

University of Windsor

Scholarship at UWindor

Electronic Theses and Dissertations

Theses, Dissertations, and Major Papers

2008

Homogeneous charge compression ignition (HCCI) engine fuelled with ethanol, iso -octane and products of in -cylinder reformation in an IDI-type engine

Gnanaprakash Gnanam
University of Windsor

Follow this and additional works at: <https://scholar.uwindsor.ca/etd>

Recommended Citation

Gnanam, Gnanaprakash, "Homogeneous charge compression ignition (HCCI) engine fuelled with ethanol, iso -octane and products of in -cylinder reformation in an IDI-type engine" (2008). *Electronic Theses and Dissertations*. 8082.

<https://scholar.uwindsor.ca/etd/8082>

This online database contains the full-text of PhD dissertations and Masters' theses of University of Windsor students from 1954 forward. These documents are made available for personal study and research purposes only, in accordance with the Canadian Copyright Act and the Creative Commons license—CC BY-NC-ND (Attribution, Non-Commercial, No Derivative Works). Under this license, works must always be attributed to the copyright holder (original author), cannot be used for any commercial purposes, and may not be altered. Any other use would require the permission of the copyright holder. Students may inquire about withdrawing their dissertation and/or thesis from this database. For additional inquiries, please contact the repository administrator via email (scholarship@uwindsor.ca) or by telephone at 519-253-3000ext. 3208.

**Homogeneous Charge Compression Ignition (HCCI) Engine
Fuelled with Ethanol, Iso-octane and Products of In-cylinder
Reformation in an IDI-type Engine**

by
Gnanaprakash Gnanam

A Dissertation
Submitted to the Faculty of Graduate Studies
through Mechanical Engineering
in Partial Fulfillment of the Requirements for
the Degree of Doctor of Philosophy at the
University of Windsor

Windsor, Ontario, Canada

2008

© 2008 Gnanaprakash Gnanam



Library and
Archives Canada

Bibliothèque et
Archives Canada

Published Heritage
Branch

Direction du
Patrimoine de l'édition

395 Wellington Street
Ottawa ON K1A 0N4
Canada

395, rue Wellington
Ottawa ON K1A 0N4
Canada

Your file *Votre référence*
ISBN: 978-0-494-47113-5
Our file *Notre référence*
ISBN: 978-0-494-47113-5

NOTICE:

The author has granted a non-exclusive license allowing Library and Archives Canada to reproduce, publish, archive, preserve, conserve, communicate to the public by telecommunication or on the Internet, loan, distribute and sell theses worldwide, for commercial or non-commercial purposes, in microform, paper, electronic and/or any other formats.

The author retains copyright ownership and moral rights in this thesis. Neither the thesis nor substantial extracts from it may be printed or otherwise reproduced without the author's permission.

AVIS:

L'auteur a accordé une licence non exclusive permettant à la Bibliothèque et Archives Canada de reproduire, publier, archiver, sauvegarder, conserver, transmettre au public par télécommunication ou par l'Internet, prêter, distribuer et vendre des thèses partout dans le monde, à des fins commerciales ou autres, sur support microforme, papier, électronique et/ou autres formats.

L'auteur conserve la propriété du droit d'auteur et des droits moraux qui protègent cette thèse. Ni la thèse ni des extraits substantiels de celle-ci ne doivent être imprimés ou autrement reproduits sans son autorisation.

In compliance with the Canadian Privacy Act some supporting forms may have been removed from this thesis.

Conformément à la loi canadienne sur la protection de la vie privée, quelques formulaires secondaires ont été enlevés de cette thèse.

While these forms may be included in the document page count, their removal does not represent any loss of content from the thesis.

Bien que ces formulaires aient inclus dans la pagination, il n'y aura aucun contenu manquant.


Canada

Author's Declaration of Originality

I hereby certify that I am the sole author of this thesis and that no part of this thesis has been published or submitted for publication.

I certify that, to the best of my knowledge, my thesis does not infringe upon anyone's copyright nor violate any proprietary rights and that any ideas, techniques, quotations, or any other material from the work of other people included in my thesis, published or otherwise, are fully acknowledged in accordance with the standard referencing practices. Furthermore, to the extent that I have included copyrighted material that surpasses the bounds of fair dealing within the meaning of the Canada Copyright Act, I certify that I have obtained a written permission from the copyright owner(s) to include such material(s) in my thesis and have included copies of such copyright clearances to my appendix.

I declare that this is a true copy of my thesis, including any final revisions, as approved by my thesis committee and the Graduate Studies office, and that this thesis has not been submitted for a higher degree to any other University or Institution.

Abstract

The major focus of this research is to analyze the individual parameters, such as, fuel chemistry, EGR, intake air temperature and engine speed that affect the HCCI combustion on-set and to utilize in-cylinder reformation as means of controlling the HCCI combustion on-set. A new in-cylinder reformation system to control the on-set of combustion has been designed and fabricated with direct injection capabilities to examine the proposed in-cylinder reformation process. The proposed reformation strategy has the advantage of temporarily varying the compression ratio during the compression stroke and controlling the HCCI combustion on-set, in addition to the effects of fuel reformation products. The methodology adopted in this thesis to identify these parameters is mostly experimental. However, there is a smaller computational component which involves HCCI cycle calculations with fuel reformation using a single-zone model. The computational part is primarily used to analyze the advantages of a proposed in-cylinder reformation strategy on HCCI combustion before implementation in the experimental set-up.

The experimental engine used for the study is a four-stroke, three cylinder In-Direct Injection (IDI) type compression ignition engine which was converted to single cylinder operation for HCCI combustion. The HCCI engine was fuelled with a lean mixture of air and fuel (ethanol, iso-octane, mixture of ethanol/iso-octane or ethanol with products of in-cylinder reformation). Based on cycle-resolved in-cylinder pressure measurements, the experimental results demonstrate that the addition of iso-octane to ethanol retards the on-set of combustion and subsequently leads to a reduction of the IMEP and thermal efficiency. The addition of EGR retards the on-set of HCCI combustion and the study indicates that ethanol allows for the use of higher percentage of EGR when compared to iso-octane. The proposed in-cylinder reformation strategy is an effective method for controlling HCCI combustion on-set (SOC) and reduces the regulated engine-out emissions. The temporary change in compression ratio that results from utilizing the proposed pre-chamber methodology has a stronger influence in controlling the HCCI combustion on-set (SOC) compared to the effects of fuel reformation products alone.

Acknowledgement

Working as a Ph.D. student in University of Windsor was a wonderful as well as challenging experience to me. In all these years, many people were instrumental directly or indirectly in shaping up my academic career. It was hardly possible for me to succeed in my doctoral work without the precious support of numerous people. Here is a small tribute to all those people.

First of all, I wish to thank my supervisor Dr. Andrzej Sobiesiak for his expert guidance, cheerful enthusiasm and ever-friendly nature that I was able to complete my research work in a respectable manner. I am also very grateful to my co-supervisor Dr. Graham Reader for his valuable suggestions and able supervision.

My graduate studies would not have been the same without the social and academic challenges and diversions provided by all my student-colleagues in the Department of Mechanical Engineering. I am particularly thankful to my friends Mwila Clarence Mulenga, Michael Johnson, Mahesh Babu, Srikanth Jonnalagedda, Hamid Toutouchian, Nima Gharib, Chunyi Xia and Mohsen Battoie. We not only studied, relaxed, and traveled well together, but also helped me in running my experiments and provided some very valuable input. Special thanks go to Michael Johnson for introducing me to the Cantera software and helping me with my numerical simulation of the single-zone model.

I also take this opportunity to express my special gratitude towards Andrew Jenner, Bruce Durfy, Mike Charron, Marc St. Pierre, Steve Budinsky, Pat Seguin, Dan Byskal and Brian Charron for providing valuable technical support during the experiment set-up construction and experimental runs.

My enormous debt of gratitude can hardly be repaid to my good friend Alben D'Silva, who always provided support with the design and development of the reformation chamber. I am also thankful to my good friends Karthi Kulandhaisamy and Kamalaveni Periasamy for their support throughout this work.

I am privileged for having Dr. David Checkel, Dr. Paul Henshaw, Dr. David Ting, Dr. Biao Zhou and Dr. Murty Madugula as my Ph.D. dissertation committee members who have spent their precious time to read the manuscript and providing me their valuable suggestions.

This dissertation would not have been possible without the help of my colleagues, Dr. Chunhua Zhang (Chang'an University) and Dale Haggith. Not only were they readily available to assist me with my experimental runs, their suggestions were always extremely perceptive, helpful, and appropriate.

I wish to express gratitude to Auto21, University of Windsor Graduate Studies and Ontario Provincial Government for providing the financial support for this work.

Finally, this journey would not have been possible without the patience and support of my family. Thus, my sincere gratitude goes to my mom, dad and my brothers (Prabhu and Vel) for their love, support, and patience over the last few years.

Despite all the assistance provided by my family, friends and colleagues, I alone remain responsible for the content of the following, including any errors or omissions which may unwittingly remain.

Table of Content

Author's Declaration of Originality	iii
Abstract	iv
Acknowledgement	v
List of figures	xii
List of tables	xxi
Nomenclature	xxii
Chapter 1	
Introduction	1
1.1 Motivation	1
1.2 HCCI engine	2
1.3 Fuel reformation	4
1.3.1 Steam reformation	5
1.3.2 Partial oxidation reformation	5
1.3.3 Auto-thermal reformation	6
1.3.4 In-cylinder reformation	6
1.4 Research hypothesis	10
1.5 Organization of dissertation	11
Chapter 2	
Literature review	12
2.1 HCCI combustion	12
2.1.1 Intake charge temperature	13
2.1.2 Intake charge boosting	14
2.1.3 Compression ratio (r_c)	15
2.1.4 Fuel injection strategies	16

2.1.5 Fuel effects	18
2.1.6 Exhaust Gas Recirculation (EGR)	19
2.1.6.1 Internal EGR using Variable Valve Timing (VVT)	20
2.1.7 Ethanol and HCCI combustion	22
2.2 In-cylinder fuel reformation	26

Chapter 3

Experimental setup and engine parameters analyzed	27
3.1 Overview	28
3.2 MTS Combustion Analysis System (CAS)	33
3.2.1 Real-time processor (V4344)	34
3.2.2 1MHz digitizer	35
3.2.3 Charge amplifier	35
3.2.4 CAS software	36
3.2.4.1 Signal pegging	36
3.2.4.2 Top Dead Center (TDC) find	37
3.3 Reformation chamber with direct injection capabilities	37
3.3.1 Design objective	38
3.3.2 Methodology	38
3.4 Horiba emissions bench	45
3.5 In-cylinder pressure sensor – validation	47
3.6 Potrable MicroGas TM emissions analyzer validation	49
3.7 Engine parameters analyzed	50
3.8 Repeatability of data	52

Chapter 4

Experimental results: Effect of intake charge temperature and fuel chemistry	54
4.1 Test conditions	54
4.2 Results and discussion	55

4.2.1 In-cylinder pressure and HRR	55
4.2.2 10% HR CA and 10-90% HR CA duration	63
4.2.3 IMEP and COV_{IMEP}	67
4.2.4 Thermal efficiency and peak pressure location	71
4.2.5 Maximum pressure rise rate	75
4.2.6 CO and UHC	78
4.3 Summary	80

Chapter 5

Experimental results: Effect of EGR **82**

5.1 Test conditions	82
5.2 Results and discussion	83
5.2.1 In-cylinder pressure and HRR ($\phi = 0.33$)	83
5.2.2 10% HR CA and 10-90% HR CA duration ($\phi = 0.33$)	90
5.2.3 In-cylinder pressure and HRR ($\phi = 0.38$)	93
5.2.4 10% HR CA and 10-90% HR CA duration ($\phi = 0.38$)	101
5.2.5 IMEP and COV_{IMEP} ($\phi = 0.33$)	104
5.2.6 IMEP and COV_{IMEP} ($\phi = 0.38$)	108
5.2.7 Thermal efficiency and maximum pressure rise rate ($\phi = 0.33$)	111
5.2.8 Thermal efficiency and maximum pressure rise rate ($\phi = 0.38$)	114
5.2.9 CO and UHC	117
5.3 Summary	121

Chapter 6

In-cylinder fuel reformation: A numerical parametric study **123**

6.1 Methodology	123
6.2 Engine parameters and test conditions	127

6.3 Results and discussion	128
6.3.1 In-cylinder reformation using Negative Valve Overlap (NVO)	132
6.3.2 Proposed in-cylinder reformation using separate reformation chamber	141
6.4 Summary	149
Chapter 7	
Experimental results: Effect of in-cylinder fuel reformation	152
7.1 Test conditions	152
7.2 Results and discussion	153
7.3 Summary	166
Chapter 8	
Conclusions and recommendations	168
8.1 Introduction	168
8.2 Conclusions	169
8.2.1 Experimental results: Effect of intake charge temperature and fuel chemistry	169
8.2.2 Experimental results: Effect of EGR	170
8.2.3 In-cylinder fuel reformation: Numerical parametric study	171
8.2.4 Experimental results: Effect of in-cylinder fuel reformation	172
8.3 Recommendations for future work	174
References	175
Appendix A: Engine specifications	182
A.1 Kubota D905 Engine specifications	182
A.2 Factory valve timing for Kubota D905	182

A.3 Performance curve for Kubota D905 engine	183
A.4 Cooling system specifications for Kubota D905	184
Appendix B: Reformation chamber design	185
Appendix C: Precision compression springs specifications	204
Appendix D: Modifications done to the experimental set-up	205
D.1 Thermocouples	205
D.2 Intake air pre-heater	206
D.3 Oil pressure sensor	207
D.4 Injector cooling system	208
D.5 Intake and exhaust pipe design	209
D.6 Differential pressure transmitter for intake air-flow measurements	209
D.7 ECU Fuel injector calibration	211
D.8 Horiba emissions bench	212
Appendix E: Statistical data from HCCI comparison runs	213
Appendix F: MATLAB program used for calculating HRR and plotting results	215
F.1: Calculating 125 cycle averaged HRR based on individual cycle in-cylinder pressure and CA data	215
F.2: Plotting the calculated HRR and in-cylinder pressure versus CA for 125 averaged cycle	216
Appendix G: MATLAB/Cantera program code used for simulation	217
G.1: In-cylinder reformation using NVO	219
G.2: In-cylinder reformation using pre-chamber	235
Vita Auctoris	236

List of figures

Figure 1.1	Compression ignition, Spark ignition and HCCI combustion.	3
Figure 1.2	In-cylinder fuel reforming as proposed by Urushihara et al. (Figure modified based on original document available at: http://www.whnet.com/4x4/cgi.html).	8
Figure 1.3	In-cylinder reformation using dedicated pre-chamber.	9
Figure 3.1a	Experimental set-up and data acquisition system.	28
Figure 3.1b	Schematic of the experimental set-up.	29
Figure 3.2	Engine and Alternating Current (AC) motor.	30
Figure 3.3	Engine head with secondary piston (and pressure sensor) and spacer arrangement.	31
Figure 3.4	Stock engine design and modified design of the pre-chamber passage.	31
Figure 3.5	Combustion Analysis System (CAS) for data acquisition.	34
Figure 3.6	Stock fuel pump used for supplying fuel for reformation.	39
Figure 3.7	Proto-type reformation chamber design.	40
Figure 3.8	Fabricated in-cylinder fuel reformation chamber with direct fuel injector.	42
Figure 3.9	In-cylinder pressure and pressure-rise rate (dP/dCA) for various motoring conditions (T_{in} : 150 °C and T_c : 75 °C).	44
Figure 3.10	Horiba emissions bench with calibration gases for analyzing engine-out emissions.	47
Figure 3.11	Comparison of in-cylinder pressure data (805 RPM, T_{in} : 25 °C, r_c : 18).	48
Figure 4.1	Cylinder pressure and rate of heat release at different intake charge temperatures (805 RPM, 100% Ethanol).	56
Figure 4.2	Cylinder pressure and rate of heat release at different intake charge temperatures (805 RPM, 50% Iso-octane & 50% Ethanol).	56

Figure 4.3	Cylinder pressure and rate of heat release at different intake charge temperatures (805 RPM, 100% Iso-octane).	57
Figure 4.4	Cylinder pressure and rate of heat release at different intake charge temperatures (1035 RPM, 100% Ethanol).	57
Figure 4.5	Cylinder pressure and rate of heat release at different intake charge temperatures (1035 RPM, 50% Iso-octane & 50% Ethanol).	58
Figure 4.6	Cylinder pressure and rate of heat release at different intake charge temperatures (1035 RPM, 100% Iso-octane).	58
Figure 4.7	Cylinder pressure and rate of heat release at different intake charge temperatures (1275 RPM, 100% Ethanol).	59
Figure 4.8	Cylinder pressure and rate of heat release at different intake charge temperatures (1275 RPM, 50% Iso-octane & 50% Ethanol).	59
Figure 4.9	Cylinder pressure and rate of heat release at different intake charge temperatures (1275 RPM, 100% Iso-octane).	60
Figure 4.10	Cylinder pressure and rate of heat release at different intake charge temperatures (1520 RPM, 100% Ethanol).	60
Figure 4.11	Cylinder pressure and rate of heat release at different intake charge temperatures (1520 RPM, 50% Iso-octane and 50% Ethanol).	61
Figure 4.12	Cylinder pressure and rate of heat release at different intake charge temperatures (1520 RPM, 100% Iso-octane).	61
Figure 4.13	10% Heat Release CA and CA duration for 10% to 90% Heat Release for different intake charge temperature and RPM (100% Ethanol, phi: 0.3).	64
Figure 4.14	10% Heat Release CA and CA duration for 10% to 90% Heat Release for different intake charge temperature and RPM (50% Ethanol and 50% Iso-octane, phi: 0.3).	65
Figure 4.15	10% Heat Release CA and CA duration for 10% to 90% Heat Release for different intake charge temperature and RPM (100% Iso-octane, phi: 0.3).	65
Figure 4.16	IMEP and COV_{IMEP} (805 RPM).	67

Figure 4.17	IMEP and COV_{IMEP} (1035 RPM).	68
Figure 4.18	IMEP and COV_{IMEP} (1275 RPM).	68
Figure 4.19	IMEP and COV_{IMEP} (1520 RPM).	69
Figure 4.20	Thermal efficiency and peak pressure location ATDC (805 RPM).	72
Figure 4.21	Thermal efficiency and peak pressure location ATDC (1035 RPM).	73
Figure 4.22	Thermal efficiency and peak pressure location ATDC (1275 RPM).	73
Figure 4.23	Thermal efficiency and peak pressure location ATDC (1520 RPM).	74
Figure 4.24	Maximum pressure rise rate (805 RPM).	75
Figure 4.25	Maximum pressure rise rate (1035 RPM) with corresponding combustion on-set CA values.	76
Figure 4.26	Maximum pressure rise rate (1275 RPM).	76
Figure 4.27	Maximum pressure rise rate (1520 RPM).	77
Figure 4.28	Carbon monoxide (CO) emissions.	79
Figure 4.29	Unburned Hydrocarbon (UHC) emissions.	83
Figure 5.1	Cylinder pressure and rate of heat release with different EGR levels (805 RPM, 100% Ethanol, ϕ : 0.33).	83
Figure 5.2	Cylinder pressure and rate of heat release with different EGR levels (805 RPM, 50% Iso-octane & 50% Ethanol, ϕ : 0.33).	84
Figure 5.3	Cylinder pressure and rate of heat release with different EGR levels (805 RPM, 100% Iso-octane, ϕ : 0.33).	84
Figure 5.4	Cylinder pressure and rate of heat release with different EGR levels (1035 RPM, 100% Ethanol, ϕ : 0.33).	85
Figure 5.5	Cylinder pressure and rate of heat release with different EGR levels (1035 RPM, 50% Iso-octane & 50% Ethanol, ϕ : 0.33).	85
Figure 5.6	Cylinder pressure and rate of heat release with different EGR levels (1035 RPM, 100% Iso-octane, ϕ : 0.33).	86
Figure 5.7	Cylinder pressure and rate of heat release with different EGR levels (1275 RPM, 100% Ethanol, ϕ : 0.33).	86
Figure 5.8	Cylinder pressure and rate of heat release with different EGR levels (1275 RPM, 50% Iso-octane & 50% Ethanol, ϕ : 0.33).	87

Figure 5.9	Cylinder pressure and rate of heat release with different EGR levels (1275 RPM, 100% Iso-octane, phi: 0.33).	87
Figure 5.10	Cylinder pressure and rate of heat release with different EGR levels (1520 RPM, 100% Ethanol, phi: 0.33).	88
Figure 5.11	Cylinder pressure and rate of heat release with different EGR levels (1520 RPM, 50% Iso-octane and 50% Ethanol, phi: 0.33).	88
Figure 5.12	Cylinder pressure and rate of heat release with different EGR levels (1520 RPM, 100% Iso-octane, phi: 0.33).	89
Figure 5.13	10% Heat Release CA and CA duration for 10% to 90% Heat Release for different EGR levels and RPM (100% Ethanol, phi: 0.33).	91
Figure 5.14	10% Heat Release CA and CA duration for 10% to 90% Heat Release for different EGR levels and RPM (50% Ethanol & 50% Iso-octane, phi: 0.33).	92
Figure 5.15	10% Heat Release CA and CA duration for 10% to 90% Heat Release for different EGR levels and RPM (100% Iso-octane, phi: 0.33).	92
Figure 5.16	Cylinder pressure and rate of heat release with different EGR levels (805 RPM, 100% Ethanol, phi: 0.38).	94
Figure 5.17	Cylinder pressure and rate of heat release with different EGR levels (805 RPM, 50% Ethanol and 50% Iso-octane, phi: 0.38).	94
Figure 5.18	Cylinder pressure and rate of heat release with different EGR levels (805 RPM, 100% Iso-octane, phi: 0.38).	95
Figure 5.19	Cylinder pressure and rate of heat release with different EGR levels (1035 RPM, 100% Ethanol, phi: 0.38).	95
Figure 5.20	Cylinder pressure and rate of heat release with different EGR levels (1035 RPM, 50% Ethanol and 50% Iso-octane, phi: 0.38).	96
Figure 5.21	Cylinder pressure and rate of heat release with different EGR levels (1035 RPM, 100% Iso-octane, phi: 0.38).	96
Figure 5.22	Cylinder pressure and rate of heat release with different EGR levels (1275 RPM, 100% Ethanol, phi: 0.38).	97

Figure 5.23	Cylinder pressure and rate of heat release with different EGR levels (1275 RPM, 50% Ethanol and 50% iso-octane, phi: 0.38).	97
Figure 5.24	Cylinder pressure and rate of heat release with different EGR levels (1275 RPM, 100% Iso-octane, phi: 0.38).	98
Figure 5.25	Cylinder pressure and rate of heat release with different EGR levels (1520 RPM, 100% Ethanol, phi: 0.38).	98
Figure 5.26	Cylinder pressure and rate of heat release with different EGR levels (1520 RPM, 50% Ethanol and 50% Iso-octane, phi: 0.38).	99
Figure 5.27	Cylinder pressure and rate of heat release with different EGR levels (1520 RPM, 100% Iso-octane, phi: 0.38).	99
Figure 5.28	10% Heat Release CA and CA duration for 10% to 90% Heat Release for different EGR levels and RPM (100% Ethanol, phi: 0.38).	102
Figure 5.29	10% Heat Release CA and CA duration for 10% to 90% Heat Release for different EGR levels and RPM (50% Ethanol and 50% Iso-octane, phi: 0.38).	102
Figure 5.30	10% Heat Release CA and CA duration for 10% to 90% Heat Release for different EGR levels and RPM (100% Iso-octane, phi: 0.38).	103
Figure 5.31	IMEP and COV_{IMEP} for different EGR levels and RPM (100% Ethanol, phi: 0.33).	105
Figure 5.32	IMEP and COV_{IMEP} for different EGR levels and RPM (50% Ethanol & 50% iso-octane, phi: 0.33).	105
Figure 5.33	IMEP and COV_{IMEP} for different EGR levels and RPM (100% Iso-octane, phi: 0.33).	106
Figure 5.34	IMEP and COV_{IMEP} for different EGR levels and RPM (100% Ethanol, phi: 0.38).	109
Figure 5.35	IMEP and COV_{IMEP} for different EGR levels and RPM (50% Ethanol and 50% Iso-octane, phi: 0.38).	109
Figure 5.36	IMEP and COV_{IMEP} for different EGR levels and RPM (100% Iso-octane, phi: 0.38).	110

Figure 5.37	Net thermal efficiency and Maximum pressure rise rate for different EGR levels and RPM (100% Ethanol, ϕ : 0.33).	112
Figure 5.38	Net thermal efficiency and Maximum pressure rise rate for different EGR levels and RPM (50% Ethanol & 50% iso-octane, ϕ : 0.33).	112
Figure 5.39	Net thermal efficiency and Maximum pressure rise rate for different EGR levels and RPM (100% Iso-octane, ϕ : 0.33).	113
Figure 5.40	Net thermal efficiency and Maximum pressure rise rate for different EGR levels and RPM (100% Ethanol, ϕ : 0.38).	115
Figure 5.41	Net thermal efficiency and Maximum pressure rise rate for different EGR levels and RPM (50% Ethanol and 50% Iso-octane, ϕ : 0.38).	116
Figure 5.42	Net thermal efficiency and Maximum pressure rise rate for different EGR levels and RPM (100% Iso-octane, ϕ : 0.38).	116
Figure 5.43	CO and UHC for different EGR levels and RPM (100% Ethanol, ϕ : 0.33).	118
Figure 5.44	CO and UHC for different EGR levels and RPM (50% Ethanol & 50% iso-octane, ϕ : 0.33).	118
Figure 5.45	CO and UHC for different EGR levels and RPM (100% Iso-octane, ϕ : 0.33).	119
Figure 5.46	CO and UHC for different EGR levels and RPM (100% Ethanol, ϕ : 0.38).	119
Figure 5.47	CO and UHC for different EGR levels and RPM (50% Ethanol and 50% Iso-octane, ϕ : 0.38).	120
Figure 5.48	CO and UHC for different EGR levels and RPM (100% Iso-octane, ϕ : 0.38).	120
Figure 6.1	Multi-step modeling of HCCI engine cyclic process with in-cylinder fuel reforming.	124
Figure 6.2	In-cylinder pressure and HRR with different intake charge temperatures and no EGR (100% Ethanol, ϕ : 0.4, T_c : 75 °C).	129

Figure 6.3	In-cylinder pressure and HRR with different EGR levels (100% Ethanol, ϕ : 0.4, T_{in} : 77 °C, T_c : 75 °C).	130
Figure 6.4	In-cylinder pressure and HRR with different fuel mechanisms (100% Ethanol, ϕ : 0.4, T_{in} : 77 °C, T_c : 75 °C).	131
Figure 6.5	In-cylinder pressure and HRR (ϕ : 0.4, T_{in} : 77 °C, 0% EGR and 30% reformation fuelling).	133
Figure 6.6	In-cylinder pressure and HRR (ϕ : 0.4, T_{in} : 77 °C, 0% EGR and 10% reformation fuelling).	135
Figure 6.7	Combustion on-set for ϕ : 0.4, T_{in} : 77 °C, 30% reformation fuelling with different % EGR addition.	136
Figure 6.8	H ₂ for ϕ : 0.4, T_{in} : 77 °C, 30% reformation fuelling with different % EGR addition.	137
Figure 6.9	Combustion on-set for ϕ : 0.4, T_{in} : 77 °C, 10% reformation fuelling with different % EGR addition.	138
Figure 6.10	H ₂ for ϕ : 0.4, T_{in} : 77 °C, 10% reformation fuelling with different % EGR addition.	139
Figure 6.11	in-cylinder pressure and HRR (ϕ : 0.4, T_{in} : 72 °C, 0% EGR and 30% reformation fuelling).	140
Figure 6.12	In-cylinder pressure and HRR (ϕ : 0.4, T_{in} : 67 °C, 0% EGR and 30% reformation fuelling).	141
Figure 6.13	In-cylinder pressure and HRR (ϕ : 0.4, T_{in} : 77 °C, 0% EGR and 30% reformation fuelling).	142
Figure 6.14	In-cylinder pressure and HRR (ϕ : 0.4, T_{in} : 77 °C, 0% EGR and 10% reformation fuelling).	143
Figure 6.15	Combustion on-set for ϕ : 0.4, T_{in} : 77 °C, 30% reformation fuelling with different % EGR addition.	146
Figure 6.16	Combustion on-set for ϕ : 0.4, T_{in} : 77 °C, 10% reformation fuelling with different % EGR addition.	147
Figure 6.17	H ₂ for ϕ : 0.4, T_{in} : 77 °C with different % EGR addition and reformation fuelling.	147

Figure 6.18	In-cylinder pressure and HRR (ϕ : 0.4, T_{in} : 67 °C with 0% EGR and 30% reformation fuelling).	149
Figure 7.1	In-cylinder pressure and pressure-rise rate (dP/dCA) for various motoring conditions (T_{in} : 150 °C and T_c : 75 °C).	153
Figure 7.2	Calculated in-cylinder temperature for various motoring conditions (T_{in} : 150 °C and T_c : 75 °C).	154
Figure 7.3	In-cylinder pressure and HRR for ϕ : 0.27, 1120 RPM and 10% fuel injected for reformation.	156
Figure 7.4	In-cylinder pressure and HRR for ϕ : 0.31, 1120 RPM condition and 10% fuel injected for reformation.	157
Figure 7.5	In-cylinder pressure and HRR for ϕ : 0.37, 1120 RPM and 10% fuel injected for reformation.	157
Figure 7.6	In-cylinder pressure and HRR for ϕ : 0.27, 1120 RPM and 25% fuel injected for reformation.	158
Figure 7.7	In-cylinder pressure and HRR for ϕ : 0.34, 1080 RPM and 20% fuel injected for reformation.	158
Figure 7.8	In-cylinder pressure and HRR for ϕ : 0.34, 1080 RPM and 25% fuel injected for reformation.	159
Figure 7.9	IMEP vs Equivalence ratio for various reformation fuelling percentage.	161
Figure 7.10	COV_{IMEP} vs Equivalence ratio for various reformation fuelling percentage.	165
Figure A.1a	Performance Curve for Kubota D905 Engine.	183
Figure A.1b	Performance Curve for Kubota D905 Engine.	184
Figure B.1	Assembly drawing of the first proto-type.	190
Figure B.2	Lower base – Item 1 in assembly drawing (first proto-type).	191
Figure B.3	Intermediate base – Item 2 in assembly drawing (first proto-type).	192

Figure B.4	Top cap – Item 3 in assembly drawing (first proto-type).	193
Figure B.5	Injector sleeve – Item 4 in assembly drawing (first proto-type).	194
Figure B.6	Injector collar – Item 5 in assembly drawing (first proto-type).	195
Figure B.7	Plunger – Item 6 in assembly drawing (first proto-type).	196
Figure B.8	Assembly drawing of the second (final) proto-type.	197
Figure B.9	Lower base restored from first proto-type– Item 1 in assembly drawing (second proto-type).	198
Figure B.10	Modified intermediate base – Item 3 in assembly drawing (second proto-type).	199
Figure B.11	Sealing plug – Item 4 in assembly drawing (second proto-type).	200
Figure B.12	Modified plunger (valve) – Item 2 in assembly drawing (second proto-type).	201
Figure B.13	Flange that holds on compressed spring – Item 5 in assembly drawing (second proto-type).	202
Figure B.14	Top cap – Item 6 in assembly drawing (second proto-type).	203
Figure D.1	Real-time unprocessed thermocouple data (Zoldak, 2005).	205
Figure D.2	Real-time unprocessed thermocouple data with shielded and grounded wires.	206
Figure D.3	Injector cooling system.	208
Figure D.4	Comparison between the Dwyer and Omega differential pressure transmitter (1000 RPM, $r_c = 20$, STP conditions).	211

List of tables

Table 3.1	Stock engine configuration	29
Table 3.2	Comparison between portable MicroGas™ analyzer and Horiba bench	49
Table 3.3	Statistical data from HCCI comparison runs	53
Table 4.1	Engine specifications and test conditions	54
Table 5.1	Engine specifications and test conditions	82
Table 6.1	Engine parameters used for simulation	128
Table 7.1	Engine specifications and test conditions	152
Table C.1	Precision compression spring specifications	204
Table D.1	Dwyer 616W pressure transmitter specifications	210

Nomenclature

ϕ, phi	Equivalence ratio [-]
γ	Ratio of specific heats [-]
CO_2	Carbon dioxide
D	Diameter (mm)
dP/dCA	Pressure rise rate (bar/ °CA)
H_2	Hydrogen
NO_x	Oxides of nitrogen
O_2	Oxygen
Q_n	Net heat release (J)
Q_{ch}	Chemical heat release (J)
T_c	Coolant temperature (°C)
T_{in}	Intake charge temperature (°C)
T_{wall}	Cylinder wall temperature (°C)
V_c	Clearance volume (cm^3)
V_d	Displacement volume (cm^3 , L)
V_{EGR}, V_e	Volume of EGR (cm^3 , L)
V_i, V_o	Volume of fresh charge (cm^3 , L)
$W_{c,i}$	Indicated work done per cycle (J)
X	Mole fraction [-]
AC	Alternating current
ATAC	Active thermo-atmosphere combustion
ATDC	After top dead center (°CA)
BDC	Bottom dead center (°CA)

BTDC	Before bottom dead center (°CA)
CA	Crank angle (°CA)
CAS	Combustion analysis system
CI	Compression ignition
CIHC	Compression ignited homogeneous charge
CNG	Compressed natural gas
CO	Carbon monoxide
COV	Coefficient of variation [-]
DEE	Diethyl ether
ECU	Electronic control unit
EGR	Exhaust gas recirculation (%)
EVC	Exhaust valve close (°CA)
EVO	Exhaust valve open (°CA)
FI	Fuel injector
FID	Flame ionization detector
HC	Hydrocarbon
HCCI	Homogeneous charge compression ignition
HR	Heat release (J)
HRR	Heat release rate (J/CA)
IC	Internal combustion
IDI	In-direct injection
IMEP	Indicated mean effective pressure (bar)
IVC	Intake valve close (°CA)
IVO	Intake valve open (°CA)

NVO	Negative valve overlap (°CA)
P	Pressure (bar)
PREDIC	Premixed lean diesel combustion
PRF	Primary reference fuel
RPM	Revolutions per minute
SI	Spark ignition
SOC	Start of combustion (°CA)
StdDev	Standard deviation [-]
TDC	Top dead center (°CA)
TS	Toyota soken
UHC	Unburned hydrocarbons
VSD	Variable speed drive
VCR	Variable compression ratio
VVT	Variable valve timing

Chapter 1 Introduction

This Ph.D. thesis investigates the combustion characteristics of an In-Direct Injection (IDI) type HCCI engine fuelled with ethanol, iso-octane and products of in-cylinder reformation for various different operating conditions. The major focus of this research is to analyze the individual parameters that affect the HCCI combustion on-set and to utilize in-cylinder reformation as a means of controlling the HCCI combustion on-set. In order to achieve this, first an extensive experimental matrix on different operating parameters has been executed for the regular HCCI combustion process without fuel reformation. Secondly, a new in-cylinder fuel reformation strategy has been proposed, implemented and experimentally tested in this work. This thesis presents the motivation, objectives and methodology for the work, then the results and findings of this work with recommendations for future work.

1.1 Motivation

The automotive industry has been forced to respond to the increasing environmental concerns of consumers and the rising cost of fossil fuels. Furthermore, the prevailing mode of operation for premixed charged engines, such as gasoline engines, is mostly in partial loading or with the throttle valve partially closed. This results in poor fuel economy and increased engine emissions. The industry is aimed at developing an alternative fueled engine that can improve engine operation at partial loads. The research community is convinced (Thring, 1989, Zhao, 2003) that the Homogeneous Charge Compression Ignition (HCCI) mode of combustion is the key to improve conventional engine operation at partial loads, which can also be achieved with minimum

modifications to the existing gasoline or diesel engines. Coupling the advantages of the HCCI mode of combustion with an alternative fuel is the solution to attain a better efficiency engine that can alleviate the dependency of fossil fuels. The alternative fuel that is our interest is ethanol since it can be produced domestically from biomass such as sugar, starch and cellulose. Furthermore, ethanol has been an attractive fuel of choice in IC engines due to the potential reduction of CO₂ (a greenhouse gas) that occurs during the production of crops used for manufacturing ethanol.

1.2 HCCI engine

The HCCI engine combines the use of premixed air and fuel, usually associated with spark ignition (SI) engines, with self-ignition induced by a high compression ratio, usually encountered in compression ignition (CI) engines. Figure 1.1 shows the different combustion processes encountered in the CI, SI and HCCI engine. From Figure 1.1 it can be noted that the charge preparation in the HCCI engine is similar to the SI engine where a premixed air-fuel mixture is brought in to the combustion chamber during the intake stroke. In the case of a CI engine, only air is induced during the intake stroke and fuel is injected directly into the combustion chamber at the end of compression stroke.

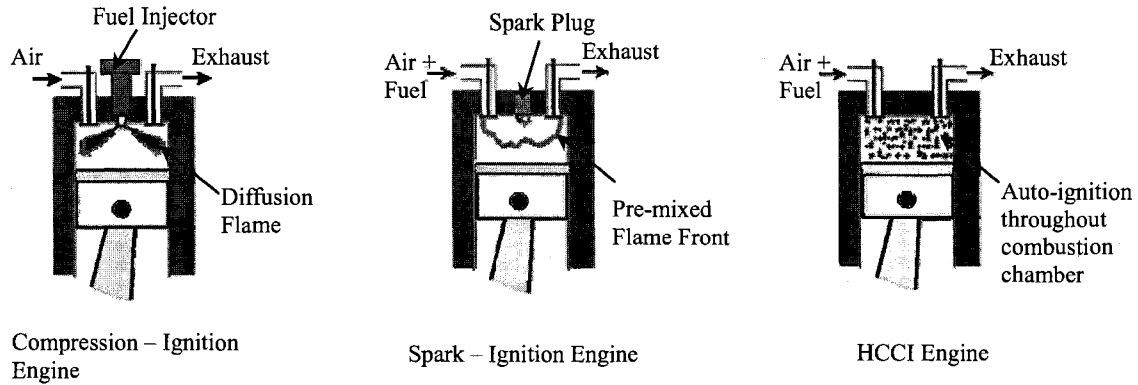


Figure 1.1: Compression ignition, Spark ignition and HCCI combustion.

In the case of a SI engine, the combustion process is initiated by electrical discharge from a spark plug at the end of the compression process. The spark kernel results in the formation of a premixed flame front that travels across the combustion chamber originating from the spark plug. Whereas, in the case of the CI engine, the combustion process is achieved by injecting fuel directly into the combustion chamber at the end of the compression stroke when air is at a very high temperature. Once the fuel is injected, it evaporates, diffuses and forms a combustible mixture with the surrounding air; then it auto-ignites. The resultant combustion is a diffusion flame front with varying fuel-air equivalence ratio that depends on the level of air and fuel mixing achieved during the combustion process. In the case of HCCI combustion, the combustion process is initiated by compressing the fuel-air mixture to its auto ignition temperature during the compression stroke. This results in multiple ignition points throughout the combustion chamber and contributes to a uniform reaction zone throughout the combustion chamber without a single flame propagation or flame front. To ensure desired ignition timing and

to moderate reaction rates during HCCI combustion, the air/fuel mixtures need to be lean or even ultra-lean.

There are numerous consequences of such an organization of the HCCI engine combustion process, such as increased thermal efficiency, lower cycle temperatures and reduced NO_x emissions. While there are numerous advantages in exploiting the HCCI mode of operation, there are also a number of issues that need to be addressed. HCCI combustion lacks a means of combustion on-set and subsequent pressure rise control, since both the spark ignition timing (SI engine) and the injection timing (CI engine) are absent. Also, the HCCI engine operation is limited to part-load only (Tabaczynski, 2000).

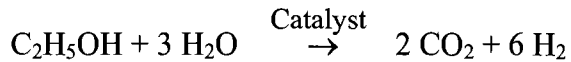
1.3 Fuel reformation

Fuel reformation is carried out to generate hydrogen or hydrogen-enriched products from primary fuel. The advantage of hydrogen is its relatively wide flammability limits and good burning quality. Fuel reformation is traditionally carried out using a dedicated reformation chamber utilizing one of these three major reformation processes:

- Steam reformation
- Partial oxidation reformation, or
- Autothermal reformation

1.3.1 Steam reformation:

Steam reformation is carried out by bringing steam and fuel into a reformation chamber in the presence of a catalyst at around 800 °C. The ideal steam reformation equation for ethanol is:

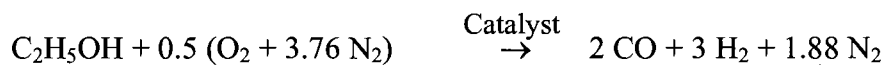


$$\text{with } X_{\text{H}_2} = \frac{6}{2+6} = 0.75$$

The main advantage of steam reformation is a higher hydrogen yield than other reformation processes. The disadvantage of steam reformation is the requirement of a heat source, supply of steam and its slow start-up time, since the catalyst has to be brought to around 800 °C for efficient conversion of fuel to hydrogen.

1.3.2 Partial oxidation reformation:

Partial oxidation reformation is carried out by combustion of a rich mixture of fuel and air. The air is generally preheated to around 200 °C for the vaporization of ethanol and the process is initiated using a glow plug. The ideal partial oxidation reformation equation for ethanol is:

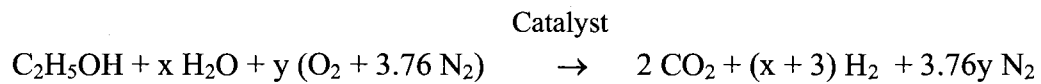


$$\text{with } X_{\text{H}_2} = \frac{3}{2+3+1.88} = 0.436$$

The main advantage of partial oxidation reformation is the quick start-up time since the reaction is exothermic. The disadvantage of partial oxidation reaction is a lower hydrogen yield than other reformation processes.

1.3.3 Auto-thermal reformation:

Auto-thermal reformation uses a combination of both partial oxidation and steam reformation. It consists of two stages. In the first stage, the fuel and air are brought together and the rich mixture is burned using a glow plug similar to partial oxidation reformation. Then in the next stage, the partially burnt fuel or combustion products that are at a high temperature are mixed with steam and reformation is carried out similar to the steam reformation. The ideal auto-thermal reformation for ethanol is:



$$\text{with } X_{\text{H}_2} = \frac{5}{2 + 5 + 1.88} = 0.563 \quad (\text{for } x = 2 \text{ and } y = 0.5)$$

The advantages of auto-thermal reformation are a higher hydrogen yield than the partial oxidation reformation and faster start-up time than the steam reformation. However, it requires multiple and difficult to control processes.

1.3.4 In-cylinder reformation:

The in-cylinder or internal reformation strategy considered in this study was first proposed by Urushihara et al. (2003) and is carried out within the engine combustion chamber. This eradicates the requirement for a dedicated external reformer for generation

of hydrogen or hydrogen-rich products from primary fuel, which consequently eliminates the reformer cost and space requirements. The in-cylinder or internal reformation strategy in general is similar to the auto-thermal reformation process. However, instead of steam and air, the lean HCCI exhaust gas or combustion product (which is ideally comprised of O_2 , H_2O , CO_2 and N_2) is used for fuel reformation. The use of exhaust gas or combustion products exploits the relatively high temperature associated with them. Higher temperatures which are favorable to the reformation reaction can be achieved by using an in-cylinder methodology, such as, Negative Valve Overlap (NVO).

a) In-cylinder reformation using NVO:

In-cylinder fuel reforming using NVO is accomplished by manipulating the valve timing to create a negative valve overlap and retaining products of combustion from the previous cycle in (Urushihara, 2003). A fraction of fuel is injected into the trapped in-cylinder combustion products and the mixture undergoes compression and reformation, as shown in Fig. 1.2. The favorable temperatures for fuel reforming are obtained by manipulating the start and duration of the reforming cycle. It should be realized that these variations in the start of the reformation cycle correspond to mean variability in the reformation cycle compression ratio and temperatures during the reformation process.

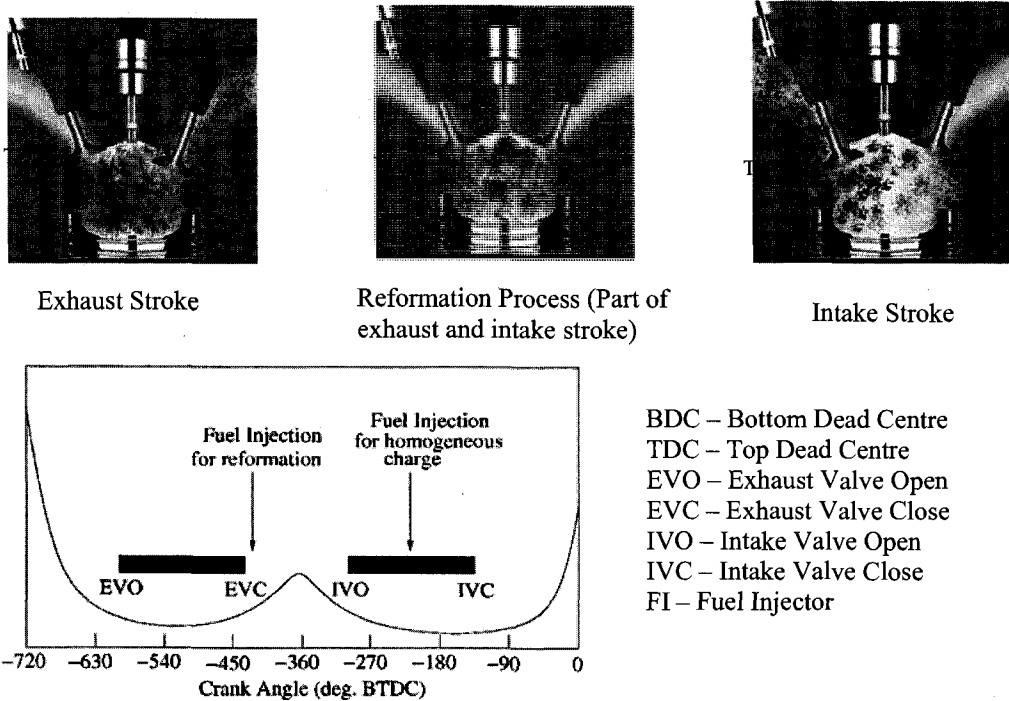


Figure 1.2: In-cylinder fuel reforming as proposed by Urushihara et al. 2003

b) In-cylinder reformation using an isolated pre-chamber (proposed in this thesis):

This reformation process is similar to the traditional in-cylinder reformation process using negative valve overlap. However, in this method the reformation process is carried out in a dedicated pre-chamber built as an integral part of the main combustion chamber (Fig. 1.3). A mechanical valve and a direct fuel injector for reformation fuelling are used to carry out the in-cylinder reformation process. The valve in the reformation chamber is used for isolating the reformation chamber volume from the main combustion chamber during the reformation process.

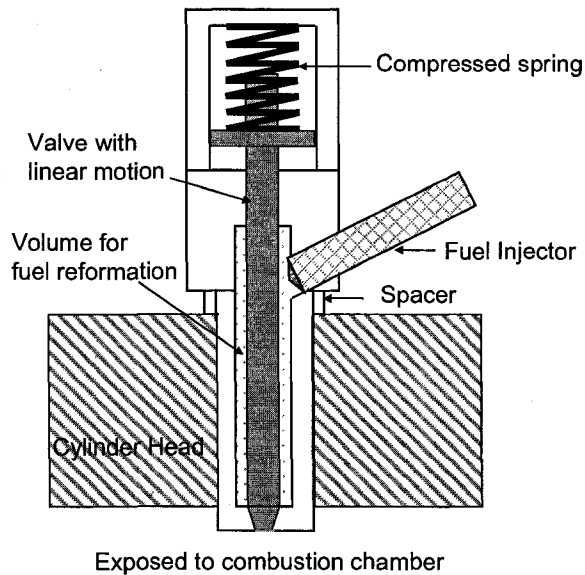


Figure 1.3: In-cylinder reformation using dedicated pre-chamber.

The first stage in fuel reformation is achieved by trapping a fraction of residual combustion products in the reformation chamber [at 80° CA After Top Dead Center (ATDC) during the expansion stroke] before the opening of the exhaust valve, minimizing the temperature loss from the expansion of gases. Then a fraction of the fuel is injected into the reformation chamber which undergoes the reformation process. Mixing of reformation products with fresh charge is accomplished at 15° CA Before Top Dead Center (BTDC) during the compression stroke of the next cycle. It should be noted that the reformation chamber is kept open from 15° CA BTDC (compression stroke) until 80° CA ATDC (expansion stroke) during which the regular HCCI combustion process takes place (in both main and reformation chamber).

The physical separation of the reformation process from the main engine operating processes (intake, compression, power and exhaust) is essential in effectively controlling

the temperature and/or the oxygen content of the trapped residual gases that participate in reformation. In the proposed method, the control over oxygen content and temperature of the trapped residual gas is achieved by manipulating the time at which the residual gases are captured during the expansion stroke. The volumetric efficiency of the engine is not affected since the intake and exhaust valve timings were not manipulated. Furthermore, the main advantage of the proposed method over the NVO strategy is that the products of reformation can be mixed with the fresh charge (next cycle) during the compression stroke rather than at the start of the intake stroke. This control over mixing of reformation products with fresh charge provides a means of direct control of the on-set or start of HCCI combustion similar to spark ignition in SI engines or direct injection in CI engines.

1.4 Research hypothesis

The overall objective of this study is to investigate the combustion characteristics of an IDI type HCCI engine fuelled with ethanol and products of in-cylinder reformation for different operating conditions. Furthermore, the effect of iso-octane addition at the on-set of HCCI combustion is also investigated experimentally. An IDI-type engine is used in this study to differentiate from the majority of the work done in HCCI combustion on DI-type engines. Hence, it is of interest to investigate the effect of the pre-chamber and the influence of its high surface-to-volume ratio in IDI-type HCCI combustion.

The major focus of this study is on identifying parameters that influence the HCCI combustion on-set, since an HCCI engine lacks a direct means of combustion on-set control. The methodology adopted here to identify these parameters is mostly

experimental. However, there is a smaller computational component which involves HCCI cycle calculations with fuel reformation using a single-zone model. The computational part was primarily used to analyze the advantages of the proposed in-cylinder reformation strategy on HCCI combustion before implementation in the experimental set-up.

1.5 Organization of dissertation

This dissertation reports on the process that was followed in achieving the objectives and is outlined as follows:

1. A literature review of the work done related to this study is provided in Chapter 2.
2. Details of the experimental apparatus are presented in Chapter 3.
3. Effect of intake charge temperature and fuel chemistry on HCCI combustion without EGR addition is provided in Chapter 4.
4. Effects of EGR addition and equivalence ratio on HCCI combustion is discussed in Chapter 5.
5. Numerical simulation using a single-zone model to analyze the advantages of proposed reformation strategy is presented in Chapter 6.
6. Experimental results and discussion of HCCI combustion with in-cylinder fuel reformation utilizing ethanol as the operating fuel is presented in Chapter 7.
7. Conclusions of the findings and Recommendations for future work are provided in Chapter 8.

Any relevant information corresponding to the above topics is provided in the Appendices.

Chapter 2 Literature review

The following literature study is focused on two topics that are relevant to this study. The first is HCCI combustion and the second is in-cylinder fuel reformation.

2.1 HCCI combustion

Over the past two decades, many studies have been performed on HCCI combustion using a variety of different fuels including ethanol, dimethyl ether, gasoline, diesel fuel, n-heptane, propane, Compressed Natural Gas (CNG) etc. The earliest studies were reported in 1979 (Onishi and Noguchi) and showed the basic characteristics of HCCI combustion, such as, very little cyclic variations and no flame propagation. Onishi et al. called the HCCI combustion Active Thermo-Atmosphere Combustion (ATAC) in their studies and Noguchi et al. termed it Toyota-Soken (TS) combustion. However, the studies in 1979 were conducted on a two-stroke engine with a low compression ratio and very high residual gas in the cylinder. Najt and Foster (1983) were the first to show that the HCCI mode of combustion is possible in a four stroke engine, which they called Compression-Ignited Homogeneous Charge (CIHC). Their study was performed on an engine with a variable compression ratio and using a mixture of iso-octane and n-heptane as fuel. Thring (1989) was the first to suggest the use of HCCI operation on part-loads and conventional SI operation at high loads. The first to test HCCI operation on a production engine utilizing pre-heated intake air (1.6L VW engine) was Stockinger et al (1992). Their tests showed that part-load efficiency can be increased from 14 to 34% by adopting a HCCI mode of operation.

Recently, interest in HCCI has been growing. Various studies on HCCI combustion covering a broad range of topics, such as, analyzing the effects of intake charge temperature, intake charge boosting, compression ratio, various fuel injection strategies, fuel effects, Exhaust Gas Recirculation (EGR), Variable Valve Timing (VVT) and Internal EGR have been reported. A summary of selected studies related to the above mentioned areas of HCCI combustion are discussed below.

HCCI engines and various strategies of HCCI combustion control, which include the use of EGR, preheating of combustion air, and steam injection, are discussed in a comprehensive review compiled by Zhao et al. (2003).

2.1.1 Intake charge temperature:

The effects of intake charge temperature on HCCI combustion on-set have been widely reported by many researchers. Najt and Foster (1983) showed that HCCI of lean mixtures could be achieved in a SI engine that has a low compression ratio with elevated intake charge temperatures (300-500°C). In general, the intake charge temperature has a strong influence on the HCCI combustion on-set, with increase in intake charge temperature advancing the combustion on-set and decreasing combustion duration. Similarly, the simulation study performed by Ng (2004) with lean ethanol-air mixtures also demonstrates that increasing the intake charge temperature leads to advancement in the combustion on-set.

Iida et al (2000) investigated the effect of intake charge temperature, compression ratio and coolant temperature on the HCCI combustion on-set. The study showed that an increase in intake charge temperature from 297 K to 325 K to 355 K, increased the peak temperature after compression and advanced the HCCI combustion on-set. Furthermore, the authors found that the effect of intake charge temperature on combustion on-set was greater for higher engine speed (1200 RPM) compared to the lower engine speed (600 RPM).

The study done by Hakan et al (2004) investigated the effect of intake temperature on HCCI operation using negative valve overlap. They tested several points in the range between 15 °C to 50 °C to investigate the effects of intake charge temperature on spark assisted and unassisted HCCI combustion stability (COV_{IMEP} and COV_{pmax}) for a particular load and negative valve overlap condition. The study showed that either increase in the residuals or intake charge temperature resulted in low COV and stabilised the combustion, with as well as without ignition. The heated air showed similar effects as increased valve overlap in terms of charge temperature.

2.1.2 Intake charge boosting

One of the factors that limit the commercial use of HCCI engine is its low IMEP that can be achieved by natural aspiration. Christensen and Johansson (1998 and 2000) showed that intake charge boosting dramatically increases the attainable IMEP for HCCI combustion. Their study in 1998 showed that an IMEP of 14 bar can be achieved with a 2 bar boost pressure and a compression of 17:1 for a HCCI engine operating on natural gas.

The maximum pressure limit for the 1998 study was set at 250 bar. Also, the study showed a decrease in HC emission with increasing boost pressure and engine load. Their second study in 2000 showed that the load limit for HCCI can be further extended by applying intake charge boosting in combination with EGR, without increasing the maximum cylinder pressure. The highest IMEP attained in the 2000 study was 15.6 bar with a boost pressure of 1.5 bar and a compression ratio of 17.2:1 for a HCCI engine operating with natural gas. The percentage EGR used for the condition was 48% and the maximum pressure obtained was below 170 bar.

The study done by Urata (2004) also showed that charge boosting is effective in expanding the operational range of a gasoline fuelled HCCI engine while maintaining low levels of NO_x emission. The authors also showed that a charge boosted HCCI engine using port injection resulted in lower NO_x levels compared to direct injection of fuel during the compression stroke (no intake pressure boosting) for the same mid-load operating condition.

2.1.3 Compression ratio (r_c)

Christensen et al. (1997, 1999) have been carefully investigating compression ratio as an effective means to achieve HCCI combustion control for several years. Their studies showed that regardless of fuel type used increasing the compression ratio (9.6:1 – 22.5:1) had a strong influence on combustion on-set and assists in decreasing the necessary intake charge temperature.

The effect of compression ratio (12:1 – 18.6:1) on combustion on-set was also reported by Hiraya et al. (2002). Their study on a gasoline HCCI engine showed that higher compression ratios allowed for lower intake charge temperature, and higher intake density for higher output. Furthermore, higher compression ratio contributed to higher thermal efficiency. The study done by Iida et al (2000) also confirmed that change in compression ratio had a strong influence on HCCI combustion on-set. Furthermore, their results showed that compression ratio had a greater effect on HCCI combustion on-set compared to changes in either intake charge temperature or coolant temperature.

The study done by Olsson et al (2002) investigated the influence of compression ratio on a natural gas fuelled HCCI engine. The experimental engine had a secondary piston that was installed in the cylinder head whose position can be varied to attain Variable Compression Ratio (VCR). In their tests, the compression ratio was modified (21:1, 20:1, 17:1 and 15:1) according to the operating condition to attain auto-ignition of the charge close to TDC. This VCR engine showed the potential to achieve satisfactory operation in HCCI mode over a wide range of operating conditions by using the optimal compression ratio for a particular operating condition. The study also showed that the maximum pressure rise rate increased with higher compression ratio for early combustion timing and a reverse effect was seen with delayed combustion on-set.

2.1.4 Fuel injection strategies

Different fuel injection strategies that use direct fuel injection with/without port fuel injection have been proposed to analyze the effects of charge preparation on HCCI

combustion. The study done by Takeda (1996) focussed on promoting fuel and air mixing to facilitate the HCCI mode of combustion in a direct injection diesel engine. The authors termed it as PREMixed lean Diesel Combustion (PREDIC). In their study two side injectors were used simultaneously to inject fuel directly (64 or 78° CA BTDC) into the cylinder and form a premixed mixture. The use of two side injectors allowed the injector sprays to collide with each other and remain in the centre region of the cylinder. Results from their study showed that the use of side injectors with early fuel injection timing reduced the NO_x emissions to 20 ppm at partial-loads (fuel:air ratio in excess of 2.7), which was not possible with conventional injection methods.

The use of two-stage diesel fuel injection to promote premixed charge mixing and control the combustion on-set was studied by Kook et al (2004). Their study used an early direct injection, termed as main injection (10 to 19 mm³), of diesel fuel to achieve premixing with air and a secondary small fuel injection (1.5 mm³) near TDC to act as an ignition promoter. Their experimental results showed that two-stage injection has prospects to control combustion on-set at lower intake air temperature. However, with high intake air temperatures the combustion on-set was advanced and the prospects of control diminished.

The effects of charge stratification on gasoline HCCI combustion was investigated by Tanet et al (2004) and Wang et al (2005). The study done by Tanet et al (2004) used two injectors; one for generating homogeneous mixture at intake system and another for direct injection into the combustion chamber. The study showed that at the lean limit of

HCCI operating range, charge stratification showed improvements in IMEP and emissions. However, at the rich limit, charge stratification was limited by high pressure rise rate and high CO and NO_x emissions.

The study by Wang et al (2005) focussed on two-stage gasoline direct injection to control the mixture formation, ignition timing and combustion rate in an HCCI engine. The first fuel stage injection (main) was accomplished during the intake stroke (100 ATDC) and the second stage injection (approx. 15% of total fuel) was done during the early stages of compression stroke (180 through 90° CA BTDC). Their results showed that two-stage injection helped in suppressing the knock and extending the HCCI load range. Furthermore, the second stage fuel injection had a more direct influence on the HCCI combustion on-set than the first stage fuel injection.

2.1.5 Fuel effects

Since combustion on-set in an HCCI engine is achieved by auto-ignition of the fuel-air mixture, the choice of fuel plays a major role on both engine design and control strategies. The effect of fuel volatility and auto-ignition characteristics plays an important factor in good combustion phasing, and a rapid bulk burn to obtain high fuel economy and minimize emission.

The study done by Furutani et al. (1998) showed that utilizing a combination of two fuels with different octane numbers, the HCCI combustion on-set can be controlled. Their study also found that with higher difference between the octane number of the two fuels

used, a wider operating range can be achieved. However, adjusting the total amount of fuel and their blending ratio to meet the torque requirement presented a major challenge for practical application. A similar study was conducted by Olsson et al. (2001) using ethanol and n-heptane. Their study also showed that using two fuels with different octane rating extended the operating range of the HCCI engine.

The study done by Asmus and Zhao (2003) focussed on using a fuel additive that acts as an ignition promoter or inhibitor to control the HCCI combustion on-set. Their results showed that with a small quantity of NO_2 as an additive to a natural gas fuelled HCCI engine, the combustion on-set can be effectively manipulated.

The effects of Reformer Gas (RG) blending to control ignition timing with three base fuels: n-heptane, iso-octane and natural gas were studied experimentally using a cooperative fuel research (CFR) engine by Hosseini and Checkel (2008). In their experiments a simulated RG was provided as a volumetric mixture of H_2 and CO , supplied from high pressure tanks. Their study investigated the effects of post-compression temperature and combustion chemistry on HCCI combustion on-set. The results from their study showed that for cases with iso-octane where high compression temperature forces rapid auto-ignition, the post compression temperature had a stronger influence on HCCI combustion on-set than the chemical effects of RG.

2.1.6 Exhaust Gas Recirculation (EGR)

EGR or recycling of burned gases is the most effective way to moderate the pressure rise rate and expand the HCCI operation to higher load regions. The studies done related to

EGR include both external EGR and internal EGR (residual combustion products) to achieve proper combustion phasing. External EGR is the more commonly utilized method for recycling exhaust gases. Exhaust gases are diverted in the exhaust manifold and brought back to the intake manifold to mix with the incoming air. However, external EGR control has issues, such as, slow response time and difficulties in handling transient operating conditions (Zoldak, 2005). Recently, there has been a number of studies that utilize variable valve timing to achieve negative valve overlap in order to trap residual combustion products (internal EGR) and achieve HCCI combustion with conventional compression ratios and less intake air preheating (Cairns, 2005 and Zhang, 2006).

The study done by Thring et al (1989) investigated the effects of EGR rate (between 13 to 33%) on the achievable HCCI operating range and engine-out emissions. Their study found out that the maximum load HCCI operating range for a 4-stroke engine was less than that of a 2-stroke engine under the selected conditions. The study done by Oakley et al (2001) showed that hydrocarbon fuels showed a much lower tolerance to air and EGR dilution than the alcohols.

2.1.6.1 Internal EGR using Variable Valve Timing (VVT)

Recently, a number of researchers examined internal EGR (utilizing variable valve timing to achieve negative valve overlap) in order to achieve HCCI combustion with conventional compression ratio and less intake air preheating (Caton et al., 2005, Xie et al., 2006 and Zhang et al., 2006).

A study done by Lavy et al (2000) was the first to operate in the HCCI mode over a limited load and speed range in a 4-stroke engine without the use of external charge heat or a high compression ratio. They analyzed the effects of internal EGR on HCCI combustion utilizing variable valve timing, lift and duration. Their study found that the degree of mixing between the fresh charge and exhaust gas residuals (internal EGR) had an impact on the HCCI combustion on-set.

Law et al (2001) investigated two methods of controlling the internal EGR rate. The first was the retention strategy similar to Lavy et al (2000), and the second involved the reinduction of exhaust gas from the exhaust port during the intake stroke. The engine used in their study is a 1.8L 4 cylinder gasoline engine converted for single cylinder operation with a Lotus active valve train. The amount of internal EGR used in their study varied from 36% to 59%, with the engine operating at stoichiometric air-fuel ratio. Their study showed that both methods are effective in controlling combustion timing and duration.

Similar studies comparing the effect of reinduction strategy and the retention strategy of residual gases on HCCI combustion were done by Kaahaaina and Caton (2001 and 2005). Their latest study showed that the reinduction strategy is tolerant to marginal combustion or misfire, while the retention strategy showed no ability to recover from marginal combustion on the previous cycle. However, both retention strategies in their study showed lower HC emissions.

2.1.7 Ethanol and HCCI combustion

The research and development of SI engines for ethanol fuel has been well documented and flexible fuel vehicles that can use both ethanol and gasoline pure or mixed in fractions have been commercialized in Brazil and the United States. In recent years, many researchers are looking into further application of ethanol in efficient combustion strategies such as HCCI combustion.

Christensen and Johansson (1998) investigated experimentally the effects of supercharging on HCCI combustion with a variety of fuels including ethanol. Two different compression ratios were used (17:1 and 19:1) in their study and for both the compression ratios analyzed, ethanol showed the best indicated efficiency. Oakley et al. (2001) experimented with different fuels, including ethanol (unblended) to determine the in-cylinder conditions necessary to obtain HCCI combustion in a 4-stroke engine. They found alcohols to be much more tolerant to air and recycled exhaust gas (EGR) dilution. A study done by Mack et al. (2005) investigated the HCCI combustion of diethyl ether and ethanol mixtures using carbon 14 tracing both experimentally and numerically. They showed that in HCCI combustion of a mixture of diethyl ether in ethanol, the diethyl ether is more reactive than ethanol.

A similar study analyzing the effects of trapped residual gas utilizing VVT on HCCI combustion with ethanol and gasoline as fuel was done by Xie et al. (2006) and Zhang et al (2006). In both the studies, the authors found that compared to gasoline, ethanol can realize HCCI combustion with a relatively leaner mixture and can extend the attainable

operating range to higher speeds. The study done by Xie et al. (2006) further looked into gasoline blended with alcohols (E50 and M50) and concluded that the HCCI combustion duration and the start of ignition for the blended fuel exhibit more like alcohols compared to gasoline.

Lü et al. (2006) experimentally investigated the auto-ignition and combustion characteristics of HCCI combustion for various blends of ethanol/n-heptane mixtures. Their results showed that, with the addition of ethanol in n-heptane, the indicated thermal efficiency can be increased up to 50% at large engine loads, but the thermal efficiency deteriorated at light engine load. In terms of operation stability of HCCI combustion, for a constant energy input, n-heptane showed an excellent repeatability and light cycle-to-cycle variation, while the cycle-to-cycle variation of the maximum combustion pressure and its corresponding crank angle, and ignition timing deteriorated with an increase in ethanol addition.

The study done by Kamio et al. (2007) focussed on investigating the effects of ethanol addition to a gasoline engine operating in a HCCI-SI mode. The study also analyzed the effects of Diethyl Ether (DEE) produced from ethanol using a fuel separator (since ethanol is supplied as fuel mixed with gasoline) and an on-board fuel reformer. The on-board reformation was carried out utilizing the exhaust gas heat and a solid acid catalyst. Their study showed that using fuel combinations involving DEE and gasoline or ethanol and PRF25 (Primary Reference Fuel), the HCCI combustion on-set can be varied. Furthermore, ethanol effectively suppressed knock in SI combustion.

A similar study investigating the effects of ethanol and DEE (produced from ethanol) on HCCI combustion of heptane by using a Rapid Compression Machine (RCM) under various conditions was carried out by Hashimoto (2007). The authors in this study investigated the effects of ethanol and DEE on HCCI combustion by comparing the hot ignition peak period calculated from the in-cylinder pressure rise rates. The results from their study also showed that HCCI combustion on-set can be effectively controlled by using ethanol and DEE. The hot ignition peak period for the 60% diethyl ether/40% ethanol fuel (by mass) was the same as that for heptane with an octane number 0. However, the hot ignition peak period for the 30% diethyl ether/ 70% ethanol was more extended than that of iso-octane having a octane number of 100.

2.2 In-cylinder fuel reformation

In-cylinder fuel reformation is a relatively new concept and has evolved in the recent years mainly due to the significant advancements made in the Variable Valve Timing (VVT) technology. The first study investigating the effects of in-cylinder reformation utilizing direct fuel injection coupled with the use of Negative Valve Overlap (NVO) was conducted experimentally by Urushihara et al. (2003).

Their results showed that a fraction of the total amount of fuel needed for combustion was injected during the NVO period and underwent fuel reformation (fuel converted to hydrogen-enriched gas which includes other intermediate species) by reaction with the internal EGR, resulting in an extension of the lean limit of HCCI operation without an

increase in NO_x emissions. Their study also showed the high speed combustion photographs taken during the NVO interval when either 3mm^3 of fuel or the entire fuel required for the cycle is injected for reformation. Based on the calculated lambda value and the combustion photographs, the authors concluded that the fuel reactions were not limited to reformation but proceeded to complete combustion reactions when all the fuel was injected during the NVO. The best fuel consumption for all the tested load levels (3 – 4.20 bar IMEP) in their study was achieved with a portion of fuel utilized for reformation (either 3mm^3 or 1mm^3) when compared to no reformation fuelling condition.

Additional experiments into HCCI combustion using NVO and early injections of fuel during the NVO were performed by (Koopmans 2003, Guohong 2006, Waldman 2007). In Koopmans (2003) the parametric study showed that the combustion phasing could be controlled by the amount of fuel injected during the NVO pilot fuel injection period. The results from Guohong (2006) and Waldman (2007) showed that fuel injection during the NVO period can indeed advance the Start of Combustion (SOC) when comparing the process to that of normal HCCI operation. The study (Guohong, 2006) showed that there is an optimal injection timing and fuel percent for each load during the NVO period which results in the lowest emissions and Indicated Specific Fuel Consumption (ISFC). The study showed the effects of the injection timing in NVO on the in-cylinder pressure and Heat Release Rate (HRR) of HCCI combustion. From their results it can be noticed that the combustion on-set or SOC advances with earlier injection during the NVO period. The effect of different split injection ratios during the NVO and regular HCCI cycle was also shown in results. With increase of the injected fuel mass in NVO, the SOC

was advanced. The total fuel mass per cycle was kept constant at 15 mg with NVO and HCCI injection timing held constant at -45 and 100° CA, respectively.

Similar results from (Waldman, 2007) also showed that there is an optimal injection timing and fuel percent for each load during the NVO period which results in the lowest emissions and ISFC. Their study showed that advancing the injection timing during the NVO resulted in an earlier HCCI SOC by up to 8° . Also, varying the percentage fuelling for reformation during the NVO period resulted in advancing the HCCI SOC by 10° in their experimental results.

Chapter 3 Experimental setup and engine parameters analyzed

The design and fabrication of the basic HCCI engine set-up was carried out as a M. Sc. thesis project (Zoldak, 2005). The detailed descriptions of the individual components used in the experimental set-up were provided in his thesis work. When the experimental set-up was taken over, it was in working condition and additions/modifications were needed to get it ready for experimentation. The following major additions were done to the experimental set-up during the course of this research work:

- Integration of a MTS Combustion Analysis System (CAS) to the experimental set-up for acquiring the in-cylinder pressure and encoder crank angle data.
- Addition of a reformation chamber with direct injection capabilities for carrying out in-cylinder reformation.
- Inclusion of a Horiba emissions bench to the experimental set-up for emission analysis. The Horiba bench was added to the set-up during the later stages of this work and hence was used only for validation of the portable MicroGas™ 5-gas analyzer.

Only an overview of the experimental apparatus and the major additions done to the experimental set-up over the course of this work are discussed below in this section. The validation of the in-cylinder pressure sensor and engine parameters analyzed based on in-cylinder pressure measurements are also provided in this section. Furthermore, it should be also realized that most of the sensors/components in the original set-up were also replaced or re-installed over the course of this work to get the set-up ready for experimentation.

3.1 Overview

Figure 3.1a and 3.1b shows the experimental setup, which consists of a four stroke, three-cylinder compression-ignition engine (Kubota D905) converted for single cylinder HCCI operation.

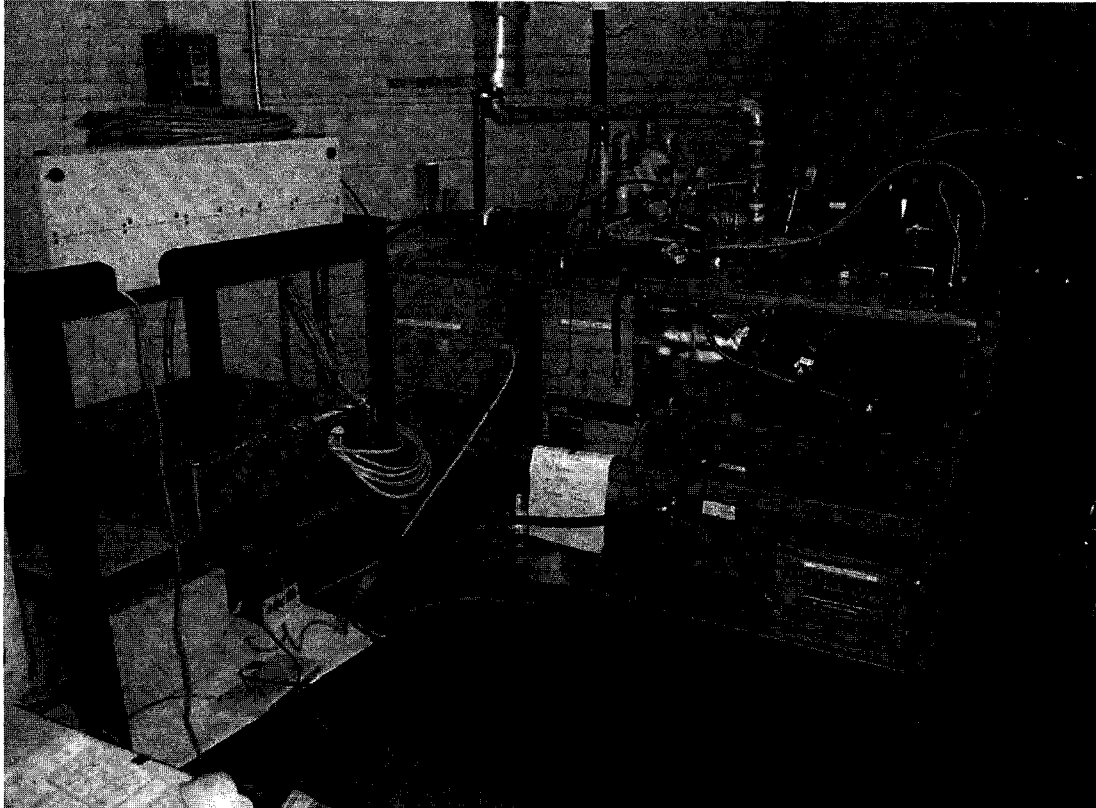


Figure 3.1a: Experimental set-up and data acquisition system.

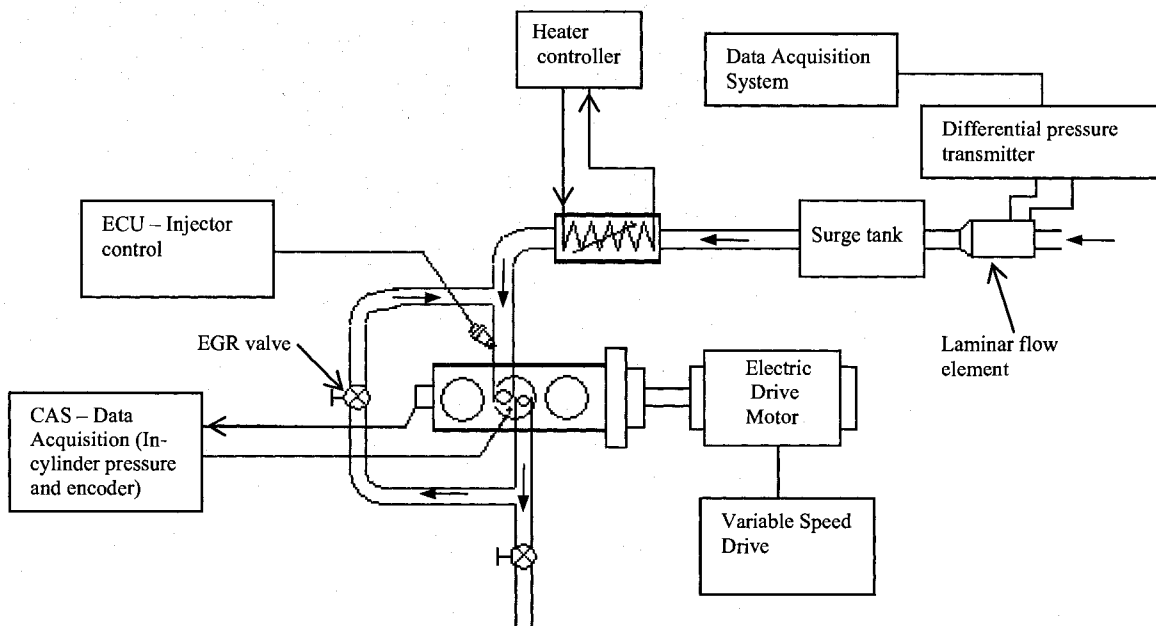


Figure 3.1b: Schematic of the experimental set-up.

The stock engine was an In-Direct Injection (IDI) type with a pre-chamber. The specifications of the stock engine are summarized in Table 3.1, while full details are available in Appendix A.

Table 3.1: Stock engine specifications

Engine Type	Vertical 4-cycle liquid cooled diesel
Number of cylinders	3
Compression ratio, r_c	20:1
Total Displacement, V_d [L (cu.in)]	0.898 (54.86)
Bore & Stroke [mm (in)]	72.0 x 73.6 (2.83 x 2.90)
Cylinder bore diameter, D [cm]	7.2
Output Power Net Continuous [kW (HP)]	12.7 (17) @ 3000 rpm 15.3 (20.5) @ 3600 rpm
Minimum idling speed [RPM]	600
Dry Weight [kg (lbs)]	110 (242.5)

The engine was motored using an AC motor (Fig. 3.2) with a Variable Speed Drive (VSD). The VSD system was used to maintain the engine speed at a desired RPM (by varying the frequency supplied by the VSD to the AC motor), during both motoring and firing scenarios. The VSD had an additional resistor brake that dissipates the additional power generated by the engine.

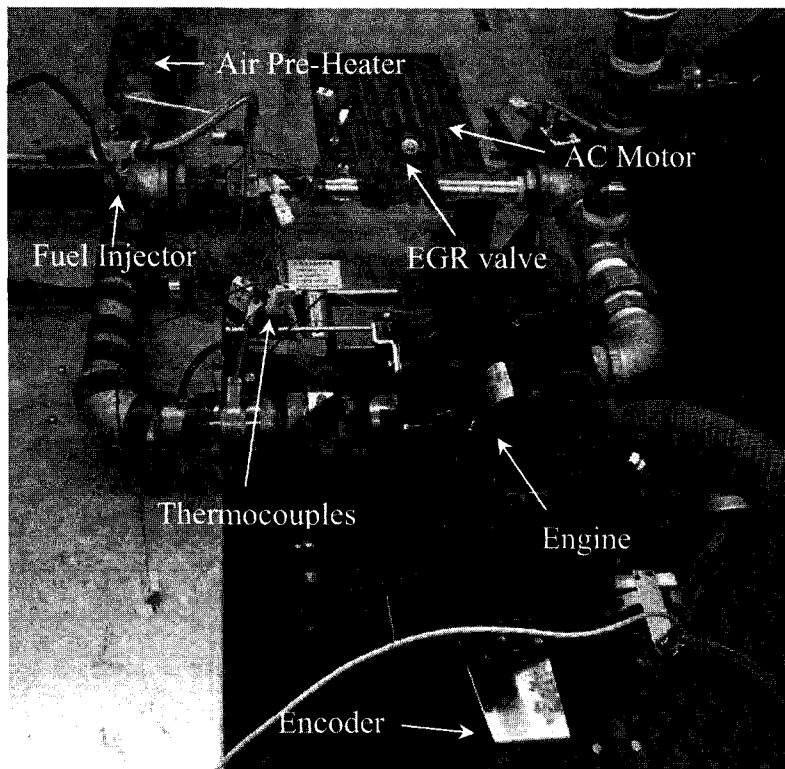


Figure 3.2: Engine and Alternating Current (AC) motor.

The converted single-cylinder engine for HCCI operation had a modified head with a secondary piston and spacer arrangement that plunges into the engine pre-chamber (Fig. 3.3). By adjusting the secondary piston plunge (spacer width), the compression ratio of the cylinder could be varied between 15:1 and 22:1. A Kistler piezoelectric 5mm wall-mounted transducer (6052A1) was mounted through the glow plug passage to acquire in-cylinder pressure measurements.

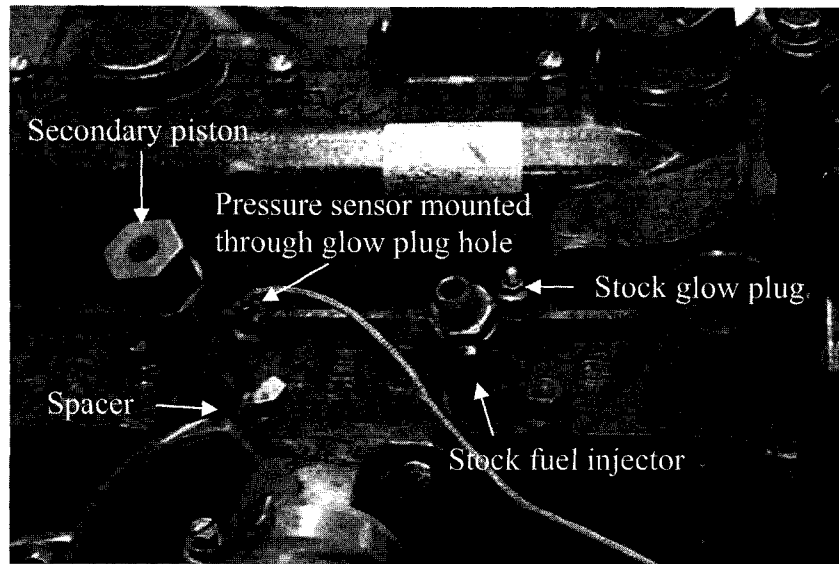


Figure 3.3: Engine head with secondary piston (and pressure sensor) and spacer arrangement.

The stock pre-chamber passage that connected the main chamber with the pre-chamber was also modified/ enlarged for the converted single cylinder. This was done to facilitate free flow of gases between the main chamber and the pre-chamber while the engine was in the HCCI mode of operation. The original stock engine configuration of the pre-chamber passage (Fig. 3.4a) and the modified pre-chamber passage (Fig. 3.4b) are shown below in Figure 3.4.

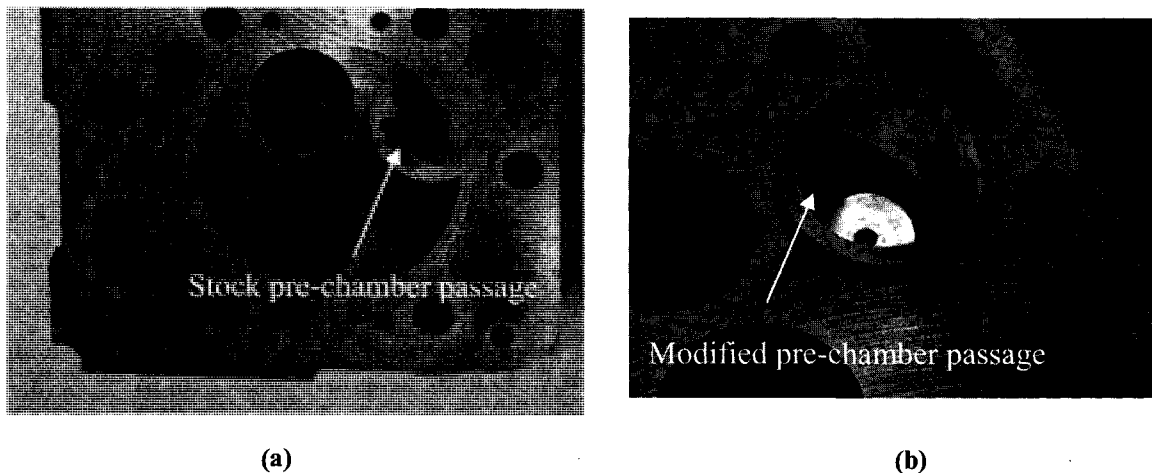


Figure 3.4: Stock engine design and modified design of the pre-chamber passage.

A Gurley optical encoder was used for crank angle measurements and to measure engine speed. The encoder outputs the following two signals:

- PPR (Pulse Per Revolution)
- CDM (Crankshaft Data Marker)

The PPR signal provided one pulse per revolution and the CDM signal output is dependant on the encoder resolution. In our case, the CDM provided one pulse per 0.1 crank angle degree totaling 3600 pulses per revolution.

The experimental set-up also consisted of an intake air pre-heater (Omega SH73343) with a power rating of 6 kW. This could provide a peak operating temperature of 700 °C for a practical flow rate up to 94.4 L/sec. The pre-heater was controlled using an Omega CNi/32 temperature controller, and used a feedback control signal from a K-Type thermocouple that was situated closer to the intake valve. The controller maintained the intake air temperature with an accuracy of ± 1.5 °C during steady state operation.

A Merriam laminar flow element with a range of up to 47.2 L/sec, in conjunction with a differential pressure transmitter was used to measure the air flow rate in the intake system of the engine. Also, a number of K-Type thermocouples were installed along the intake and exhaust pipes to record the intake and exhaust gas temperatures. The intake and exhaust system design also had the capability for Exhaust Gas Recirculation (EGR) and the percentage EGR utilized is measured using the following equation:

$$\% \text{ EGR} = \left(\frac{\dot{V}_{\text{EGR}}}{\dot{V}_i + \dot{V}_{\text{EGR}}} \right) * 100$$

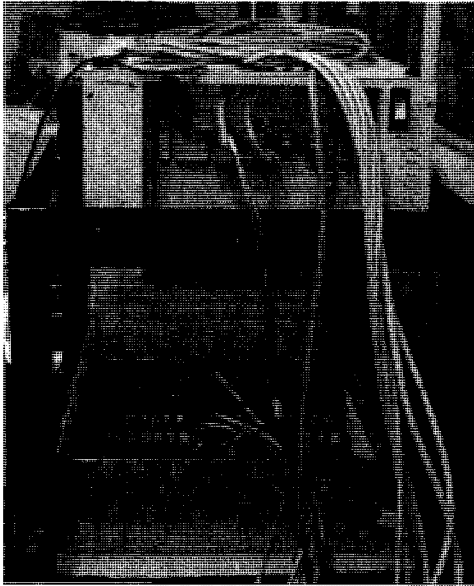
where \dot{V}_{EGR} and \dot{V}_i are the volume of EGR and fresh charge inducted per cycle. The volume flow rate, \dot{V}_{EGR} , was measured as the difference in the intake volume flow rate at zero EGR and the intake volume flow rate with percentage EGR addition for a particular operating condition.

The fuel system consisted of a fuel tank, fuel pump, filter, pressure regulator, injector, fuel rail, main and return fuel lines, and fittings. The system was designed to be compatible for operation with alcohols. The fuel injector used for the experiments was a Delphi # 2532087 with a dynamic flow rate of 2.18 g/s at 400 KPa fuel rail pressure. A programmable ECU with a programmable fuel pulse width generator was used to operate the fuel injector. The injector pulse width was chosen based on the engine speed, measured airflow rate and equivalence ratio (since the experiments were run at constant speed). The fuel injector was calibrated by measuring the amount of fuel delivered over a period of time for various injector pulse widths at different RPM settings for a constant fuel-line pressure. The engine-out emissions were evaluated using a portable MicroGas™ 5-gas analyzer that measures carbon dioxide (CO₂), carbon monoxide (CO), nitrogen oxide (NO), oxygen (O₂) and unburned hydrocarbons (UHC).

3.2 MTS combustion analysis system (CAS)

The MTS advanced drivetrain and powertrain testing Combustion Analysis System (CAS) was added to the experimental set-up in order to collect and analyze the in-cylinder pressure and the encoder data on an individual cycle and cycle averaged basis.

The CAS system (Fig. 3.5) consisted of a real-time processor and a charge amplifier for processing and analyzing the acquired pressure signal.



Real-time processor and 1 MHz digitizer



Charge amplifier for pressure sensor

Figure 3.5: Combustion Analysis System (CAS) for data acquisition.

The following are some of the main features of the MTS CAS system and its components:

3.2.1 Real-time processor (V4344):

The real-time processor present in the CAS system has the following capabilities:

- Logging of continuous cycle-based combustion data for multiple cylinders at up to thousands of engine cycles. Encoder error recovery supported.
- Logs real-time combustion data and analysis parameters to disk for post-test processing.

- Acquires “raw” unprocessed cylinder pressure data (and other signals) in local memory for post-test analysis. Over 2000 consecutive engine cycles of raw data can be stored for an 8-cylinder engine at 1-degree resolution.
- Acquires non-pressure cylinder signals such as temperature and manifold air pressure and correlates their values per engine cycle to the combustion data.
- Supports up to three different sampling rates at different parts of the engine cycle, allowing for more efficient storage of data.
- Performs real-time calculations of combustion parameters such as IMEP, peak pressure, peak pressure location, etc.
- Connects to a laptop PC via Ethernet for data logging and post processing of data.

3.2.2 1MHz digitizer:

The CAS system also has a 1MHz digitizer that has the following capabilities:

- Digitizes crank angle based cylinder pressure signals (maximum 8 channels) and has another eight channels for analog signals.
- Programmable input gains (± 10 , 5, 2 and 1).
- 12-bit 1Msample/sec/channel conversion rate.

3.2.3 Charge amplifier:

The charge amplifier is part of the CAS system sub-components and provides the following features:

- Amplifies and conditions raw cylinder pressure signals.
- Auto-tracking with programmable signal off-set and drift compensation.
- Module uses proprietary circuits to self-calibrate each signal.

3.2.4 CAS software:

The CAS system also includes proprietary CAS software that is utilized for the following functions:

- Configure experimental trials specific to the engine type used and specify performance parameters that are acquired.
- Real-time display of the calculated values (such as IMEP, IMEP Misfires, PMEP, NMEP, Peak Pressure, Peak Pressure Location, Peak Rise Rate, Peak Rise Rate Location, Polytropic Coefficients of Expansion and Compression) on a cycle-to-cycle basis.
- Logging and storage of the acquired data.
- Signal pegging
- Top Dead Center (TDC) find

3.2.4.1 Signal pegging:

The Piezoelectric transducer used for the in-cylinder pressure measurement was a differential pressure transducer and does not provide the absolute pressure measurements. Hence, a reference signal(s) is required to obtain the absolute pressure values. CAS provides options to peg these signals to an absolute reference. In the case of in-cylinder pressure transducers, MAP (Manifold Absolute Pressure) or Exhaust manifold pressures

are commonly used as references. In our case, the reference value is taken from the MAP sensor added to the intake manifold. To use this technique, the reference needs to be applied at some known point in the engine cycle where it closely represents cylinder pressure. In a typical application, when the crankshaft has reached Bottom Dead Center (BDC) and the intake valve remains open, the pressure in the cylinder and that in the intake are considered nearly equal. The MAP signal is sampled between -190° CA (BTDC) and -170° CA (BTDC) and the average value calculated from it is applied to the cylinder pressure signal at -180° degrees.

3.2.4.2 Top dead center (TDC) find:

This function in the CAS software allows us to find the difference in $^{\circ}$ CA between the location of the Pulse per Revolution (PPR) signal and the TDC of cylinder. The method uses an interpolation technique to compute TDC. After computing the average waveform, the CAS uses linear interpolation to find amplitudes on the right side of the curve equal to amplitudes on the left side of the curve. The average of all crankshaft intervals divided by two is the resultant TDC. The method assumes that peak pressure during motoring occurs at TDC.

3.3 Reformation chamber with direct injection capabilities

The reformation strategy used in the experimental approach is the proposed in-cylinder reformation method (discussed earlier in Chapter 1) that utilizes a dedicated chamber with direct injection capabilities for carrying-out fuel reformation.

3.3.1 Design objective:

The main objective in the design and implementation of the proposed in-cylinder reformation method is to achieve in-cylinder reformation with minimum modifications to the existing experimental set-up and minimize the cost of implementation. In order to meet this objective the following constraints were drawn:

- The in-cylinder reformation chamber with direct injection capabilities must be incorporated into an operating cylinder without making any modifications to either the existing HCCI cylinder head or the HCCI combustion chamber.
- The direct injection capability required for the fuel reformation should be accomplished with minimum additions to the existing experimental set-up.

3.3.2 Methodology:

The following methodology is adopted to meet the above constraints for the in-cylinder reformation chamber design:

- The secondary piston used for varying the compression ratio is replaced by a reformation chamber that utilizes the original fuel injector passage. This allows the compression ratio to be varied by adjusting the spacer width.
- An additional direct fuel injector (pencil type) is used for the injection of fuel into the dedicated reformation chamber. A pencil type injector is primarily chosen because of restrictions in the available space to build the reformation chamber.
- The injector fuel-injection pressure was reduced to match the stock fuel pump (mechanical) injection pressure (125 bar) which is used for the reformation

fuel injection system. This eliminates the cost and requirement for a new fuel injection system.

- A valve with linear motion is used in the reformation chamber design to trap the combustion products from each previous cycle for fuel reformation and to bring the products of reformation into the current cycle (which has a fresh charge) closer to TDC.

The stock fuel pump used for the reformation fuel injection is shown in Figure 3.6. The original pump is designed to deliver fuel to all of the three cylinders. In the present configuration, the fuel cam inside the pump was re-machined such that fuel is delivered only to one injector (firing cylinder). From Figure 3.6 it can be noted that there is a lever in the fuel pump that controls the amount of fuel delivered to the fuel injector. During the experimental trials the lever position was adjusted according to the required mass flow rate of fuel for reformation.

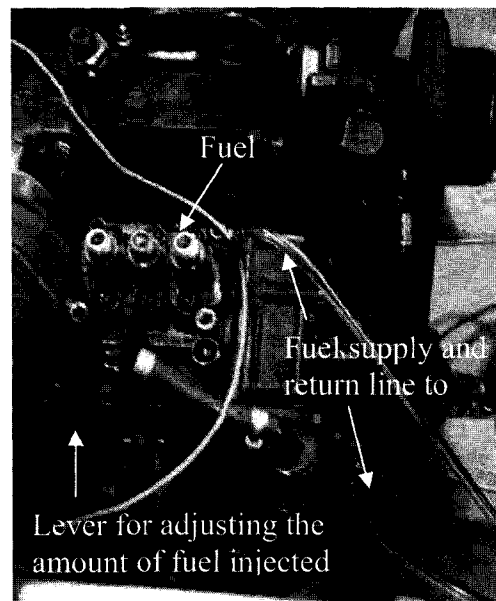


Figure 3.6: Stock fuel pump used for supplying fuel for reformation.

Figure 3.7 shows the proto-type reformation chamber developed to test the above proposed in-cylinder reformation concept in Chapter 1. It should be realized that the final implemented reformation chamber design is based on modifications made to a first proto-type that was manufactured and tested. Appendix B shows the detailed drawings of the individual components involved in the fabrication of the first proto-type and the modifications that were made to it in order to obtain the final implemented reformation chamber design.

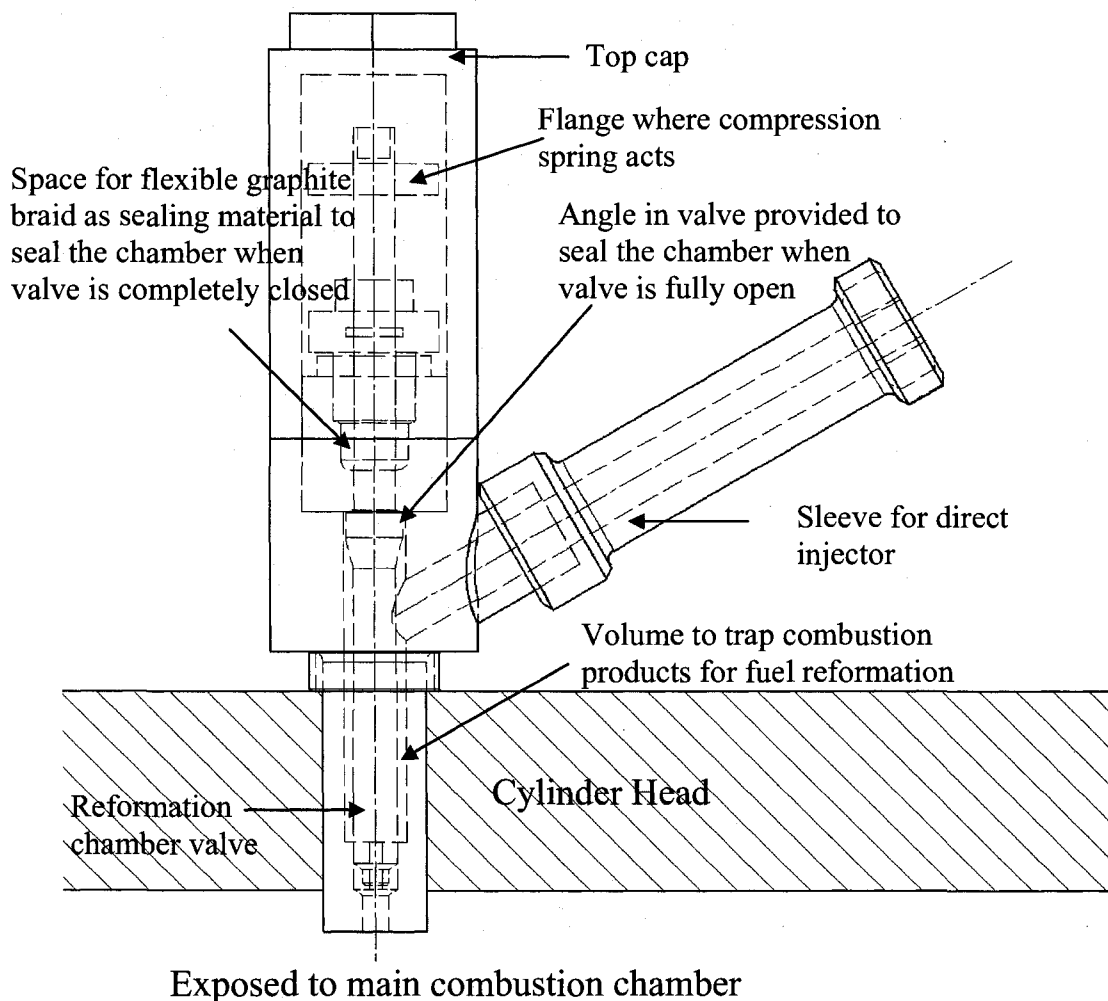


Figure 3.7: Proto-type reformation chamber design.

The pencil-type direct fuel injector in conjunction with the stock mechanical fuel pump used for fuel injection during the reformation process can also be viewed in Figure 3.8. The direct injector fuel-injection pressure was reduced to match the stock fuel pump (mechanical) injection pressure (125 bar). The valve with linear motion which is utilized to trap the combustion products and to isolate the reformation chamber from the main chamber is also shown in Fig. 3.8. The valve opens and allows mixing of the reformation products (contained in the reformation chamber) with fresh charge during the next cycle at 15° CA BTDC (compression stroke). In the current configuration a pre-compressed precision compression spring acts on the top surface of the reformation valve and the opening or closing of the valve is dictated by the in-cylinder pressure acting on the bottom surface of the valve (Fig. 3.7). Depending on the spring design parameters and the amount by which the spring is pre-compressed, the CA at which the cylinder pressure (acting on the valve) that overcomes the spring force during the compression stroke can be manipulated. The springs used for the experimental trials were precision compression springs with varying spring diameter. The specifications of the springs are provided in Appendix C. In the experimental trials, the spring diameter and the amount of pre-compression required to open the valve closer to TDC were determined by trial and error method. An ideal control for the precise opening and closing of the reformation chamber valve would be through the use of a Variable Valve Timing (VVT).

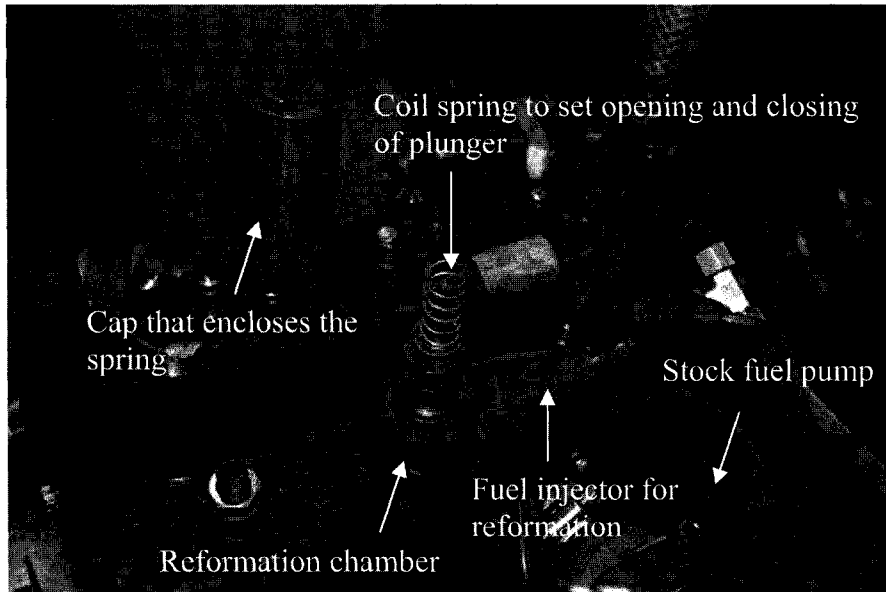
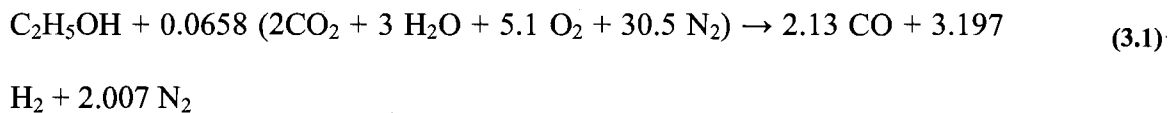


Figure 3.8: Fabricated in-cylinder fuel reformation chamber with direct fuel injector.

The volume of the fabricated reformation chamber that traps the combustion products for reformation is 5cc. This volume corresponds to 3% of the total cylinder volume at BDC (main chamber plus the reformation chamber). It should be noted that the exhaust valve opens at 125° ATDC during the expansion stroke. Hence, care must be taken such that the reformation chamber valve closes before the exhaust valve opens (125° CA ATDC) in order to avoid a drop in the temperature of trapped combustion products resulting from expansion of the gases to atmospheric pressure and outflow of the combustion products from the chamber. The theoretical reformation reaction for ethanol with combustion products from previous cycle with an equivalence ratio of 0.37 is



The heat of reaction for Equation 3.1 based on the enthalpies of products and reactants is +99.07 MJ/kmol. For the experimental engine operating at an equivalence ratio of 0.37

with reformation valve closing at 80° CA ATDC, the amount of fuel that corresponds to the above theoretical reformation fuel-oxidizer equivalence ratio is 40.5% of the total fuel injected per cycle (by mass). This amount is based only on the oxygen content in the combustion products. It should be realized that the temperature of the trapped combustion products also plays a vital role in the reformation process and hence the amount of fuel that is ideal for reformation might be less than the 40.5%. Also consider the fact that ethanol has a higher latent heat of vaporization than gasoline and the amount of fuel injected for fuel reformation will have an impact on the overall temperature of the trapped combustion products. Furthermore, it should be realized that any change in the engine operating equivalence ratio will lead to either an increase or decrease in the oxygen content of the trapped combustion products. An increase in the engine operating equivalence ratio in turn will lead to a decrease in the above indicated fuel percentage that provides the theoretical reformation equivalence ratio. However, trapping the combustion products before 80° CA ATDC should increase the amount of combustion products in the reformation chamber and therefore the oxygen content (because of higher cylinder pressure). The temperature of the trapped combustion products will also increase with both early closing of the reformation valve and increase in equivalence ratio. Hence, the CA at which the reformation valve closes during the expansion stroke is important in dictating the favorable temperature of the trapped combustion products and the amount of fuel used for reformation. Other experimental studies (Guohong, 2006 and Waldman, 2007) confirm that the temperature and the oxygen content of the trapped combustion products plays an important role in attaining higher hydrogen yield during the reformation process. It should be said here that in all the experimental runs below, a

platinum wire of 0.0254 mm thickness was wrapped around a small spring and inserted in to the reformation chamber to act as a catalyst during the reformation process. The total volume occupied by the spring with platinum wire is less than 0.3 cm³ and it is present in the chamber at all times during both the reformation and no reformation fuelling runs.

Figure 3.9 shows the in-cylinder pressure and the pressure-rise rates for the engine motoring condition with various reformation chamber opening and closing conditions.

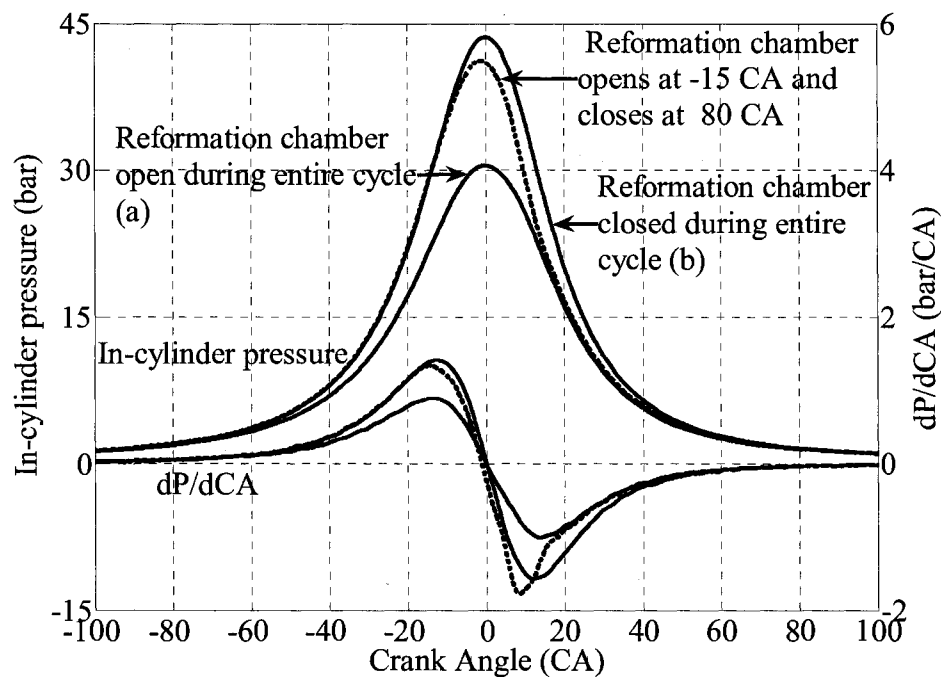


Figure 3.9: In-cylinder pressure and pressure-rise rate (dP/dCA) for various motoring conditions (T_{in} : 150 °C and T_c : 75 °C).

The two solid lines [marked as (a) and (b) in Fig. 3.9] represent the pressure traces when the reformation chamber is kept open (a) or closed (b) throughout the entire cycle. The difference in their peak pressure is due to difference in the clearance volumes between cases (a) and (b). The clearance volume is decreased by 25% for the case (b) resulting in

an increased overall compression ratio of the engine. The mechanical compression ratio of the engine with reformation chamber kept closed throughout the compression stroke is 21:1. The dotted line in Fig. 3.9 represents the pressure trace when the reformation chamber is opened at 15° BTDC and closed at 80° CA ATDC (current configuration). It should be noted that clearance volume at TDC for this motoring condition (dotted line) is equal to the case (a) (motoring condition with 30 bar peak pressure). However, manipulation of the reformation chamber opening time during the compression stroke results in temporarily varying the compression ratio of the engine during the intermediate period of the compression stroke. The intermediate change in the compression ratio results in a higher peak pressure and temperature at the end of the compression stroke (TDC) than the solid line (a). This can be viewed from Fig. 3.9 where the dotted line at first follows the pressure curve with the chamber closed (solid line b) until 15° CA BTDC and then shifts down to the pressure curve that represents chamber open condition (solid line a) after 10° CA ATDC. This results in attaining a higher TDC pressure and temperature than the regular engine compression, an inherent advantage of the proposed reformation methodology. Simply by varying the reformation chamber opening time during the compression stroke, the Start of Combustion (SOC) can be altered for a particular intake charge and coolant temperature. This is tested later from our experimental results in Chapter 7.1.

3.4 Horiba emissions bench

A Horiba emissions bench (Figure 3.10) was added to the experimental set-up during the later stages of this work. The emissions bench was donated by the DaimlerChrysler

Automotive Research and Development Centre (ARDC) and is a complete set-up with capabilities for conditioning the exhaust gas before being analyzed by five individual gas analyzers. Figure 3.10 shows the Horiba emissions bench with calibration gases for the individual analyzers present in it. The bench utilizes solenoid valves and pumps for directing the gases (zero, span, sample) to the various analyzers. The exhaust gas analyzed by the emissions bench is on a dry basis and the measured gases are: CO, CO₂, THC, NO_x and O₂. The CO and CO₂ gases were analyzed by two Non-Dispersive Infrared Analyzers which provides continuous determination of the CO and CO₂ gas concentrations in the exhaust stream. The THC is measured by the Horiba bench using a Hydrocarbon Analyzer that utilizes the principle of Flame Ionization Detection (FID). The Oxygen content in the exhaust sample is measured using a Magneto-parametric Analyzer that works based on the paramagnetism of the oxygen. The Oxides of Nitrogen (NO_x) in the exhaust sample is analyzed using a Chemiluminescent Analyzer. The NO_x analyzer was not in operation when the emissions bench was donated and requires some components from manufacturer. The measured data from the Horiba bench is monitored and acquired from the individual analyzer using a data acquisition card and a LabVIEW program running through a laptop.

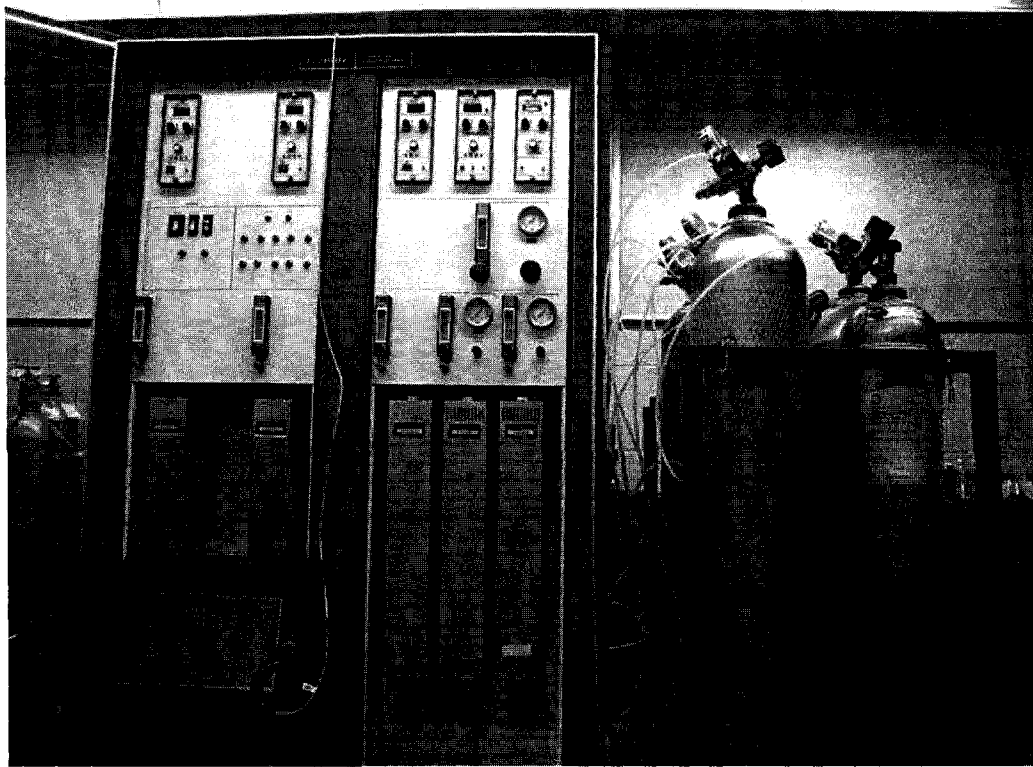


Figure 3.10: Horiba emissions bench with calibration gases for analyzing engine-out emissions.

Other modifications made to the experimental set-up are detailed in Appendix D.

3.5 In-cylinder pressure sensor - validation

The pressure measurements from the in-cylinder pressure transducer used in the experimental trials were verified with two other spark plug mounted Kistler transducers. The spark plug mounted transducers were mounted using an adaptor through the glow plug passage. At that time, the wall-mounted in-cylinder pressure sensor (used in this study) was located in the secondary piston. This allowed us to operate the wall-mounted in-cylinder sensor and the spark plug mounted sensor simultaneously. Figure 3.11 show the comparison between the wall-mounted pressure sensor with the two other spark mounted transducers. From Figure 3.11 it can be noted that the pressure signals do not

vary significantly during the compression and expansion stroke. However, there is about 2.5 bar difference in the peak pressure attained between the three sensors tested. The wall-mounted sensor showed the highest peak pressure value of 43 bar. The lowest peak pressure value obtained (40.5 bar) was with one of the tested spark-mounted sensor. The obtained results were consistent with the findings of Roth (2002), where the author compared both wall mounted and spark mounted Kistler transducers.

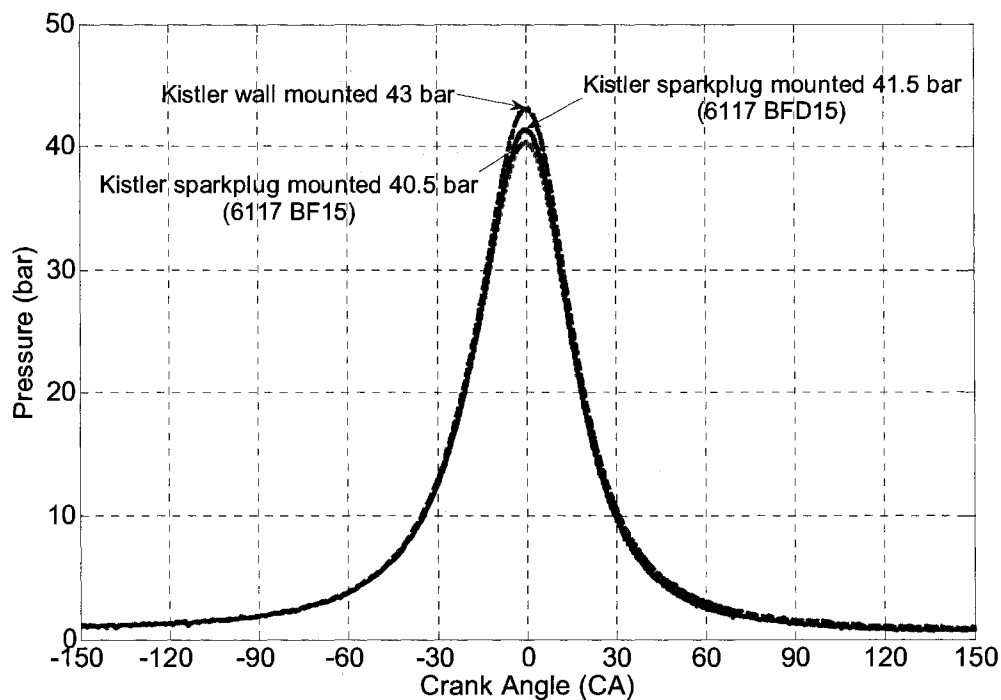


Figure 3.11: Comparison of in-cylinder pressure data (805 RPM, T_{in} : 25 °C, r_c : 18).

The results from Roth (2002) showed that the wall mounted transducer showed a higher peak pressure than the spark mounted transducers based on the test data from a V-8 CNG fuelled test engine.

3.6 Potrable microGasTM emissions analyzer validation:

The emissions measurements of the Horiba bench and portable MicroGasTM 5-gas analyzer were compared in order to validate the portable gas analyzer. The comparison was done by sending the engine-out emissions sample to both the Horiba bench and the 5-gas MicroGas analyzer simultaneously while the HCCI engine was in operation. As mentioned earlier, the Horiba bench does not have a working NO_x analyzer and hence, the NO_x analyzer was not used in the validation of the portable Microgas analyzer. Table 3.2 shows the percentage difference in the emissions results for each gas analyzed between the two analyzers.

Table 3.2: Comparison between potable MicroGasTM analyzer and Horiba bench

Description	% difference between Horiba and MicroGas TM analyzer
Phi, ϕ	3.98 %
CO	8.20 %
UHC	11.3 %
O ₂	2.52 %
CO ₂	10.8 %
NO _x	N/A

From Table 3.2 it can be noted that the difference in the equivalence ratio (calculated based on individual gas measurements) and O₂ measurements were less than 4%. However, the CO₂, CO and UHC had a higher difference, around 10% between the Horiba bench and the portable 5-gas analyzer. This is primarily due to the broader operating range for the MicrogasTM analyzer compared to that of the Horiba bench, which

can be calibrated according to the engine operating condition. However, the difference between the two analyzers remained the same for the operating range used in this study. Hence, the trends with respect to CO and UHC when comparing between different operating conditions was consistent with respect to the Horiba bench.

3.7 Engine parameters analyzed

The engine performance parameters, such as IMEP, HRR, combustion on-set and thermal efficiency were evaluated based on cycle-resolved in-cylinder measured pressure and crank angle data. The following equations were used for estimating the engine performance parameters (Heywood, 1988):

a) Indicated Mean Effective Pressure (IMEP):

The Indicated Mean Effective Pressure (IMEP) is calculated as the work done over the entire cycle divided by the cylinder displacement volume,

$$\text{IMEP} = \frac{W_{c,i}}{V_d} = \frac{\oint p dV}{V_d}$$

where V_d is the cylinder displacement volume.

b) Net Heat Release Rates (HRR):

The Heat Release Rate (HRR) is the difference between the gross heat-release rate and the heat-transfer rate to the walls. It equals the rate at which work is done on the piston plus the rate of change of sensible internal energy of the cylinder contents.

$$\frac{dQ_n}{dCA} = \frac{dQ_{ch}}{dCA} - \frac{dQ_{ht}}{dCA} = \frac{\gamma}{\gamma-1} p \frac{dV}{dCA} + \frac{1}{\gamma-1} V \frac{dp}{dCA}$$

c) On-Set of Combustion:

The on-set of combustion was estimated based on the Total Heat Release (HR) calculated from the HRR. The crank angle corresponding to the 10% HR (Start of Combustion or SOC) value is taken as the combustion on-set.

$$10\% \text{ HR} = 0.10 * \int_{-180}^{180} \frac{dQ_n}{dCA} dCA$$

d) Thermal Efficiency:

The thermal efficiency is calculated as the ratio of indicated work produced per cycle to the amount of fuel energy supplied per cycle that can be released during the combustion process.

$$\eta_{th} = \frac{W_{c,i}}{m_f Q_{HV}}$$

where m_f is the mass of fuel inducted per cycle and Q_{HV} is the heating value of the fuel.

e) Coefficient of Variation of IMEP (COV_{IMEP}):

The Coefficient of Variation of IMEP (COV_{IMEP}) is the ratio of standard deviation to the mean of the IMEP values calculated for 125 individual cycles.

$$COV_{IMEP} = \frac{StdDev_{IMEP}}{Mean_{IMEP}} * 100$$

where the StdDev (Standard Deviation) and the mean IMEP values are calculated as follows:

$$Mean_{IMEP} = \frac{1}{N} \sum_{i=1}^{i=N} IMEP_i$$

$$\text{StdDev}_{IMEP} = \sqrt{\frac{1}{N} \sum_{i=1}^{i=N} (IMEP_i - \text{Mean}_{IMEP})^2}$$

N is the total number of individual cycles analyzed (125 cycles).

f) Maximum Pressure-rise rate:

The calculation of the maximum rise rate value is based on a calculation of the first derivative of the pressure curve with respect to crank angle. The formula for the derivative is a 5-point data fit (CAS Software, 2005), as follows:

$$\frac{dP_i}{dCA} = \frac{1}{12 * \Delta CA} * (P_{i-2} - 8 * P_{i-1} + 8 * P_{i+1} - P_{i+2})$$

The maximum pressure rise rate value is the most-positive data value of the derivative in the crank angle interval. In the case in which multiple points have the same maximum rise rate, the first data point is reported as the maximum rise rate location.

The results and discussion of the above parameters analyzed for the experimental HCCI engine under various operating conditions with and without EGR for the different fuels (ethanol, iso-octane and its blend) tested were provided in the next Chapters.

3.8 Repeatability of data

The repeatability of the data presented in this thesis was verified by repeating the experiment at a selected operating point at a different time (after days or weeks) during the course of this experimentation. The repeated points were HCCI firing runs and performed with same initial conditions as the selected operating point. A summary of statistical data based on twelve sets of repeated data is shown in Table

3.3, with full details of each operating condition provided in Appendix E. The summary in Table 3.3 shows the maximum difference obtained for each parameter observed in the repeatability tests.

Table 3.3: Statistical data from HCCI comparison runs

Recorded Data	Maximum % difference between the repeated runs (based on 12 different operating conditions repeated after couple of days/weeks of the original run)
Engine speed [rpm]	0.50
Exhaust Air/Fuel Ratio[-]	2.15
IMEP [bar]	4.65
Peak Pressure [bar]	4.76
Intake charge temperature [°C]	1.97
Coolant temperature [°C]	1.47

From Table 3.3 it can be noted that the maximum percentage difference between the runs repeated after a couple of days/weeks after the original run is less than 5 %. This shows that the error margin for comparison runs reported in this thesis for similar operating conditions is less than 5 %.

Chapter 4 Experimental results: Effect of intake charge temperature and fuel chemistry

In this chapter the effects of intake charge temperature and the fuel chemistry on the HCCI combustion on-set were analyzed. The study was carried-out by maintaining a constant compression ratio, and a constant equivalence ratio with no EGR addition. The parameters that were varied are the intake charge temperatures and the fuel composition. The details of the test conditions are provided below in the next section.

4.1 Test conditions

The fuels used in this study are 100% ethanol, 100% iso-octane and 50% ethanol & 50% iso-octane blend by volume. The engine specifications and conditions used in the experimental study are as follows:

Table 4.1: Engine specifications and test conditions

Compression ratio, r_c	20:1
Bore & Stroke [mm]	72.0 x 73.6
Equivalence ratio, ϕ	0.3
Engine Speed [RPM]	805, 1035, 1275 & 1520
Coolant Temperature, T_c [°C]	75 (\pm 2)
Intake charge temperature, T_i [°C]	120 – 150 (\pm 1.5)

The results discussed below are averaged data based on samples of 125 consecutive cycles. The HCCI combustion is initiated by maintaining a high compression ratio ($r_c = 20$) and adjusting the intake charge temperature from 120 to 150 °C. The volumetric

efficiency of the engine was between 80% and 72% for the range of engine speed used in this section. The volumetric efficiency decreases with increasing engine speed and intake air temperature. The relatively low level of volumetric efficiency was due to the lengthening of the stock intake pipes to accommodate the air pre-heater, airflow sensors, and EGR section. The discussion of the results includes the engine performance in terms of the HRR, IMEP, and Coefficient of Variation of IMEP (COV_{IMEP}), thermal efficiency, and regulated engine-out emissions. The codes written in Matlab/Cantera for calculating the HRR based on in-cylinder pressure measurements and cylinder volume changes (dV/dCA) are provided in Appendix F.

4.2 Results and discussion

4.2.1 In-cylinder pressure and HRR:

Figures 4.1 through 4.12 depict the in-cylinder pressure and the rate of heat release for the three fuels tested over different intake charge temperatures and engine speed. The intake charge temperature for ethanol is varied between 120 °C and 140 °C. For iso-octane and ethanol/iso-octane blend, the charge temperature is varied between 130 °C and 150 °C.

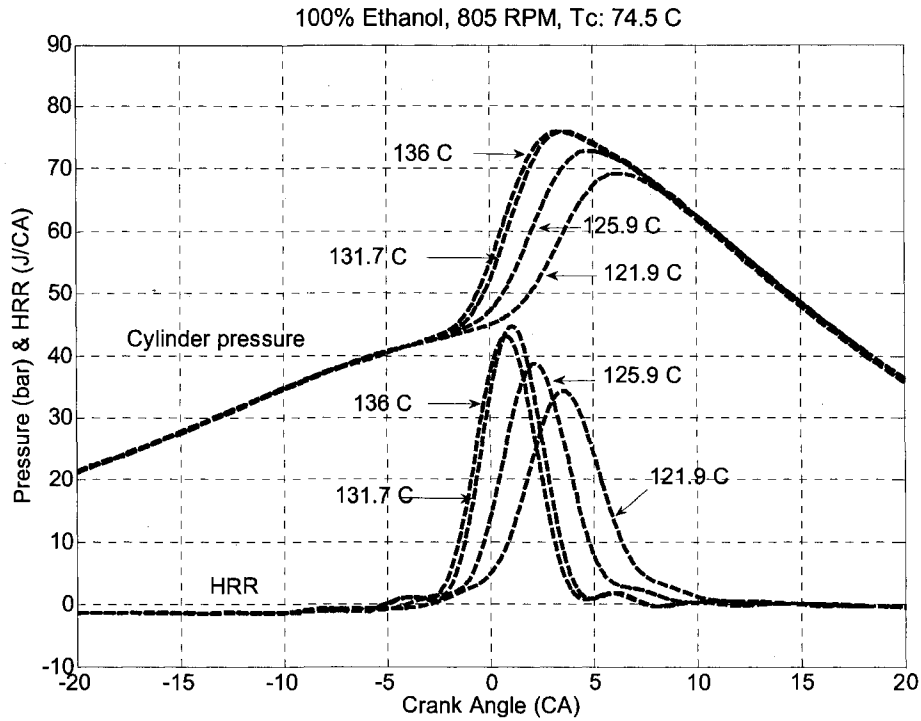


Figure 4.1: Cylinder pressure and rate of heat release at different intake charge temperatures (805 RPM, 100% Ethanol).

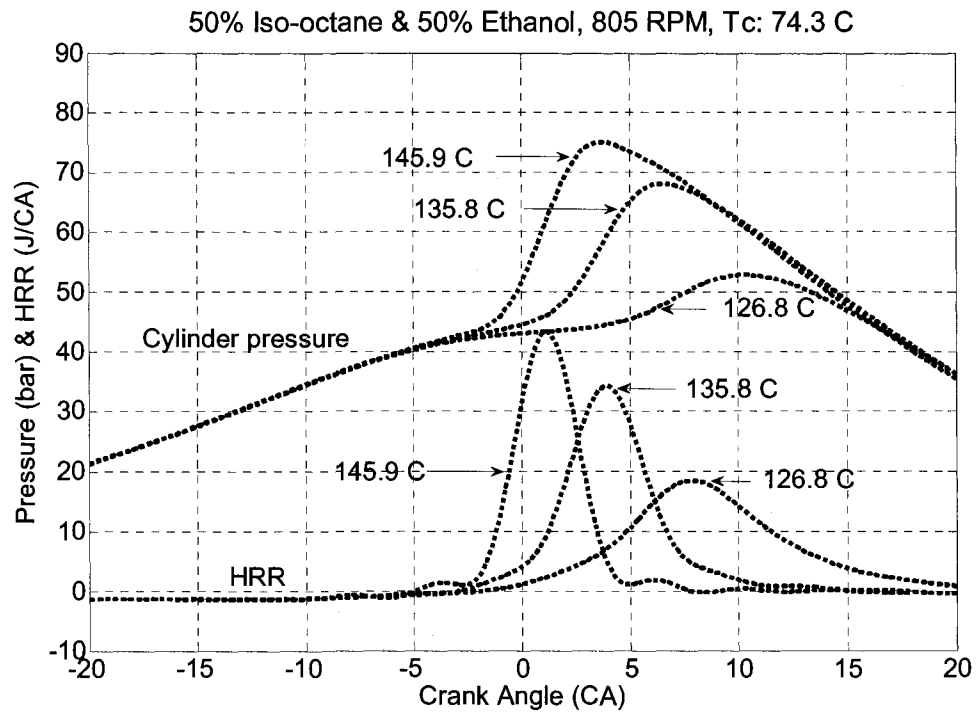


Figure 4.2: Cylinder pressure and rate of heat release at different intake charge temperatures (805 RPM, 50% Iso-octane & 50% Ethanol).

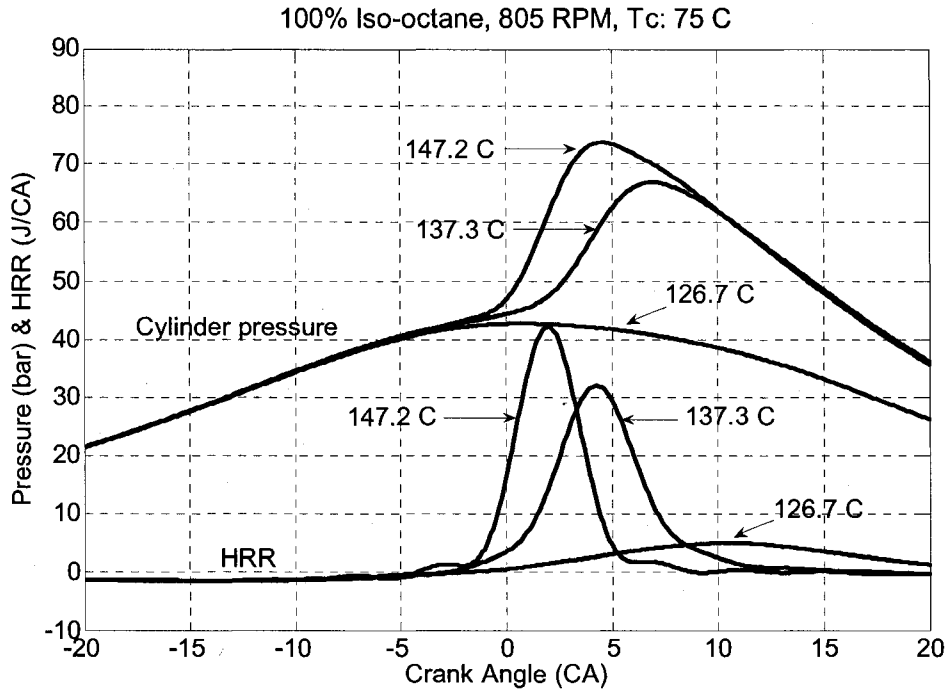


Figure 4.3: Cylinder pressure and rate of heat release at different intake charge temperatures (805 RPM, 100% Iso-octane).

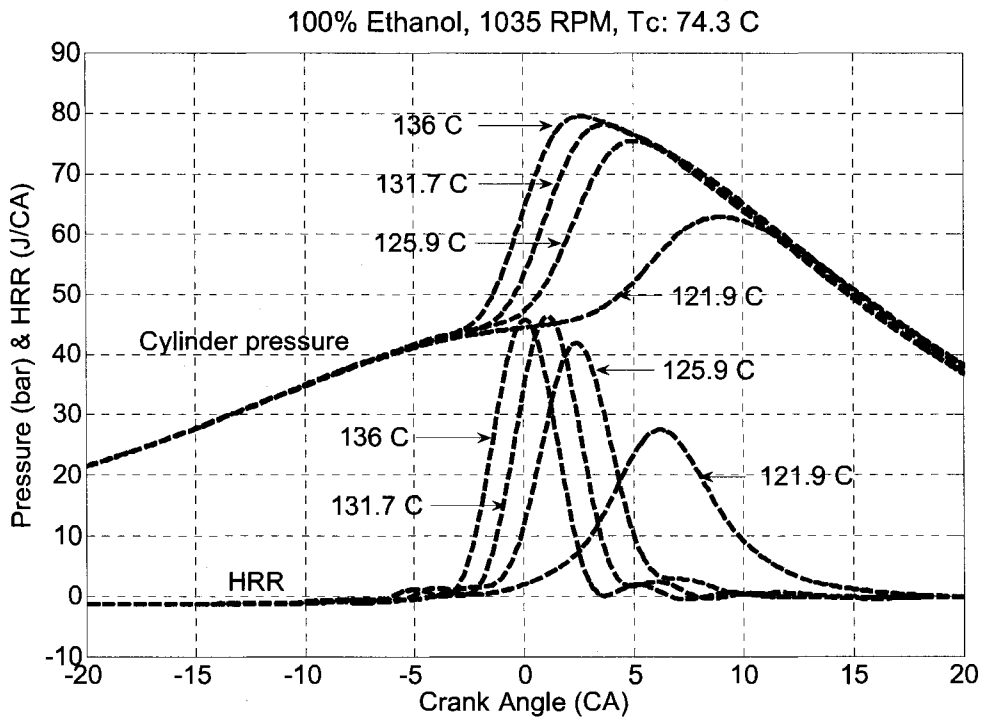


Figure 4.4: Cylinder pressure and rate of heat release at different intake charge temperatures (1035 RPM, 100% Ethanol).

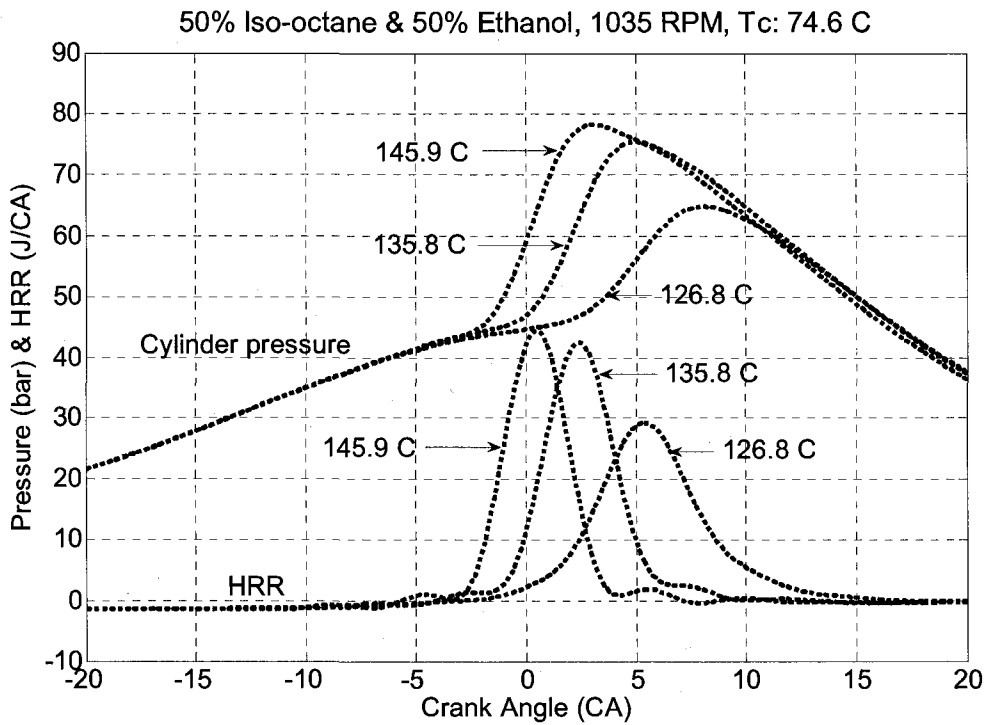


Figure 4.5: Cylinder pressure and rate of heat release at different intake charge temperatures (1035 RPM, 50% Iso-octane & 50% Ethanol).

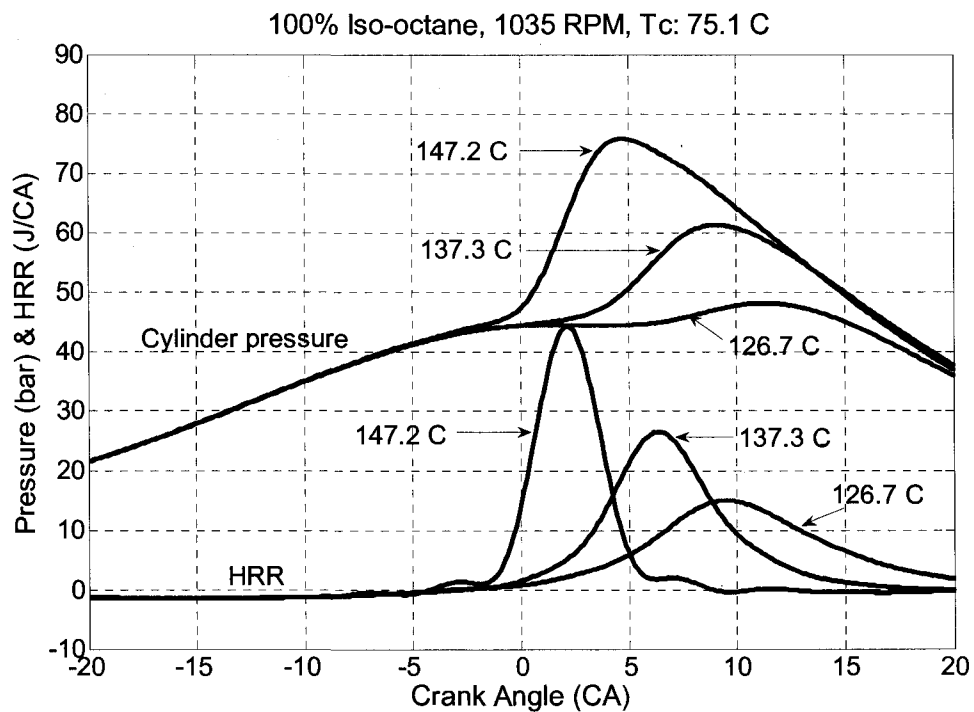


Figure 4.6: Cylinder pressure and rate of heat release at different intake charge temperatures (1035 RPM, 100% Iso-octane).

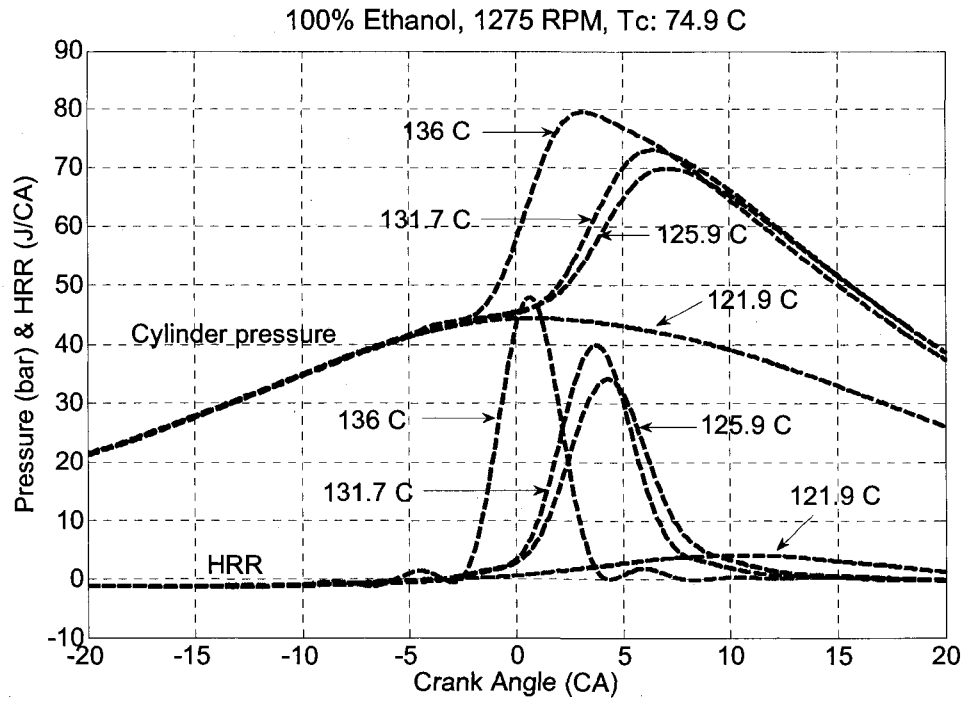


Figure 4.7: Cylinder pressure and rate of heat release at different intake charge temperatures (1275 RPM, 100% Ethanol).

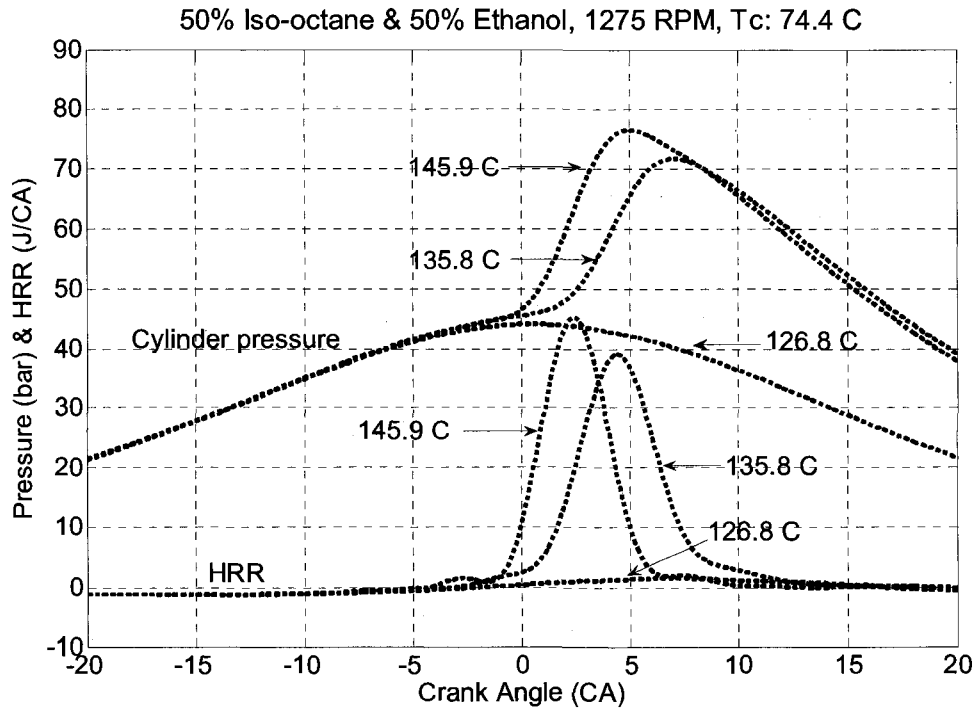


Figure 4.8: Cylinder pressure and rate of heat release at different intake charge temperatures (1275 RPM, 50% Iso-octane & 50% Ethanol).

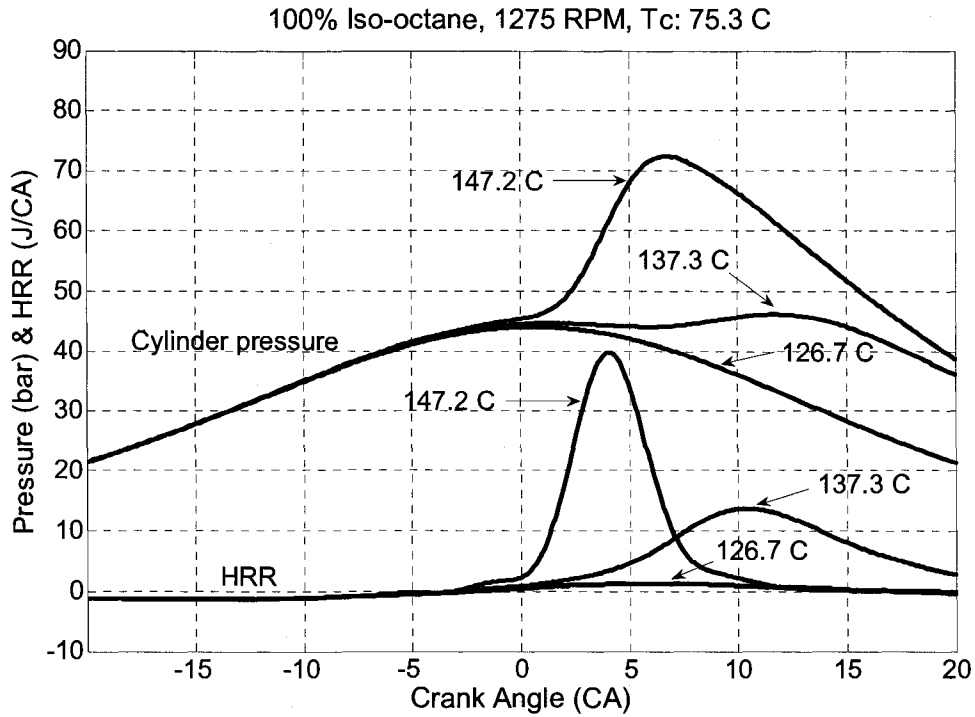


Figure 4.9: Cylinder pressure and rate of heat release at different intake charge temperatures (1275 RPM, 100% Iso-octane).

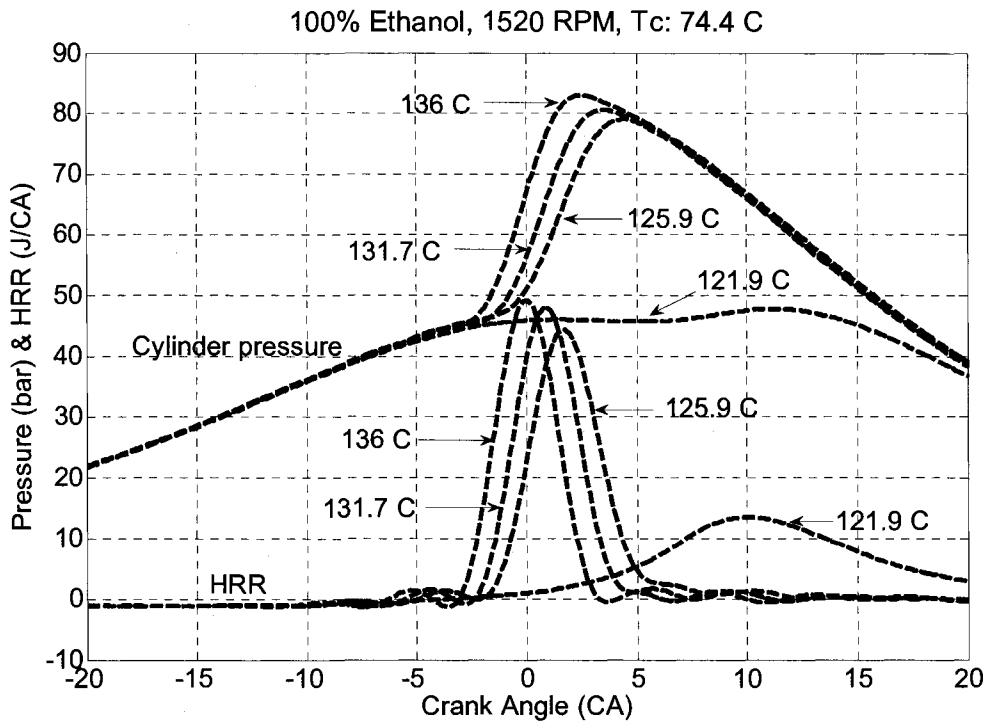


Figure 4.10: Cylinder pressure and rate of heat release at different intake charge temperatures (1520 RPM, 100% Ethanol).

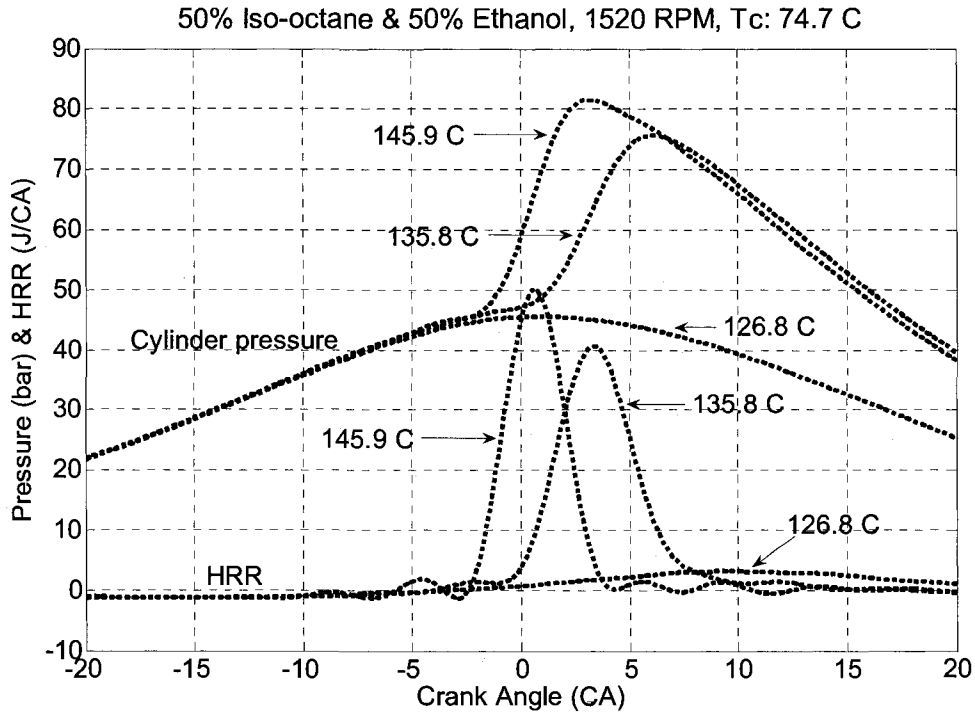


Figure 4.11: Cylinder pressure and rate of heat release at different intake charge temperatures (1520 RPM, 50% Iso-octane and 50% Ethanol).

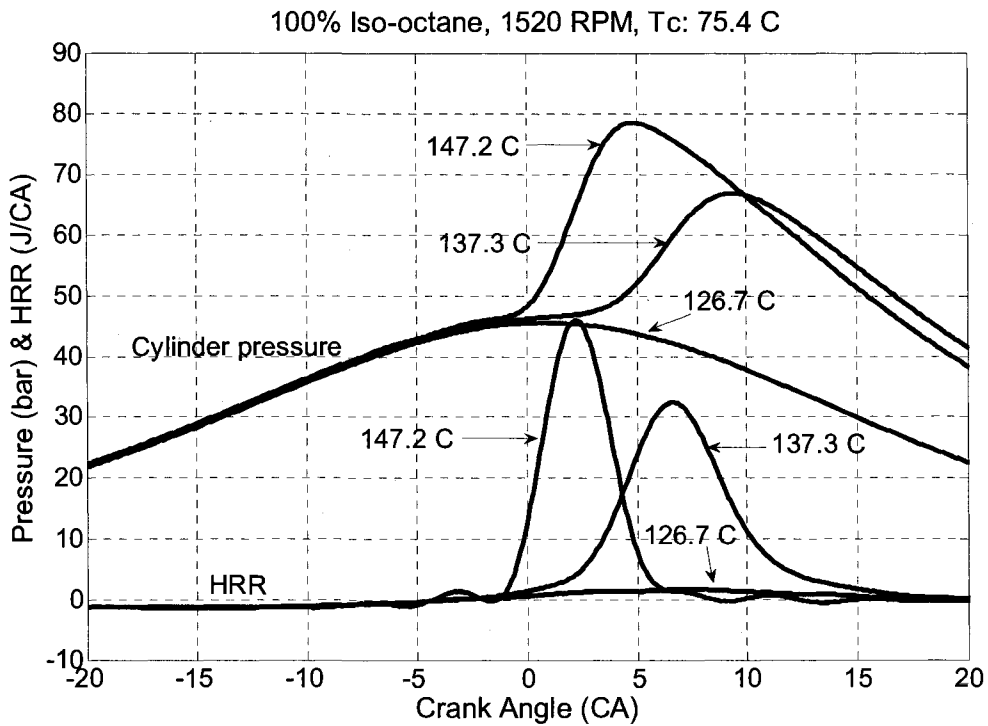


Figure 4.12: Cylinder pressure and rate of heat release at different intake charge temperatures (1520 RPM, 100% Iso-octane).

Data in Figures 4.1 through 4.12 indicate that for a particular fuel and engine speed, the intake charge temperature has a strong impact on the on-set of combustion. For example, in Figure 4.1 the on-set of combustion (the CA corresponding to 10% of HRR) advances from 0.8° CA BTDC to 1.3° CA BTDC when the intake charge is increased from 121.9°C to 136.0°C . This influence has been reported by several other researchers earlier, (Ayoma 1996, Christensen 1999, Martinez-Frias 2000, Marriot 2002, Tanaka 2003, Xie 2006). Also, for a particular engine speed and intake charge temperature, it can be noted that ethanol advances the on-set of combustion when compared with iso-octane. For example, the on-set of combustion in the case of pure ethanol and pure iso-octane at 1035 RPM and 136°C are 5.6 and 2.9° CA BTDC respectively (Figures 4.4 and 4.6). This trend is confirmed when fuelling with the iso-octane/ethanol blend (Figure 4.5) where the on-set of combustion at 1035 RPM and 136°C is 3.8° CA BTDC, which lies between the values of pure ethanol and pure iso-octane. Similar results have been reported in Christensen (1998) and Xie (2006). The advancement in on-set of combustion suggests that alcohols might be advantageous fuels for HCCI combustion. Concurrently, it should also be noted that ethanol has a higher enthalpy of vaporization (0.84 MJ/kg) compared to that of iso-octane (0.351 MJ/kg).

There is an interesting trend that separates the lower speed conditions (805 and 1035) from the higher speed conditions (1275 and 1520) when the intake charge temperatures are low. From the rate of heat release it can be noted that for the lower speeds (805 and 1035) the ethanol and the ethanol/iso-octane blend show consistent ignition without misfire. Whereas, for the same fuels and operating conditions, the higher speeds (1275

and 1520) show either total or partial misfire. This behavior is also observed for pure iso-octane with total misfire at higher speeds while at lower speeds there is either partial or consistent ignition. This particular effect of either partial or total misfire at higher speeds for the lower intake charge temperature conditions can be linked to two factors:

- heat losses due to heat transfer, and
- effect of residence time on fuel chemistry.

The engine used in this study is an In-Direct Injection (IDI) type and the surface to volume ratio for the cylinder is high and this contributes to increased heat transfer losses. In addition, at higher engine speeds, the in-cylinder gas velocity increases and hence, the convective heat transfer rate. The overall increase in heat transfer rate can reduce the overall temperature of the charge at the end of compression stroke leading to misfire at higher speeds. However, it should also be noted that the residence time of the charge in the cylinder decreases with increasing engine speed. The shorter residence time will decrease the overall energy transferred as heat during the compression stroke and act to attain a higher charge temperature at the end of the compression stroke. Later in this section, looking at the thermal efficiency, it is seen that the shorter residence time plays a more important role than the increase in in-cylinder gas velocity and contributes to lower heat transfer losses at higher speeds.

4.2.2 10% HR CA and 10-90% HR CA duration:

Figures 4.13 through 4.15 show the CA corresponding to the 10% HR (on-set of combustion) and the heat release (HR) duration in CA from 10% and 90% HR for various operating conditions. As mentioned earlier, it can be noted from Figures 4.13 through

4.15 that the increase in intake charge temperature advances the 10% HR (on-set of combustion) CA for all the fuels and RPM conditions. Furthermore, when studying the HR duration (Figures 4.13 through 4.15) it is evident that the reduction in intake charge temperature increases the duration for all the operating conditions. Another interesting trend is that the presence of iso-octane in fuel prolongs the HR duration. For instance, in Figures 14.14 and 14.15, at the 136 °C intake charge condition; for 50% ethanol/iso-octane blend the HR duration is between 4° CA and 8° CA for all the RPM conditions. Whereas, at the same 136 °C intake charge condition when fuelling with pure iso-octane (Fig. 14.15) the HR duration varies from 7 to 16° CA for all the RPM conditions.

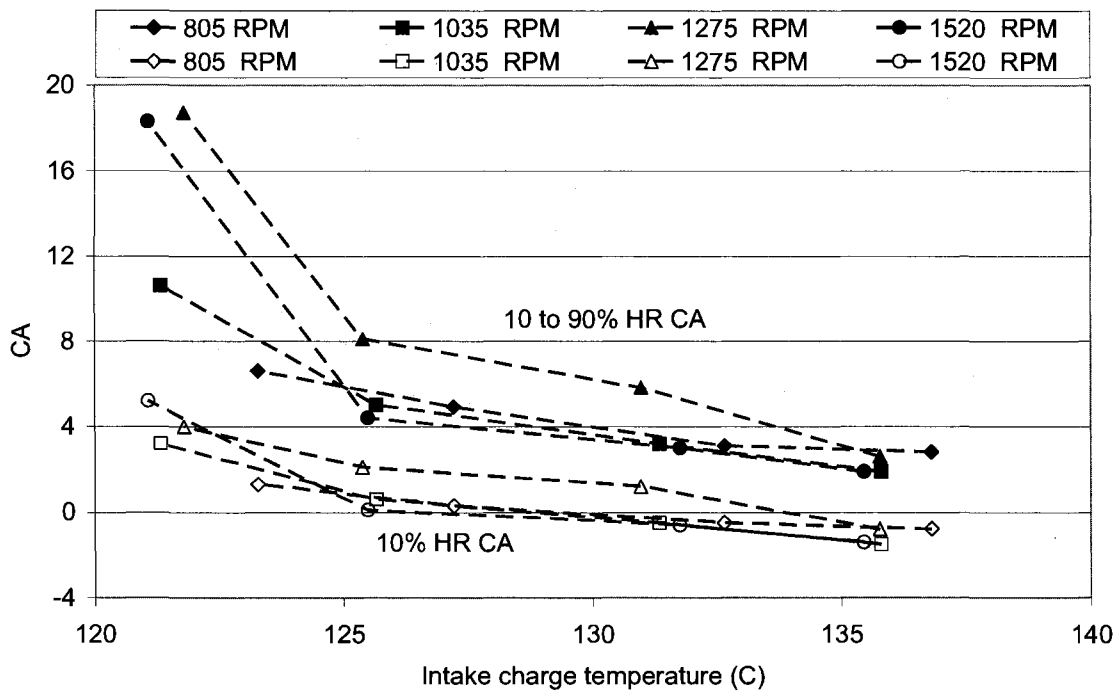


Figure 4.13: 10% Heat Release CA and CA duration for 10% to 90% Heat Release for different intake charge temperature and RPM (100% Ethanol, phi: 0.3).

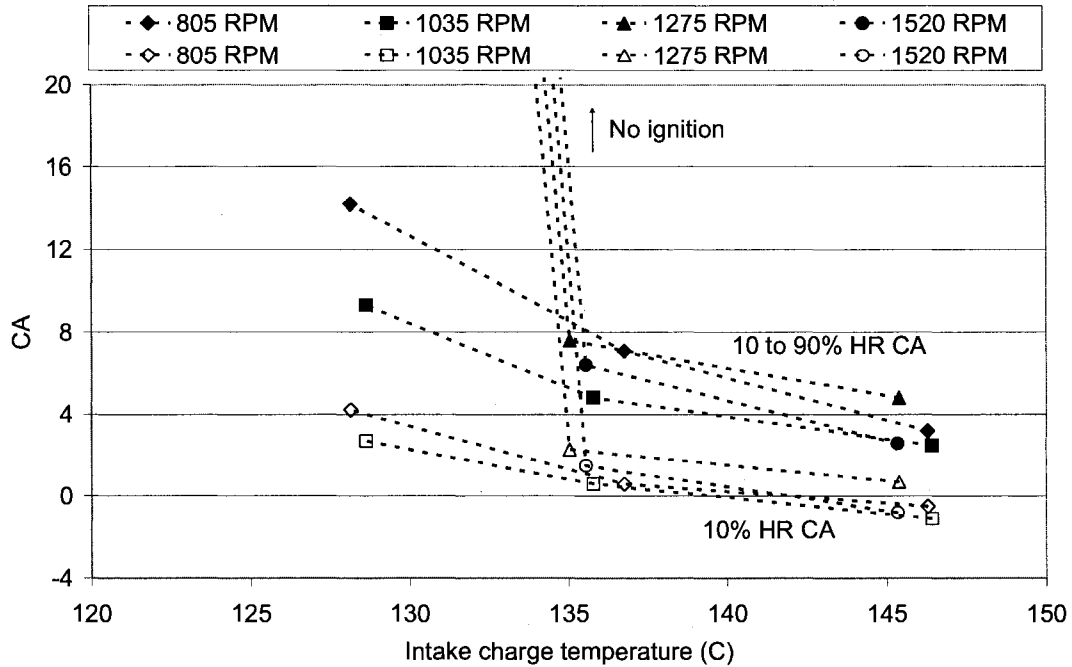


Figure 4.14: 10% Heat Release CA and CA duration for 10% to 90% Heat Release for different intake charge temperature and RPM (50% Ethanol and 50% Iso-octane, ϕ : 0.3).

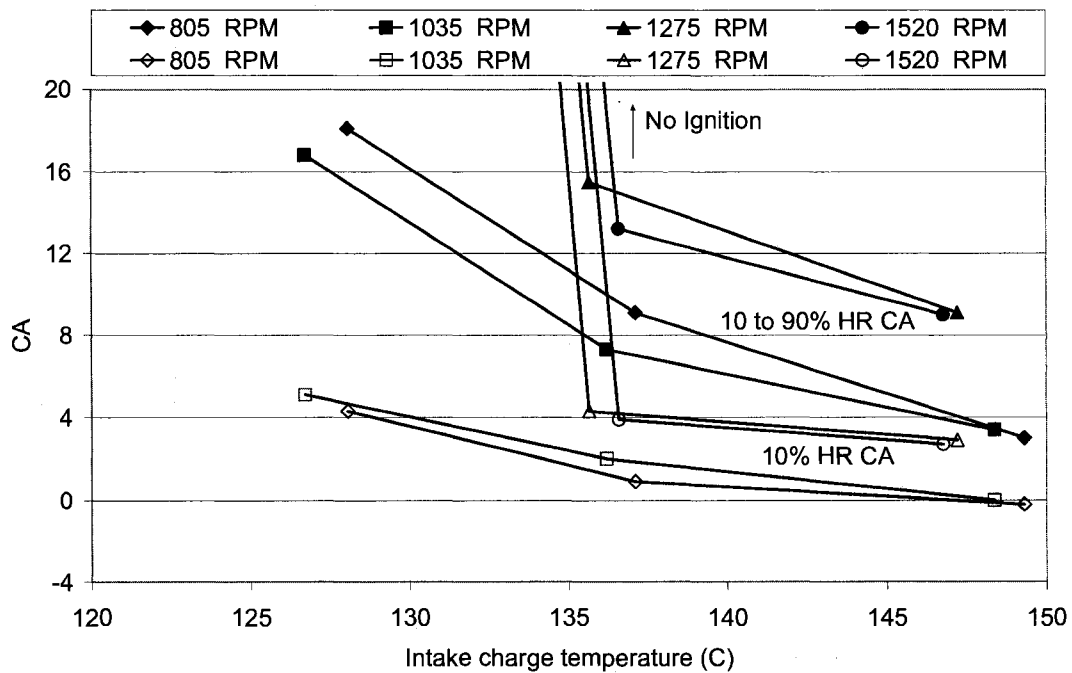


Figure 4.15: 10% Heat Release CA and CA duration for 10% to 90% Heat Release for different intake charge temperature and RPM (100% Iso-octane, ϕ : 0.3).

The effect of fuel chemistry and residence time at higher RPM conditions (Figures 4.13 through 4.15) can be recognized when comparing the 147 °C condition for the fuels tested. For ethanol (Fig. 4.13) it is clear that the 10% HR CA (combustion on-set) and the HR duration do not change significantly with change of RPM. However, from Figures 4.14 and 4.15 it can be noted that once iso-octane is added there is significant change in the CA values with respect to RPM. The combustion on-set (10% HR) is delayed and the HR duration increases for the higher RPM conditions (1275 and 1520 RPM) compared to the lower RPM conditions (805 and 1035 RPM). This shows that the reaction rates for iso-octane at these lean operation conditions are affected by the residence time during both early (10% HR) and regular combustion periods (10 to 90% HR). This interference of residence time on fuel chemistry leads to delay in the on-set of combustion and subsequent misfire at higher engine speeds especially for the lower intake charge temperatures. This effect is not as pronounced when fuelling with pure ethanol at higher engine speeds where the reaction rates during the early (10% HR) and regular combustion (10 – 90% HR) are less affected by the residence time. Further, it should be noted that due to the presence of the pre-chamber in this IDI type engine, there is trapped residual mass that acts as an ignition source for subsequent cycles once the initial firing (combustion) cycles occur. The amount of trapped residual mass is not measured here. The pre-chamber occupies 5% of the total cylinder volume at BDC.

4.2.3 IMEP and COV_{IMEP} :

Figures 4.16 through 4.19 show the IMEP and the coefficient of variation in the IMEP for the various operating conditions. The IMEP reported here are the net values which include pumping losses. From the figures it can be noted that the COV_{IMEP} has very high levels at the low initial charge temperature conditions where there is partial or complete misfire. Also, looking at pure iso-octane for different operating conditions, there is a specific charge temperature that gives the best IMEP combustion timing. This trend can be also seen clearly for the ethanol and an ethanol/iso-octane blend at higher engine speeds (Figures 4.18 and 4.19).

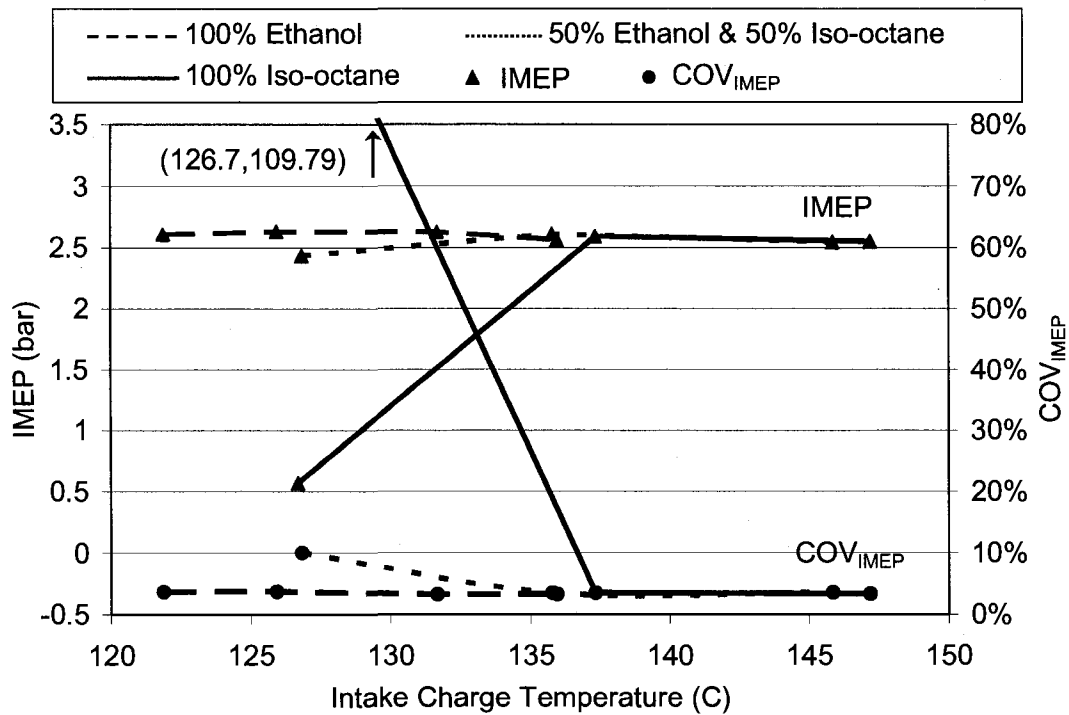


Figure 4.16: IMEP and COV_{IMEP} (805 RPM).

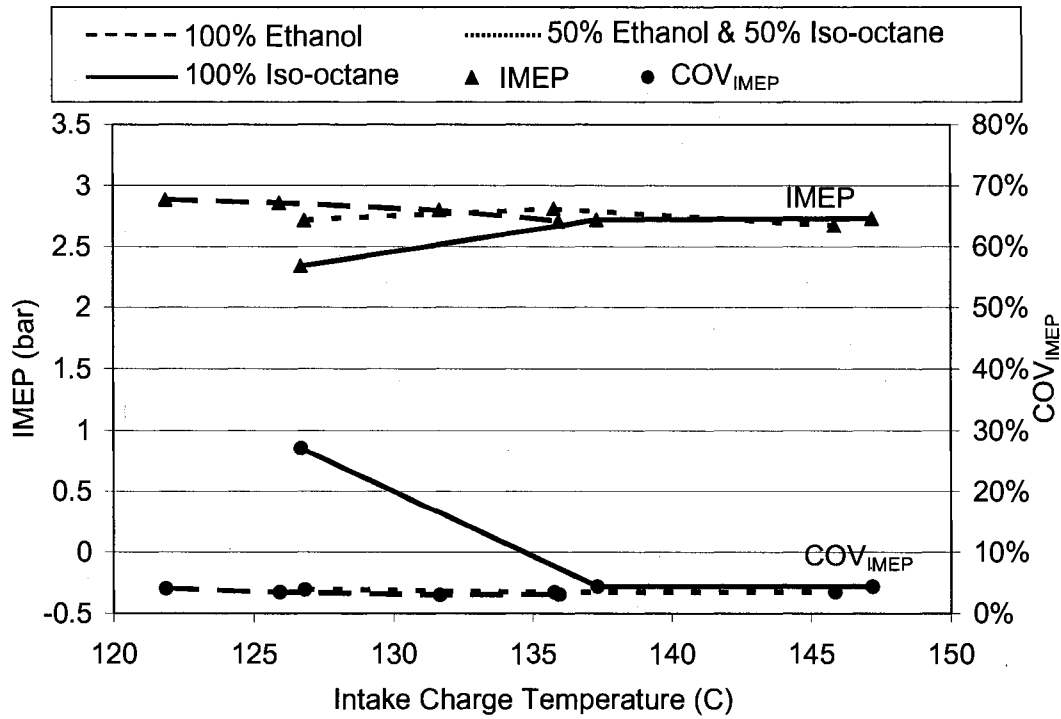


Figure 4.17: IMEP and COV_{IMEP} (1035 RPM).

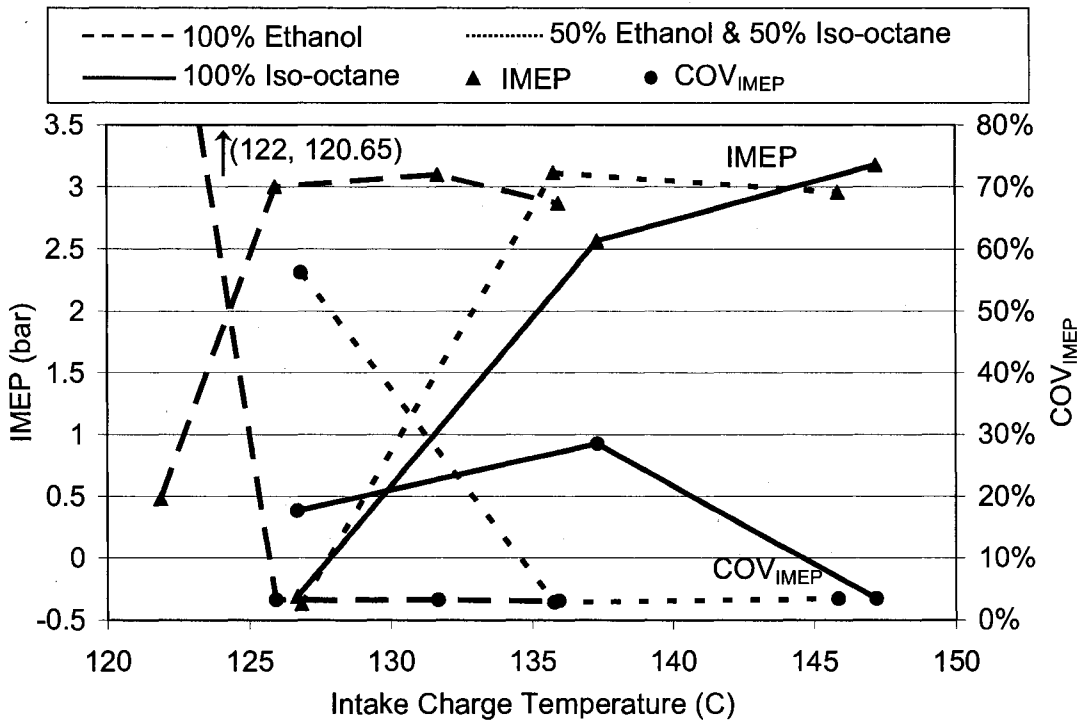


Figure 4.18: IMEP and COV_{IMEP} (1275 RPM).

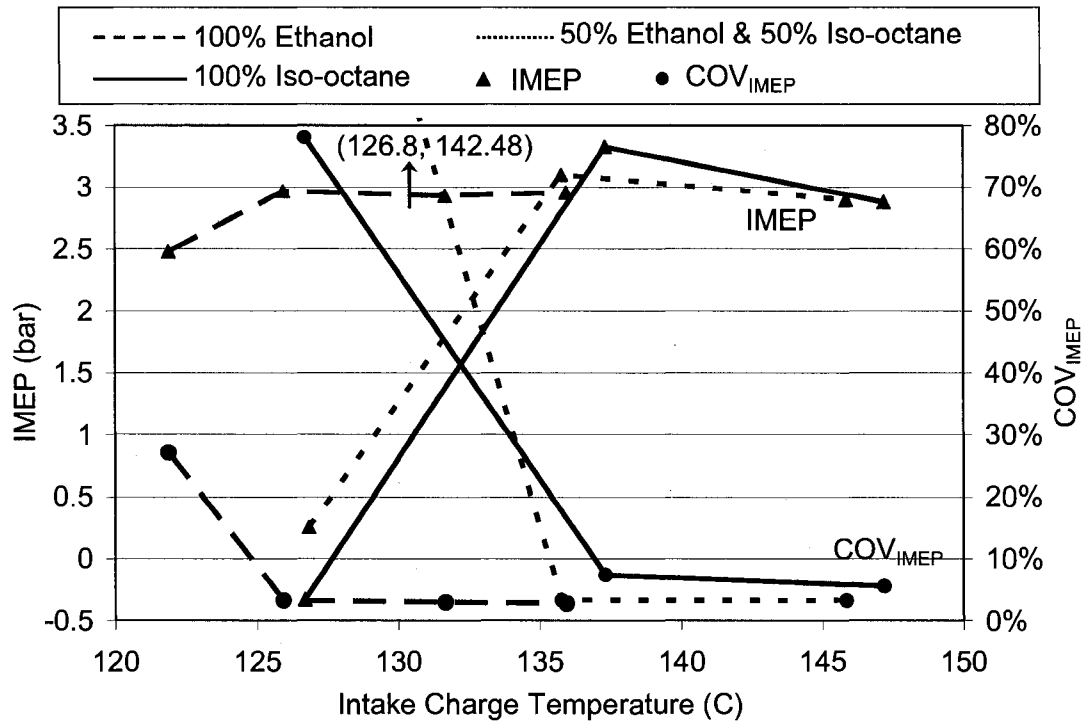


Figure 4.19: IMEP and COV_{IMEP} (1520 RPM).

For pure iso-octane, the 147.2 °C gives the best IMEP value for 1035 and 1275 RPM. At 1275 RPM it is evident from the HRR and pressure profile that this operating point features better combustion characteristics than at other temperatures. Whereas, at 1035 RPM and at 147.2 °C and 137.3 °C intake temperatures, very similar IMEP values are attained even though there are significant differences in their pressure and HRR profiles (Figure 4.3). At 147.2 °C only a little improvement in IMEP is gained (Fig. 4.17). A closer look at the pressure profile (Fig. 4.6) will reveal that the 137.3 °C pressure curve at first stays below the 147.2 °C pressure curve until 15 crank angle ATDC. At this point, the 137.3 °C pressure curve crosses above the 147.2 °C. It should be noted that the cylinder volume change is minimum when the piston is close to the TDC and significant volume change occurs only during the 30 to 150° CA region of the expansion stroke.

Hence, the above noted shift in the pressure curve plays a role in the work done during the expansion stroke. Also, the peak pressures and therefore temperatures for the 137.3 °C case are lower compared to the 147.2 °C case. This in effect reduces the heat transfer losses for the 137.3 °C condition, especially when the piston is close to the TDC. This combined effect due to the shift in the pressure curve and difference in the heat transfer losses results in similar IMEP values at both 147.2 °C and 137.3 °C even though they show different pressure and HRR profile. A similar trend is seen for pure iso-octane at 805 and 1520 RPM, where the 137.3 °C shows a better IMEP value compared to that of the 147.2 °C condition.

For the ethanol/iso-octane blend the 135.8 °C initial charge temperature gives the highest IMEP value for all the tested speeds even though the 145.9 °C shows a pressure profile that has an earlier and higher peak. This is again due to lower heat transfer rates resulting from lower peak temperatures compared to the 145.9 °C case, and also due to the shift in the pressure curve between these two temperatures during the 30 to 150° CA region of the expansion stroke where the change in cylinder volume is maximum. In the case of ethanol, there is not much difference in the IMEP values at 805 and 1035 RPM, with 125.9 °C and 121.9 °C giving a slightly higher IMEP values compared to other initial charge temperatures at 805 and 1035 RPM. Whereas in the case of 1275 RPM the optimum temperature is 131.7 °C and for 1520 RPM the 125.9 °C gives a better IMEP value than the other higher initial charge temperature conditions.

For all the test conditions that produce the highest IMEP values and also for the conditions that are closer to the highest IMEP values irrelevant of the fuel type used, the COV_{IMEP} values remain less than 5%. The only exception from this is the pure iso-octane for the 1520 RPM condition where the COV_{IMEP} is around 6%. COV_{IMEP} values less than 5% are within the stable operating region. Similar values were seen for richer mixtures ($\phi = 0.8$ to 1) with very high amounts of trapped residual gas at 1500 RPM in Zhang (2006). In the same paper, the authors also reported a sharp increase in the COV_{IMEP} with the leanest mixture studied ($\phi = 0.8$). In our experiments the mixture is very lean compared to that of the one used in (Zhang, 2006), and still the COV_{IMEP} stays below 5%. One of the reasons for stable operation can be due to presence of the pre-chamber in this IDI type engine, where there is trapped residual mass that acts as an ignition source for subsequent cycles once the initial cycle with combustion occurs.

4.2.4 Indicated thermal efficiency and peak pressure location:

Figures 4.20 through 4.23 depict the indicated thermal efficiency, which is calculated as the ratio of net indicated work to product of fuel inducted per cycle and lower heating value of fuel. In addition, the figures show the peak pressure location for different operating conditions. The trends in thermal efficiency are similar to the IMEP since the amount of input energy remains constant for a fixed equivalence ratio. The thermal efficiency of the engine is between 30% and 41% and increases with the engine speed. The net indicated thermal efficiencies reported in (Christensen, 1998) for similar lean charges of ethanol and iso-octane were about 38% and 40% (compression ratio used in that study was 18 and the equivalence ratios used were $\phi = 0.33$ for ethanol and $\phi = 0.35$

for iso-octane). The efficiency values reported here are lower than those of (Christensen, 1998) because of the IDI type engine used here.

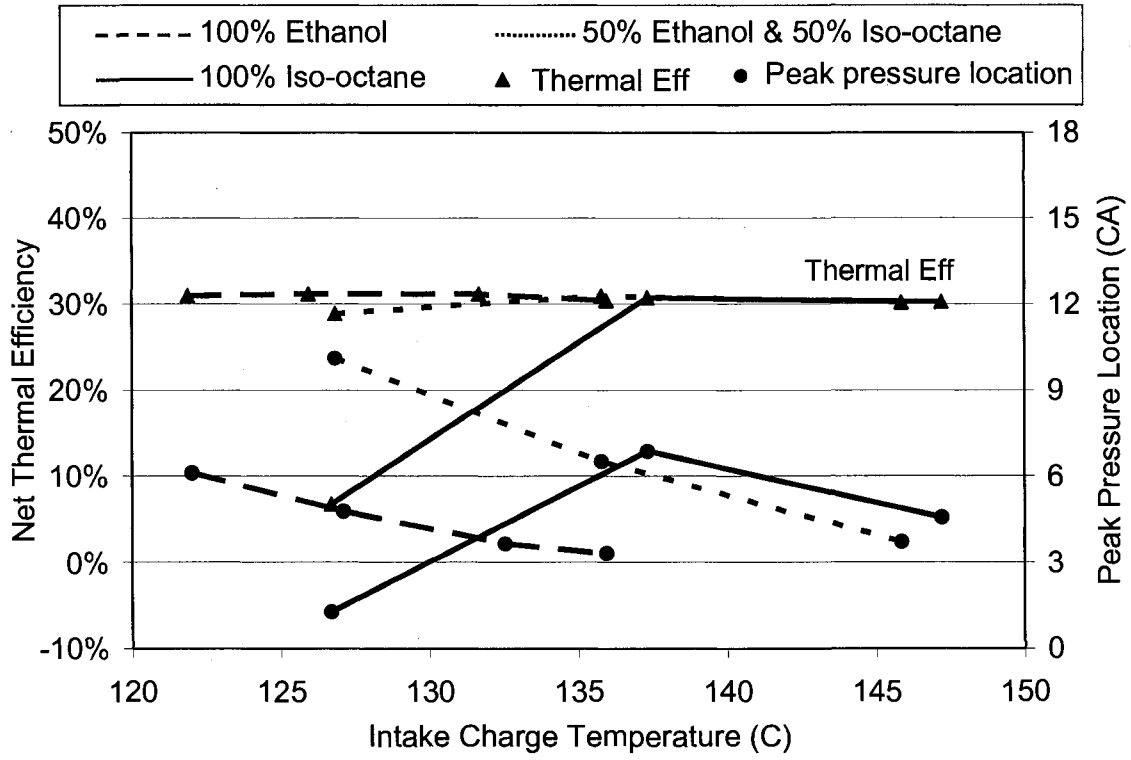


Figure 4.20: Thermal efficiency and peak pressure location ATDC (805 RPM).

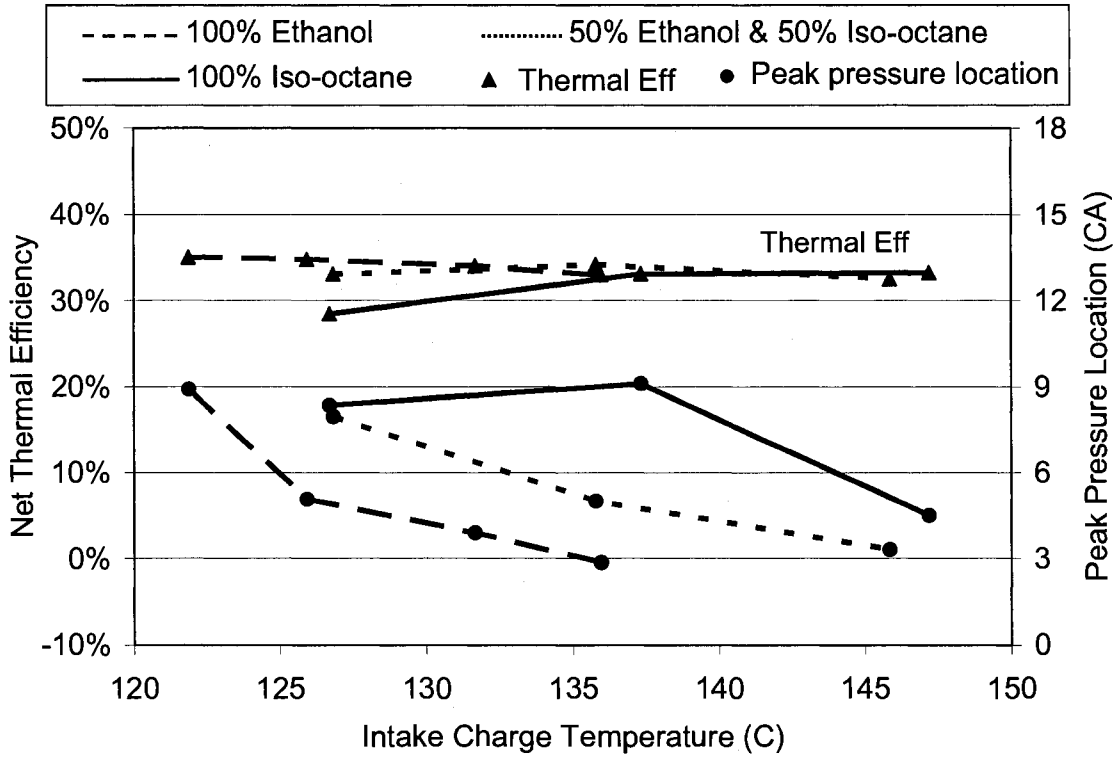


Figure 4.21: Thermal efficiency and peak pressure location ATDC (1035 RPM).

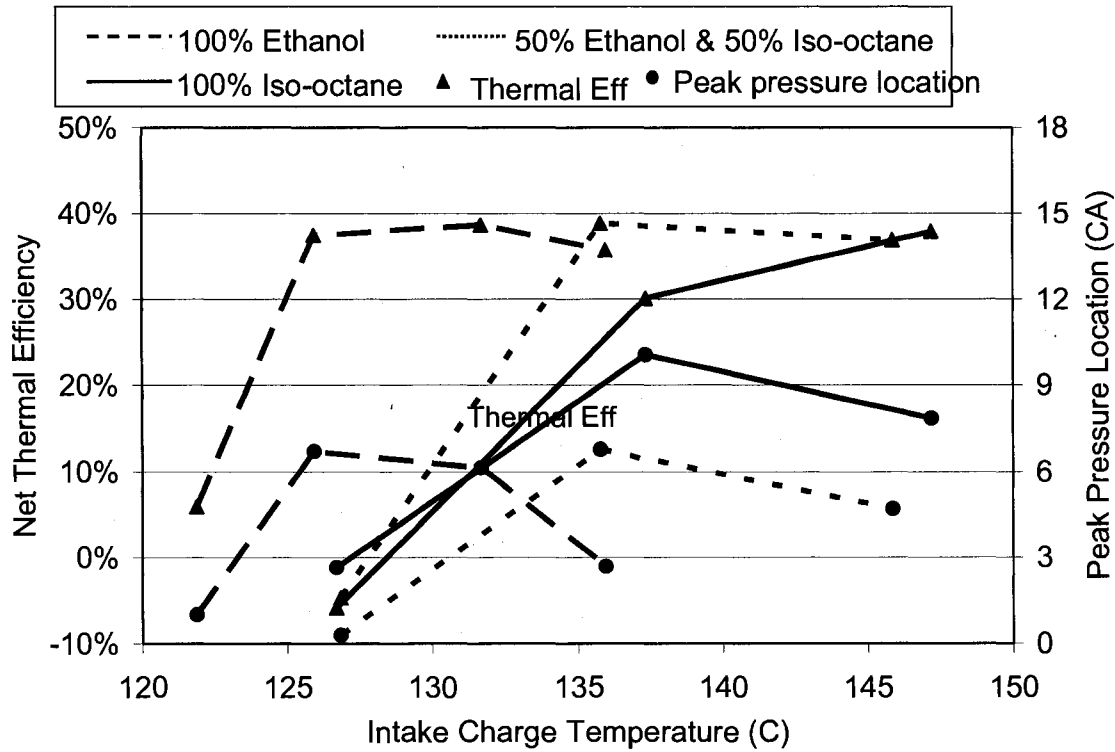


Figure 4.22: Thermal efficiency and peak pressure location ATDC (1275 RPM).

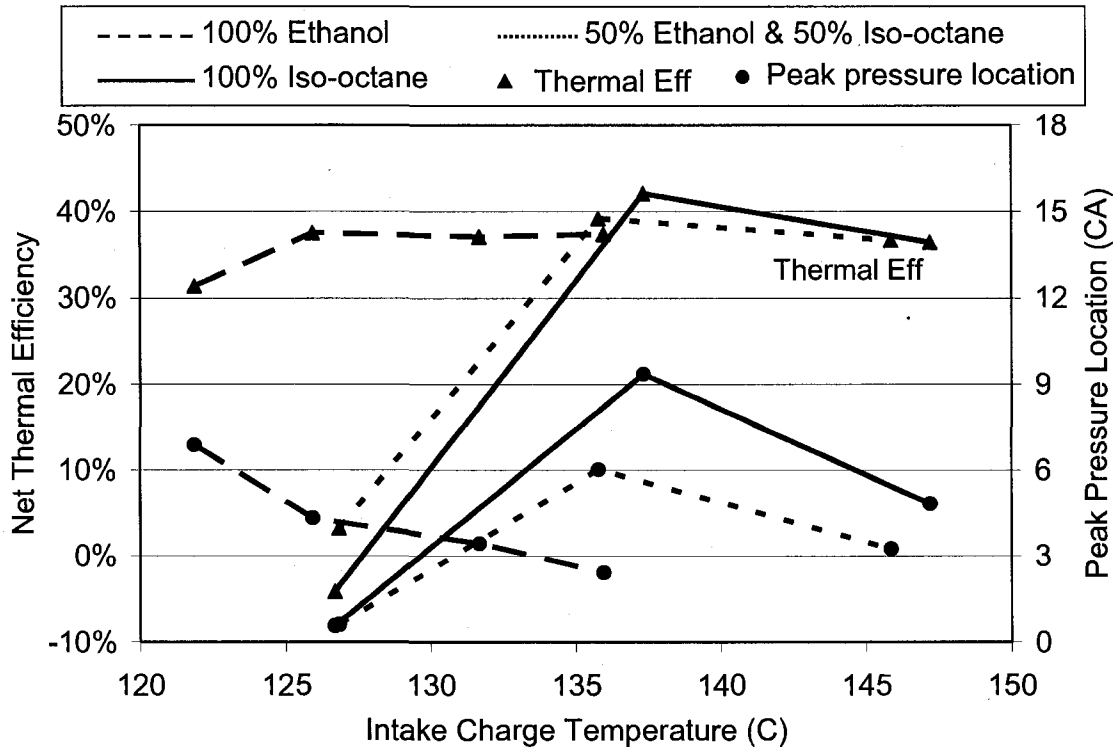


Figure 4.23: Thermal efficiency and peak pressure location ATDC (1520 RPM).

As mentioned earlier, the thermal efficiency increases with engine speed irrespective of the type of fuel used. It should be noted that the volumetric efficiency for a given intake temperature condition drops by 6% when the engine speed is increased from 805 to 1520 RPM. Hence, the amount of intake charge per cycle does not change significantly with increasing engine speed. From engine-out emission results in Section 4.2.6, the combustion quality does not improve significantly with increased thermal efficiency. From the results obtained, it appears that the heat transfer losses decrease with increasing engine speed, which results in improved thermal efficiency of the engine.

4.2.5 Maximum pressure rise rate:

Figures 4.24 through 4.27 show the maximum pressure rise rate (average of 125 cycle) for the various fuels at different operating conditions. The maximum pressure rise rates for all the tested conditions are less than 10 bar/CA. The maximum stress limit for IDI engines is about 5-6 bar/CA, (Xie, 2006). However, in Christensen (1999), the authors reported that their diesel engine (normal stress limit: 6-10 bar/CA) modified for HCCI operation has been running at 15-20 bar/CA for extended time periods without significant wear. Hence, the pressure rise rates shown here are within the acceptable range. The lowest values for the maximum pressure rise rate in Figures 4.24 through 4.28 occurred at conditions where the engine started to misfire.

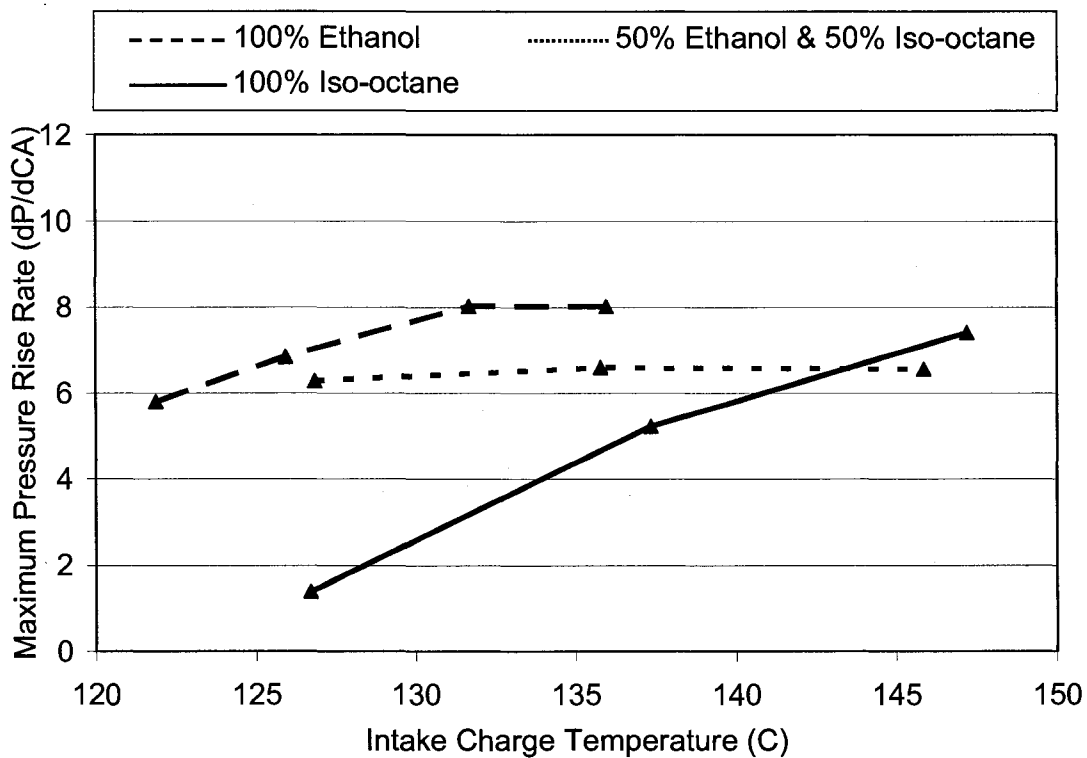


Figure 4.24: Maximum pressure rise rate (805 RPM).

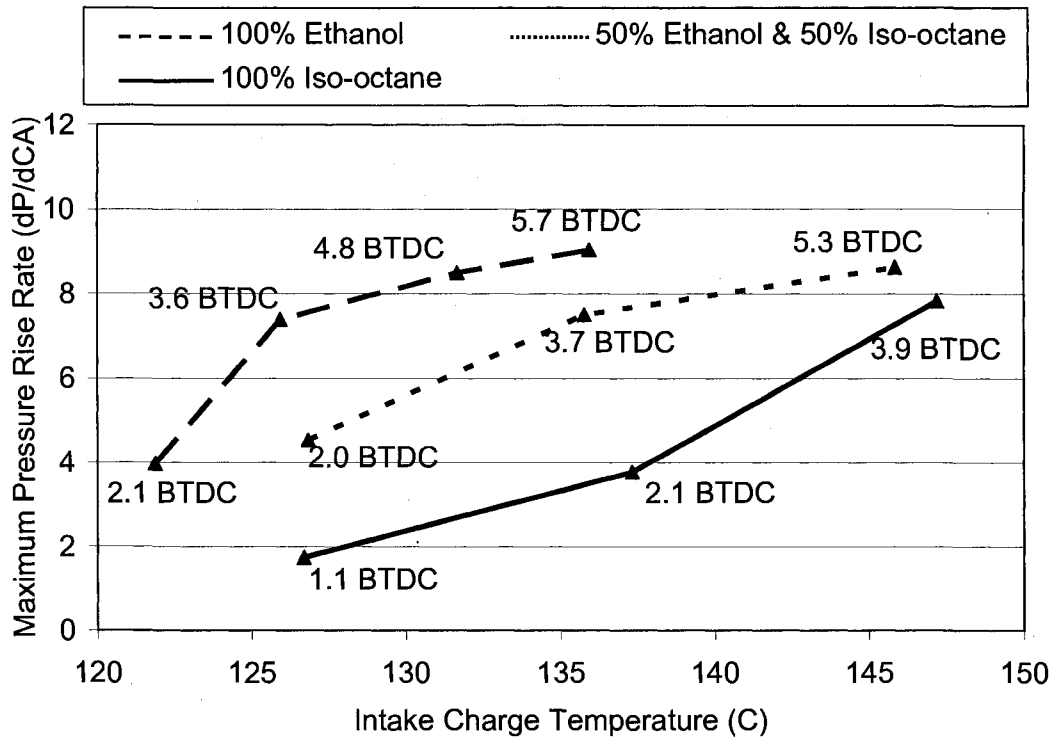


Figure 4.25: Maximum pressure rise rate (1035 RPM) with corresponding combustion on-set CA values.

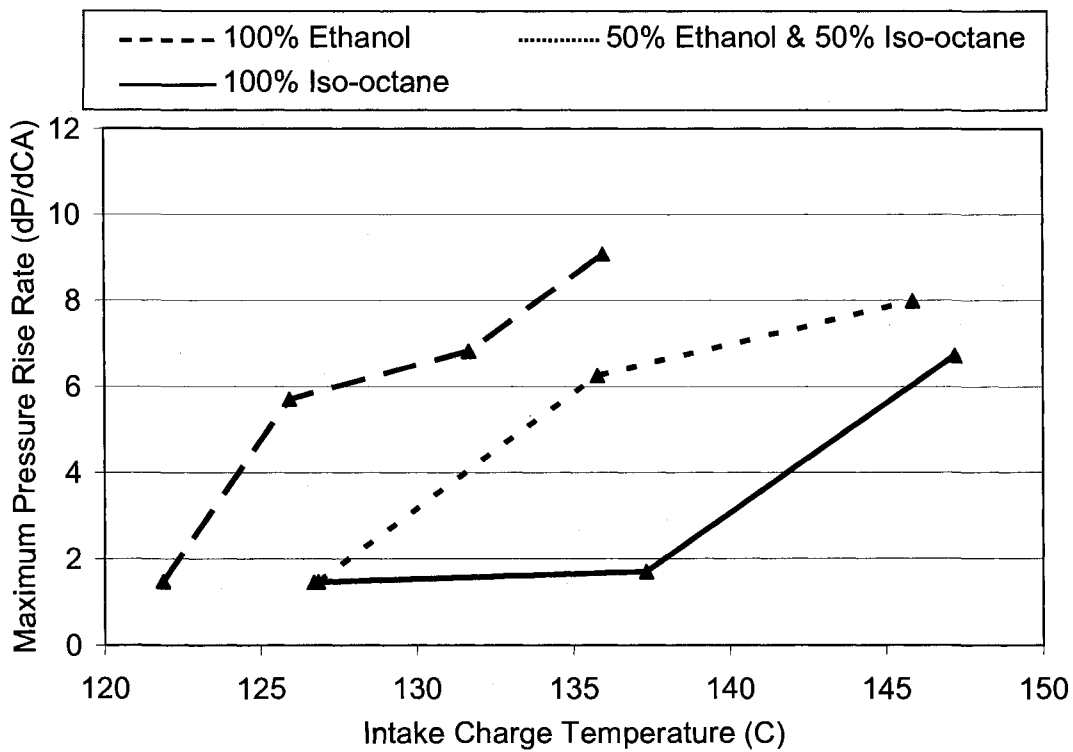


Figure 4.26: Maximum pressure rise rate (1275 RPM).

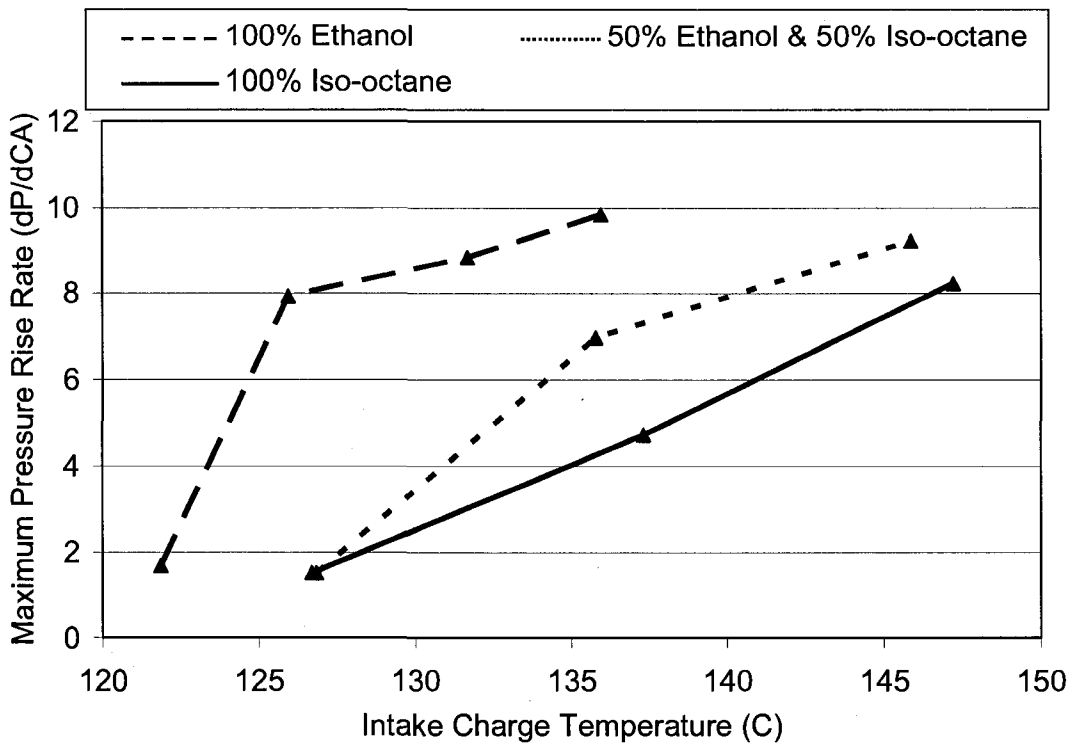


Figure 4.27: Maximum pressure rise rate (1520 RPM).

In general, the maximum pressure rise rate increases with intake charge temperature for a given fuel irrespective of the engine speed. The only exception is the ethanol/iso-octane blend at 805 RPM condition where there is no major difference in the maximum pressure rise rate for different intake charge temperatures. There is also no direct correlation between the maximum pressure rise rate and the best IMEP values. However, there is a direct correlation between the maximum pressure rise rate and the on-set of combustion. Figure 4.25 shows the on-set of combustion values displayed next to the plotted maximum pressure rise rate for each operating condition. From the values it is clear that the combustion on-set has a strong influence on the subsequent pressure rise rate. For most of the operating conditions the best IMEP values were obtained for the maximum

pressure rise rate of about 7 to 8 bar/CA. However, in the case of pure ethanol for 1035 RPM, the best IMEP is obtained when the maximum pressure rise rate is only 4 bar/CA. Similarly, for the ethanol/iso-octane blend for the 805 and 1520 RPM conditions, the maximum pressure rise rates are about 5 bar/CA.

4.2.6 CO and UHC:

Figure 4.28 and 4.29 show the carbon monoxide (CO) and non-methane unburned hydrocarbon (UHC) engine-out emissions that corresponds to the intake charge temperature and the fuel type, which showed overall best thermal efficiency values for all the tested RPM conditions. Hence, the intake charge temperature is different for ethanol when compared to the other two fuel types used. The intake charge temperature that showed overall best thermal efficiency for all the RPM conditions in the case of ethanol was 130 °C. Whereas, for the iso-octane and the ethanol/iso-octane blend it is 136 °C. The oxides of nitrogen (NO_x) are not shown in the figure since the maximum value read is less than 10 ppm for the entire set of test conditions. This shows that near-zero NO_x emissions can be obtained using a lean charge. Similar results for NO_x at an equivalence ratio of 0.321 were reported in (Van Blarigan et al, 1998) for iso-octane.

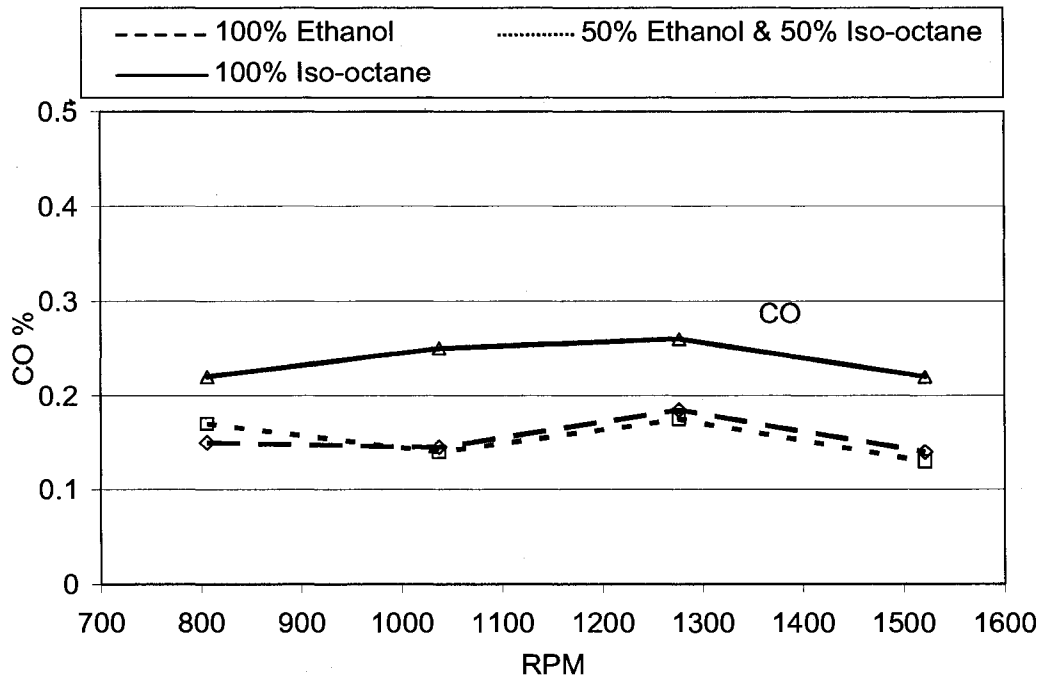


Figure 4.28: Carbon monoxide (CO) emissions.

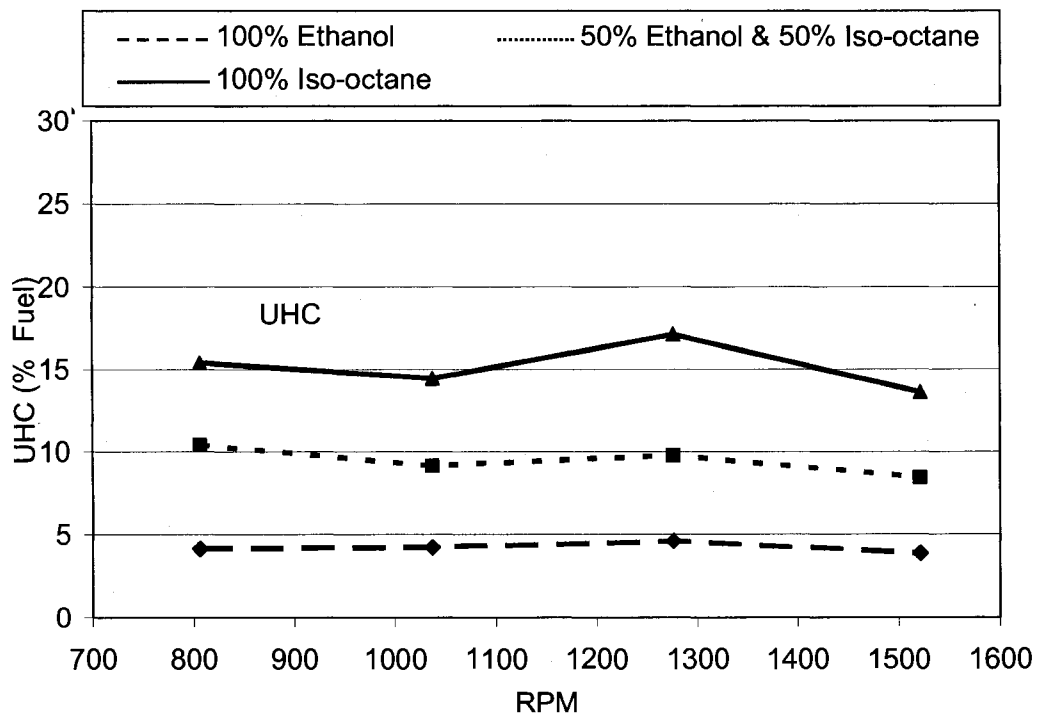


Figure 4.29: Unburned Hydrocarbon (UHC) emissions.

It should be noted that the UHC levels shown in Fig. 4.28 is in terms of percentage intake fuel. Also, the amount of fuel does not vary much between the different engine speed tested for a particular intake charge temperature condition. In general, the CO and UHC levels are high and require exhaust gas after-treatment. Again, these high levels in CO and UHC emissions are due to the IDI type of engine being used here, which has greater heat losses that contribute to incomplete combustion especially closer to the cylinder walls. Similar levels of UHC and CO for iso-octane are reported in (Van; 1998). An interesting trend with both CO and UHC emissions is that, for any given operating condition, the presence of ethanol decreased the CO and UHC levels. This trend is clear when comparing the emissions level for iso-octane and the ethanol/iso-octane blend where the intake charge temperature is the same for both the fuel type. In the case of iso-octane the CO and UHC levels are 0.23% and 15%. Whereas, for the ethanol/iso-octane blend the CO and UHC levels are 0.15% and 10%. This further confirms that presence of iso-octane in fuel prolongs the HR duration and leads to incomplete combustion when compared to ethanol for this lean operating condition.

4.3 Summary

For the same intake charge temperature and engine speed, the on-set of combustion for ethanol occurs ahead of that for iso-octane. For example, the on-set of combustion in the case of ethanol and iso-octane at 1035 RPM and 136 °C are 5.6 and 1.9° CA BTDC, respectively. It should be noted that ethanol has a higher enthalpy of vaporization than iso-octane, but this has no effect since the intake charge temperature is maintained constant.

The HRR and in-cylinder pressure traces in this IDI engine indicate that residence time has more impact on the on-set of combustion at lower charge temperatures and engine speeds.

The indicated thermal efficiency (30 – 41%) values reported in this study are comparable to other HCCI experimental results reported elsewhere and these values are better than those for typical SI engines which are less than 30%, especially during low load operating conditions.

The presence of the pre-chamber in this IDI type engine ensures stable operation (COV_{IMEP} stays below 5%) due to trapping of residual mass that acts as an ignition source for subsequent cycles once the initial cycle with combustion occurs.

The NO_x emissions were very low (less than 10 ppm) for the tested conditions and do not require after-treatment. However, the UHC and CO levels are higher and would require after-treatment.

For a particular operating condition, the presence of ethanol reduced the CO and UHC levels on this HCCI engine operating with iso-octane at a lean fuel-air equivalence ratio.

Chapter 5 Experimental results: Effect of EGR

In this chapter the effect of EGR on the HCCI combustion on-set is analyzed. The study is done by maintaining a constant compression ratio, and a constant intake charge temperature (for a particular fuel type used). The parameters that were varied are percentage EGR addition, equivalence ratio and the fuel composition. The details of the test conditions are provided below in the next section.

5.1 Test conditions

The fuels used in this study are 100% ethanol, 100% iso-octane and 50% ethanol & 50% iso-octane blend by volume, which were similar to the previous study done in Chapter 4. The engine specifications and conditions used in the experimental study are as follows:

Table 5.1: Engine specifications and test conditions

Compression ratio, r_c	20:1
Equivalence ratio, ϕ , ϕ	0.33, 0.38
Engine Speed [RPM]	805, 1035, 1275 & 1520
EGR [% by vol.]	0 – 40 %
Coolant Temperature, T_c [°C]	75 (± 2)
Intake charge temperature, T_i [°C]	133 or 150 (± 2)

The results reported in the next section are averaged data based on a sample of 125 consecutive cycles. The discussion of the results includes the engine performance in terms of the in-cylinder pressure, HRR, 10% and 90% HR, IMEP, and COV_{IMEP} , indicated thermal efficiency, and regulated engine-out emissions.

5.2 Results and discussion

5.2.1 In-cylinder pressure and HRR ($\phi = 0.33$):

Figures 5.1 through 5.12 show the in-cylinder pressure and HRR for the fuels tested over various engine speeds and different levels of EGR addition for a fuel-air equivalence ratio of $\phi = 0.33$. The intake charge temperature for ethanol is maintained during the trials at 135 °C. For iso-octane and 50% ethanol/iso-octane blend the charge temperature is kept constant at 150 °C. Our earlier results in Chapter 4 showed that intake charge temperature has a strong impact on the on-set of combustion for a particular engine speed and ethanol advances the on-set of combustion when compared with iso-octane. The initial charge temperatures in this study were chosen such that the on-set of combustion is close to the TDC for all the fuel types used.

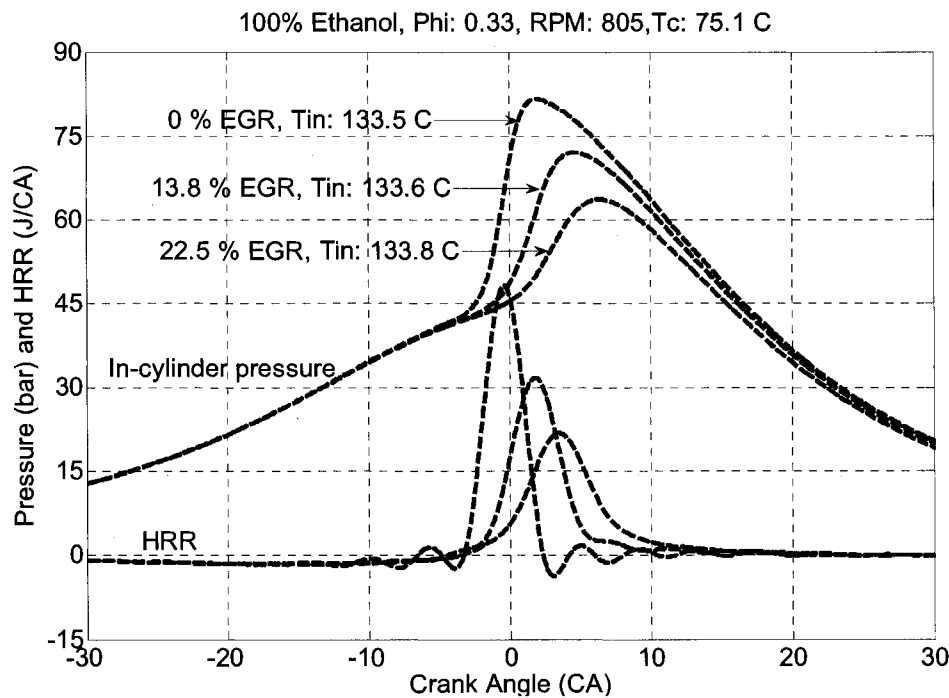


Figure 5.1: Cylinder pressure and rate of heat release with different EGR levels (805 RPM, 100% Ethanol, phi: 0.33).

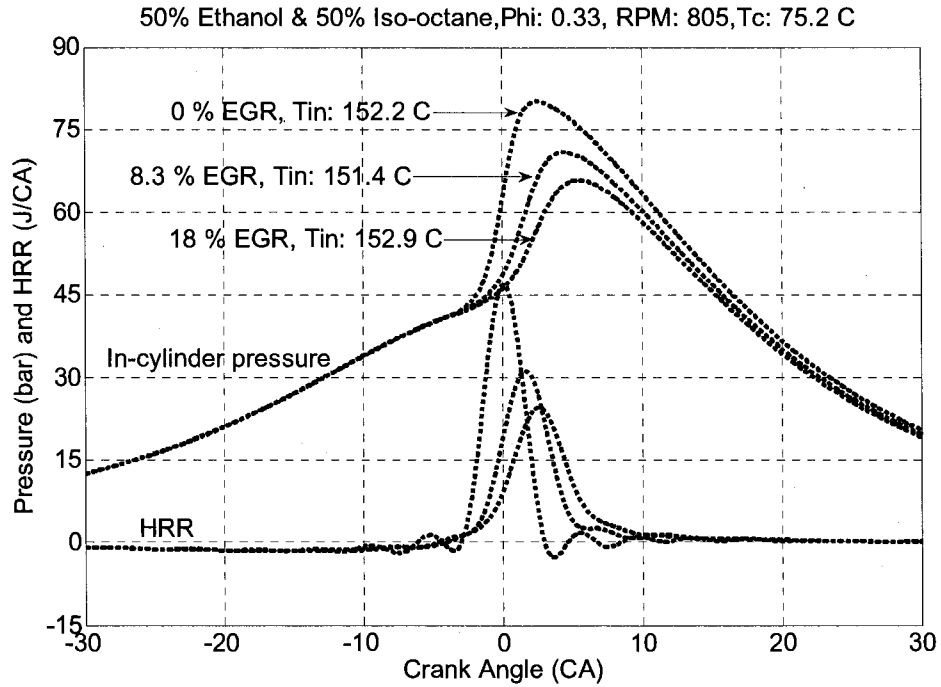


Figure 5.2: Cylinder pressure and rate of heat release with different EGR levels (805 RPM, 50% Iso-octane & 50% Ethanol, phi: 0.33).

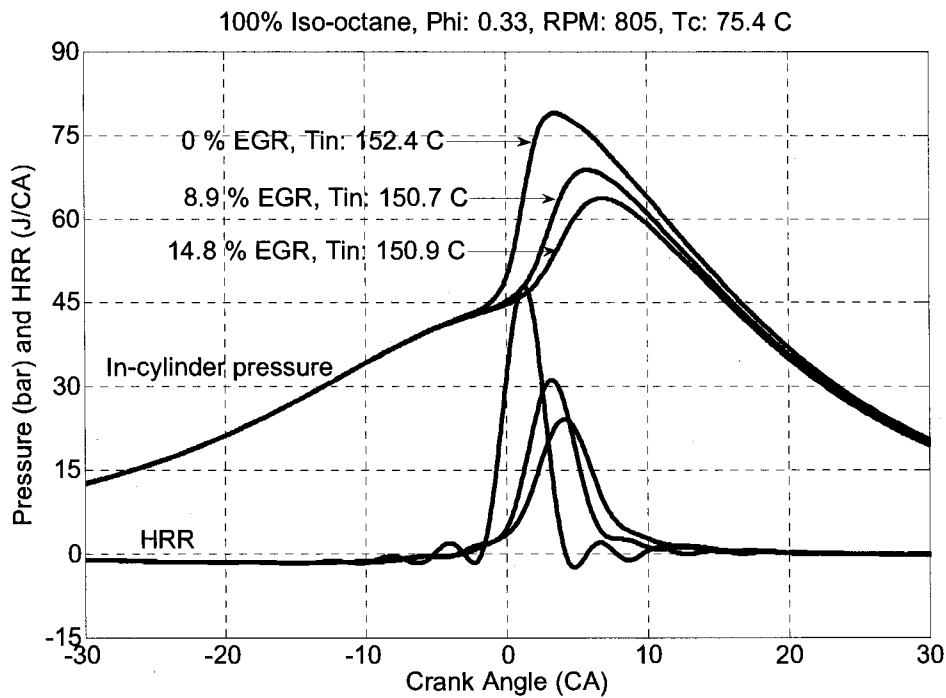


Figure 5.3: Cylinder pressure and rate of heat release with different EGR levels (805 RPM, 100% Iso-octane, phi: 0.33).

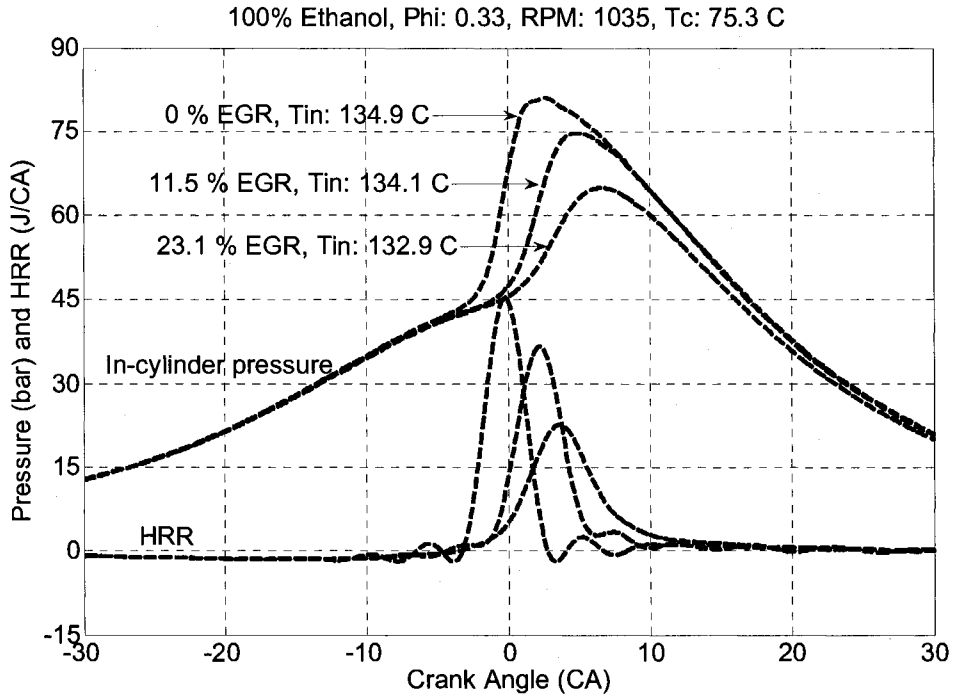


Figure 5.4: Cylinder pressure and rate of heat release with different EGR levels (1035 RPM, 100% Ethanol, phi: 0.33).

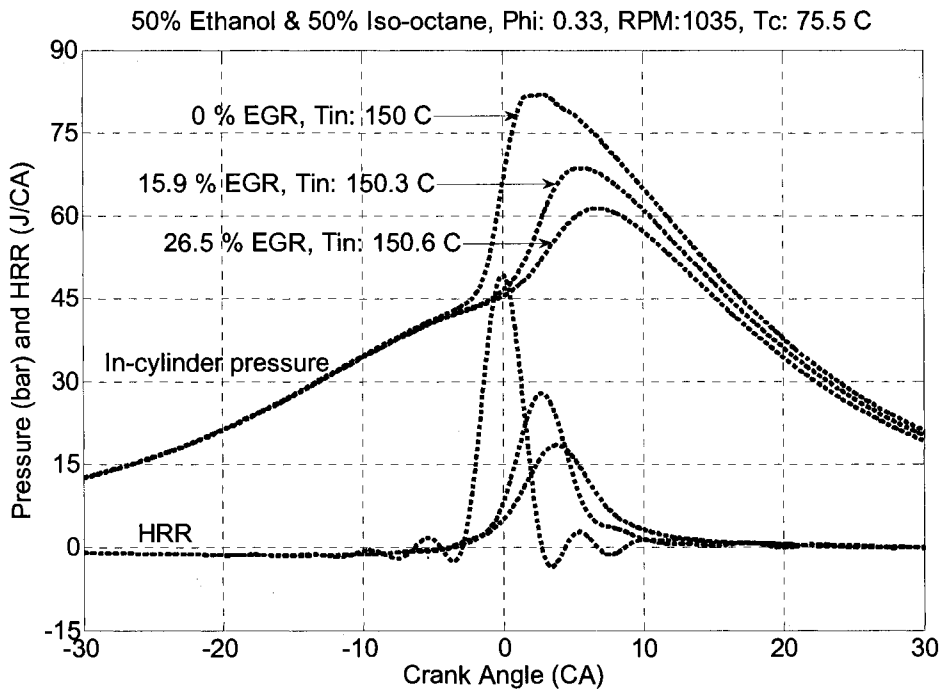


Figure 5.5: Cylinder pressure and rate of heat release with different EGR levels (1035 RPM, 50% Iso-octane & 50% Ethanol, phi: 0.33).

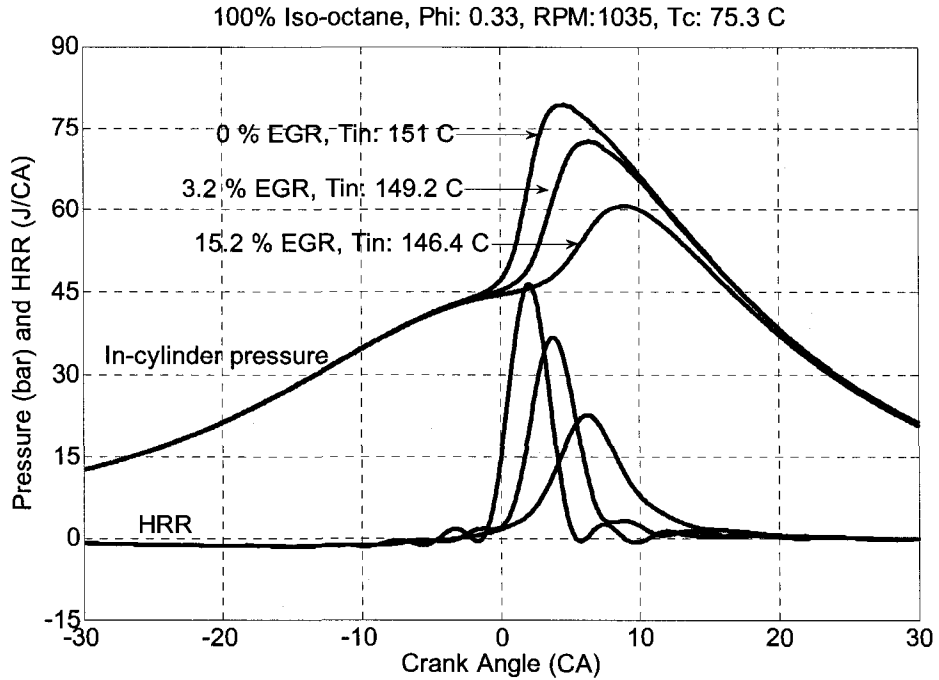


Figure 5.6: Cylinder pressure and rate of heat release with different EGR levels (1035 RPM, 100% Iso-octane, phi: 0.33).

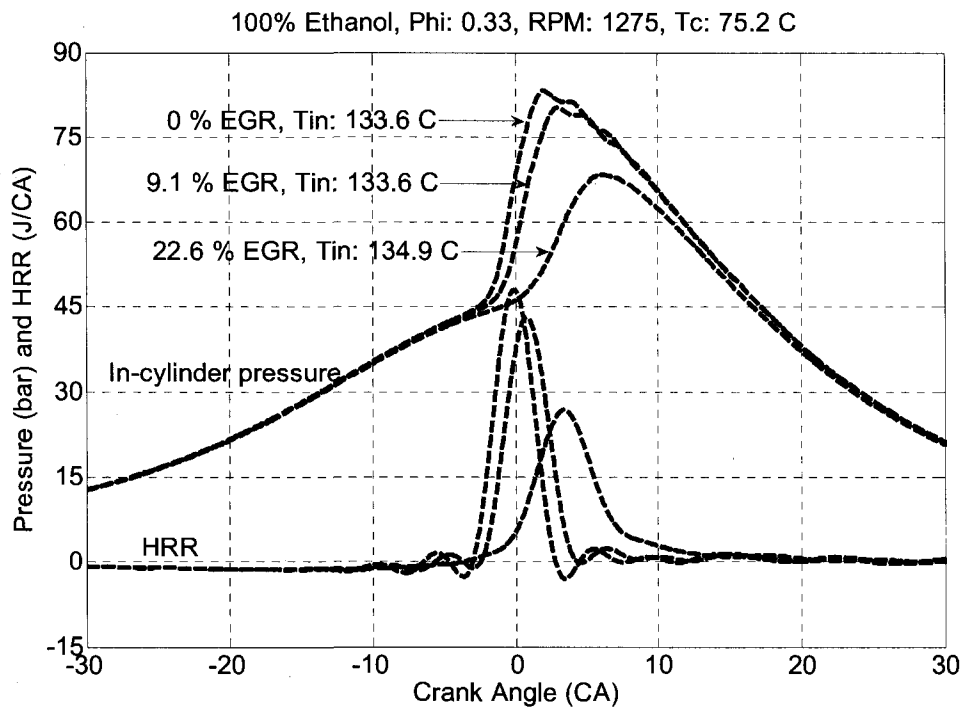


Figure 5.7: Cylinder pressure and rate of heat release with different EGR levels (1275 RPM, 100% Ethanol, phi: 0.33).

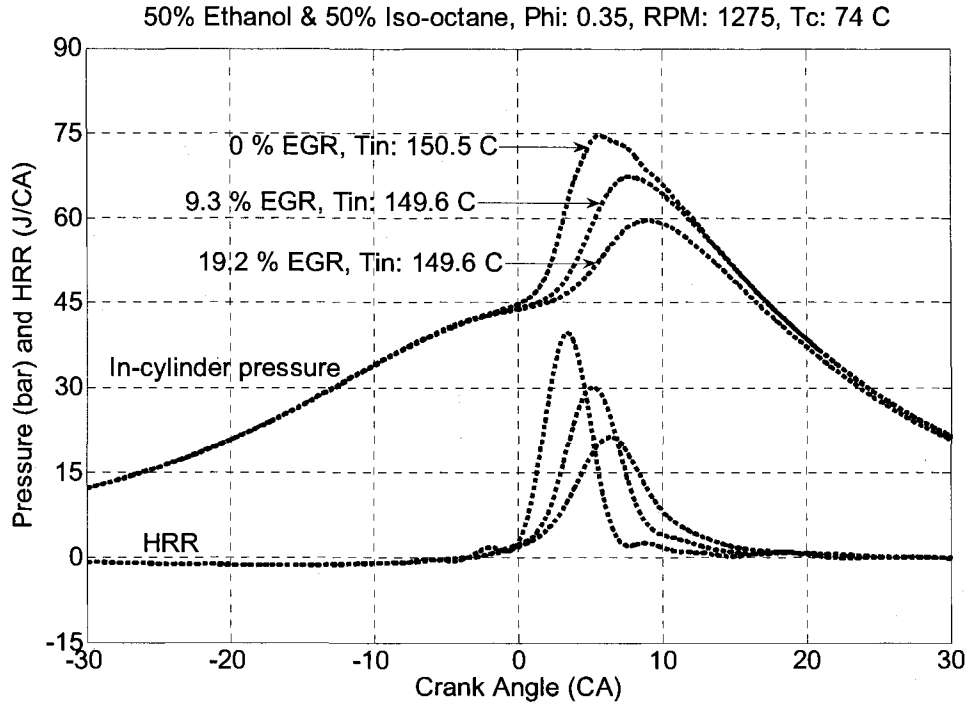


Figure 5.8: Cylinder pressure and rate of heat release with different EGR levels (1275 RPM, 50% Iso-octane & 50% Ethanol, phi: 0.33).

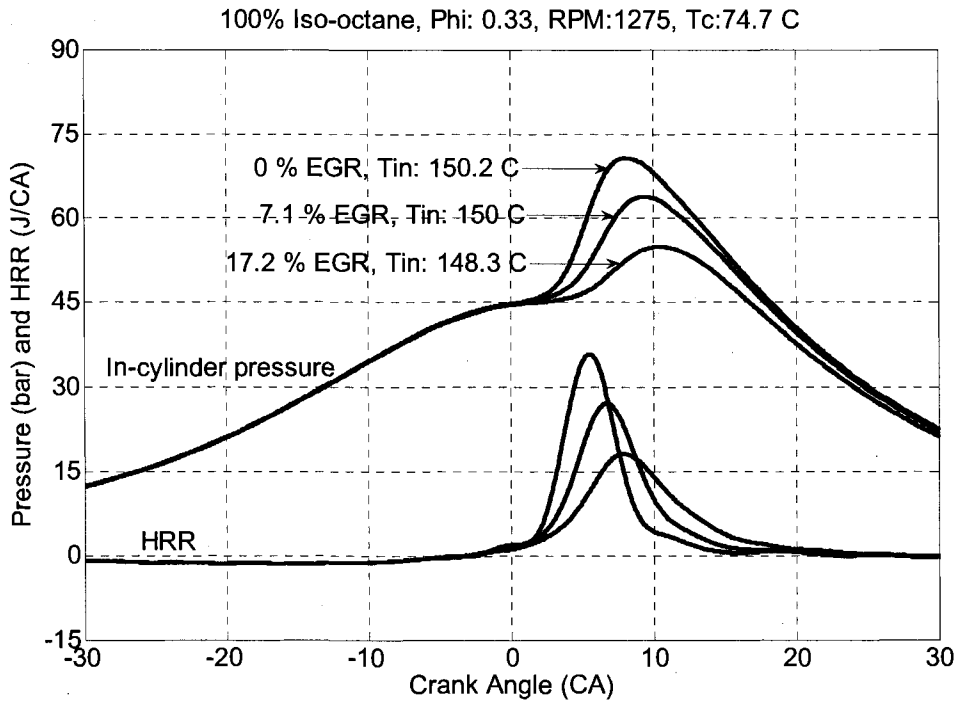


Figure 5.9: Cylinder pressure and rate of heat release with different EGR levels (1275 RPM, 100% Iso-octane, phi: 0.33).

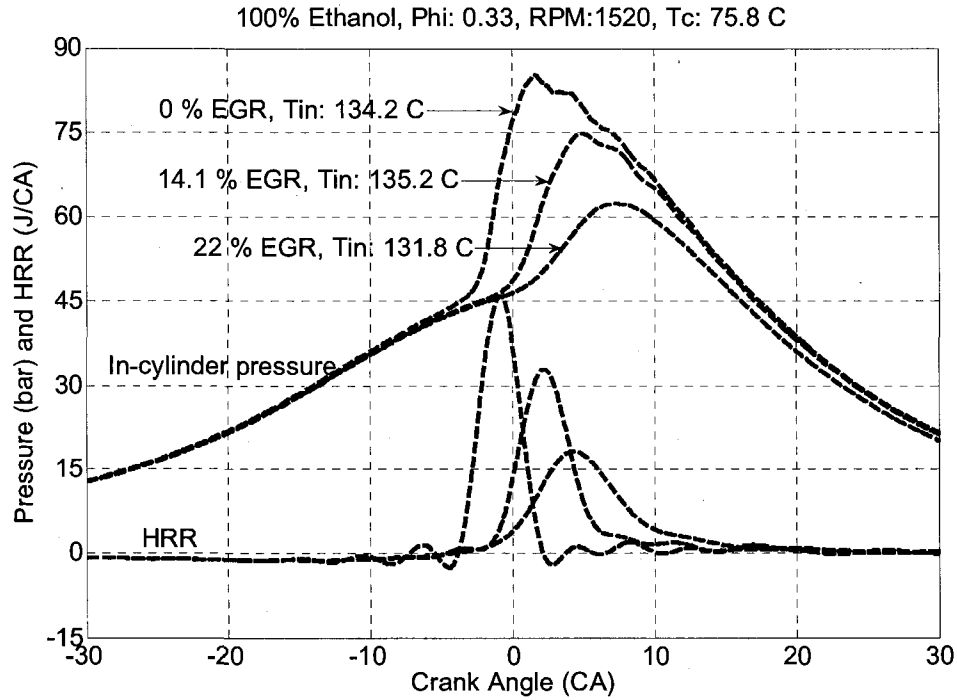


Figure 5.10: Cylinder pressure and rate of heat release with different EGR levels (1520 RPM, 100% Ethanol, phi: 0.33).

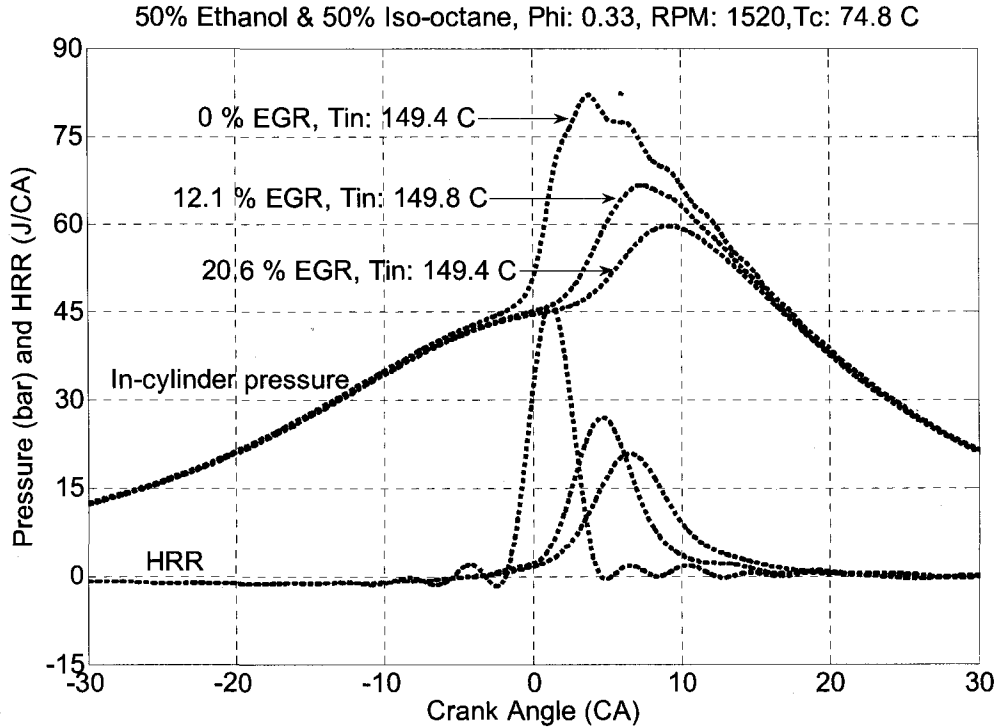


Figure 5.11: Cylinder pressure and rate of heat release with different EGR levels (1520 RPM, 50% Iso-octane and 50% Ethanol, phi: 0.33).

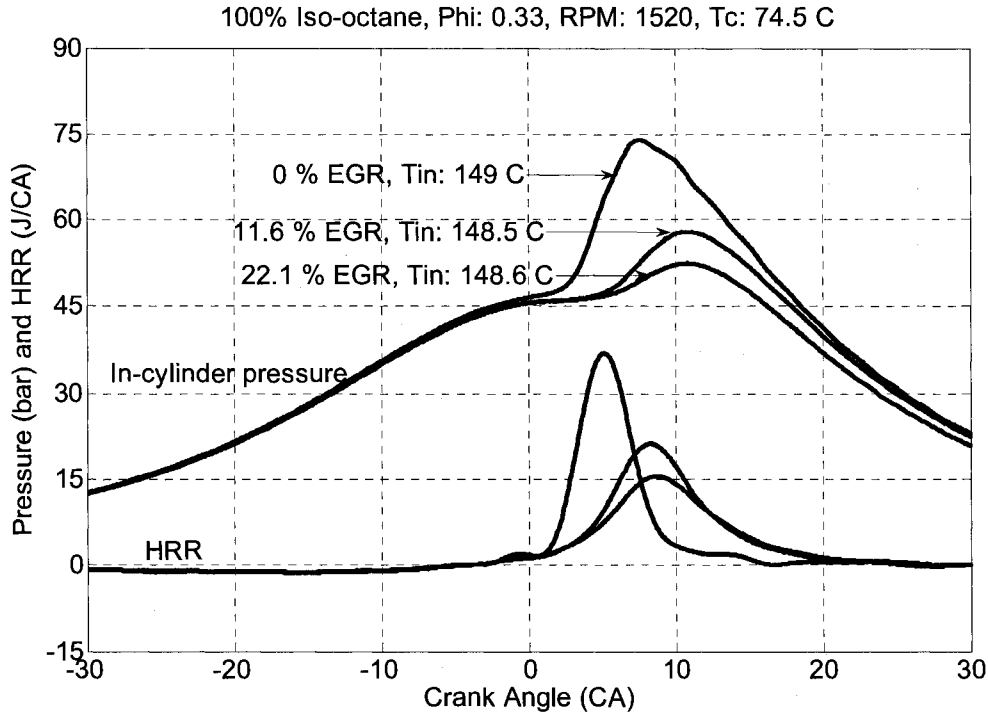


Figure 5.12: Cylinder pressure and rate of heat release with different EGR levels (1520 RPM, 100% Iso-octane, phi: 0.33).

Results in Figures 5.1 through 5.12 indicate that for a particular fuel and engine speed, the EGR addition has a strong impact on the on-set of combustion. For example, the on-set of combustion (CA corresponding to the 10% HR) in the case of pure ethanol ($\phi = 0.33$) with 0%, 13.8% and 22.5% EGR addition for the 805 RPM (Fig. 2) are 1.8 CA BTDC, 0.2 CA BTDC and 0.8 CA ATDC. The trend of delayed on-set of combustion with respect to the addition of EGR is confirmed when fuelling with the 50% iso-octane/ethanol blend and pure iso-octane for 805 RPM (Figures 5.2 and 5.3). This influence has been reported by several other researchers, (Oakley et al. 1994, Zhao et al. 1994, Zhang et al. 2006). Furthermore, the EGR addition also reduces the peak pressure and moderates the HRR. For example, the peak pressure for the pure ethanol ($\phi = 0.33$)

and 1035 RPM (Fig. 5.4) decreases from 81 bar to 65 bar with 23% EGR addition. The HRR for the same condition drops from 45 J/CA to 20 J/CA.

There is also an interesting trend that differentiates the lower speed conditions (805 and 1035 RPM) from the higher speed conditions (1275 and 1520 RPM) when there is no EGR addition. When analyzing the in-cylinder pressure it can be noted that for the lower speeds (805 and 1035 RPM) there is no engine ringing. Whereas, when comparing pressure curves of the higher RPM ranges to the lower RPM pressure curves it can be noted that there are distinguishable variations which signify engine ringing. This behavior is very prominent at 1520 RPM with ethanol as fuel (Fig. 5.10). The engine ringing tendency associated with ethanol can be confirmed by comparing the 1520 RPM and 0% EGR for the remaining two fuelling conditions; 50% ethanol/iso-octane blend, and 100% iso-octane (Figures 5.11 and 5.12). In both, Figures 5.11 and 5.12, the initial charge temperature and coolant temperature were kept constant at 149 °C and 74 °C. From the above-mentioned figures it can be noted that the engine ringing is more pronounced with addition of ethanol. Also, from Figures 5.10 through 5.12 it can be seen that the addition of EGR to the 1520 RPM condition terminates the ringing and moderates the HRR for all the fuel types used.

5.2.2 10% HR CA and 10-90% HR CA duration ($\phi = 0.33$):

Figures 5.13 through 5.15 show the CA corresponding to the 10% HR (on-set of combustion) and the heat release (HR) duration in CA from 10% and 90% HR for fuel-air equivalence ratio of 0.33 for various operating conditions. As mentioned earlier it can be

noted from Figures 5.13 through 5.15 that the addition of EGR delays the 10% HR (onset of combustion) CA for all the fuels and RPM conditions. Furthermore, when studying the HR duration (Figures 5.13 through 5.15) it is evident that the EGR addition increases the duration for all the operating conditions. Another interesting trend is that the presence of iso-octane in fuel prolongs the HR duration. For instance, in Figures 5.14 and 5.15, at the 15% EGR condition; for 50% ethanol/iso-octane blend ($\phi = 0.33$) the HR duration is between 7.5 CA and 9.5 CA for all the RPM conditions. Whereas, at the same 15% EGR when fuelling with pure iso-octane (Fig. 5.15) the HR duration varies from 7.8 to 11 CA for all the RPM conditions

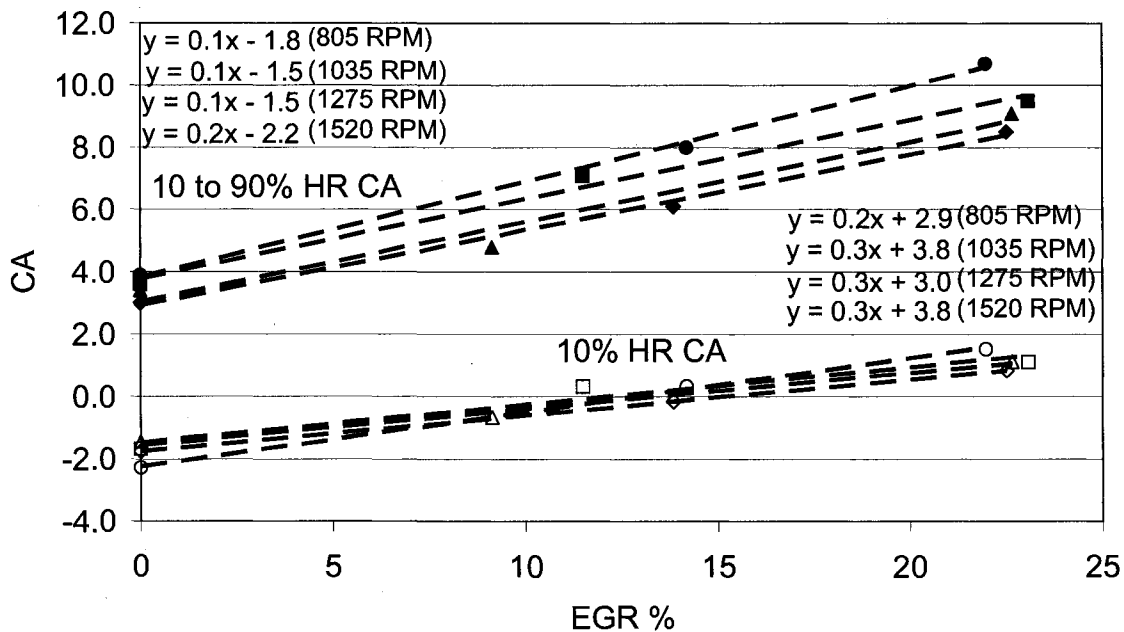


Figure 5.13: 10% Heat Release CA and CA duration for 10% to 90% Heat Release for different EGR levels and RPM (100% Ethanol, ϕ : 0.33).

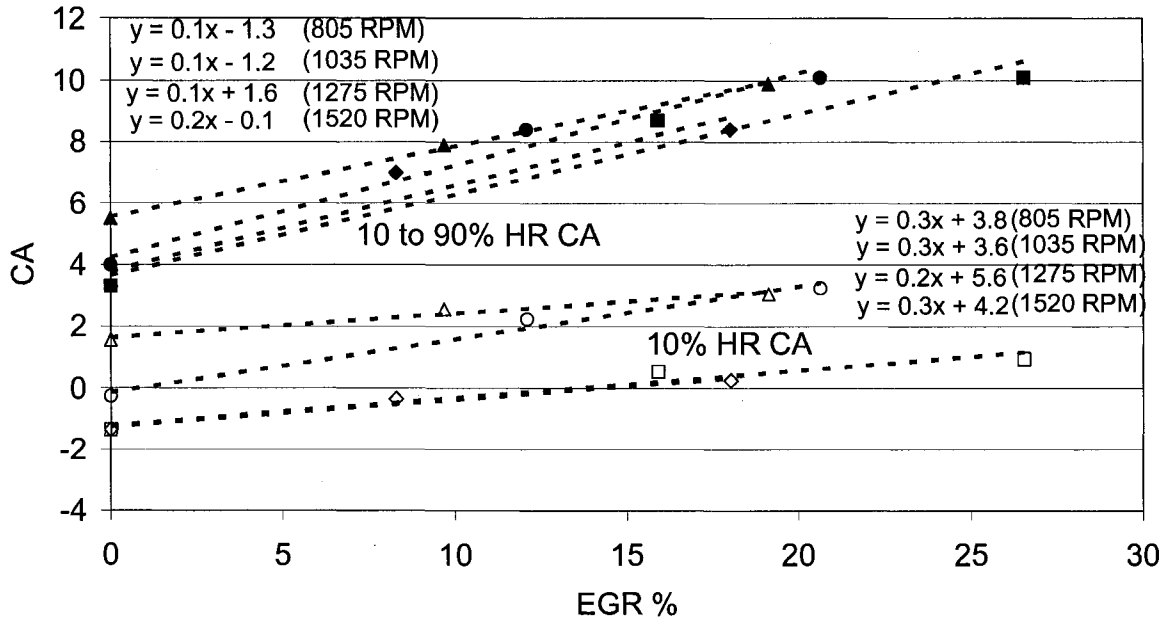


Figure 5.14: 10% Heat Release CA and CA duration for 10% to 90% Heat Release for different EGR levels and RPM (50% Ethanol & 50% Iso-octane, phi: 0.33).

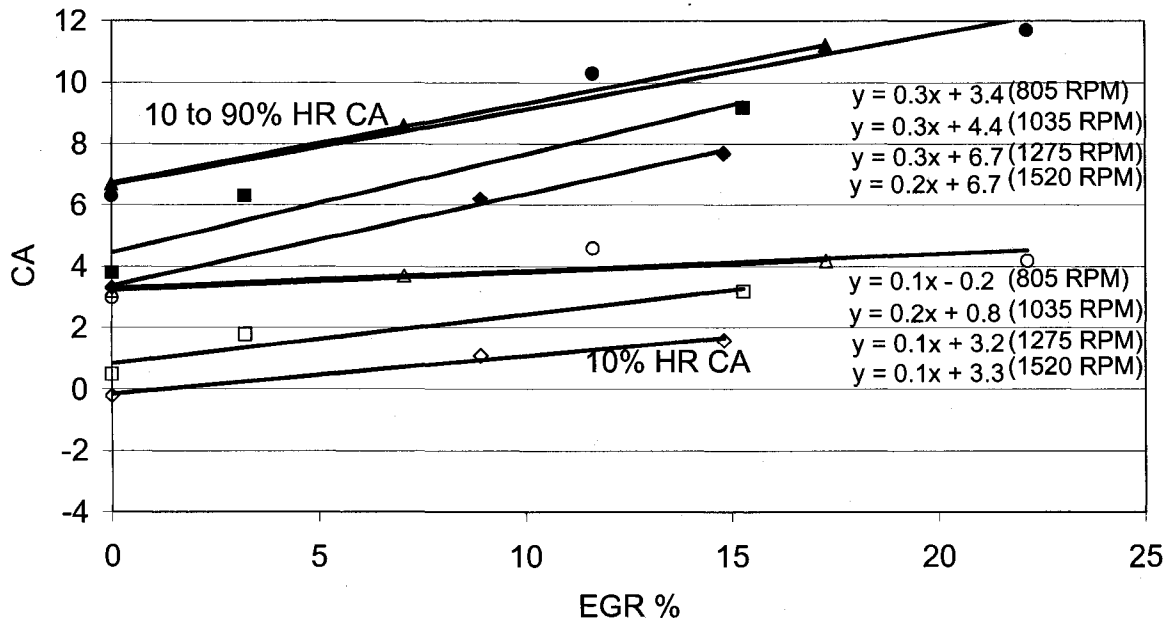


Figure 5.15: 10% Heat Release CA and CA duration for 10% to 90% Heat Release for different EGR levels and RPM (100% Iso-octane, phi: 0.33).

Another interesting trend in Figures 5.13 through 5.15 can be identified for the 0% EGR condition when comparing all of the fuels tested. For ethanol (Fig. 5.13) it is clear that

the 10% HR CA (combustion on-set) and the HR duration do not change significantly with change of RPM. However, from Figures 5.14 and 5.15 it can be noted that once iso-octane is added there is significant change in the CA values with respect to RPM. The combustion on-set (10% HR) is delayed and the HR duration increases for the higher RPM conditions (1275 and 1520 RPM) compared to the lower RPM conditions (805 and 1035 RPM). This shows that the reaction rates for iso-octane at the lean operation conditions ($\phi = 0.33$) are affected by the residence time during both early and regular combustion periods, causing the delay in the on-set of combustion and prolonged HR durations at higher engine speeds. This effect is not seen when fuelling with pure ethanol where the reaction rates during the early (10% HR) and regular combustion (10 – 90% HR) are not affected by the residence time.

5.2.3 In-cylinder pressure and HRR ($\phi = 0.38$):

Figures 5.16 through 5.27 depict in-cylinder pressure and HRR for the fuels tested over various engine speeds and different levels of EGR addition for a fuel-air equivalence ratio of 0.38. The intake charge temperature for ethanol is maintained during the trials at 135 °C, similar to the previous case ($\phi = 0.33$). For iso-octane and a 50% ethanol/iso-octane blend the charge temperature is kept constant at 150 °C. It should be noted that the percentage EGR addition range used for the 0.38 equivalence ratio is higher than the 0.33 equivalence ratio. This is primarily done to eliminate pressure ringing and to keep the peak pressure-rise rates below 10 bar/CA. Similar to the previous case ($\phi = 0.33$), it can be noticed (Fig. 5.16 through 5.27) that the EGR addition delays the on-set of combustion, reduces the peak pressure and moderates the HRR.

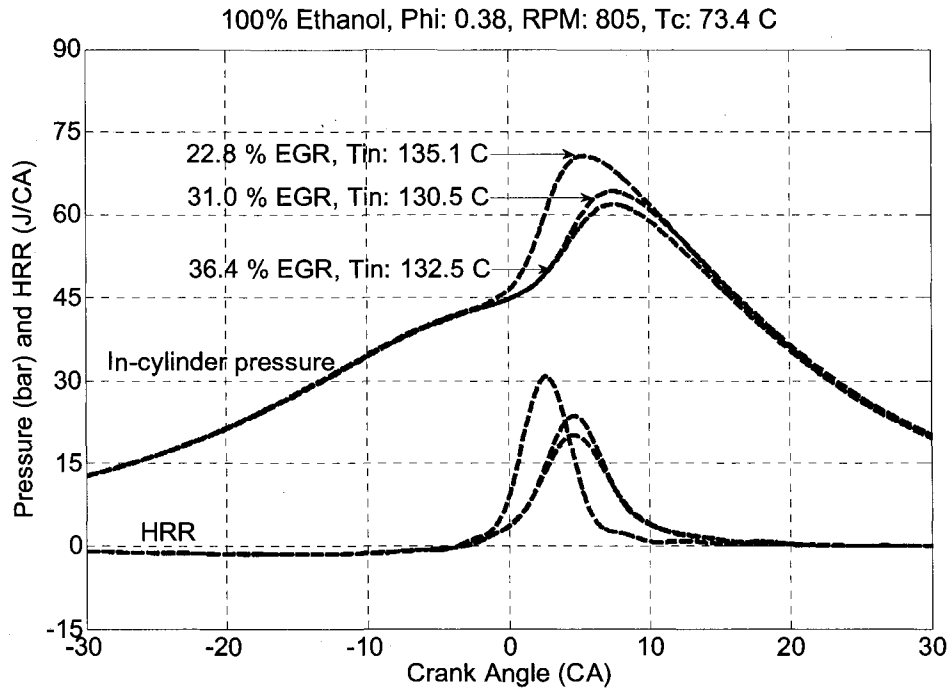


Figure 5.16: Cylinder pressure and rate of heat release with different EGR levels (805 RPM, 100% Ethanol, phi: 0.38).

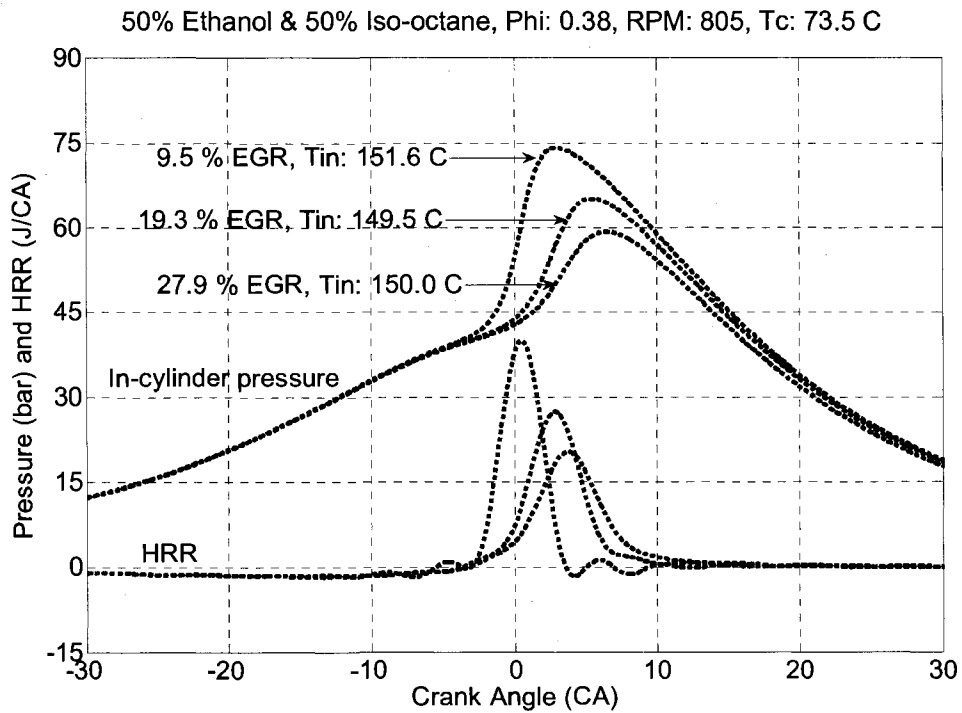


Figure 5.17: Cylinder pressure and rate of heat release with different EGR levels (805 RPM, 50% Ethanol and 50% Iso-octane, phi: 0.38).

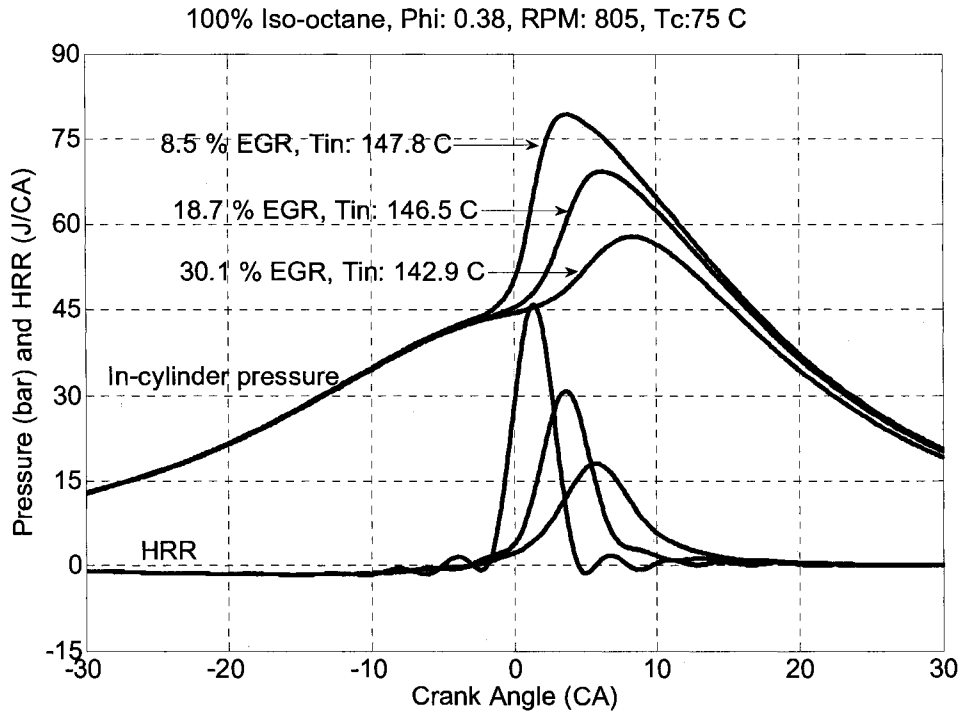


Figure 5.18: Cylinder pressure and rate of heat release with different EGR levels (805 RPM, 100% Iso-octane, phi: 0.38).

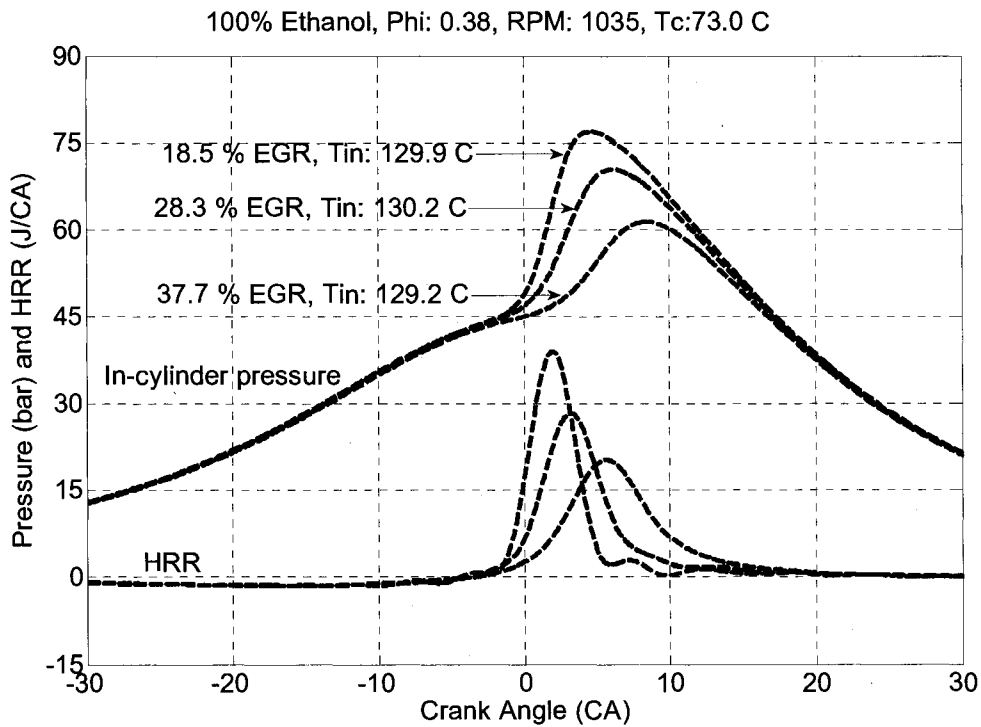


Figure 5.19: Cylinder pressure and rate of heat release with different EGR levels (1035 RPM, 100% Ethanol, phi: 0.38).

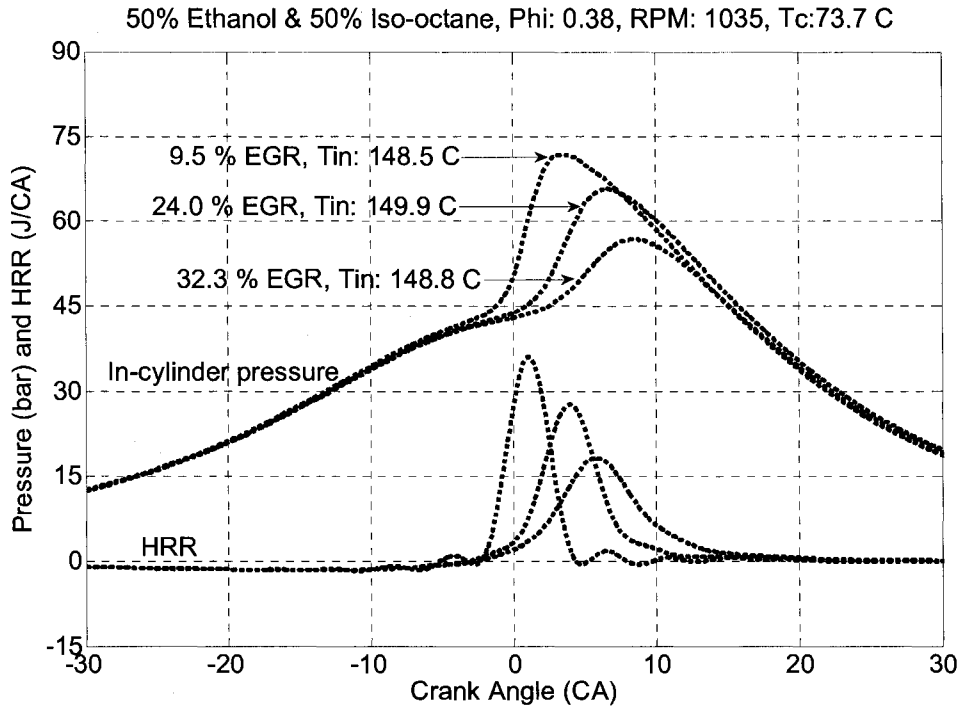


Figure 5.20: Cylinder pressure and rate of heat release with different EGR levels (1035 RPM, 50% Ethanol and 50% Iso-octane, phi: 0.38).

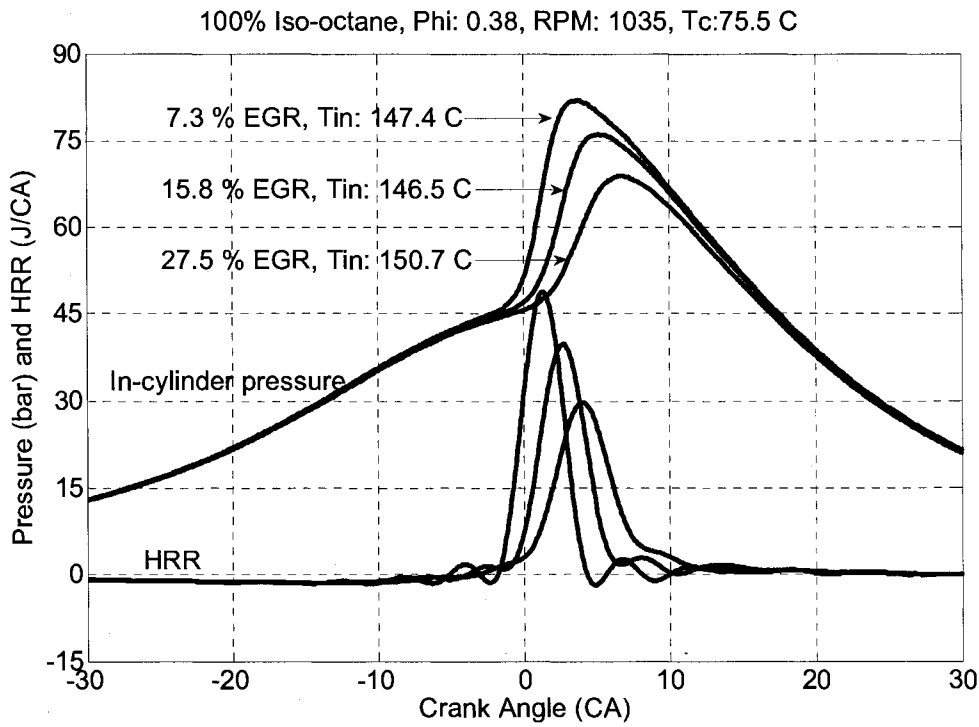


Figure 5.21: Cylinder pressure and rate of heat release with different EGR levels (1035 RPM, 100% Iso-octane, phi: 0.38).

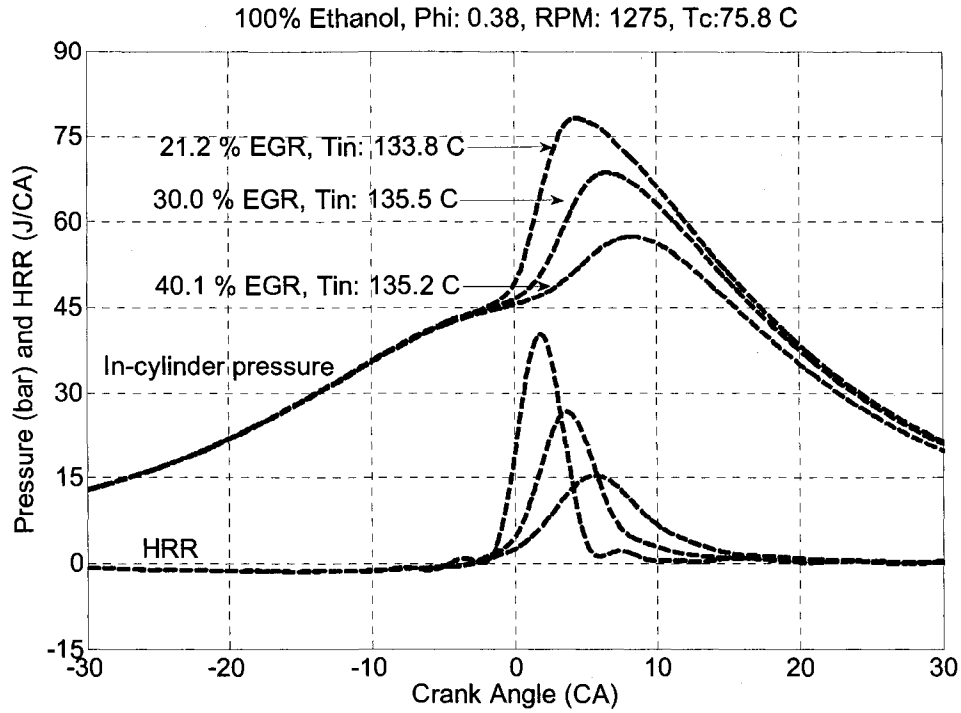


Figure 5.22: Cylinder pressure and rate of heat release with different EGR levels (1275 RPM, 100% Ethanol, phi: 0.38).

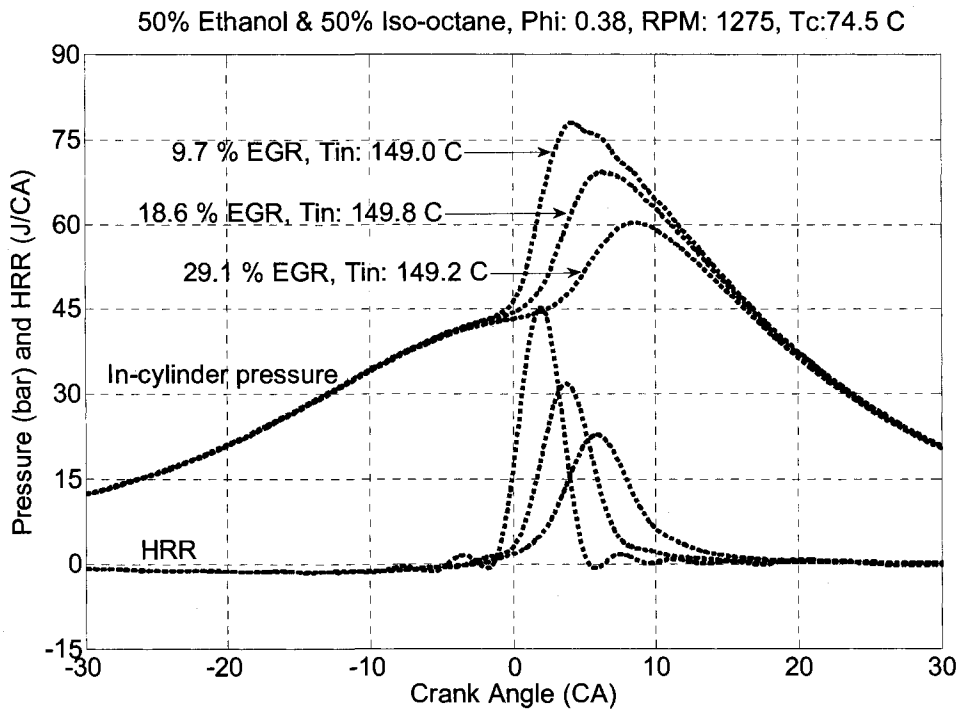


Figure 5.23: Cylinder pressure and rate of heat release with different EGR levels (1275 RPM, 50% Ethanol and 50% iso-octane, phi: 0.38).

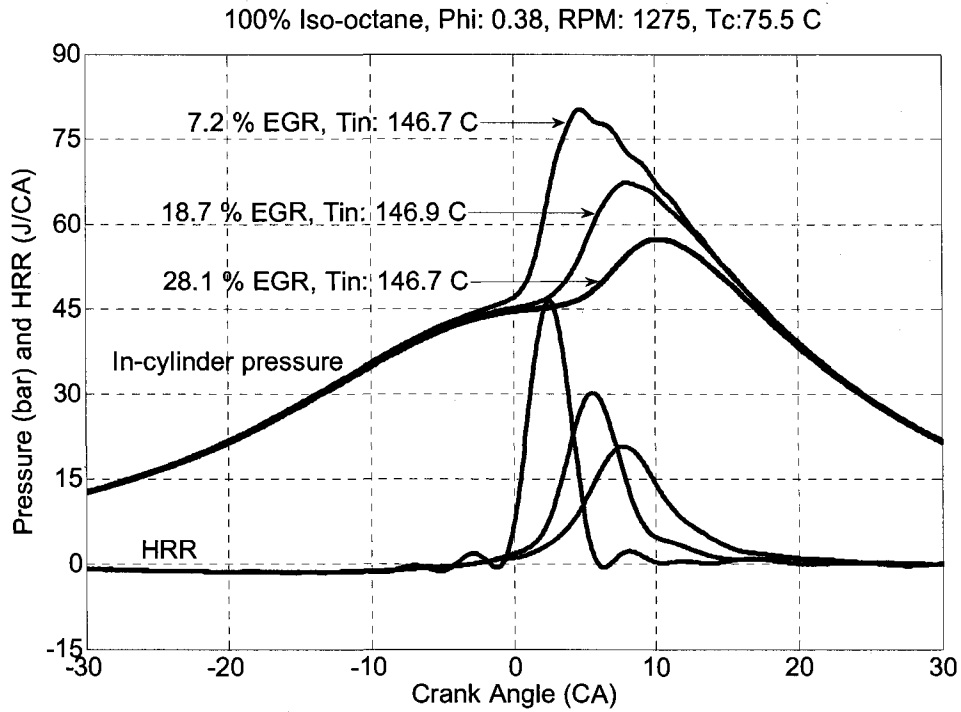


Figure 5.24: Cylinder pressure and rate of heat release with different EGR levels (1275 RPM, 100% Iso-octane, phi: 0.38).

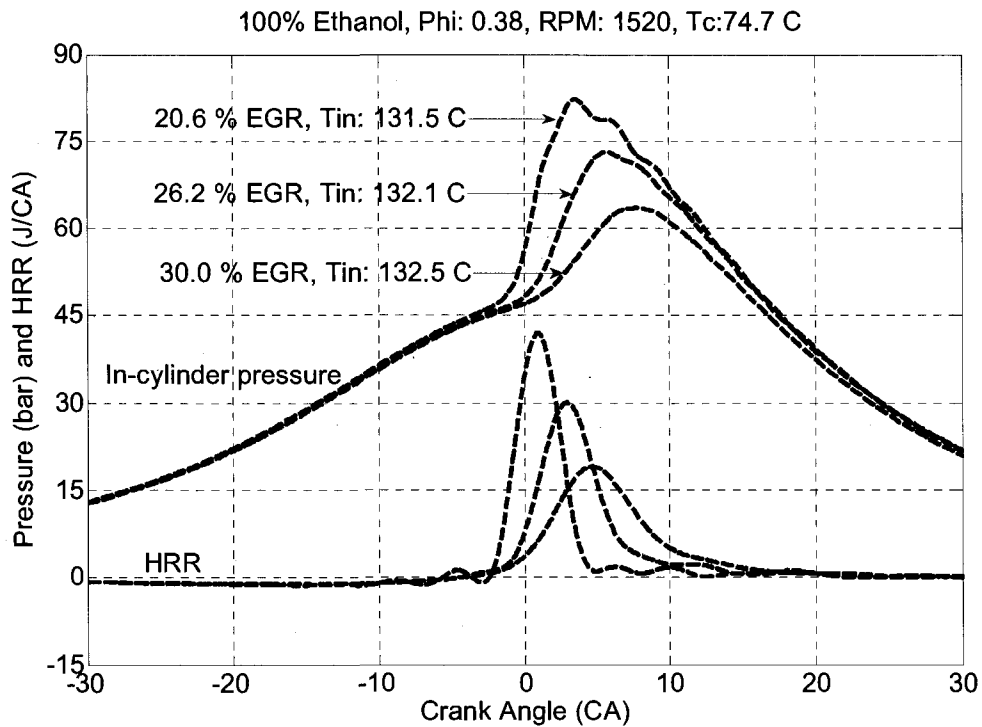


Figure 5.25: Cylinder pressure and rate of heat release with different EGR levels (1520 RPM, 100% Ethanol, phi: 0.38).

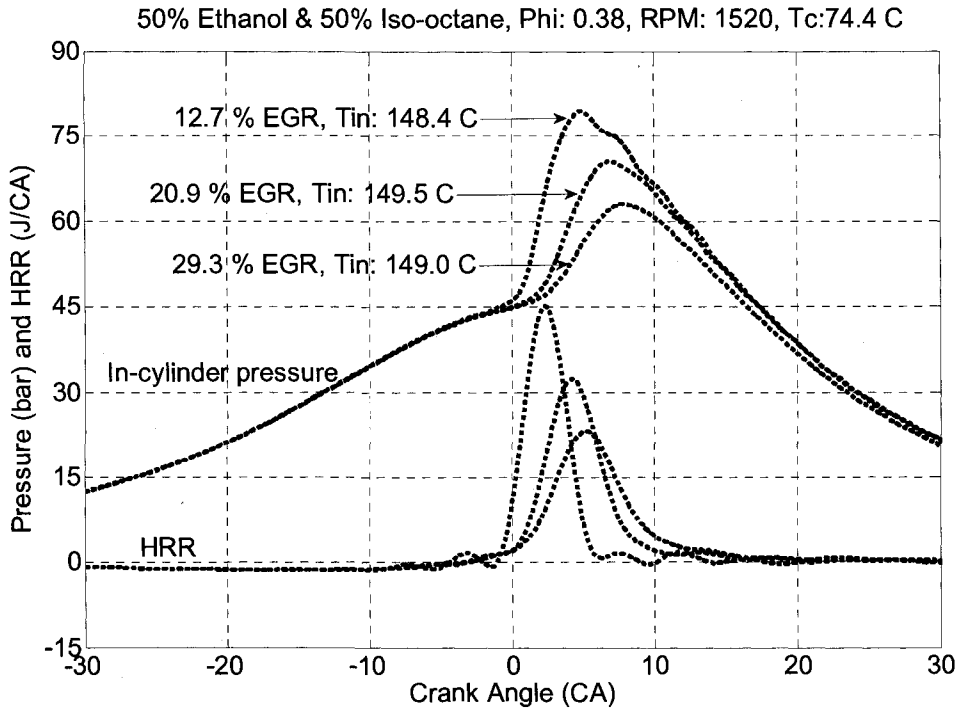


Figure 5.26: Cylinder pressure and rate of heat release with different EGR levels (1520 RPM, 50% Ethanol and 50% Iso-octane, phi: 0.38).

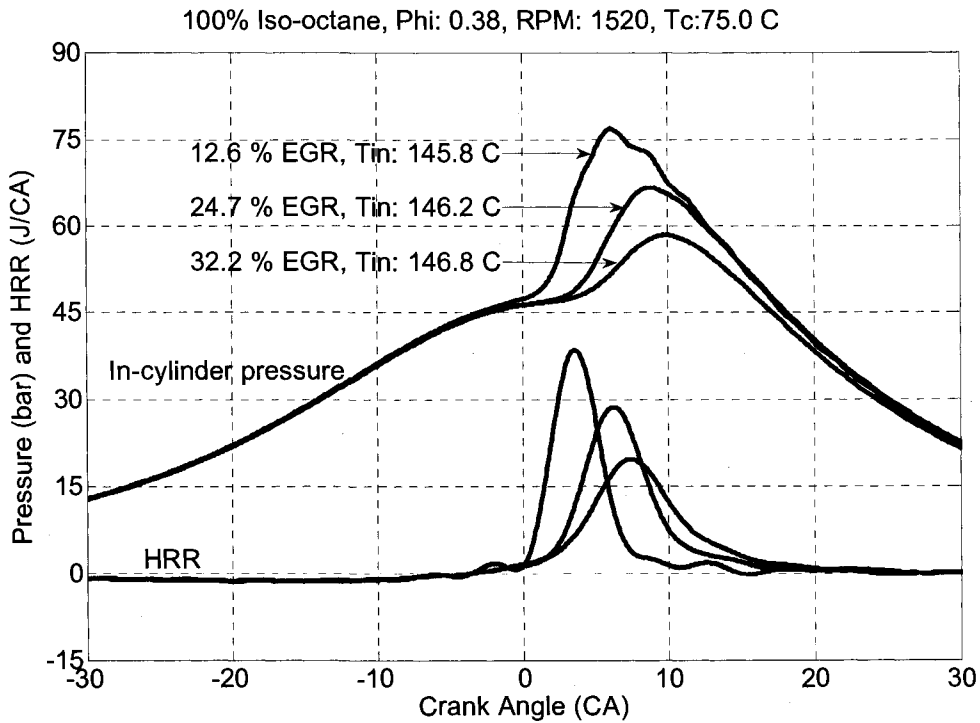


Figure 5.27: Cylinder pressure and rate of heat release with different EGR levels (1520 RPM, 100% Iso-octane, phi: 0.38).

From Figures 5.16 through 5.27 it can be also noted that the higher equivalence ($\phi = 0.38$) results in a higher peak pressure and higher peak HRR value compared to that of $\phi = 0.33$ for the same EGR percentage addition and intake charge temperature condition. For example, in the case of pure ethanol ($\phi = 0.38$) for the 805 RPM and 22.8% EGR addition (Fig. 5.16) the peak pressure and HRR obtained is 72 bar and 30 J/CA. Whereas, for the same fuel with $\phi = 0.33$ and similar EGR addition (22.5%), the peak pressure and HRR values obtained are 63 bar and 20 J/CA (Fig. 5.1). Similar trends were also seen for the other types of fuels analyzed. For instance, the peak pressure and HRR for blend (1275 RPM and 9.7% EGR) with $\phi = 0.38$ (Fig. 5.23) are 76 bar and 47 J/CA. While for the same fuel at similar operating conditions with 9.7% EGR addition and $\phi = 0.33$ (Fig. 5.8), the peak pressure and HRR drops to 67 bar and 28 J/CA. This behavior is expected since more fuel enters the combustion process at the higher equivalence ratio (for the same percentage EGR addition) resulting in higher peak pressure values.

Similar to the previous case ($\phi = 0.33$) the 0.38 equivalence ratio condition also shows no presence of engine ringing at lower engine speeds (805 and 1035 RPM). With higher RPM conditions (1275 and 1520 RPM) there are distinguishable oscillations in the pressure curve that signifies engine ringing similar to $\phi = 0.33$. For the lower equivalence ratio ($\phi = 0.33$) the oscillations in the pressure signal were prominent only for the 1520 RPM condition irrespective of the fuel type tested (Fig. 5.10). However, with higher equivalence ratio ($\phi = 0.38$) it can be seen that the 1275 RPM condition (Fig. 5.23 and 5.24) also shows the presence of engine ringing, especially for the pure iso-octane and blend where the percentage EGR addition are low. This again points out that

the percentage EGR addition is critical in eliminating the presence of engine ringing and moderating the in-cylinder and HRR profiles.

5.2.4 10% HR CA and 10-90% HR CA duration ($\phi = 0.38$):

Figures 5.28 through 5.30 show the CA corresponding to the 10% HR (on-set of combustion) and the heat release (HR) duration in CA from 10% and 90% HR for fuel-air equivalence ratio of 0.38 for different operating conditions. As mentioned earlier in the case of $\phi = 0.33$, it is noted from Figures 5.28 through 5.30 that the addition of EGR delays the 10% HR CA (on-set of combustion) and increases the duration for all the fuels and RPM conditions. An interesting trend in Figures 5.28 through 5.30 is that irrespective of the fuel type used, for a constant percentage EGR addition, the combustion on-set advances and the HR duration decreases with an increase in equivalence ratio. For example, in the case of ethanol with $\phi = 0.33$ and 20% EGR addition (Fig. 5.13), the on-set of combustion is at around 1 CA ATDC and the HR duration is around 7 – 10 CA for the tested RPM range. While for the same operating conditions with $\phi = 0.38$ (Fig. 5.28) the combustion on-set is at TDC and the HR duration decreases to 6 – 7 CA. This effect can be also seen in the case of pure iso-octane and the blend (Fig. 5.29 and 5.30).

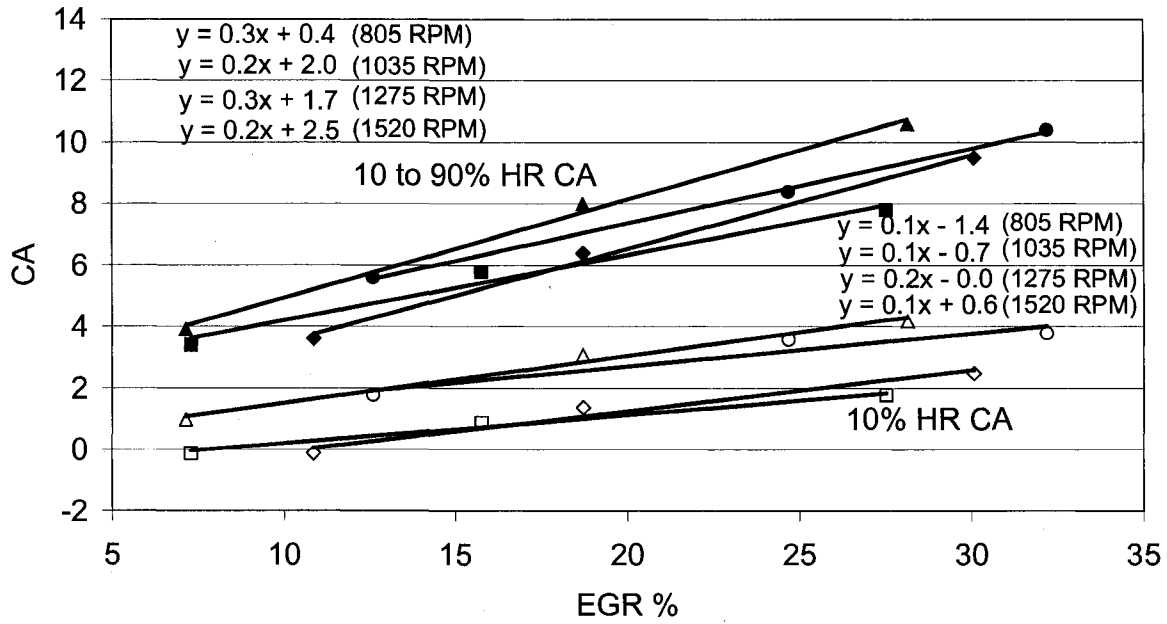


Figure 5.28: 10% Heat Release CA and CA duration for 10% to 90% Heat Release for different EGR levels and RPM (100% Ethanol, ϕ : 0.38).

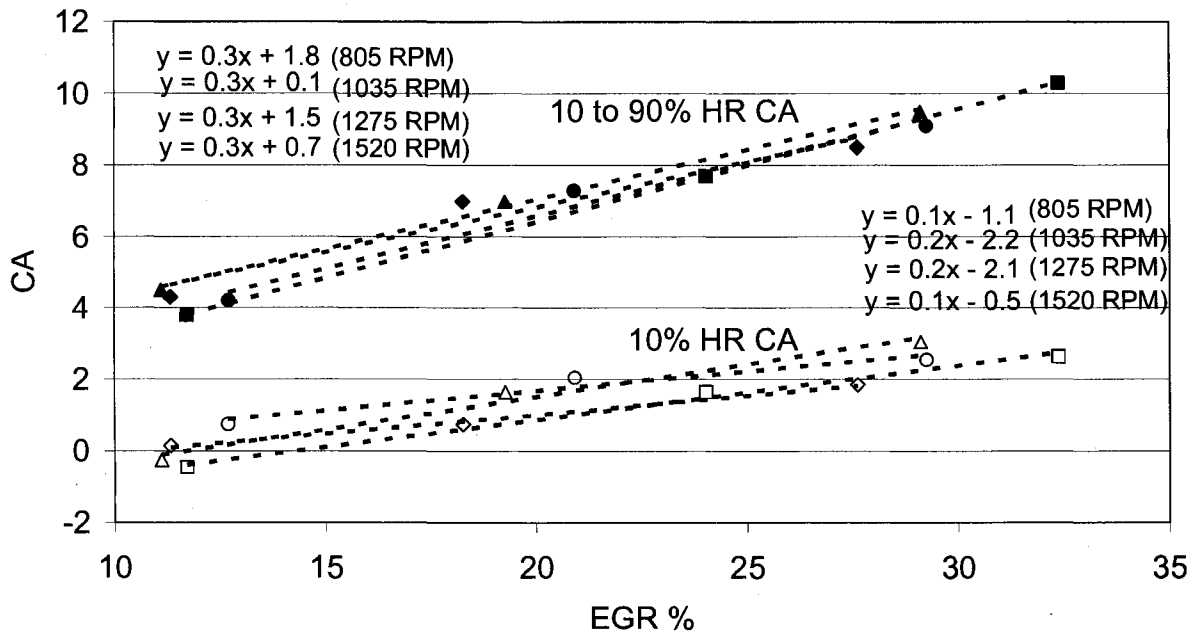


Figure 5.29: 10% Heat Release CA and CA duration for 10% to 90% Heat Release for different EGR levels and RPM (50% Ethanol and 50% Iso-octane, ϕ : 0.38).

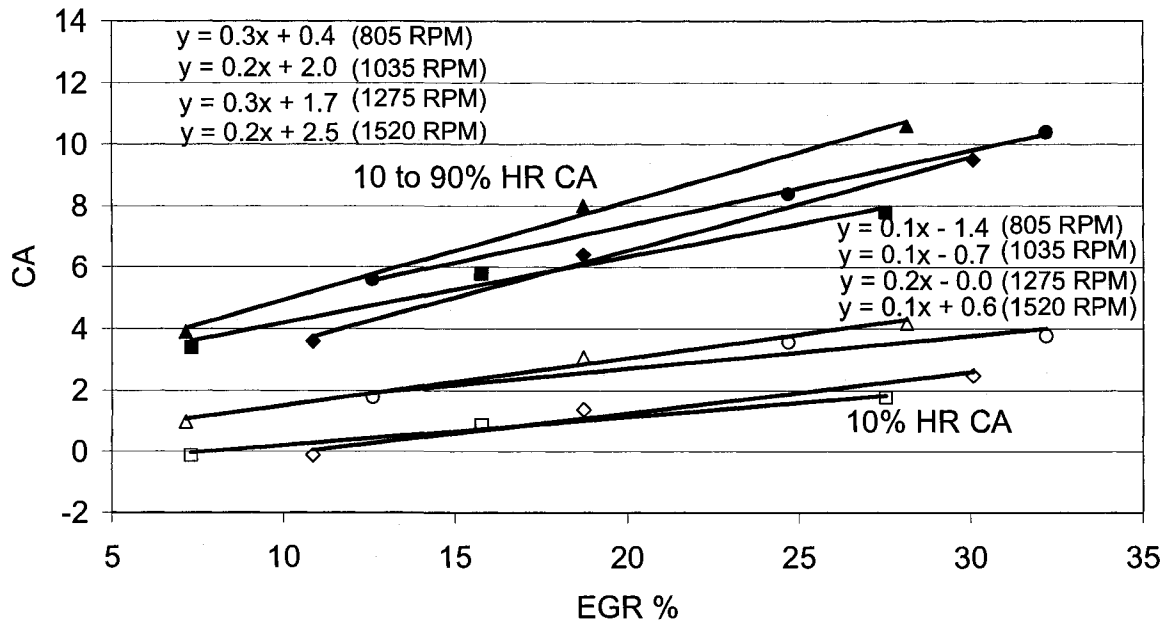


Figure 5.30: 10% Heat Release CA and CA duration for 10% to 90% Heat Release for different EGR levels and RPM (100% Iso-octane, ϕ : 0.38).

Another interesting trend with increase in equivalence ratio is that the 10% HR CA (combustion on-set) and the HR duration do not change significantly with change of RPM for ethanol and the blend (Fig. 5.28 and 5.29). The only fuel that shows significant change in 10% HR CA with increase in RPM is pure iso-octane (Fig. 5.30). The combustion on-set (10% HR) is delayed for the higher RPM conditions (1275 and 1520 RPM) compared to the lower RPM conditions (805 and 1035 RPM). However, the HR duration does not show any significant difference with respect to RPM as in the case of $\phi = 0.33$ (Fig. 5.15). This effect can also be confirmed when comparing the 10% HR and HR duration for the blend with different equivalence ratio. For $\phi = 0.33$ (Fig. 5.14), it can be seen that there is delayed combustion on-set (10% HR CA) with an increase in RPM, but with increase in equivalence ratio ($\phi = 0.38$) this effect is eradicated. This shows that the reaction rates for iso-octane are sensitive to the fuel-air equivalence ratio and with

increase in an equivalence ratio, the effect of engine speed on reaction rates during the early (10% HR) and regular combustion (10 – 90% HR) is eliminated.

5.2.5 IMEP and COV_{IMEP} ($\phi = 0.33$):

Figures 5.31 through 5.33 show the IMEP and the Coefficient of Variation of IMEP (COV_{IMEP}) for $\phi = 0.33$ for various operating conditions. The IMEP reported here are the net values that include pumping losses. The IMEP values in general decrease with EGR addition for a given RPM condition. This reduction in IMEP with can be linked to two factors: reduction in the amount of charge which is replaced by EGR and decrease in the quality of combustion. The latter is evident in Section 5.2.9, where it will be noted that CO levels increase with percentage EGR addition, irrelevant of the type of fuel and RPM condition. Furthermore, for a particular engine speed and EGR condition, the drop in IMEP with EGR addition for 100% ethanol (Fig. 5.31) is less when compared to either a 50% ethanol/iso-octane blend (Fig. 5.32) or 100% iso-octane (Fig. 5.33). This clearly indicates that ethanol is more tolerant to EGR than iso-octane.

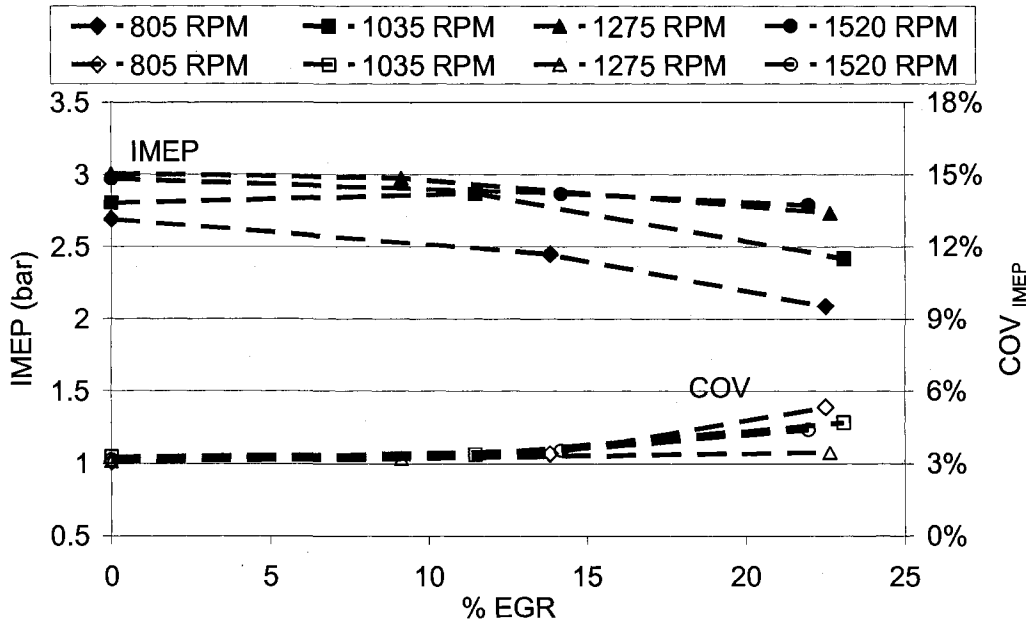


Figure 5.31: IMEP and COV_{IMEP} for different EGR levels and RPM (100% Ethanol, phi: 0.33).

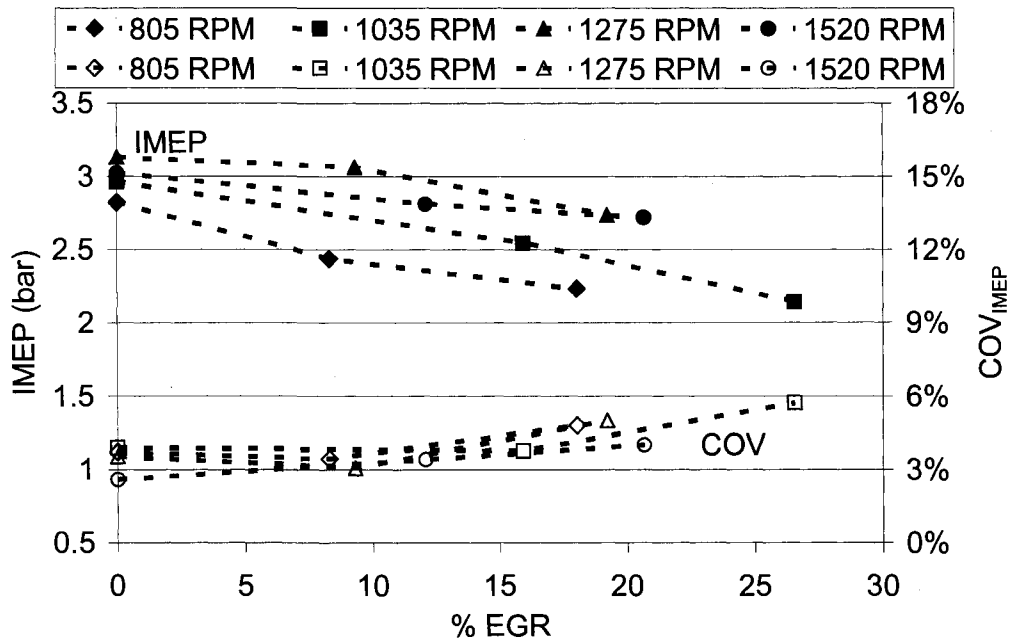


Figure 5.32: IMEP and COV_{IMEP} for different EGR levels and RPM (50% Ethanol & 50% iso-octane, phi: 0.33).

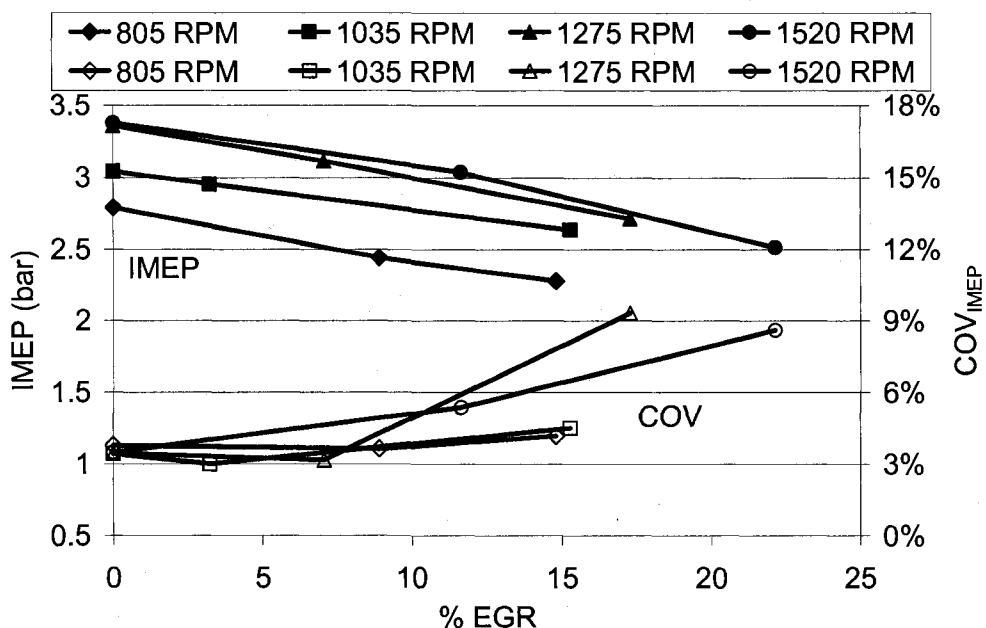


Figure 5.33: IMEP and COV_{IMEP} for different EGR levels and RPM (100% Iso-octane, phi: 0.33).

An interesting trend in the IMEP curves emerges when comparing the 0% EGR condition for the different fuels tested. The IMEP increases with engine speed irrelevant of the type of fuel used. It should be noted that the volumetric efficiency for a given intake temperature condition drops by 6% when the engine speed is increased from 805 to 1520 RPM. Hence, the amount of intake charge per cycle does not change significantly with increasing engine speed. From engine-out emission results in Section 5.2.9, the combustion quality also does not improve significantly with increased engine speeds. Hence, the only factor that affects the IMEP is heat transfer losses. From the results obtained, it appears that the residence time of the in-cylinder charge and hence the heat transfer losses decrease with increasing engine speed and result in improved IMEP of the engine. Furthermore, the increase in IMEP with increase in RPM is well represented by results for the pure iso-octane and less pronounced in the results for the 50% ethanol/iso-

octane blend. For pure iso-octane the IMEP values are close to 3.4 bar at higher RPM conditions (Fig. 5.33) compared to 3 bar obtained for 50% ethanol/iso-octane blend (Fig. 5.32). This is primarily due to the longer combustion duration in the case of pure iso-octane (Fig. 5.15) compared to the 50% ethanol/iso-octane blend (Fig. 5.14) during these RPM conditions. This in effect moderates the HRR and results in lower peak pressure values (Figures 5.8 through 5.11). Lower peak pressure values will contribute to lower peak temperature within the combustion chamber and reduced heat transfer losses. Even though ethanol shows better combustion characteristics, the heat transfer loss plays a more important role in achieving higher IMEP values in this IDI-type engine than quality of combustion.

From Figures 5.31 through 5.33 it can be noted that there is increase in the COV_{IMEP} values after 10% EGR addition regardless of the fuel types used. Furthermore, the increase in the COV_{IMEP} values are less when fuelled with ethanol compared to iso-octane, specifically for the higher RPM conditions. For example, the maximum COV_{IMEP} for the 50% ethanol/iso-octane blend (Fig. 5.32) stays within 6% for the 1275 and 1520 RPM. For the same operating conditions the COV_{IMEP} values are around 9% when fuelled with iso-octane. For most of the test conditions that produce the highest IMEP values and also for the conditions that are close to the highest IMEP values, irrelevant of the fuel type used, the COV_{IMEP} remains less than 4%, within the stable operating region. The notable exception is for ethanol at 805 rpm where it is 5%. Similar values were seen for a richer mixtures (ϕ - 0.8 to 1) with very high amounts of trapped residual gas at 1500 RPM in Zhang et al (2006). In the same paper, the authors also reported a sharp increase

in the COV_{IMEP} with the leanest mixture studied ($\phi = 0.8$). In our experiments the mixture was very lean compared to those of Zhang et al (2006) and still the COV_{IMEP} stayed below 4%. One of the reasons for stable operation can be due to presence of the pre-chamber in this IDI type engine, where there is trapped residual mass that acts as an ignition source for subsequent cycles.

5.2.6 IMEP and COV_{IMEP} ($\phi = 0.38$):

Figures 5.34 through 5.36 depict the IMEP and the Coefficient of Variation of IMEP (COV_{IMEP}) for $\phi = 0.38$ for various operating conditions. Similar to the $\phi = 0.33$ condition the IMEP values in general decrease with EGR addition for a given RPM condition. Also, the trend of an increase in the IMEP with increasing engine speed irrelevant of the type of fuel used is also seen here for the higher equivalence ratio, similar to $\phi = 0.33$. Comparing Figures 5.31 through 5.33 ($\phi = 0.33$) with Figures 5.34 through 5.36 ($\phi = 0.38$) it can be noted that for the same level of EGR addition, a higher equivalence ratio leads to a higher IMEP value for the fuels tested. For example, in the case of pure ethanol $\phi = 0.33$ for the 20% EGR condition (Fig. 5.31) gives a IMEP value of 2.25 to 2.75 bar. While for the same 20% EGR condition with $\phi = 0.38$ (Fig. 5.34), the IMEP value obtained is 2.75 to 3.25 bar. This effect is also confirmed when comparing the pure iso-octane and the blend.

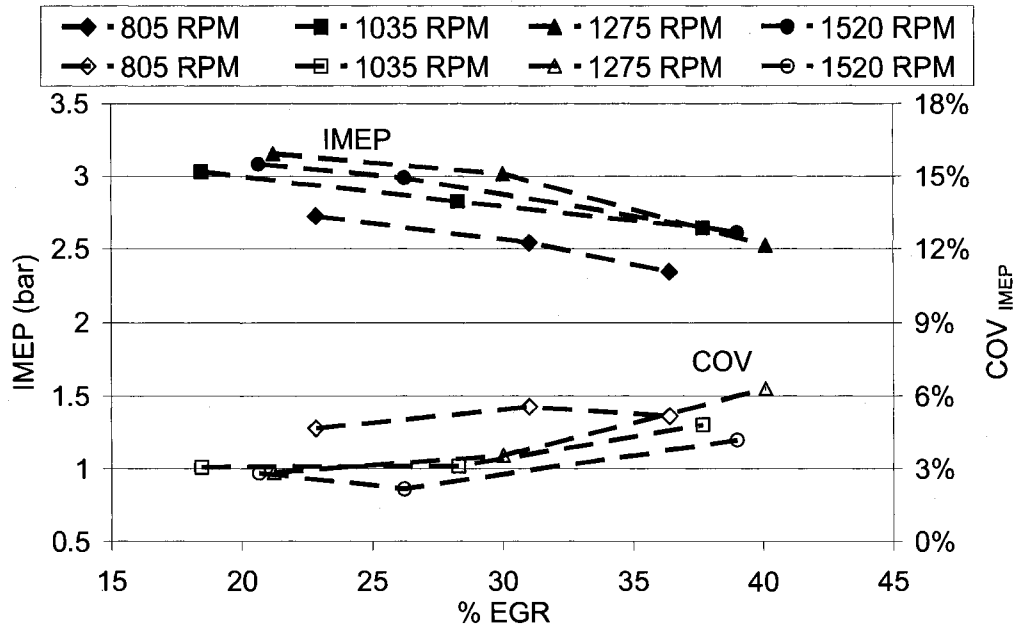


Figure 5.34: IMEP and COV_{IMEP} for different EGR levels and RPM (100% Ethanol, phi: 0.38).

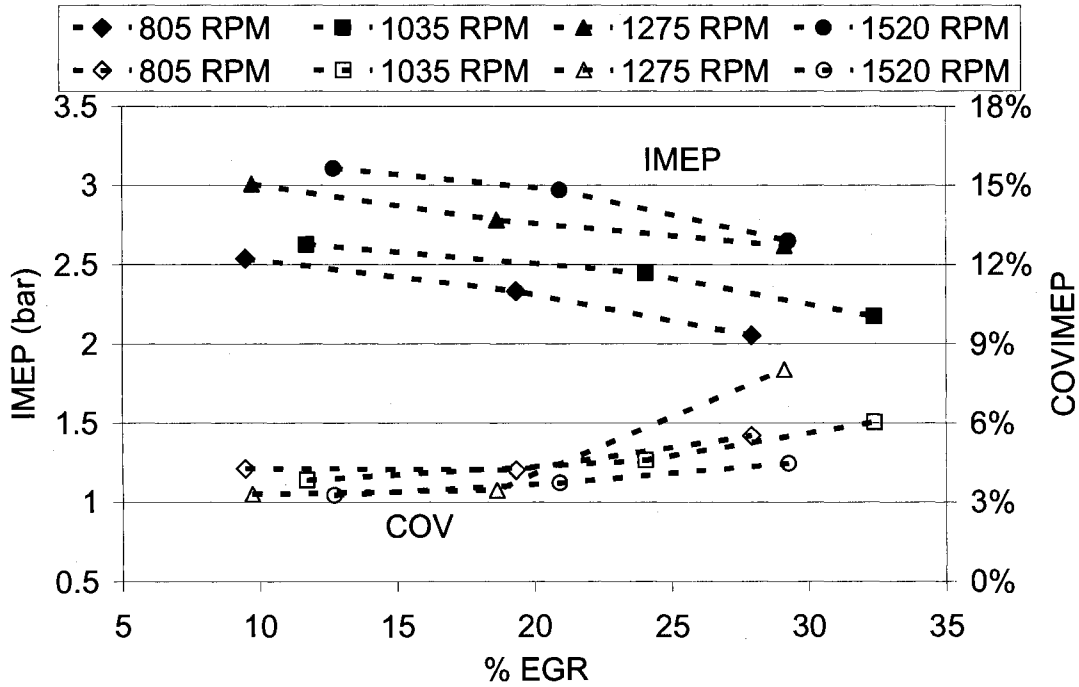


Figure 5.35: IMEP and COV_{IMEP} for different EGR levels and RPM (50% Ethanol and 50% Iso-octane, phi: 0.38).

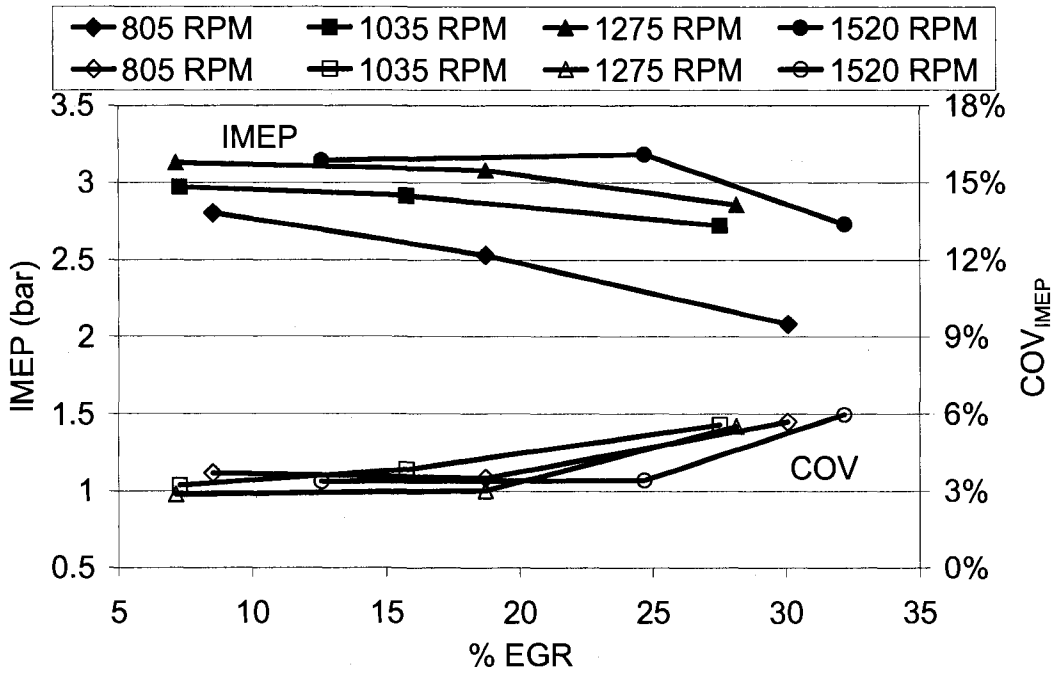


Figure 5.36: IMEP and COV_{IMEP} for different EGR levels and RPM (100% Iso-octane, ϕ : 0.38).

Furthermore, the COV_{IMEP} values for $\phi = 0.38$ (Fig. 5.34 through 5.36) remain below 6% for most of the test conditions. The notable exception is for the 50% ethanol and 50% iso-octane blend with 30% EGR where the COV_{IMEP} is 8%. There is also an interesting trend in the case of pure iso-octane when comparing the COV_{IMEP} for different equivalence ratio. From Figure 5.33 it can be noted that the peak COV_{IMEP} values for $\phi = 0.33$ at higher RPM conditions (1275 and 1520 RPM) are closer to 9% and the trend shows that any increase in EGR level above 12% leads to COV_{IMEP} values above 6%. However, when looking into the COV_{IMEP} values for $\phi = 0.38$, it can be noted that for pure iso-octane (Fig. 5.36) the values are less than 6% for EGR levels up to 30%. This shows that with an increase in equivalence ratio, lower COV_{IMEP} values can be attained even with higher EGR levels.

5.2.7 Thermal efficiency and maximum pressure rise rate ($\phi = 0.33$):

Figures 5.37 through 5.39 depict the thermal efficiency and the maximum pressure rise rates for the various fuels at different operating conditions for $\phi = 0.33$. The thermal efficiency is calculated as the ratio of net indicated work to product of fuel inducted per cycle and lower heating value of fuel [$\eta_{th} = W_{NET} / (HV * m_{fuel})$]. The thermal efficiency increases with engine speed irrelevant of the type of fuel used and is between 28% and 42%. The thermal efficiency in general either increases or stays constant with percentage EGR addition. This is interesting since the combustion quality reduces (CO increases) with EGR addition (Section 5.2.9). This is again due to the low heat transfer losses that result from moderate HRR profiles and low peak pressures with EGR addition. The best thermal efficiency values (29% – 35%) and best IMEP for pure ethanol ($\phi = 0.33$) are obtained for the 10% EGR condition (Fig. 5.37). In the case of pure iso-octane ($\phi = 0.33$, Fig. 5.39), the best thermal efficiency (30% - 40%) and best IMEP values are obtained for the 0% EGR condition. For 50% ethanol/iso-octane blend ($\phi = 0.33$) thermal efficiency (32% - 36%) and best IMEP values are also obtained for the 0% EGR condition (Fig. 5.38). The net indicated thermal efficiencies reported in Christensen et al. (1999) for similar lean charges of ethanol and iso-octane were about 38% and 40% (the compression ratio used in that study was 18 and the equivalence ratio used were $\phi = 0.35$ for iso-octane and $\phi = 0.33$ for ethanol). The efficiency values reported here are lower than that of Christensen et al. (1999) because of the IDI type engine used here that has higher heat transfer losses.

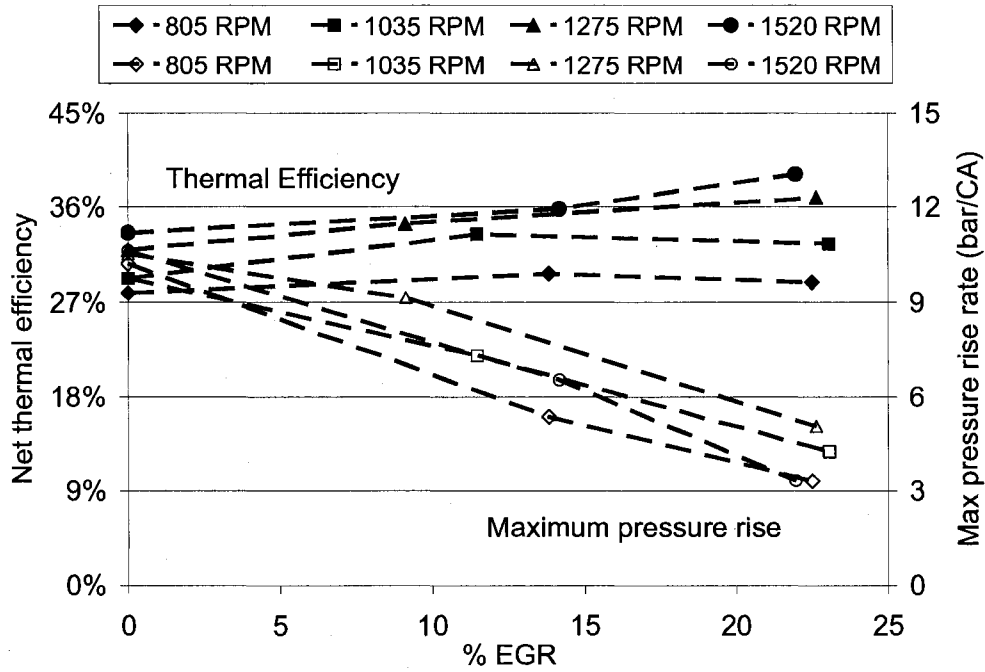


Figure 5.37: Net thermal efficiency and Maximum pressure rise rate for different EGR levels and RPM (100% Ethanol, ϕ : 0.33).

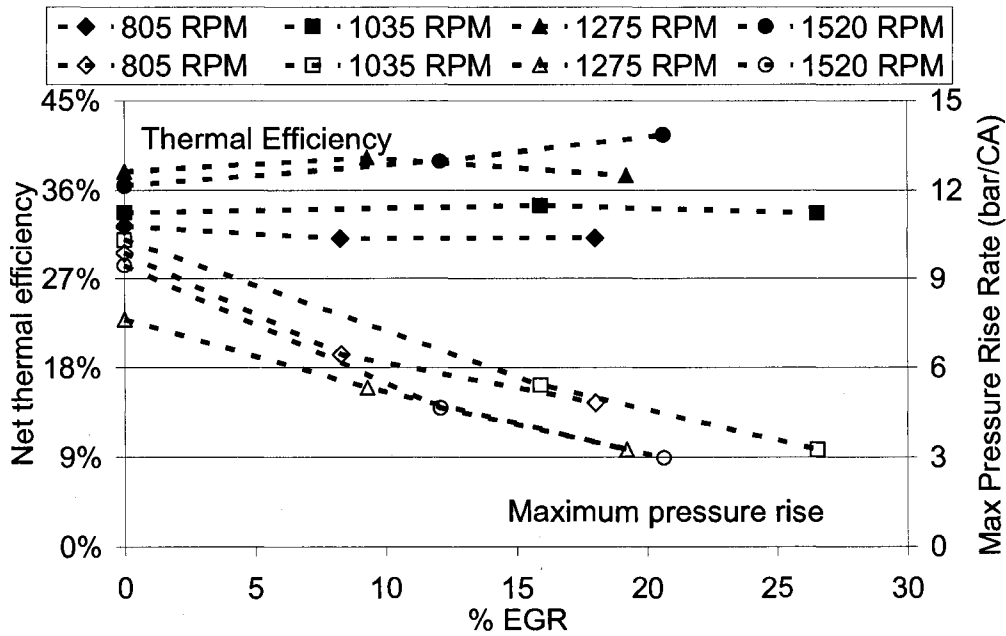


Figure 5.38: Net thermal efficiency and Maximum pressure rise rate for different EGR levels and RPM (50% Ethanol & 50% iso-octane, ϕ : 0.33).

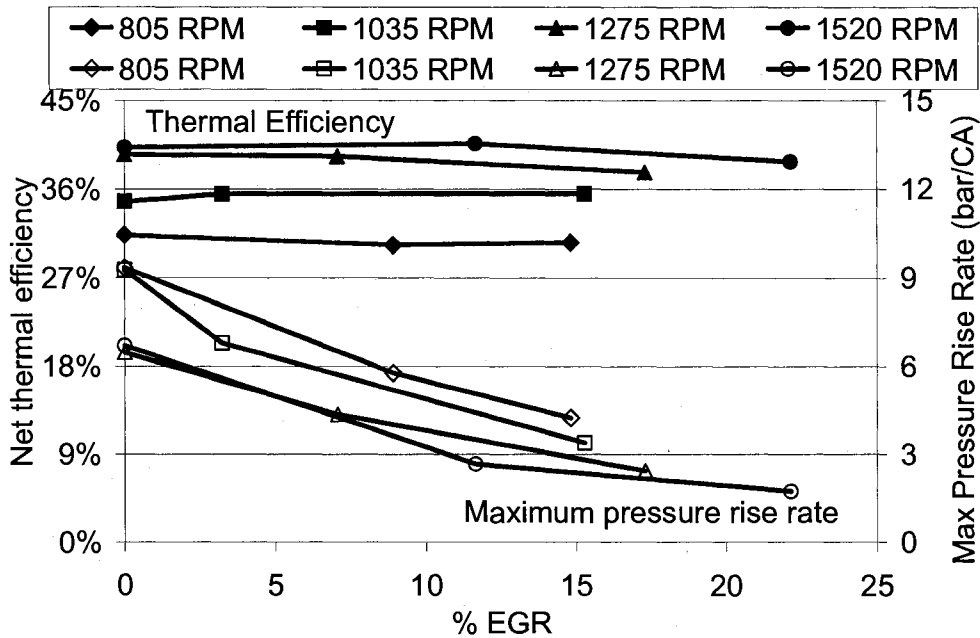


Figure 5.39: Net thermal efficiency and Maximum pressure rise rate for different EGR levels and RPM (100% Iso-octane, ϕ : 0.33).

Another interesting trend can be identified in Figures 5.38 and 5.39 for the 0% EGR and $\phi = 0.33$ condition at higher engine speeds. For 50% ethanol/iso-octane blend (Fig. 5.38) the thermal efficiency values at higher RPM conditions with no EGR and $\phi = 0.33$ are about 37%. However, for the same RPM conditions with no EGR, the thermal efficiency values for 100% iso-octane (Fig. 5.39) are about 40%. From Figures 5.44 and 5.45 it is clear that the 50% ethanol/iso-octane blend shows better combustion characteristics (less CO and UHC) compared to 100% pure iso-octane for the above mentioned operating conditions. Hence, the increase in thermal efficiency values for 100% pure iso-octane are not due to improvement in the combustion quality. The improvements in the thermal efficiency are due to the reaction rates when fuelling with pure iso-octane. As mentioned earlier, the combustion on-set (10% HR) is delayed and the HR duration increases for the

higher RPM conditions when fuelled with iso-octane. This leads to lower maximum pressure rise rates (Figures 5.38 and 5.39) and peak pressure values that subsequently reduces net heat transfer losses. The reduced heat transfer losses result in increased thermal efficiency even though the emissions deteriorate for these operating conditions (1275 and 1520 RPM, 100% iso-octane). This shows that reaction rates and residence time plays a major role in the thermal efficiency of HCCI combustion at higher RPM conditions.

The maximum pressure rise rate for all the tested conditions for $\phi = 0.33$ are generally within 10 bar/CA which is within the acceptable range (discussed in Chapter 4). In general, the maximum pressure rise rate decreases with EGR addition for a given fuel irrespective of the engine speed. This shows that moderate pressure rise rates at higher equivalence ratios can be obtained by using EGR. Furthermore, for a given EGR condition there is no significant difference in the maximum pressure rise rates with respect to RPM in the case of pure ethanol ($\phi = 0.33$). Whereas, in the case of pure iso-octane ($\phi = 0.33$) the maximum pressure rise rates dropped with increase in engine speed for a particular EGR condition (Fig. 5.39). This is again due to the longer HR duration at higher engine speeds for iso-octane compared to ethanol.

5.2.8 Thermal efficiency and maximum pressure rise rate ($\phi = 0.38$):

Figures 5.40 through 5.42 show the thermal efficiency and the maximum pressure rise rates for the various fuels at different operating conditions for $\phi = 0.38$. Similar to the previous case ($\phi = 0.33$), the thermal efficiency increases with engine speed irrelevant of

the type of fuel used and is between 27% and 42%. Furthermore, the trend with percentage EGR addition and thermal efficiency (where the efficiency in general either increases or stays constant) is also seen for the higher equivalence ratio. There is an also interesting trend when comparing the two equivalence ratio for different fuels. From Figure 5.34 and 5.40 it can be noticed that the $\phi = 0.38$ condition with 20% EGR gives a higher IMEP value and better thermal efficiency value than the maximum value obtained with $\phi = 0.33$ and 0% EGR condition (Fig. 5.31 and 5.37). Whereas, in the case of pure iso-octane (Fig. 5.33 and 5.39) and the blend (Fig. 5.32 and 5.38), the best IMEP and thermal values obtained were for the $\phi = 0.33$ and 0% EGR condition, when comparing the two equivalence ratios. This shows that fuel chemistry and the level of EGR plays a vital role in shaping the pressure and HRR profiles that contribute to maximum IMEP attained.

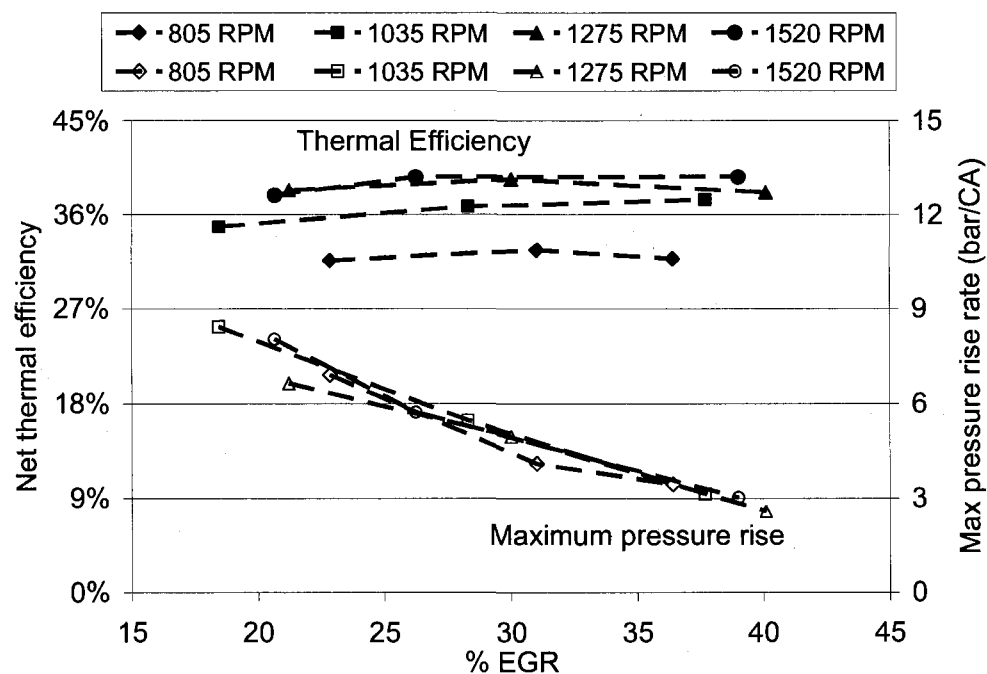


Figure 5.40: Net thermal efficiency and Maximum pressure rise rate for different EGR levels and RPM (100% Ethanol, $\phi = 0.38$).

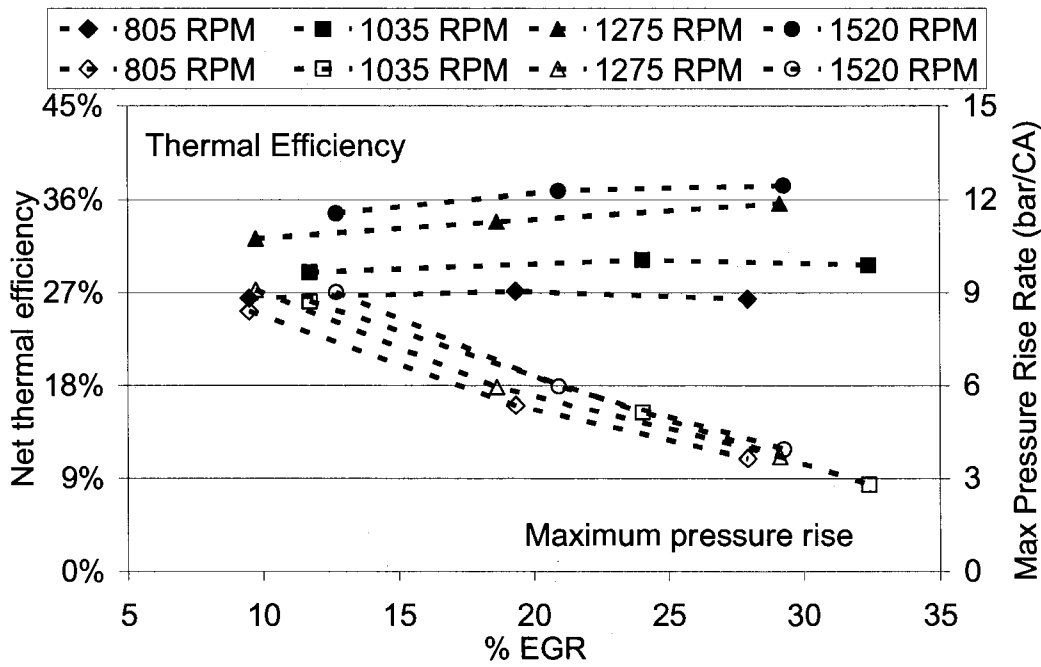


Figure 5.41: Net thermal efficiency and Maximum pressure rise rate for different EGR levels and RPM (50% Ethanol and 50% Iso-octane, phi: 0.38).

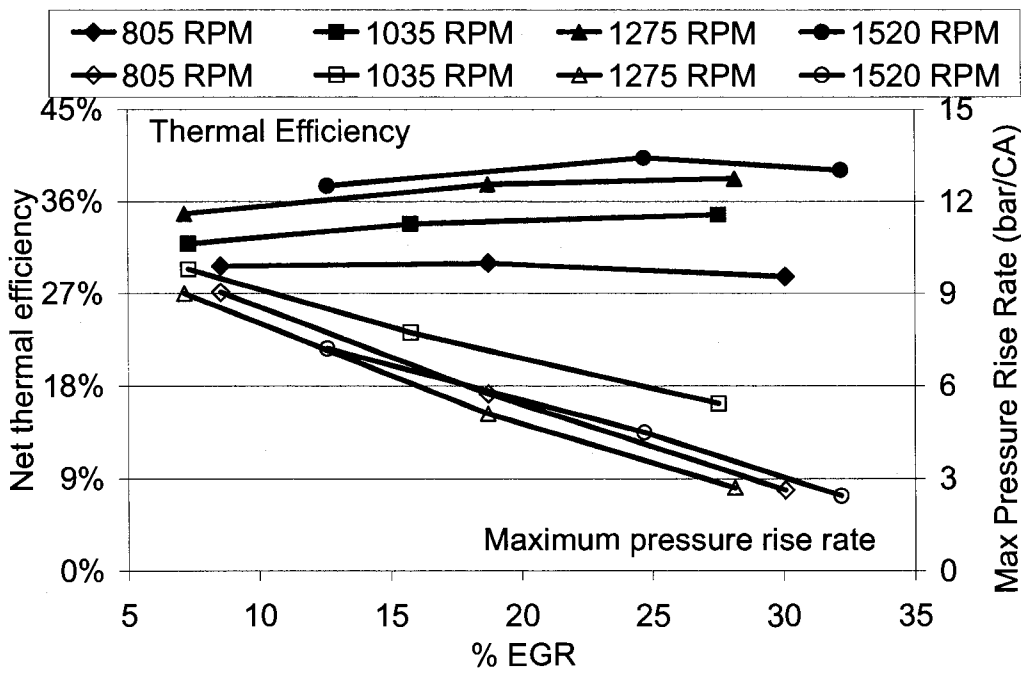


Figure 5.42: Net thermal efficiency and Maximum pressure rise rate for different EGR levels and RPM (100% Iso-octane, phi: 0.38).

From Figure 5.40 through 5.42, it can be noted that the maximum pressure rise rate in the case of $\phi = 0.38$ are under 10 bar/CA for all the tested conditions. Similar to the previous condition ($\phi = 0.33$), the maximum pressure rise rate decreases with EGR addition for a given fuel irrespective of the engine speed. Furthermore, in the case of $\phi = 0.38$ there is no major difference in the maximum pressure rise rates with respect to RPM for all the tested fuels. This is in contrast to the previous case ($\phi = 0.33$) where the maximum pressure rise rates dropped with an increase in engine speed for a particular EGR condition in the case of pure iso-octane (Fig. 5.39). This change in trend again shows that the reaction rates for iso-octane are sensitive to the fuel-air equivalence ratio and with an increase in equivalence ratio, the effect of engine speed on reaction rates during the early (10% HR) and regular combustion (10 – 90% HR) are eliminated.

5.2.9 CO and UHC:

Figures 5.43 through 5.48 show the carbon monoxide (CO) and non-methane unburned hydrocarbon (UHC) engine-out emissions for both the equivalence ratios ($\phi = 0.33$ and $\phi = 0.38$) at all the operating conditions. The oxides of nitrogen (NO_x) are not reported since the maximum value read is less than 10ppm for the duration of these tests conditions. This shows that near-zero NO_x emissions can be obtained using a lean charge. Similar results of NO_x for the equivalence ratio of 0.321 were reported in Van et al., 1998, for iso-octane. It should be noted that the UHC levels reported here are in terms of percentage intake fuelling. In general, the CO and UHC levels are high and would require exhaust gas after-treatment. Again, these high levels in CO and UHC emissions might be due to the IDI type of engine being used here, which has greater heat losses that

contribute to incomplete combustion especially closer to the cylinder walls. However, similar levels of UHC and CO for iso-octane are reported in Van et al., 1998.

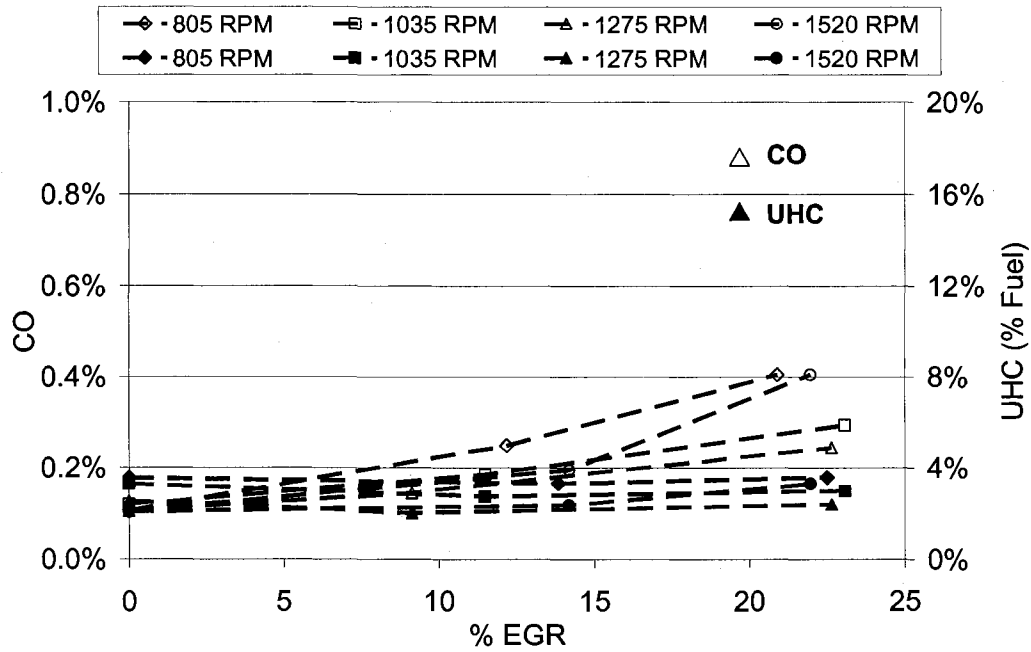


Figure 5.43: CO and UHC for different EGR levels and RPM (100% Ethanol, $\phi = 0.33$).

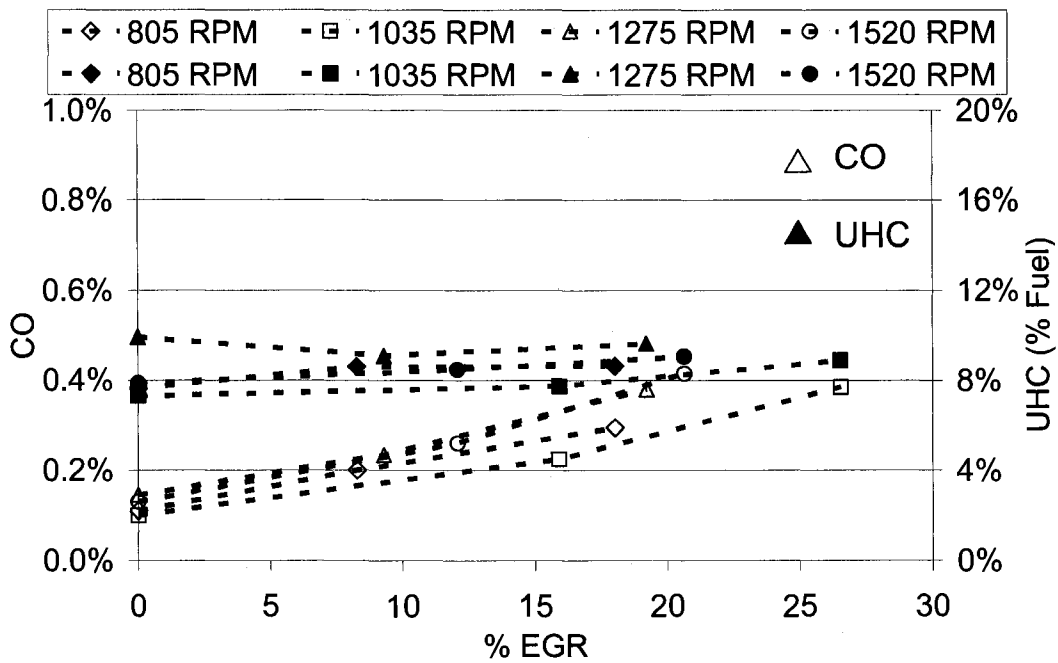


Figure 5.44: CO and UHC for different EGR levels and RPM (50% Ethanol & 50% iso-octane, $\phi = 0.33$).

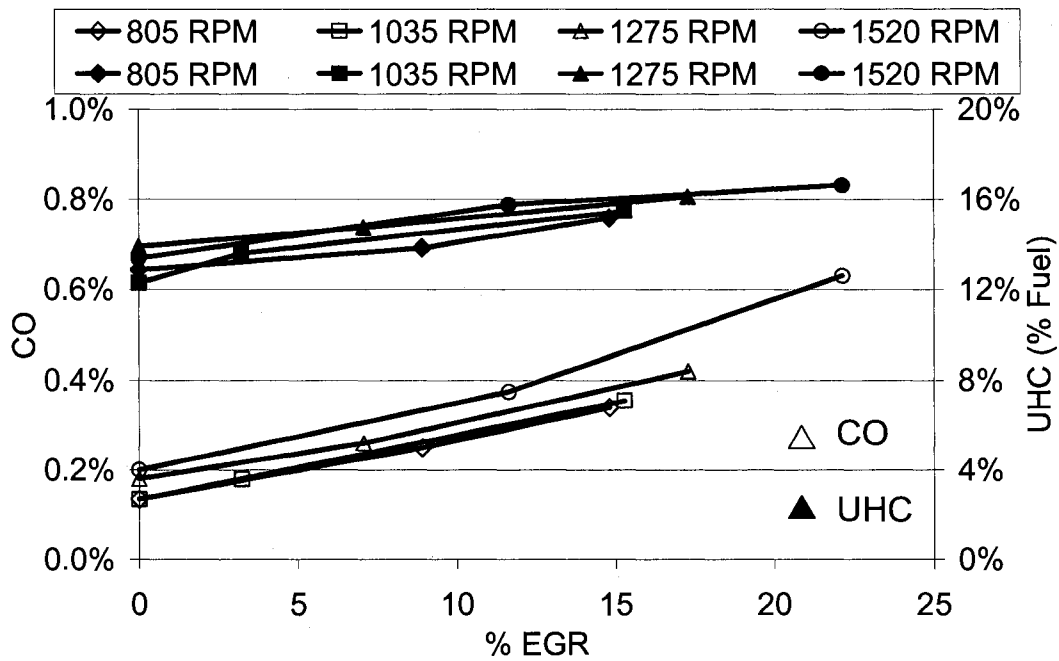


Figure 5.45: CO and UHC for different EGR levels and RPM (100% Iso-octane, ϕ : 0.33).

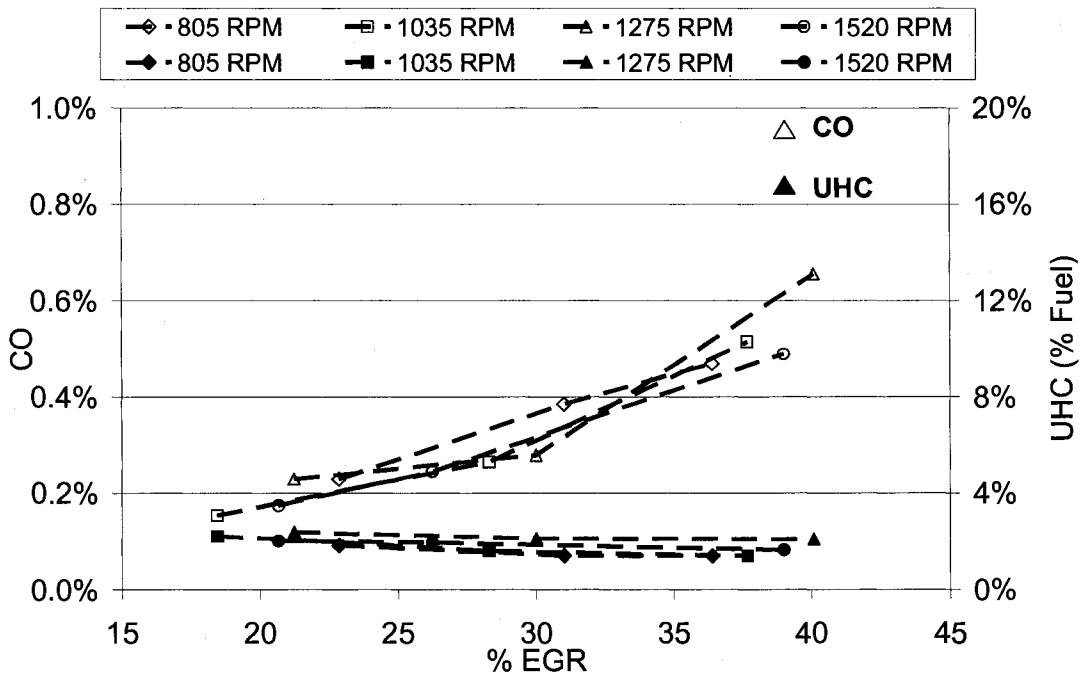


Figure 5.46: CO and UHC for different EGR levels and RPM (100% Ethanol, ϕ : 0.38).

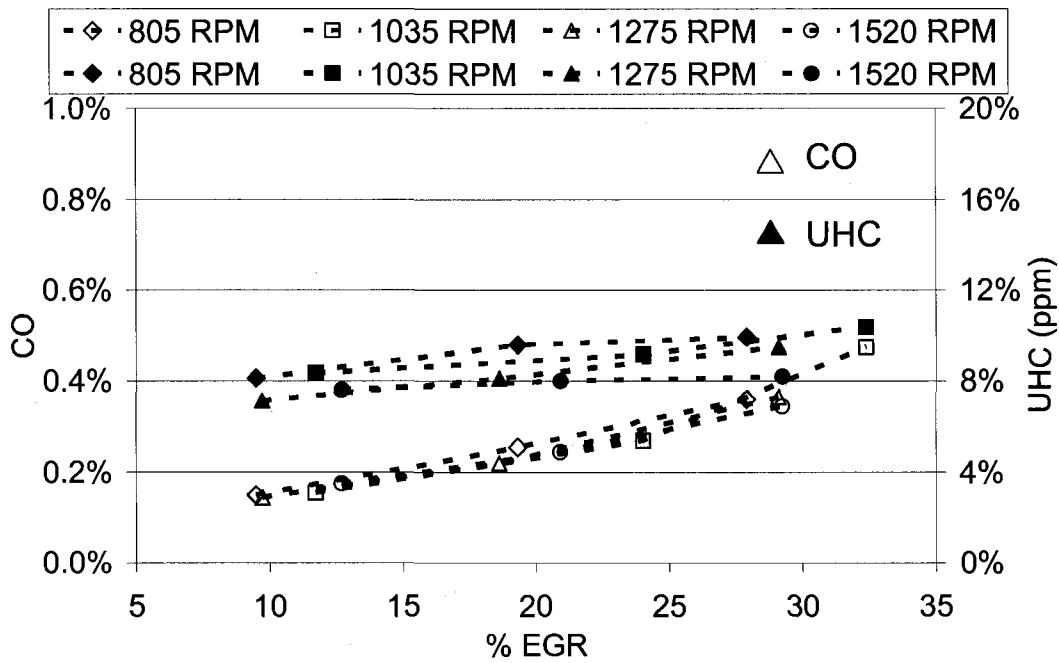


Figure 5.47: CO and UHC for different EGR levels and RPM (50% Ethanol and 50% Iso-octane, ϕ : 0.38).

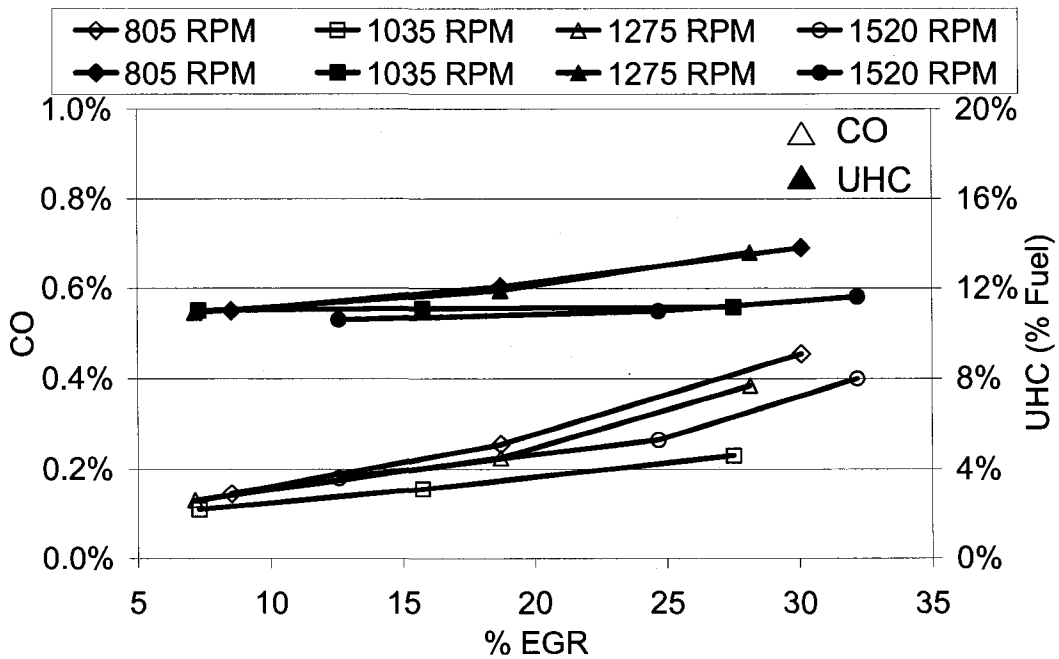


Figure 5.48: CO and UHC for different EGR levels and RPM (100% Iso-octane, ϕ : 0.38).

The CO emissions increase with percentage EGR addition for all the fuels tested. Also, the CO and UHC emissions are higher for pure iso-octane than pure ethanol for a (any) given operating condition. For example, in the case of 50% ethanol/iso-octane blend the CO and UHC levels for all the RPM conditions are around 0.18-0.25% and 7-10% with 10% EGR addition (Fig. 5.44). Whereas, for the same operating conditions with pure iso-octane the CO and UHC levels are around 0.25-0.35% and 14-16%. This again shows that the combustion quality decreases with the addition of iso-octane for a particular RPM condition and percentage EGR addition.

5.3 Summary

For the same intake charge temperature and engine speed, the on-set of combustion and the HR duration increases with EGR addition irrespective of the fuel type used in this study. This influence has been reported by several other researchers elsewhere.

The IMEP and COV_{IMEP} values also indicate that ethanol allows for the use of a higher percentage of EGR when compared to iso-octane.

The COV_{IMEP} values for the maximum IMEP values are within the stable operating conditions (below 4%) for the tested conditions.

The maximum thermal efficiency (30 – 40%) values obtained in this study are comparable to other HCCI experimental results reported elsewhere. The heat transfer

losses decrease with engine speed and have a major effect in this IDI-type engine at lower RPM conditions.

Trends in the thermal efficiency indicate that the residence time and combustion reaction rates play an important role at higher RPM conditions. For higher RPM conditions (1275 and 1520 RPM) fuelling with iso-octane showed slower combustion characteristics that obtained the maximum thermal efficiency when compared to 50% ethanol/iso-octane blend.

In general, operation with ethanol present showed better emissions and more complete combustion compared to fuelling with iso-octane. The CO and UHC levels were higher when fuelled with iso-octane when compared with a 50% ethanol/iso-octane blend.

The NO_x emissions are very low (less than 10 ppm) for the tested conditions and do not require after-treatment. However, the UHC and CO levels are higher and would require after-treatment.

Chapter 6 In-cylinder fuel reformation: A numerical parametric study

This numerical parametric study is focused on evaluating the advantages of the proposed in-cylinder fuel reformation strategy over the in-cylinder fuel reformation strategy using NVO. The model used in this study is comprised of a single-zone perfectly reactor for both HCCI combustion and fuel reformation. A single-zone model is chosen for its simplicity. Furthermore, our primary interest is to simulate and capture the trends when analyzing the effect of different reformation strategies on the HCCI combustion. The simulations were performed using Matlab/Cantera (Mathworks, 2005 and Goodwin, 2003) software. The code used for simulation of the results discussed in this Chapter is provided in Appendix G. The mechanisms used for ethanol and iso-octane are from Marinov (1998) and Curran (2002), which are commonly used by many other researchers for HCCI modeling.

6.1 Methodology

The numerical modeling of the HCCI combustion with in-cylinder fuel reformation is carried out through a multi-step HCCI engine cyclic process that includes only compression and expansion (no gas exchange process), as shown in Fig. 6.1. Each step involves a HCCI engine cycle simulation with a unique purpose for that step. The initial three steps are devoted to the production of the reformat gas in a reformation process that includes a homogenous mixture of fuel and retained products of combustion from the

preceding HCCI cycle that has EGR. The final step is a targeted HCCI cycle that involves the premixed products of in-cylinder reforming, fresh fuel/air mixture and EGR.

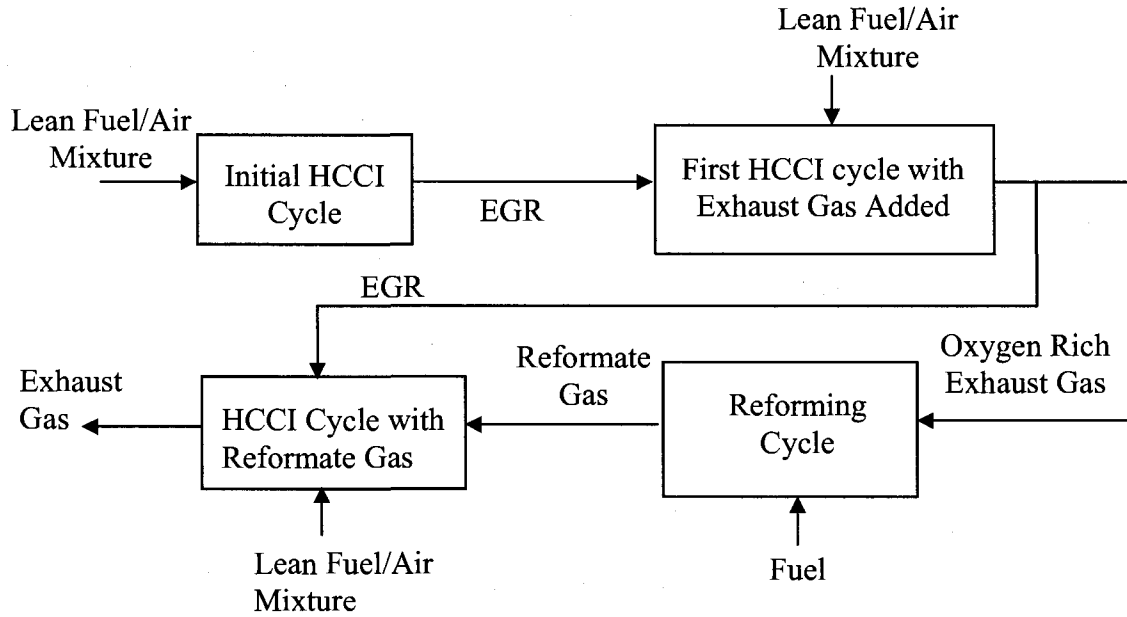
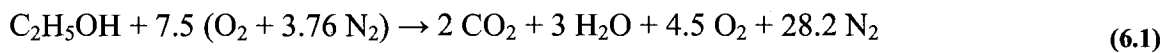


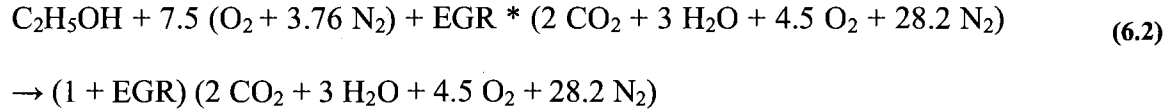
Figure 6.1 Multi-step modeling of HCCI engine cyclic process with in-cylinder fuel reforming.

The ideal balance equations representing the lean combustion, reforming, and fully reformed fuel combustion of ethanol at the equivalence ratio $\phi = 0.4$ may be written as follows.

Step 1: Initial HCCI cycle - HCCI combustion with lean fuel/air mixture.



Step 2: First HCCI cycle with Exhaust Gas Added - HCCI combustion with lean fuel/air mixture and varying percentage of EGR.



In this reaction EGR is calculated by:

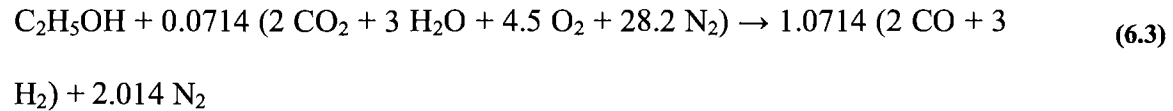
$$\text{EGR} = \left(\frac{V_o - V_e}{V_o} \right) * 100$$

where V_o = volume of fresh charge inducted per cycle with no EGR.

V_e = volume of fresh charge inducted per cycle with EGR.

Step 3: Reforming Cycle

The combustion products from the second step are used in this step for both the traditional and proposed in-cylinder reformation strategy, which involves the calculation of the reforming process. The ideal reforming reaction with no EGR and 7% retained products is given below:



In this reaction the requirements are that: all fuel hydrogen is converted into H_2 , all fuel carbon into CO , and no molecular oxygen is left. Under this requirement the H_2 yield is 43%, with a clear indication that in order to achieve the high degree of conversion the volume fraction of retained products of combustion should not be more than 7%. If more of the products of combustion are retained, the H_2 yield will be lower since other paths for hydrogen oxidation will open due to higher oxygen concentrations. Concurrently, it is feasible that under those conditions some of the CO will oxidize into CO_2 .

a) In-cylinder reformation using NVO:

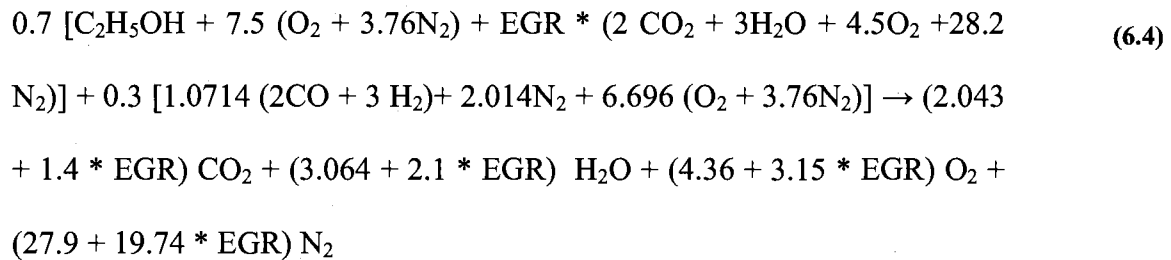
The initial temperature of the mixture entering the traditional in-cylinder reforming cycle is calculated under the assumption that the exhaust gas from the preceding HCCI cycle has expanded isentropically to ambient pressure at the end of the expansion process from the previous cycle. In this cyclic process, the compression ratio is reduced to simulate the early closing of the exhaust valve and recompression of the retained products of combustion from the preceding cycle and fraction of fuel. The duration of the reformation process is varied from 72° crank angle (CA) to 152° CA in 20° intervals. This corresponds to a start angle of between 327° BTDC and 287° BTDC. Starting with a 20 CR, the changes in the compression ratio during reformation for the above crank angle durations are 2.5, 3.4, 4.5, 5.7 and 7. In the NVO reformation process the peak temperature during reformation depends on various factors such as the level of compression used during reformation and the temperature of the exhaust gases from the previous HCCI cycle, which again varies depending on the previous cycle's initial charge temperature.

b) Proposed in-cylinder reformation:

For the proposed reformation strategy, the initial temperature of the mixture is calculated based on when the residual gasses are trapped during the expansion process. In our study the residual gases are captured at 80° CA ATDC during the expansion stroke. The volume of the reformation chamber is 5 cc. The reforming cycle is modeled as a constant volume combustion chamber with a reformation chamber wall temperature maintained at 75 °C.

The duration of the reforming cycle varies depending on the time between 80° CA ATDC during expansion stroke (the moment when the combustion products are trapped for reformation) and the instant when the reformation products are introduced back into the main combustion chamber during the compression cycle. In our simulation it is 180° BTDC, 45° BTDC, 15° BTDC and 5° BTDC during the compression cycle.

Step 4: HCCI Cycle with Reformate Gas - In this step, the reformate gas produced in step 3 is mixed with a fresh lean fuel/air mixture and a varying percentage of EGR. The new mixture now constitutes a charge for the first HCCI cycle with products of reforming. For example, where 30% fuel was used for reforming:



It should be noted that the products of combustion from step 4 do not differ significantly from the products of combustion from step 2. Hence, there is no need to repeat the reformation step (3) more than once with the composition of recycled products from step 4.

6.2 Engine parameters and test Conditions

The engine parameters used for the numerical model are provided in Table 6.1. The parameters used are similar to the experimental engine specifications.

Table 6.1: Engine parameters used for simulation

Compression Ratio, r_c	20:1
Total Displacement, V_d [L (cu.in)]	0.898 (54.86)
Engine Speed [rpm]	1000
Starting crank angle of simulation [$^\circ$ BTDC]	180
Number of revolutions of the crank to be simulated	1 rev
Bore & Stroke [mm]	72 x 73.6
Cylinder wall temperature, T_{wall} [$^\circ$ C]	75
Initial charge temperature (beginning of compression) [$^\circ$ C]	57 or 77
EGR [% by vol.]	0, 15, 30 or 45
Fuel used for reformation [% by mass]	0, 10 or 30
Initial charge pressure (beginning of compression)	0.8 bar

A lean mixture of fuel and air at an equivalence ratio of $\phi = 0.4$ is examined in this study. The ethanol reaction mechanism and thermodynamic data are taken from Marinov et al (1998), which involves 372 reactions and 58 species. The iso-octane reaction mechanism and thermodynamic data are taken from Curran et al (2002).

6.3 Results and discussion

Before analyzing the effects of reformation processes using the numerical model, the trends from the HCCI cycle (Step 1) with the two individual fuel chemistry mechanisms (iso-octane and ethanol) were compared with the experimental results obtained from Chapter 4 and 5. Figure 6.2 and 6.3 shows the in-cylinder pressure and HRR curves for HCCI cycle (Step 1) using the MATLAB/Cantera single-zone model. From the figures it

can be noted that the correlation between intake charge temperature/EGR and on-set of combustion was strong, similar to the experimental results seen here (Figures 4.1 and 5.1) and elsewhere. However, the predicted pressures and their respective rise rates after ignition are excessive compared to the experimental results [more than the allowable 5-6 bar/CA, (Xie, 2006)]. The excessive predictions in the pressures and their rise rates are due to the inherent nature of the single-zone models and similar results have been reported in (Ng et al., 2004).

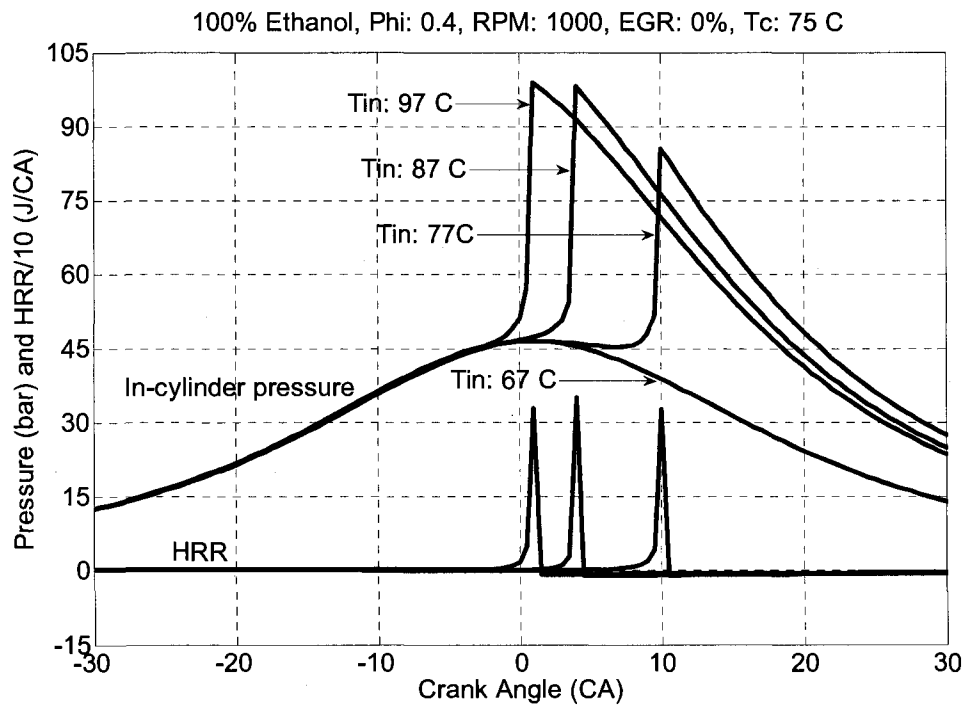


Figure 6.2: In-cylinder pressure and HRR with different intake charge temperatures and no EGR (100% Ethanol, phi: 0.4, T_c: 75 °C).

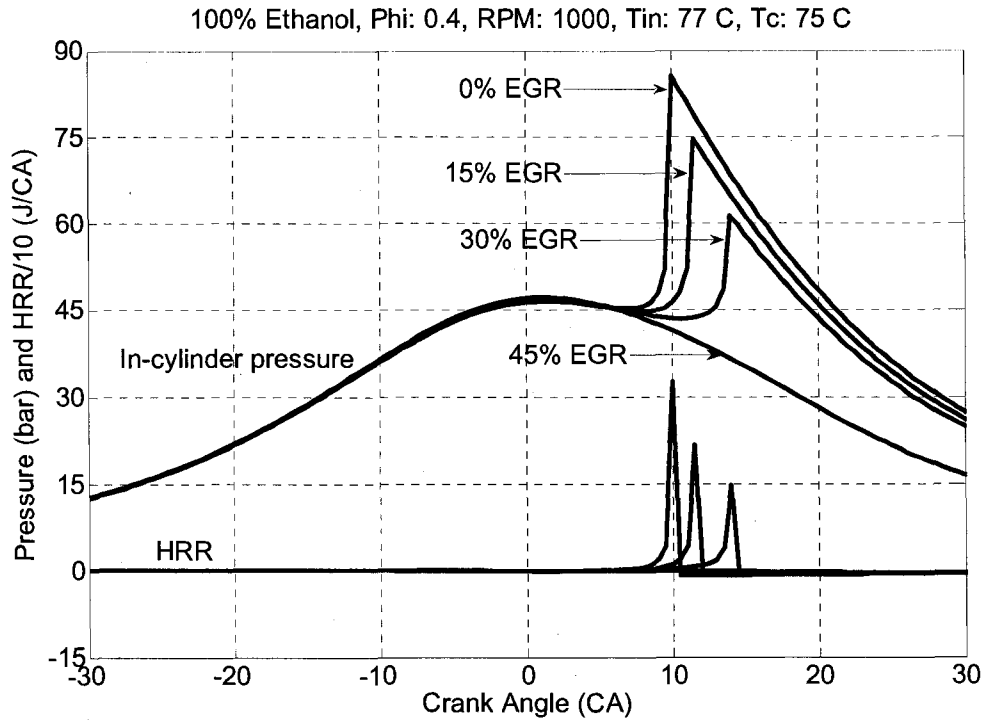


Figure 6.3: In-cylinder pressure and HRR with different EGR levels (100% Ethanol, ϕ : 0.4, T_{in} : 77 °C, T_c : 75 °C).

As mentioned earlier, the trends between experimental and single-zone model are similar when analyzing a particular fuel. However, there is a reverse in the experimental and numerical trends when comparing the on-set of combustion between different fuel mechanisms (pure ethanol and pure iso-octane) for a particular operating condition. Figure 6.4 show the pressure and HRR from numerical simulations using the single-zone model when fuelled with ethanol and iso-octane. The experimental engine specifications from Table 6.1 were used in the simulation.

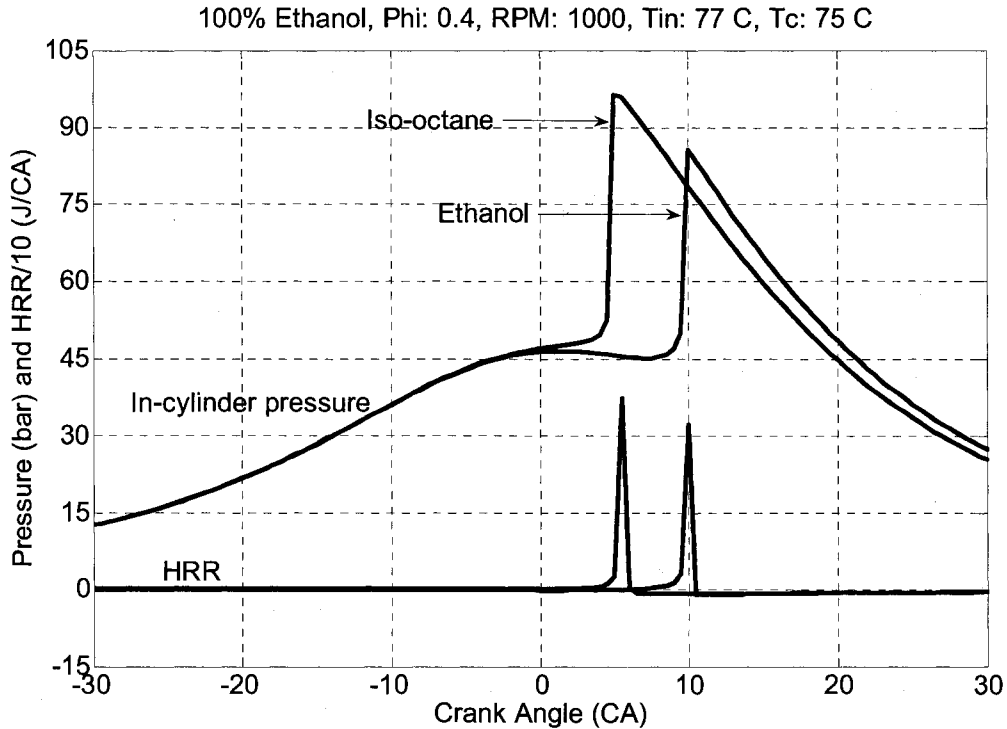


Figure 6.4: In-cylinder pressure and HRR with different fuel mechanisms (100% Ethanol, ϕ : 0.4, T_{in} : 77 °C, T_c : 75 °C).

From Fig. 6.4, it can be noted that the iso-octane on-set of combustion is approximately 1° CA ahead of the on-set of combustion for ethanol for the given intake charge temperature and engine speed. This is in contrast to the experimental results reported here (Figures 4.1 and 4.3) and elsewhere (Ida, 2000). As mentioned earlier, the mechanisms when analyzed individually do show similar trends between intake charge temperature/EGR and on-set of combustion compared to the experimental results. The inability of the mechanisms to capture the trends when comparing different fuels can be attributed solely to the fact that these mechanisms are validated at a much lower pressure than those encountered within the engine cylinder.

Due to the mechanisms inability to capture the experimental trends with respect to fuel effects, further numerical simulations were performed only with one fuel (pure ethanol). Also, an attempt was made by combining the individual ethanol and iso-octane mechanisms and the combined mechanism failed to predict the trend with ethanol and iso-octane on-set of combustion measured in the experiments. Hence, the investigation of ethanol/iso-octane blends was not considered here. The discussion of the simulation results is focused mainly on analyzing the effect of two different in-cylinder reformation processes on the on-set of HCCI combustion with varying levels of EGR.

6.3.1 In-cylinder reformation using Negative Valve Overlap (NVO):

Figure 6.5 shows the in-cylinder pressure and the HRR versus crank angle for the HCCI cycle with and without fuel reformation for a initial charge temperature of 77 °C, $\phi = 0.4$ and 0% EGR. The solid line in Fig. 6.5 represents the HCCI cycle without fuel reformation and the dashed line represents the HCCI cycle that includes products of fuel reformation. The amount of fuel used for reformation in this case is 30% by mass. The different dashed lines in the Fig. 6.5 represents the HCCI cycle with different reformation durations (NVO), which is varied from 72° crank angle (CA) to 152° CA in 20° intervals. From Fig. 6.5 it can be noted that the HCCI combustion on-set occurs a short time after Top Dead Center (TDC) for all the cases (with and without reformation fuelling) and the subsequent combustion process is almost instantaneous with a very steep pressure rise.

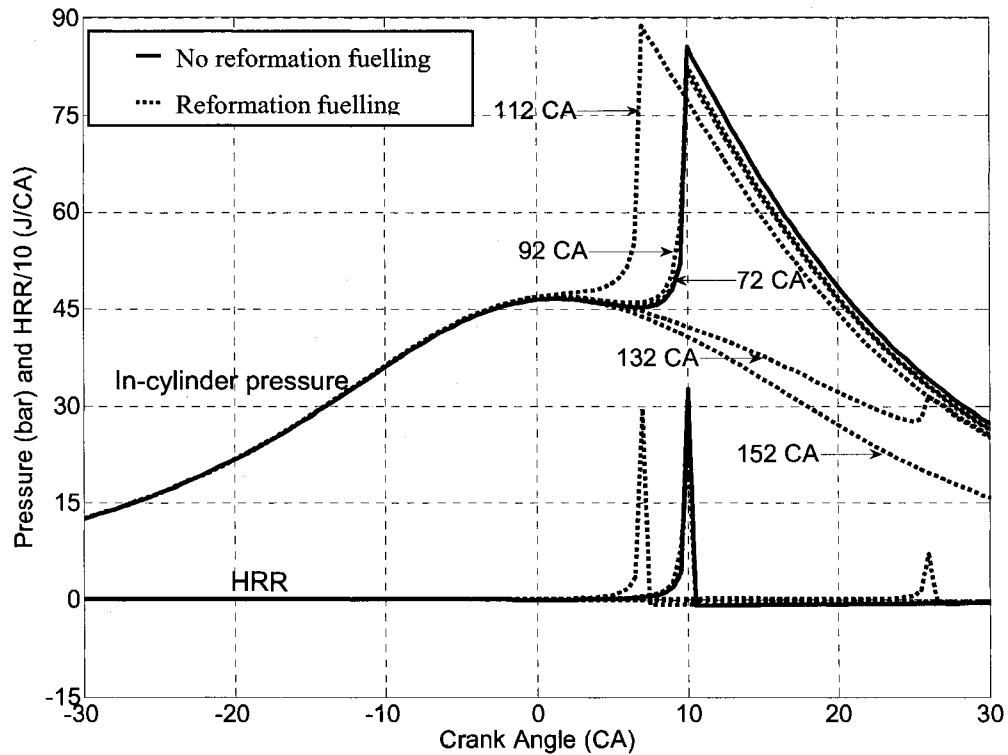


Figure 6.5: in-cylinder pressure and HRR (ϕ : 0.4, T_{in} : 77 °C, 0% EGR and 30% reformation fuelling).

There is also an interesting trend in Fig. 6.5 when comparing the combustion on-set for the HCCI cycle with various reformation cycle/process durations. Depending on the reformation duration utilized, the HCCI combustion on-set either advances, retards or stays the same when compared to the no reformation fuelling condition. For example, the HCCI combustion on-set is advanced with the 92° and 112° CA duration reformation products when compared to the no reformation fuelling condition. With the 72° CA duration reformation products the HCCI combustion on-set does not change when compared to the no reformation fuelling condition. However, it should be noted that the peak pressure obtained for this case is less than the no reformation fuelling due to the reformation process. Whereas, for the HCCI combustion with 132° CA duration reformation products the HCCI combustion on-set is delayed when compared to the no

reformation fuelling condition. The worst scenario is for the HCCI combustion with the 152° CA duration reformation products where it misfires. This shows that there is optimal reformation duration depending on the HCCI engine operation condition, which has a positive impact on the HCCI combustion cycle. It should be realized that the change in reformation duration alters the amount of trapped residual gas and hence the oxygen content during the reformation cycle. Furthermore, the increase in reformation duration also increases the amount of compression achieved during the NVO period and leads to higher temperature during the reformation stage. The oxygen content and temperature are the two important factors that dictate whether the fuel injected during the reformation cycle proceeds towards favorable reformation products (Eq. 6.3) or complete conversion of reformation fuel to CO₂ and H₂O (which will act like EGR as seen in Fig. 6.5 for the 132 and 152° CA duration). The existence of the above mentioned optimal reformation duration is further confirmed by trends shown in Fig. 6.6 where the percentage reformation fuelling is reduced to 10% during the NVO. The other parameters for this condition are maintained similar to the previous case (Fig. 6.5). From Fig. 6.6 it can be seen that, similar to Fig. 6.5, the HCCI combustion on-set with different reformation duration products either advances or retards when compared to the no reformation fuelling condition. However, the influence of the individual reformation duration on the HCCI combustion is different for the 10% reformation fuelling case when compared to the 30% reformation fuelling condition.

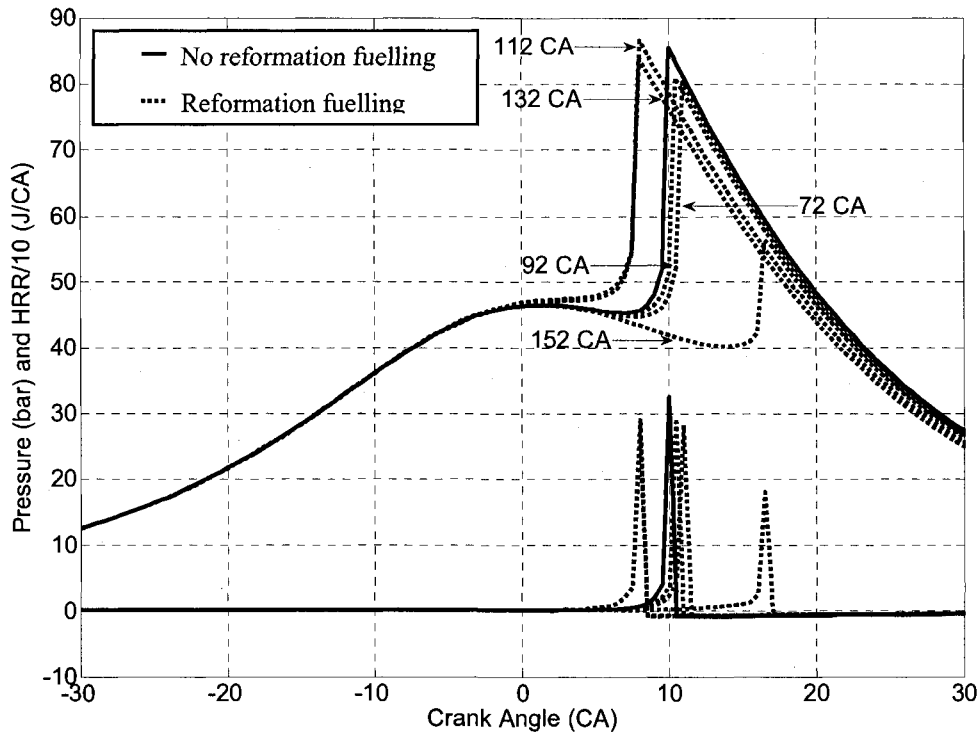


Figure 6.6: In-cylinder pressure and HRR (ϕ : 0.4, T_{in} : 77 °C, 0% EGR and 10% reformation fuelling).

For example, the 132° CA and 152° CA reformation cycle durations (Fig. 6.5 and 6.6) have a opposite effect on the HCCI combustion on-set when the reformation fuelling percentage is decreased from 30% to 10%. With 10% reformation fuelling and 132° duration the on-set of combustion is advanced when compared to the no reformation fuelling condition. Whereas, with 30% reformation fuelling for the same 132° CA duration (Fig. 6.5) were the HCCI combustion on-set was delayed compared to the no reformation fuelling condition. Conversely, for the 152° CA reformation duration with 10% reformation fuelling showed delayed on-set for both reformation fuelling conditions. This shows that there is indeed an optimal reformation cycle duration depending on the engine operating condition and percentage reformation fuelling.

The variation in the combustion on-set for 30% reformation fuelling with varying levels of EGR is shown in Fig. 6.7. The percentage EGR addition used is either 15, 30 or 45%. The intake charge temperature, charge equivalence ratio and the reformation cycle duration used in the simulation is similar to the previous operating conditions (Figs. 6.5 and 6.6). The solid line in Fig. 6.7 represents the combustion on-set for the no reformation fuelling condition and the dashed lines represent the reformation fuelling conditions. From Fig. 6.7 it can be seen that for the no reformation fuelling condition, an increase in percentage EGR addition delays the HCCI combustion on-set. Similar to Figs. 6.5 and 6.6, the combustion on-set for HCCI cycle with reformation and EGR is delayed or advanced depending on the duration of the reformation process utilized when compared to the no reformation fuelling condition.

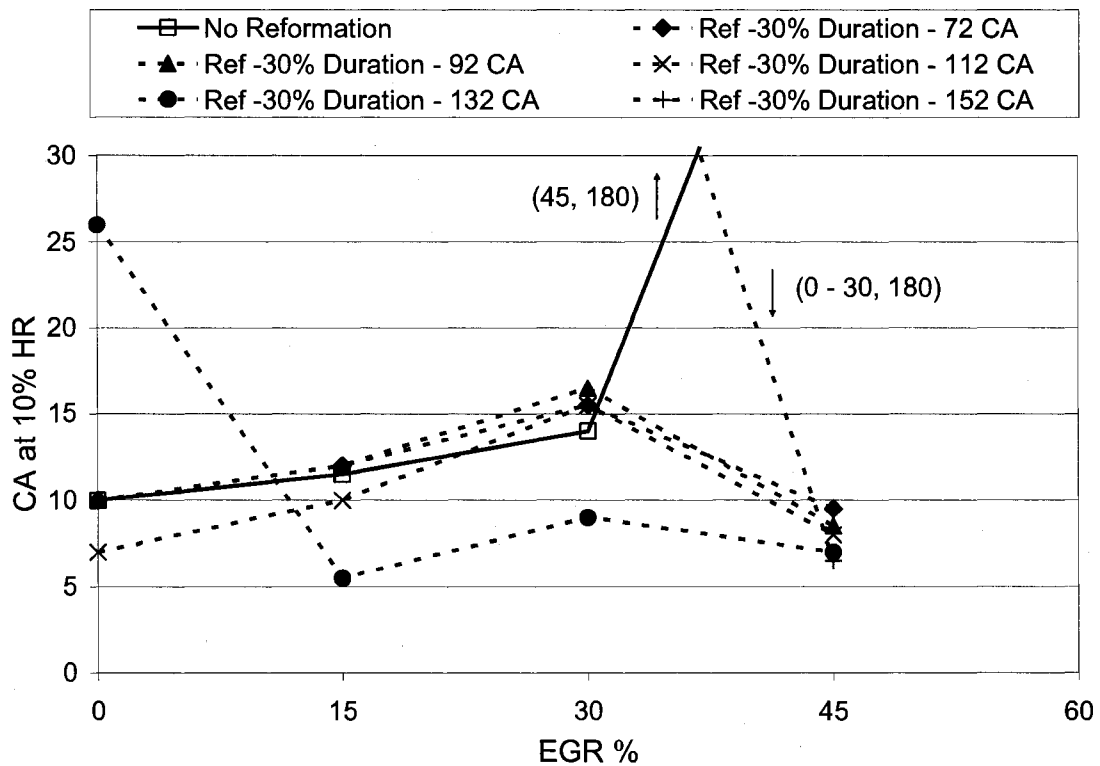


Figure 6.7: Combustion on-set for ϕ : 0.4, T_{in} : 77 °C, 30% reformation fuelling with different % EGR addition.

There is also an interesting trend when comparing the combustion on-set times for the 30% reformation fuelling condition (Fig. 6.7) and their respective hydrogen yield during the reformation process (Fig. 6.8). In general, for the conditions which showed high hydrogen yield (signifying favorable reformation reaction) during the reformation process, the subsequent HCCI combustion which included those reformation products showed advanced combustion on-set compared to the no reformation fuelling condition. For example, the HCCI cycle with 15% EGR and 132° CA reformation duration products (which produced an H₂ yield of 400 ppm) advanced the combustion on-set by 7° CA compared to the no reformation fuelling condition. Similarly, in the case of 45% EGR all the reformation durations showed a H₂ yield of more than 200 ppm and resulted in extension of the HCCI operating range (the no reformation fuelling condition with 45% EGR misfired).

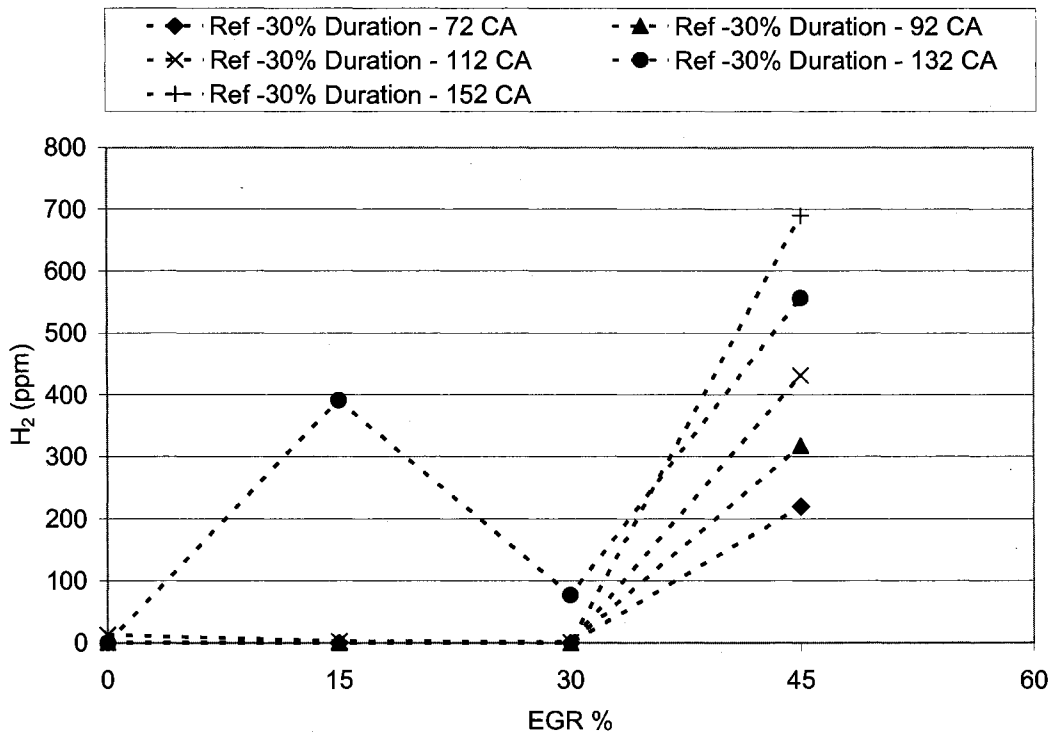


Figure 6.8: H₂ for phi: 0.4, T_{in}: 77 °C, 30% reformation fuelling with different % EGR addition.

Figure 6.9 and 6.10 show the combustion on-set crank angle and the hydrogen yield for the 10% reformation fuelling condition with varying levels of EGR. Similar to the 30% reformation fuelling condition (Fig. 6.8), the 10% reformation fuelling condition that produced a hydrogen yield resulted in the advancement of HCCI combustion on-set when compared to the no reformation fuelling condition. Furthermore, similar to the 30% reformation fuelling condition, the 45% EGR condition resulted in higher H₂ yield for all the reformation durations tested and showed extension of the HCCI operating range (the no reformation fuelling condition with 45% EGR misfired).

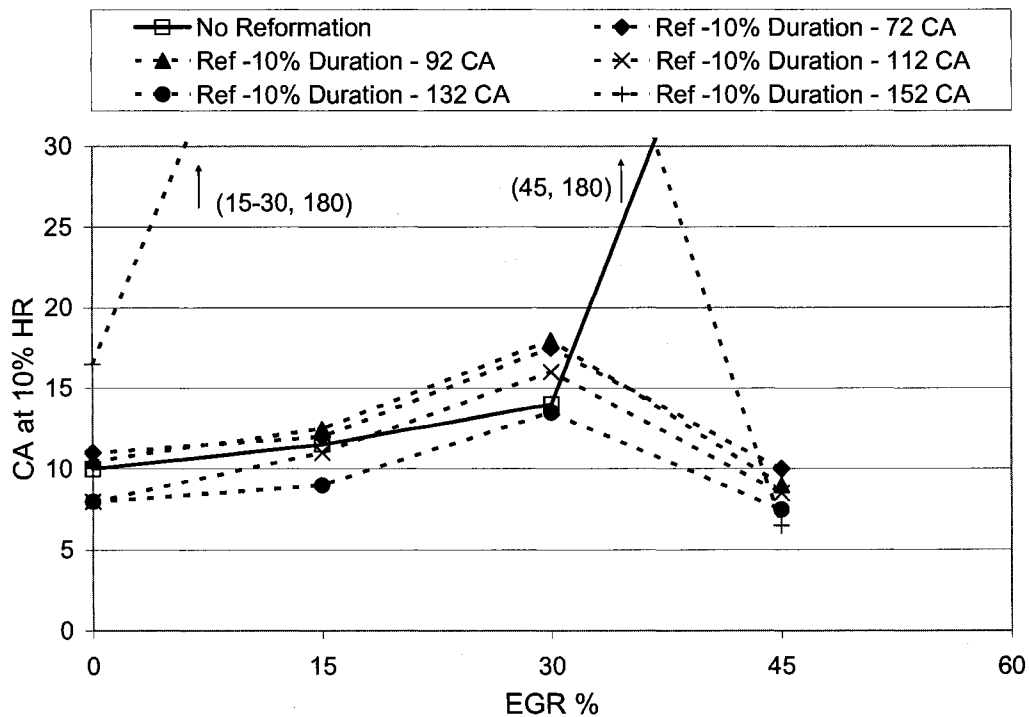


Figure 6.9: Combustion on-set for ϕ : 0.4, T_{in} : 77 °C, 10% reformation fuelling with different % EGR addition.

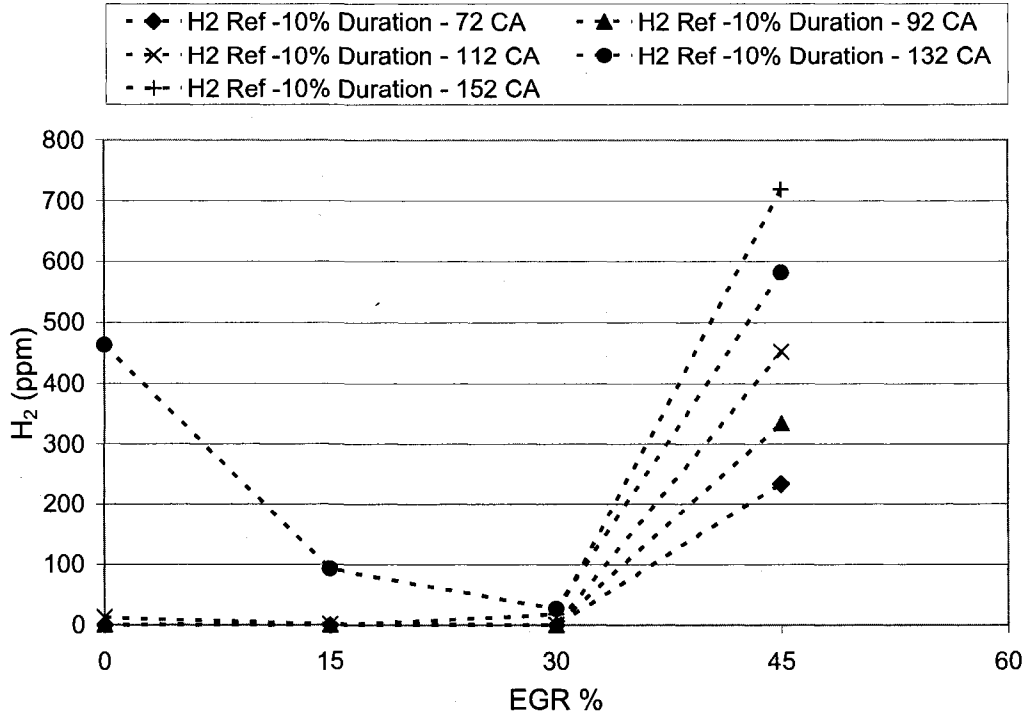


Figure 6.10: H₂ for ϕ : 0.4, T_{in} : 77 °C, 10% reformation fuelling with different % EGR addition.

Figure 6.11 shows the in-cylinder pressure and the HRR versus crank angle for the HCCI cycle with and without reformation fuelling for a initial charge temperature of 72 °C, $\phi = 0.4$ and 0% EGR. The solid line in the Fig. 6.11 represents the HCCI cycle without fuel reformation and the dashed line represents the HCCI cycle which included fuel reformation products. The amount of reformation fuelling used for this case is 30% by mass. From Fig. 6.11 it can be seen that the lower initial charge temperature (compared to Fig. 6.5) leads to misfire for the no reformation fuelling condition. Whereas, for the same operating condition with products of fuel reformation, the HCCI cycle shows combustion irrespective of the reformation duration used. Similar results that show extension in the HCCI operating range were reported by Urushihara et al. (2003).

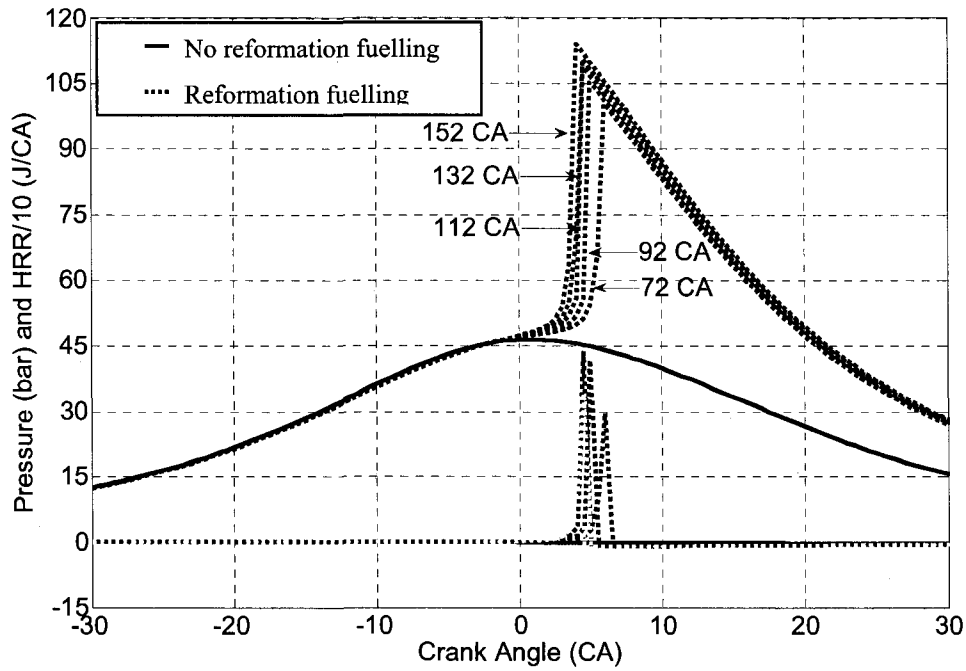


Figure 6.11: in-cylinder pressure and HRR (ϕ : 0.4, T_{in} : 72 °C, 0% EGR and 30% reformation fuelling).

Figure 6.12 shows the pressure and HRR versus crank angle for the HCCI cycle with and without reformation fuelling for a charge with initial temperature of 67 °C, $\phi = 0.4$ and 0% EGR. From figure it can be seen that lowering the initial charge temperature further compared to the one used in Fig. 6.11 lead to misfire for both the reformation and no reformation fuelling conditions.

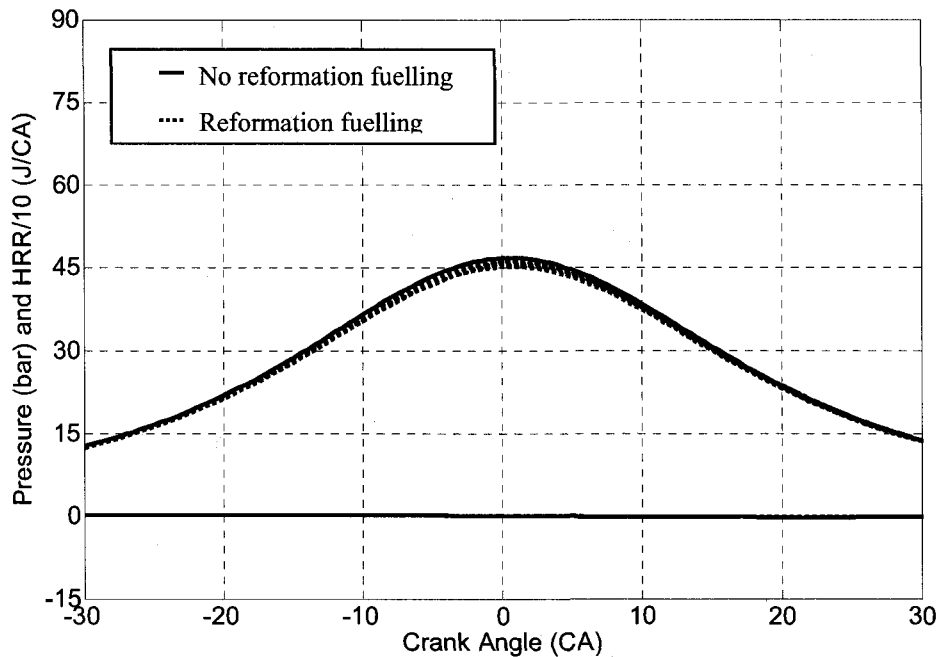


Figure 6.12: In-cylinder pressure and HRR (ϕ : 0.4, T_{in} : 67 °C, 0% EGR and 30% reformation fuelling).

6.3.2 Proposed in-cylinder reformation using separate reformation chamber:

Figure 6.13 shows the in-cylinder pressure and the HRR versus crank angle for the HCCI cycle with and without reformation fuelling for a initial charge temperature of 77 °C, $\phi = 0.4$ and 0% EGR. The two dashed curves [marked as (a) and (b) in Fig. 6.13] represent the pressure traces when the reformation chamber is kept closed (a) or open (b) throughout the entire cycle. The difference in their peak pressure is due to the difference in the clearance volumes between cases (a) and (b). The clearance volume is decreased by 25% for case (a) resulting in an increased overall compression ratio of the engine. The solid line in the figure represents the HCCI cycle without fuel reformation. The dotted line in Fig. 6.13 represents the in-cylinder pressure and HRR when the reformation chamber is opened at 45° BTDC and closed at 80° CA ATDC (current configuration in

experiments). The amount of reformation fuelling used for this case is 30% by mass and the reformation products are introduced into the HCCI compression cycle at 15 BTDC.

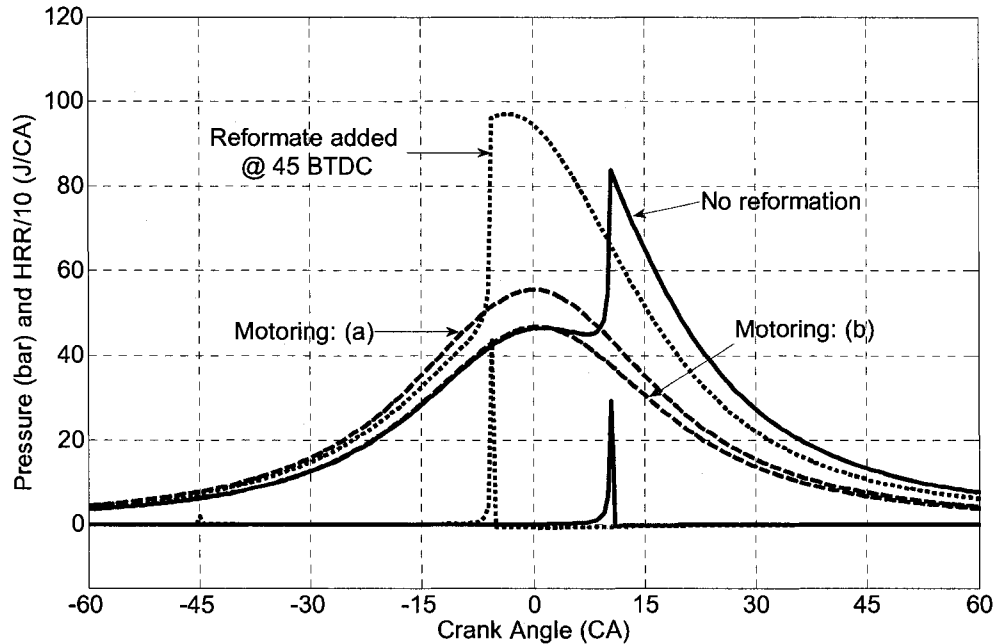


Figure 6.13: In-cylinder pressure and HRR (ϕ : 0.4, T_{in} : 77 °C, 0% EGR and 30% reformation fuelling).

From Fig. 6.13 it can be noted that the in-cylinder pressure during the compression stroke (from -45° CA BTDC) is different for the HCCI combustion with and without fuel reformation. The difference is due to the manipulation of the reformation chamber opening time during the compression stroke (for HCCI cycle with fuel reformation) which results in temporarily varying the compression ratio of the engine during the intermediate period of the compression stroke. This results in attaining a higher TDC pressure and temperature than the regular HCCI cycle compression, an inherent advantage of the proposed reformation methodology. It should be realized that at the TDC, the clearance volume is the same for both the HCCI cycle with reformation and

without fuel reformation. Hence, the overall compression ratio of the engine is not varied during the reformation and no reformation cycle. From Fig. 6.13, it is evident that HCCI cycle with fuel reformation advances the combustion on-set by 15° CA when compared to the HCCI cycle no fuel reformation condition.

Figure 6.14 shows the in-cylinder pressure and the HRR versus crank angle for the HCCI cycle with and without reformation fuelling for a initial charge temperature of 77°C , $\phi = 0.4$ and 0% EGR (similar to the previous condition). However, the percentage reformation fuelling used for this case is reduced to 10% by mass compared to Fig. 6.13.

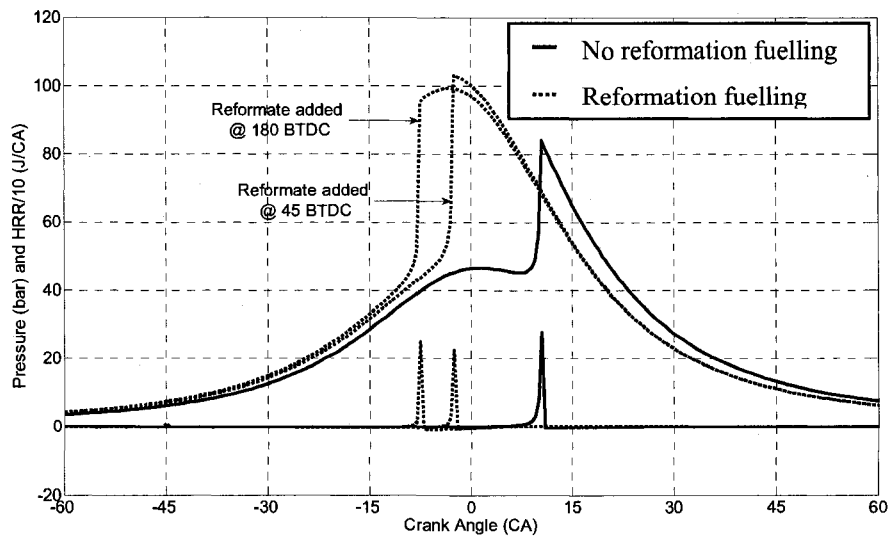


Figure 6.14: in-cylinder pressure and HRR (ϕ : 0.4, T_{in} : 77°C , 0% EGR and 10% reformation fuelling).

Furthermore, in Fig. 6.14 two different crank angles (180 and 45 BTDC) were used for admission of the reformate products during the HCCI compression stroke which includes products of in-cylinder fuel reformation. In general, it can be noted that the HCCI cycle with products of in-cylinder fuel reformation has an advanced combustion on-set

compared to the no-reformation condition. There is an interesting trend when comparing the combustion on-set between the two HCCI cycle with reformation products (Fig. 6.14). Depending on the CA at which the products of reformation are brought in to the HCCI compression stroke, the advance in HCCI combustion on-set (for the HCCI cycle with reformation products) is varied. For example, for the HCCI cycle with reformation products introduced at 180° CA BTDC the combustion on-set is advanced by 5° CA compared to the HCCI cycle where the products of reformation are introduced at 45° CA BTDC. This shows that the proposed in-cylinder reformation methodology has the potential to control the HCCI combustion on-set similar to the direct injection strategy used in diesel engines. Furthermore, there is also another interesting trend when comparing the combustion on-set in Figs. 6.13 and 6.14 for the HCCI cycle where reformation products are introduced at 45° CA BTDC. Depending on the percentage fuel utilized in the reformation process (30% for Fig. 6.13 and 10% in Fig. 6.14), the advance in the combustion on-set for the HCCI cycle with reformation products varies compared to the no reformation fuelling condition. In the case of Fig. 6.13, the combustion on-set for the HCCI cycle with reformation products (added at 45° CA BTDC) is 6.5° CA BTDC compared to the same condition in Fig. 6.14 where the HCCI cycle on-set is at 4° CA BTDC. This shows that similar to the NVO method, there is an optimal reformation fuelling percentage depending on the engine operating condition.

The variation in the combustion on-set for 30% and 10% reformation fuelling with varying levels of EGR is shown in Fig. 6.15 and Fig. 6.16. Also, the hydrogen yield during the reformation process for the two reformation fuelling condition (30% and 10%)

with different EGR conditions are shown in Fig. 6.17. The percentage EGR addition used is either 15, 30 or 45%. The intake charge temperature, charge equivalence ratio and the reformation cycle duration used in Figs. 6.15 and 6.16 are the same as the previous NVO operating conditions. In Figs. 6.15 and 6.16, three different crank angles (180, 45 and 15° CA BTDC) were used for admission of the reformat products during the compression stroke for the HCCI cycle that includes reformation fuelling. In general, similar to the no EGR condition, the HCCI cycle with EGR (Fig. 6.15 and 6.16) results in an advanced combustion on-set for the HCCI cycle with reformation fuelling compared to their no reformation condition. Furthermore, the 30% reformation fuelling condition (Fig. 6.15) resulted in an earlier HCCI combustion on-set when compared to the 10% reformation fuelling condition (Fig. 6.16) for any given percentage EGR condition.

There is also an interesting trend when comparing the combustion on-set and the CA at which the products of in-cylinder fuel reformation are brought into the HCCI cycle (Fig. 6.15 and 6.16). Irrespective of the reformation fuelling percentage used, the 45° CA BTDC condition resulted in a delayed combustion on-set when compared to the 175° CA and 15° CA BTDC condition. It should be realized that with late admission of the reformation products there is a temporary change in the compression ratio that results in a higher pressure and temperature at the end of the compression stroke. Hence, it should have been expected that the 175° CA BTDC condition should have resulted in the most delayed HCCI combustion on-set when compared to the other two conditions (45 and 15° CA BTDC). However, it should be realized that the products of in-cylinder reformation are captured at 80° CA ATDC which is at a higher pressure when compared to the initial

charge pressure (0.8 bar) at th

CA at which the products of

depending on the relative cyli

increases or decreases with

reformation products earlier d

overall initial cylinder pressur

end of the compression strok

shows an advanced HCCI c

condition.

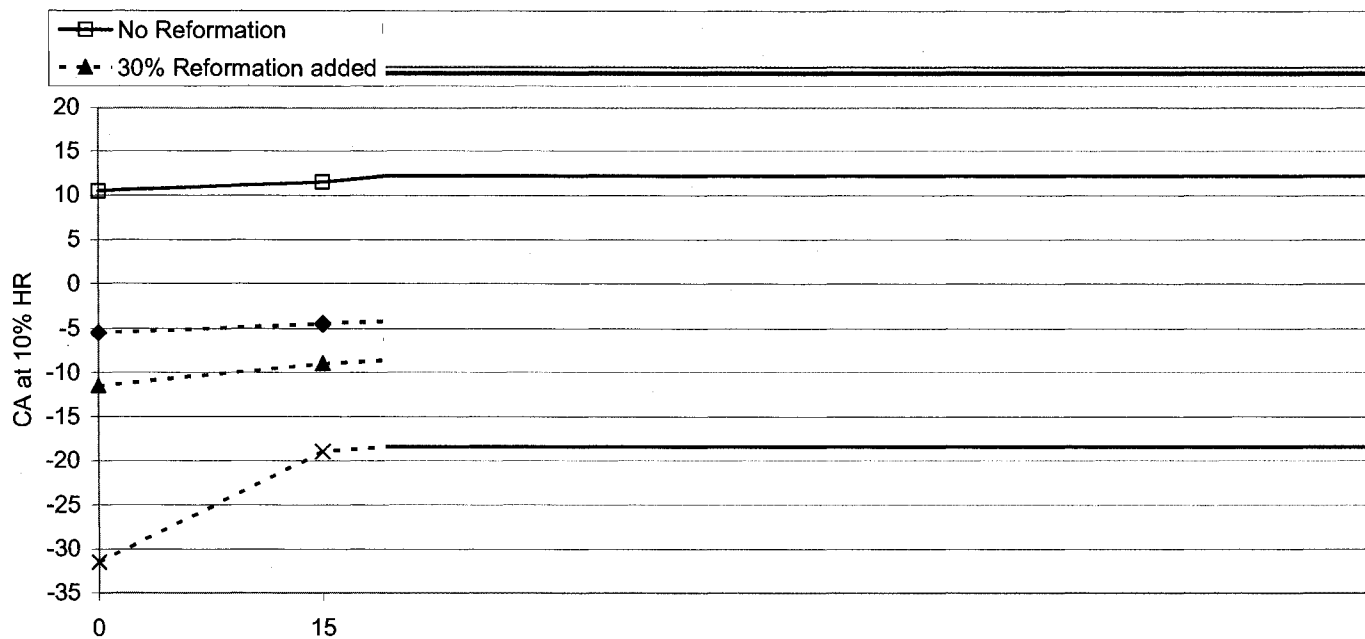


Figure 6.15: Combustion on-set for
EGR addition.

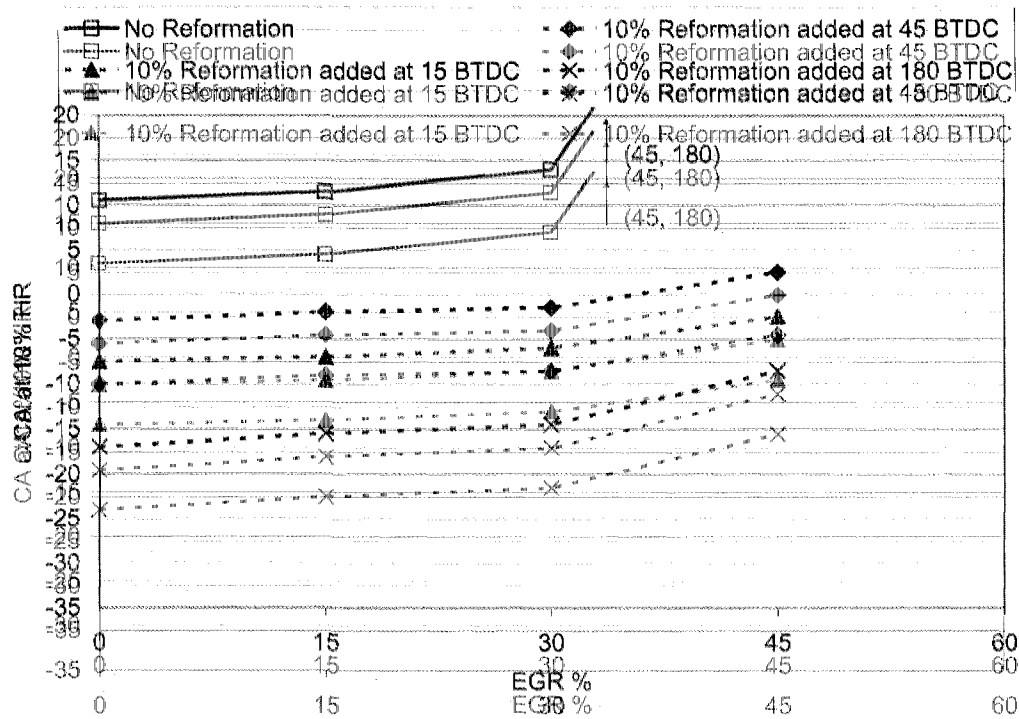


Figure 6.16: Combustion on-set for ϕ : 0.4, T_{in} : 77 °C, 10% reformation fuelling with different % EGR addition.
 Figure 6.16: Combustion on-set for ϕ : 0.4, T_{in} : 77 °C, 10% reformation fuelling with different % EGR addition.
 Figure 6.16: Combustion on-set for ϕ : 0.4, T_{in} : 77 °C, 10% reformation fuelling with different % EGR addition.

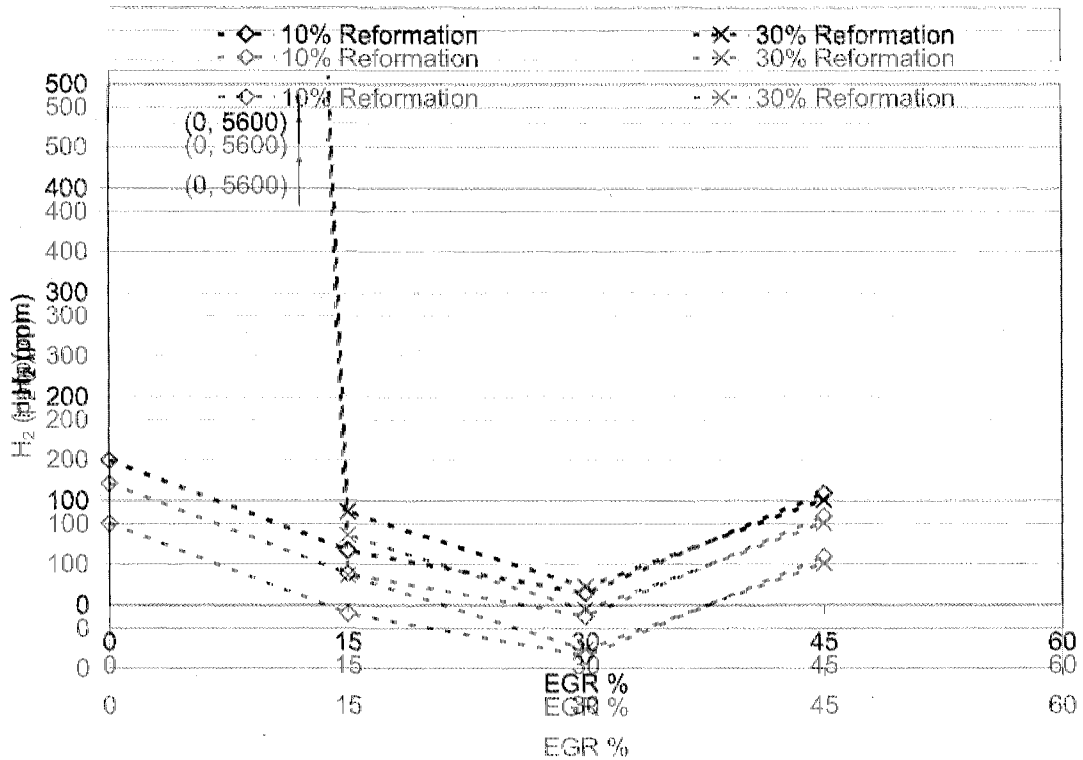


Figure 6.17: H₂ for ϕ : 0.4, T_{in} : 77 °C with different % EGR addition and reformation fuelling.
 Figure 6.17: H₂ for ϕ : 0.4, T_{in} : 77 °C with different % EGR addition and reformation fuelling.
 Figure 6.17: H₂ for ϕ : 0.4, T_{in} : 77 °C with different % EGR addition and reformation fuelling.

There is also another interesting trend when comparing the H₂ yield with respect to the percentage EGR addition (Fig. 6.17). From Fig. 6.17 it can be noted that the 30% EGR condition results in a lower hydrogen yield compared to the other EGR conditions tested irrespective of the reformation fuelling percentage used. It should be realized that with an increase in EGR, the oxygen content and the temperature of the trapped exhaust products for reformation decreases. These are the two main factors that are critical in attaining favorable reformation reaction; and any change in them affects the H₂ yield. This again shows that there is an optimum fuel reformation percentage for each operating condition.

Figure 6.18 shows the in-cylinder pressure and the HRR versus crank angle for the HCCI cycle with and without reformation fuelling for a initial charge of 67 °C, $\phi = 0.4$ and 0% EGR. The amount of reformation fuelling used for this case is 30% by mass. From Fig 6.18 it can be seen that the HCCI cycle with no reformation fuelling condition did not produce a combustion event and misfired. Whereas, the two HCCI cycle with reformation fuelling showed combustion with the HCCI combustion on-set occurring either before or after TDC depending on the CA at which the reformation products are introduced in to the HCCI compression stroke. This shows that similar to the NVO method, the proposed method has prospects of extending the HCCI operating range. However, there is also an added advantage with the proposed reformation methodology which can be seen when comparing Figs. 6.12 and 6.18. The HCCI cycle with the proposed reformation methodology results in a combustion event for the 67 °C initial charge temperature condition compared to Fig. 6.18 were the HCCI cycle with reformation products from the NVO methodology resulted in misfire. This shows the proposed methodology has the

potential to expand the HCCI operating range to a greater extent than the NVO methodology.

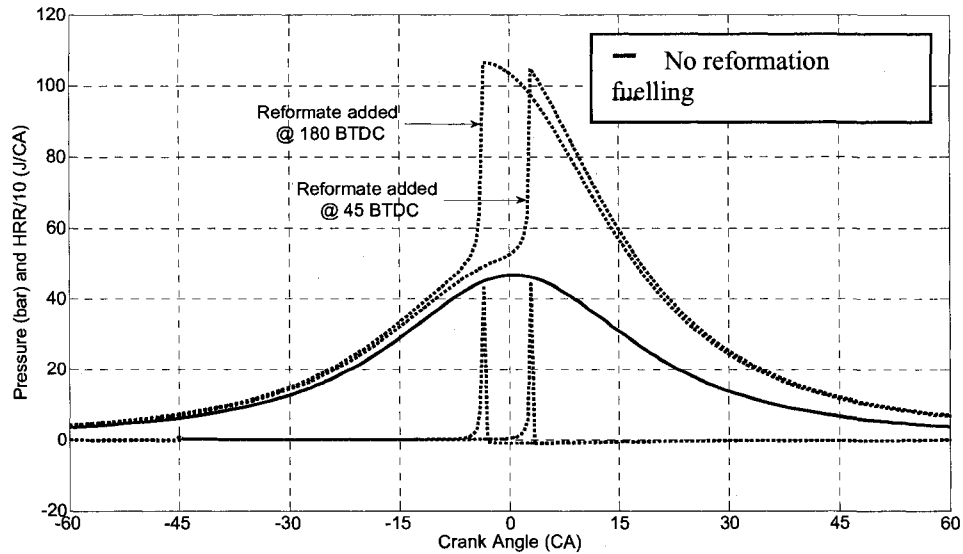


Figure 6.18: In-cylinder pressure and HRR (ϕ : 0.4, T_{in} : 67 °C with 0% EGR and 30% reformation fuelling).

6.4 Summary

In this Chapter, the numerical parametric study has demonstrated that multi-step calculation of a perfectly-stirred reactor undergoing compression and expansion processes capture several trends in the behavior of the HCCI engine cycle with internal reforming.

The predicted pressures and their respective rise rates after ignition are excessive compared to the experimental results. The excessive predictions in the pressure and their rise rates are due to the inherent nature of the single-zone models and similar results have been reported by other researchers.

The trends between experimental and single-zone model are similar when analyzing a particular fuel. However, there is a reverse in the experimental and numerical trends when comparing the on-set of combustion between different fuel mechanisms (pure ethanol and pure iso-octane) for a particular operating condition.

The in-cylinder fuel reforming using NVO extends the operational range of a HCCI engine. The no reformation fuelling condition with 45% EGR misfired, while the same condition with 30% of the fuel undergoing the reformation process fired.

The NVO reforming process also shows that there is optimal reformation duration and reformation fuelling percentage depending on the HCCI engine operation condition, which has a positive impact on the HCCI combustion cycle.

The in-cylinder fuel reformation using a pre-chamber also shows extension in the operating range similar to the NVO method. However, the pre-chamber method shows higher degree of controllability in varying the HCCI combustion on-set by manipulating the duration at which the reformation products are added to the main HCCI combustion event.

Furthermore, in-cylinder reformation using a pre-chamber also extends the HCCI operating limit to lower initial charge temperatures than those feasible with the NVO method for a particular operating condition.

Similar to the NVO method, the pre-chamber method also shows that there is optimal reformation duration and reformation fuelling percentage depending on the HCCI engine operation condition.

Chapter 7 Experimental results: Effect of in-cylinder fuel reformation

In this chapter the effect of in-cylinder fuel reformation on the HCCI combustion on-set is analyzed. The study was done with the compression ratio kept constant, and a constant intake charge temperature. The parameters that were varied were: percentage fuel used for reformation and equivalence ratio. The details of the test conditions are provided below in the next section.

7.1 Test conditions

The fuel used in this study is 100% ethanol. The engine specifications and conditions used in the experimental study are as follows:

Table 7.1: Engine specifications and test conditions

Compression ratio with reformation pre-chamber open, r_c	16:1
Compression ratio with reformation pre-chamber closed, r_c	21:1
Equivalence ratio, ϕ	0.27, 0.34 and 0.37
Engine Speed [RPM]	1080 and 1120
Fraction of fuel injected in to the reformation chamber [% by mass]	0, 10, 20 and 25
Coolant Temperature, T_c [°C]	75 ± 2
Intake charge temperature, T_i [°C]	150 ± 2

The results reported in the next section are averaged data from 125 individual cycles. The discussion of the results includes the engine performance in terms of the in-cylinder pressure, HRR, 10% and 90% HR, IMEP, and COV_{IMEP} , indicated thermal efficiency, and regulated engine-out emissions.

7.2 Results and discussion

Figure 7.1 shows the in-cylinder pressure and the pressure-rise rates for the engine motoring condition under different reformation chamber opening and closing conditions. From Fig. 7.1 it can be clearly seen that manipulating the reformation chamber opening during the compression stroke (dotted curve in Fig. 7.1) results in a temporary change in the compression ratio leading to higher peak pressure. However, it should also be realized that the volume at TDC is the same for all the curves in Fig. 7.1 since the reformation chamber is open at TDC for all the conditions.

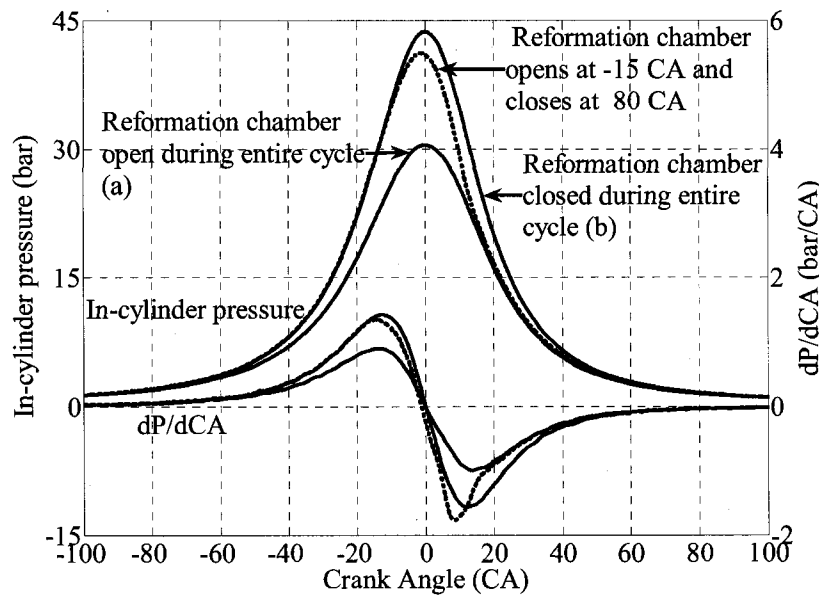


Figure 7.1: In-cylinder pressure and pressure-rise rate (dP/dCA) for various motoring conditions (T_{in} : 150 °C and T_c : 75 °C).

The manipulation of the reformation chamber opening time also results in attaining a higher peak gas temperature at TDC (Fig. 7.2) due to change in temporary compression ratio. The in-cylinder temperatures shown in Fig. 7.2 are calculated from the above pressure profiles and assuming ideal gas conditions. This shows that utilizing the proposed reformation strategy, excluding the effects of fuel reformation products, the compression ratio during the compression stroke can be temporarily varied and the HCCI combustion on-set can be effectively controlled. This is further verified from our experimental runs, where keeping the reformation chamber open throughout the cycle did not produce any combustion for any of the above test condition. For the same conditions, opening the chamber at 15 CA BTDC resulted in HCCI combustion (Figs. 7.3 through 7.8). The local drop in temperature at TDC for the motoring condition (a) arises due to the throttling losses across the reformation chamber valve. Similar drop can be seen at 10 CA ATDC in the case of the motoring condition where the reformation chamber opens at 15 CA BTDC.

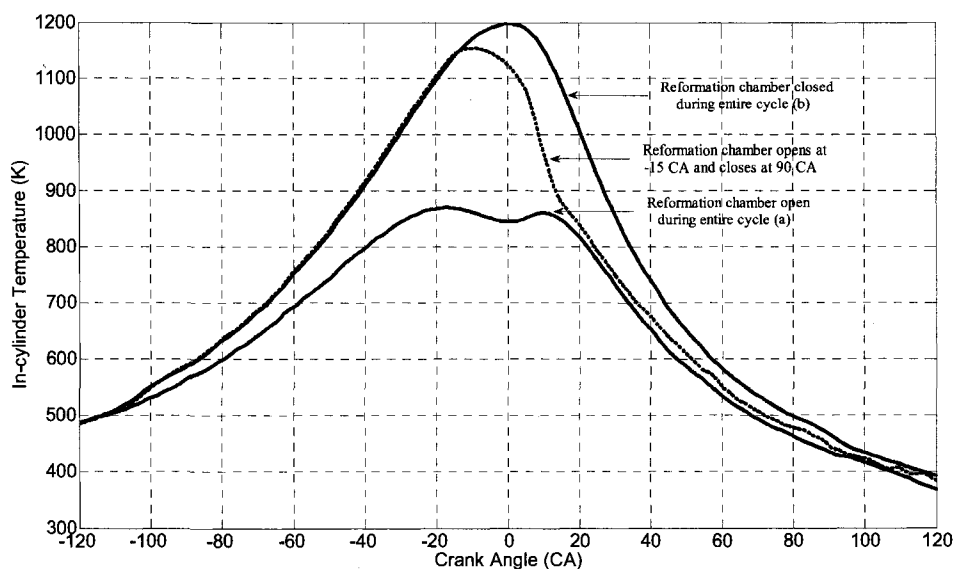


Figure 7.2: Calculated in-cylinder temperature for various motoring conditions (T_{in} : 150 °C and T_c : 75 °C).

Ideally, in the following experiments, the no reformation runs (similar to the Numerical Parametric study in Chapter 6) should have been the firing scenarios that correspond to the motoring case (a) in Fig. 7.1. Since the no reformation runs did not result in any combustion for the above test conditions during our experimental runs, it is of our interest to analyze only the effects of reformation products on HCCI combustion on-set and neglecting the additional advantage of temporarily changing in the HCCI cycle compression ratio (which is an integral part of the proposed reformation strategy). Hence, the no reformation fuelling case in this chapter is defined as the firing scenario that correspond to the motoring case (b) in Fig. 7.3 where the trapped products from the previous cycle are re-entered into the current cycle. The only difference between the reformation and no reformation is with respect to whether a percentage of the fuel is supplied or not using the direct injector into the reformation chamber for fuel reformation.

Figures 7.3 through 7.8 show the in-cylinder pressure and HRR for various engine operating conditions. In all the figures, the solid line represents the no reformation fuelling case and the dotted line represents the case when a percentage fuel is injected for reformation. The intake charge temperature (T_{in}), coolant temperature (T_c) and the equivalence ratio for each particular operating condition are displayed next to the in-cylinder pressure traces. The SOC, CO and UHC values are also shown next to the respective HRR curves for comparison between the no reformation and reformation fuelling case. The displayed UHC values are calculated as a percentage of the total fuel injected rather than ppm for a particular operating condition. It can be noticed that there

is a local maximum in the HRR curve at 15° CA BTDC at which point the reformation chamber valve starts to open and rapidly increases the cylinder volume. This local HRR maximum is an artifact of the HRR calculation method when this volume rapidly changes (dV/dCA). In this work, the dV/dCA was assumed to be a linear function of the CA between 15 and 10° CA BTDC, which might not be the actual case (e.g. non-linear). The 5° CA duration was chosen based on the in-cylinder pressure trace from motoring condition (Fig. 7.1), where the pressure has a negative dP/dCA at 10 CA BTDC signifying the reformation chamber is open. This is confirmed by examining Figs. 7.3 through 7.8 where there is a similar rise in the HRR value at 15° CA BTDC for the no reformation fuelling condition (solid line in Figs. 7.3 through 7.8).

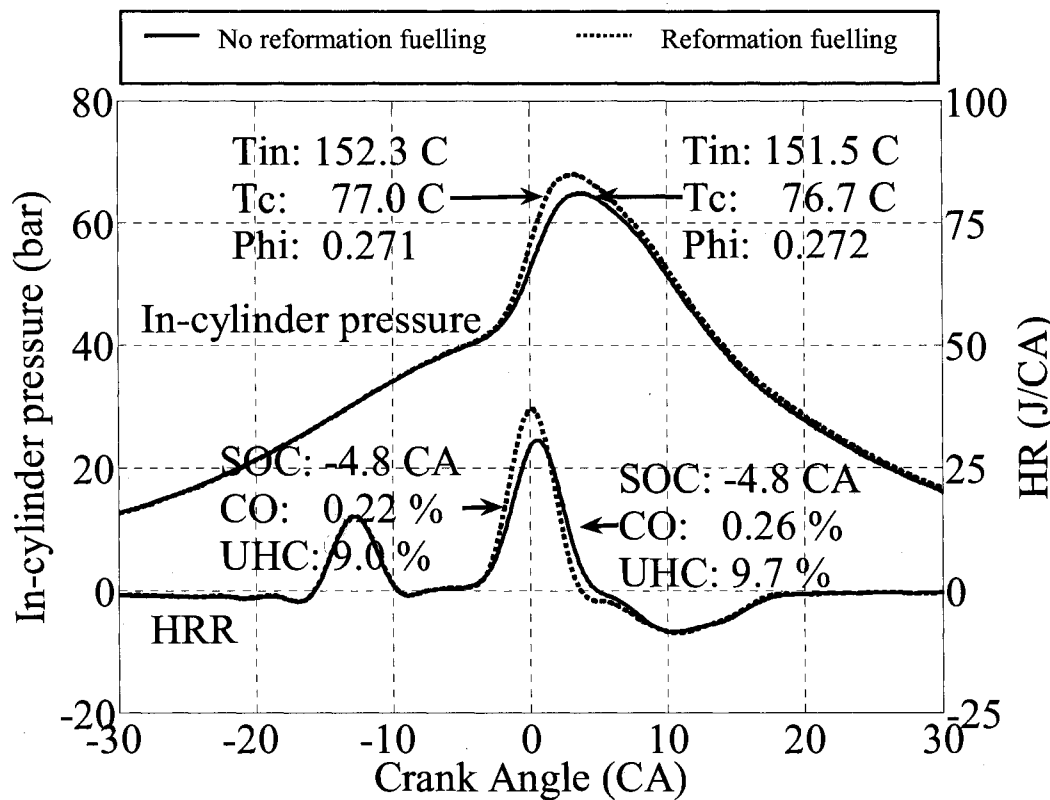


Figure 7.3: In-cylinder pressure and HRR for ϕ : 0.27, 1120 RPM and 10% fuel injected for reformation.

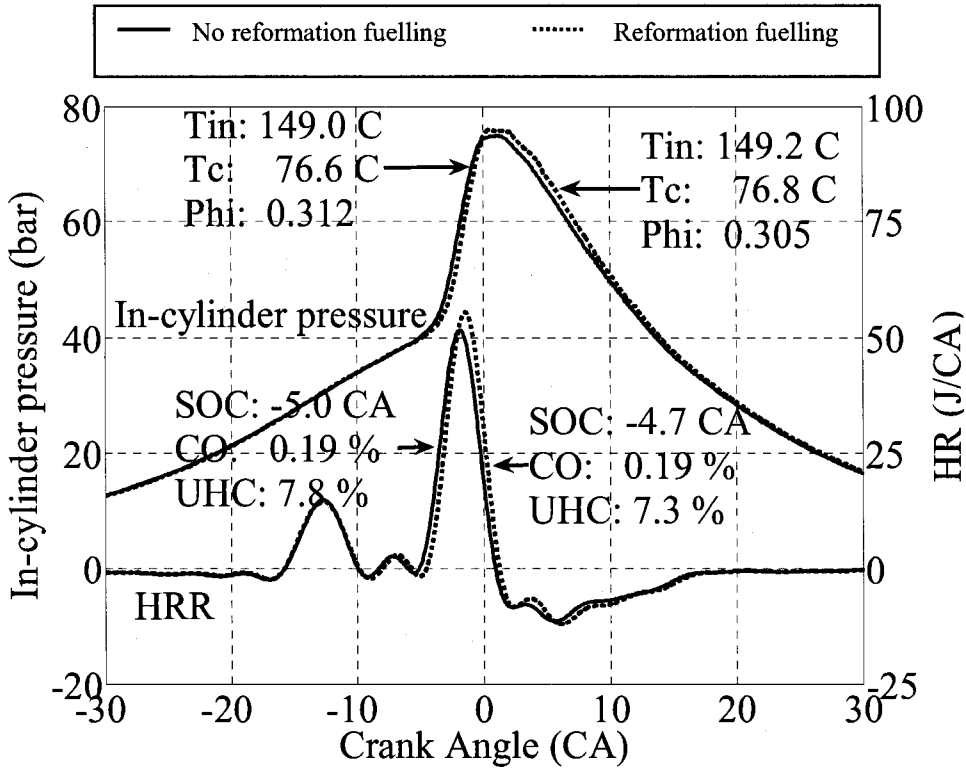


Figure 7.4: In-cylinder pressure and HRR for ϕ : 0.31, 1120 RPM condition and 10% fuel injected for reformation.

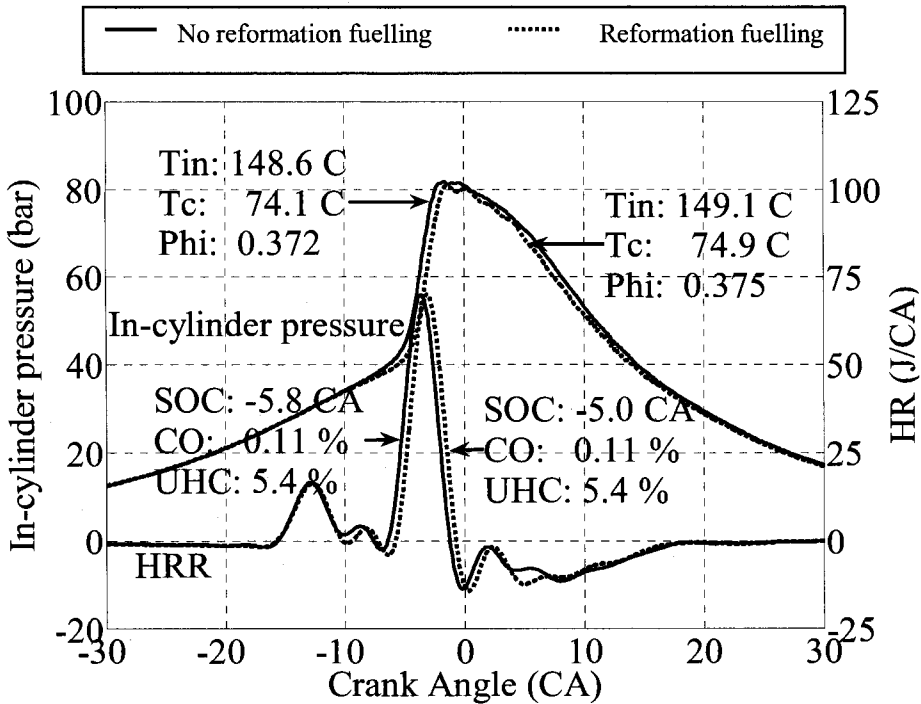


Figure 7.5: In-cylinder pressure and HRR for ϕ : 0.37, 1120 RPM and 10% fuel injected for reformation.

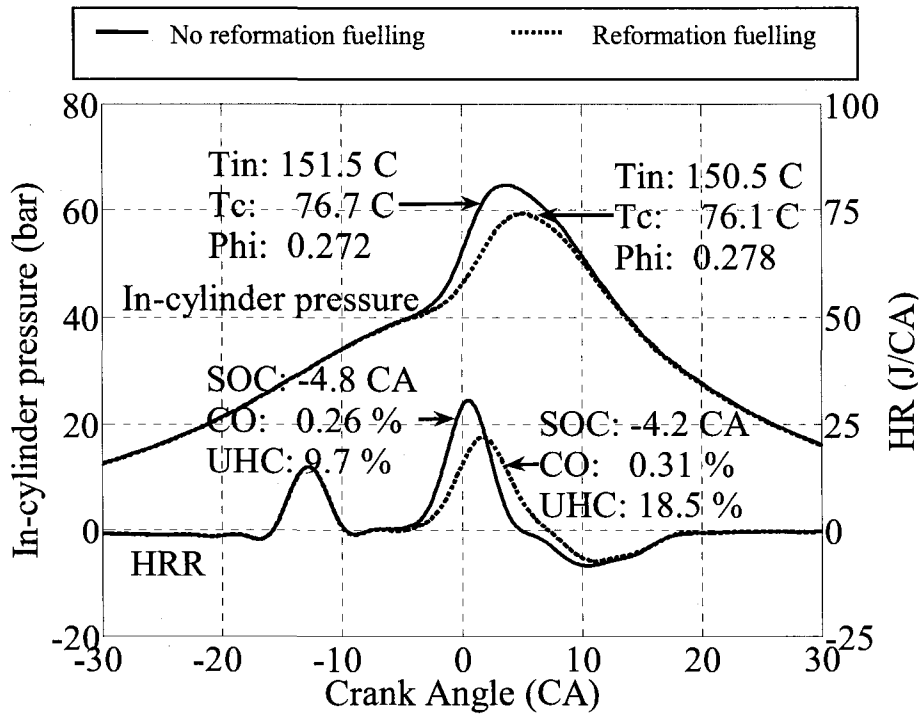


Figure 7.6: In-cylinder pressure and HRR for ϕ : 0.27, 1120 RPM and 25% fuel injected for reformation.

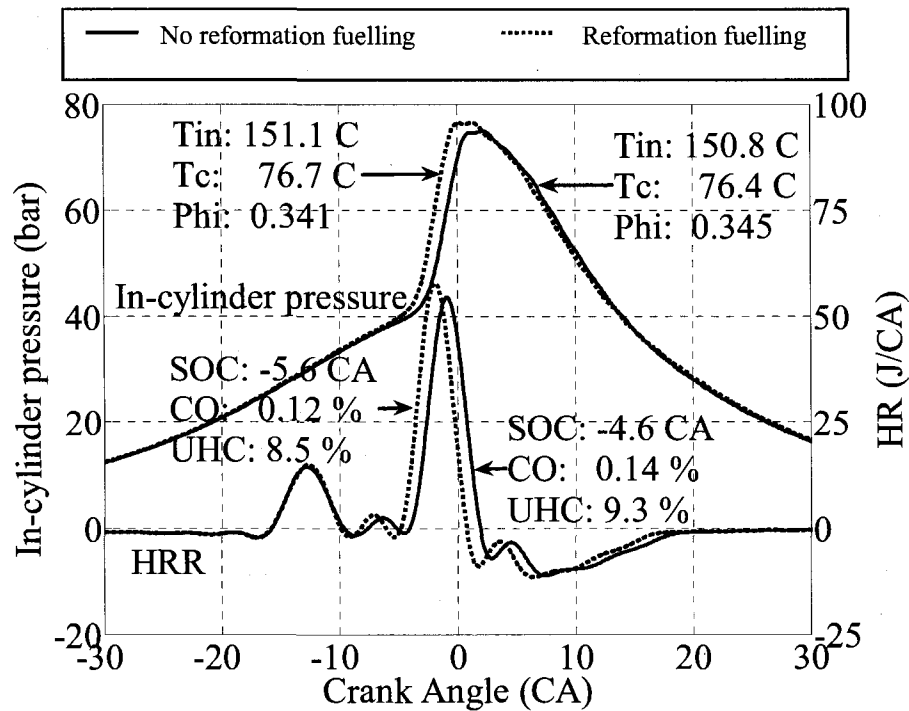


Figure 7.7: In-cylinder pressure and HRR for ϕ : 0.34, 1080 RPM and 20% fuel injected for reformation.

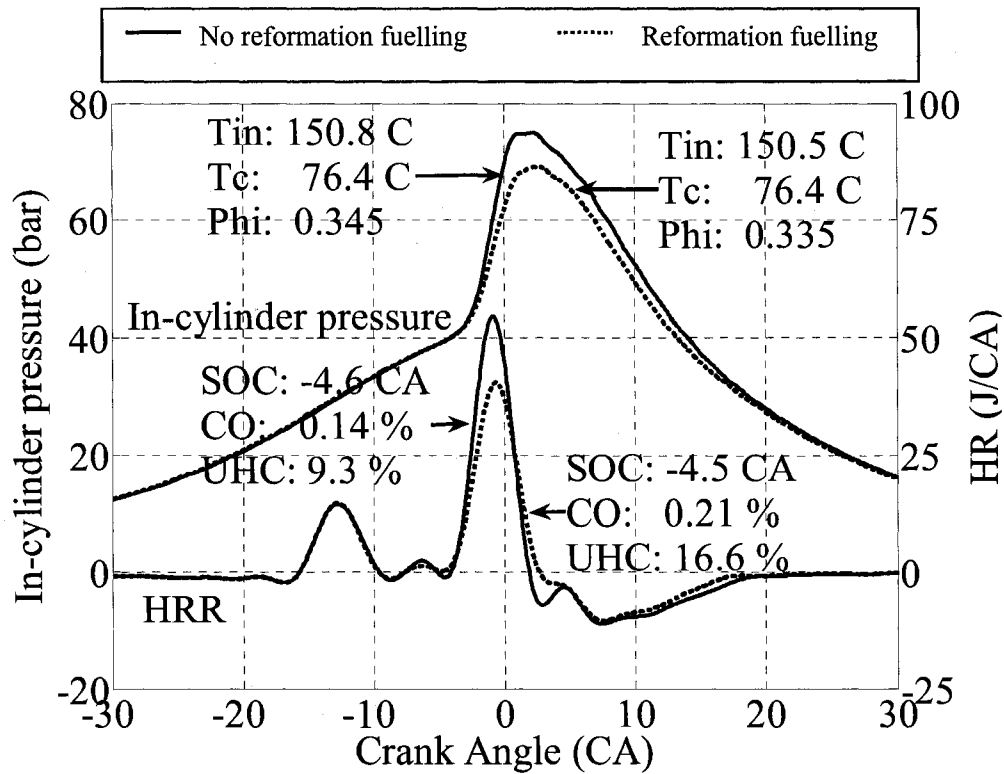


Figure 7.8: In-cylinder pressure and HRR for ϕ : 0.34, 1080 RPM and 25% fuel injected for reformation.

In Figures 7.3 through 7.5 the intake charge temperature and the percentage fuelling (10% of total fuel per cycle) were kept constant and the only parameter varied was the fuel-air equivalence ratio. In general, comparing the no reformation fuelling case (solid line) in Figs. 7.3 through 7.5, it can be noticed that the SOC is advanced with an increase in equivalence ratio for the same operating condition. Also, the CO and UHC level in the exhaust decreases with an increase in the equivalence ratio. This trend with equivalence ratio was also seen in Section 5.2.9 where the influence of EGR and equivalence ratio on HCCI combustion was analyzed without in-cylinder fuel reformation.

It should be realized that the reformation pre-chamber is open to the main chamber only during about one eighth of the cycle time and this occurs when temperatures reach their highest values. It is estimated that because of the pre-chamber volume (20% of the entire combustion chamber at TDC), the heat transfer losses across the pre-chamber walls (30 % of the pre-chamber walls protrudes into the main combustion chamber and remaining 70% is in the cylinder head) have only a small impact on the main charge state. However, the bigger impact in the current configuration is due to the throttling and mixing of the reformation products with the main charge through the connecting channel between the pre-chamber and the main chamber. Furthermore, the reformation reaction (equation 3.1) is endothermic and there is a long wait for the pre-chamber to open, occupying 7/8th of the cycle time. Both factors lead to overall decrease of the reformation products temperature. Hence, the advancement in the SOC utilizing the reformation process employed here suggests that the effect on HCCI combustion due to the reformation process is more of chemical than thermal in nature.

From Fig. 7.3, for $\phi = 0.27$, it can be noticed that with 10% reformation fuelling (dotted line) the CO and UHC levels are slightly reduced when compared to the no reformation fuelling case (solid line). Furthermore, the peak HRR value is higher and the HRR duration is shorter for the reformation case. This shows that the hydrogen-enriched reformation products help in attaining higher fuel conversion efficiency during the HCCI combustion of lean fuel-air mixture. The advantage of the in-cylinder reformation on HCCI combustion is also evident from the IMEP value (Fig. 7.9) obtained for the 10% reformation fuelling case (2.38 bar) which is higher than the no reformation fuelling case

(2.18 bar). A similar reduction in UHC and CO levels with higher HR values was seen in (Waldman, 2007) with in-cylinder reformation using NVO. However, in Fig. 7.3 there was no significant change in the SOC between the reformation and the no reformation fuelling conditions.

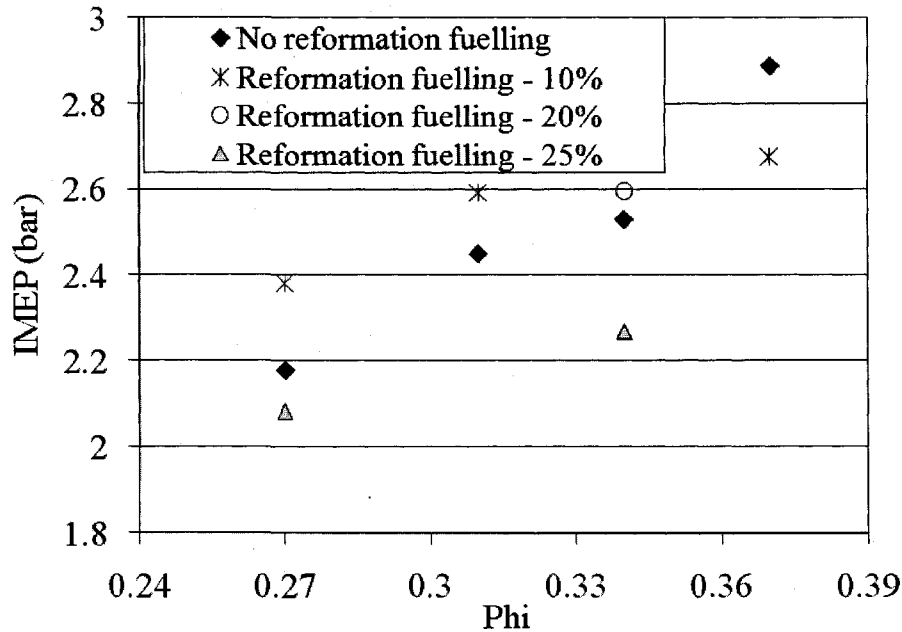


Figure 7.9: IMEP vs Equivalence ratio for various reformation fuelling percentage.

An interesting trend emerges for the 10% reformation case when the equivalence ratio is changed. As the equivalence ratio is increased, the SOC retardation and the decrease in CO, UHC levels are diminished when compared to their corresponding no reformation fuelling case. The difference in the HRR peak value and the HRR duration is also reduced with an increase in the equivalence ratio for the reformation fuelling case. Specifically in Fig. 7.5, the reformation products act more like EGR by delaying SOC with no reduction in HRR duration, UHC and CO levels. The trend is also witnessed with

the IMEP (Fig. 7.9), where the high rise in IMEP for the 10% in-cylinder reformation fuelling condition over the corresponding no reformation fuelling case diminished with an increase in engine operating equivalence ratio. In Fig. 7.4 with $\phi = 0.31$, the corresponding IMEP (Fig. 7.9) for the 10% reformation fuelling case is 2.59 bar, slightly higher than the no reformation condition (2.45 bar). Whereas, for Fig. 7.5 ($\phi = 0.37$), the 10% reformation fuelling case showed a lower IMEP value of 2.68 bar (Fig. 7.9) when compared to the no reformation case (2.89 bar). It should be realized that the combustion products are trapped for reformation at 80° CA ATDC during the expansion stroke in all runs and most of the equivalence ratios analyzed are lower than that of Eq. 6.3 ($\phi = 0.4$). Furthermore, the percentage reformation fuelling (10%) is much less than the theoretical reformation level (40.5% at $\phi = 0.37$), which was calculated based on only the oxygen content of the trapped combustion products. Hence, in theory, considering only the oxygen content, an engine operating at a lower equivalence ratio should provide an environment which favors the reformation reaction (Eq. 6.3) towards complete combustion compared to the engine operating at a higher equivalence ratios. However, the trend is reversed when comparing Figs 7.3 through 7.5. This is mainly due to a lower temperature of the trapped combustion products which enter the reformation process for the engine operating at $\phi = 0.27$ when compared to the higher equivalence ratios ($\phi = 0.31$ and $\phi = 0.37$). For the $\phi = 0.27$ condition, even with higher oxygen content in the trapped combustion products, the lower temperature of the trapped combustion products leads to a favorable reformation condition and does not allow for complete conversion of the fuel injected to CO₂ and H₂O. Whereas, with increase in equivalence ratio the temperature of the trapped combustion products increases and the fuel injected for

reformation approaches complete combustion (CO_2 and H_2O) rather than reformation. This can be clearly seen with Fig. 7.5 where the reformation products act more like EGR when compared to Fig. 7.3. This indicates that the temperature and the oxygen content play a critical role during the reformation period in either achieving hydrogen enriched reformat gas or complete combustion during the reformation period. In order to clarify this effect the percentage reformation fuelling was increased in the experiments which led to Fig. 7.6 though 7.8. Figure 7.6 shows the in-cylinder pressure and HRR comparison between the no reformation fuelling and 25% reformation fuelling case. The fuel-air equivalence ratio used for this condition is 0.27, as in Fig. 7.3. Comparing Fig. 7.3 and 7.6 it can be noted that with an increase in the reformation fuelling percentage from 10% to 25%, the SOC is retarded and the combustion efficiency also deteriorates (CO and UHC increases). This is also seen in the IMEP trend (Fig. 7.9) where the 25% reformation fuelling case (2.07 bar) falls below the no reformation fuelling condition (2.18 bar). Even though excess oxygen content of the trapped combustion products favors a higher reformation fuelling percentage in the case of $\phi = 0.27$, it should be realized that the temperature of the trapped combustion products decreases with an increase in the reformation fuelling percentage due to the high enthalpy of vaporization of ethanol. This in turn leads to a decrease in the overall temperature during the reformation process and does not favor the reformation reaction, which is evident during the subsequent HCCI combustion with the reformation products in Fig. 7.6. This phenomenon of an optimal reformation fuel percentage for a particular operating condition is further confirmed when looking into Figs. 7.7 and 7.8.

Figure 7.7 shows the in-cylinder pressure and HRR comparison between the no reformation fuelling condition and the 20% reformation fuelling condition. The fuel-air equivalence ratio for this condition is 0.34 which lies between the equivalence ratios in Figs. 7.4 and 7.5. As mentioned above, from Figs. 7.4 and 7.5, it was clear that the 10% reformation fuelling was not the optimal amount since the increase in trapped combustion products temperature (with increase in engine operating equivalence ratio) shifted the reformation reactions towards complete combustion. From Fig. 7.7 it can be seen that the increase in the reformation fuelling percentage (20%) with higher equivalence ratio ($\phi = 0.34$) favors the reformation process and has a positive impact on the subsequent regular HCCI combustion process. The IMEP for the 20% reformation fuelling condition was 2.6 bar compared to 2.53 bar for the no reformation fuelling condition. The 20% reformation fuelling condition advances SOC and decreases the CO and UHC levels when compared to the no reformation case. However, with further increase in the percentage reformation fuel to 25% (Fig. 7.8) the SOC is retarded and the combustion efficiency deteriorates (CO and UHC increases). This is also evident from the IMEP where the 25% reformation fuelling condition (Fig. 7.9) drops to 2.27 bar when compared to the no reformation fuelling condition (2.53 bar). This shows that for the 0.34 equivalence ratio the optimal reformation fuelling percentage that has a desired impact on the HCCI combustion is 20%.

Figure 7.10 shows the COV_{IMEP} values for the different tested reformation fuelling and no reformation fuelling conditions. It can be seen from Fig. 7.10 that all the reformation fuelling conditions except one (0.27 equivalence ratio and 25% reformation fuelling condition) showed lower COV_{IMEP} values compared to their respective no reformation

fuelling condition. However, it should be realized that IMEP values for the $\phi = 0.37$ with 10% reformation fuelling condition and $\phi = 0.34$ with 25% reformation fuelling were lower compared to their respective no reformation fuelling conditions. This shows that even at operating conditions where the reformation fuelling percentage is not at its optimized value, the products of fuel reformation help in attaining a lower COV_{IMEP} values compared to their respective no reformation fuelling conditions.

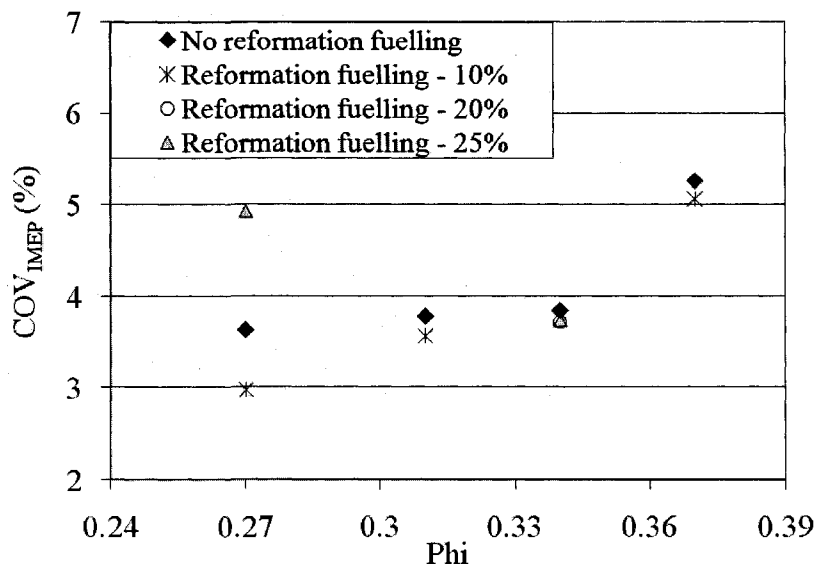


Figure 7.10: COV_{IMEP} vs Equivalence ratio for various reformation fuelling percentage.

It should be said here that the CO and UHC levels for all the above experimental runs were high and would require exhaust after-treatment. Similar higher levels of CO and UHC were also reported by (Van Blarigan, 1998).

7.3 Summary

In this chapter, a new in-cylinder reformation strategy to control the on-set of HCCI combustion was tested in an experimental HCCI engine fuelled with lean ethanol/air mixtures.

The in-cylinder reformation methodology utilizing a pre-chamber does not affect the volumetric efficiency of the engine as in the case of NVO technology and provides control over the mixing of the reformation products with fresh charge when compared with other processes.

Employing the proposed pre-chamber methodology results in controlling the HCCI combustion on-set (SOC) in two ways:

- Simply manipulating the reformation chamber opening time during the compression stroke (excluding the effects of reformation products) results in temporary change in compression ratio and has a strong influence in controlling the HCCI combustion on-set (SOC).
- Excluding the benefits of temporary change in compression ratio (that results from utilizing the proposed methodology), the fuel reformation products shows further prospects in controlling the HCCI combustion on-set. However, the influence of reformation products on the HCCI combustion on-set has a lesser influence compared to the temporary change in compression ratio that results from utilizing the proposed pre-chamber methodology.

The experimental results from the proto-type reformation chamber demonstrate that the products from in-cylinder reformation are effective for most conditions in accelerating the HCCI combustion on-set (SOC) and reduce the regulated engine-out emissions.

The experimental results also indicate that there is an optimal in-cylinder reformation fuelling percentage for each operating condition.

Chapter 8 Conclusions and recommendations

8.1 Introduction

The overall objective of this study is to investigate the combustion characteristics of an IDI type HCCI engine fuelled with ethanol and products of in-cylinder reformation for different operating conditions. Furthermore, the effect of iso-octane addition at the on-set of HCCI combustion is also investigated experimentally. An IDI-type engine is used in this study since to differentiate from the majority of the work done in HCCI combustion on DI-type engines. Hence, it is of our interest to investigate the effect of a pre-chamber and the influence of a high surface to volume ratio in an IDI-type on the HCCI combustion.

The major focus of the study is on identifying parameters that influence the HCCI combustion on-set, since the HCCI engine lacks a direct means of combustion on-set control. The methodology adopted here to identify these parameters is mostly experimental. However, there is a smaller computational component which involves HCCI cycle calculations with fuel reformation using a single-zone model. The computational part is primarily used to analyze the advantages of the proposed in-cylinder reformation strategy on HCCI combustion before implementation in the experimental set-up.

The above objective is met by first executing an extensive experimental matrix on different operating parameters for the regular HCCI combustion process without fuel reformation. Secondly, a new in-cylinder fuel reformation strategy has been proposed,

implemented and experimentally tested in this work. This chapter presents the conclusions of the experimental and simulation work with recommendations for future studies.

8.2 Conclusions

8.2.1 Experimental results: Effect of intake charge temperature and fuel chemistry

- For the same intake charge temperature and engine speed, the on-set of combustion for ethanol occurs ahead of that for iso-octane. For example, the on-set of combustion in the case of ethanol and iso-octane at 1035 RPM and 136 °C are 5.6 and 1.9° CA BTDC, respectively. It should be noted that ethanol has a higher enthalpy of vaporization than iso-octane, but this has no effect since the intake charge temperature is maintained constant.
- The HRR and in-cylinder pressure traces in this IDI engine indicate that residence time has more impact on the on-set of combustion at lower charge temperatures and engine speeds.
- The indicated thermal efficiency (30 – 41%) values reported in this study are comparable to other HCCI experimental results reported elsewhere and these values are better than those for typical SI engines which are less than 30%, especially during low load operating conditions.
- The presence of the pre-chamber in this IDI type engine ensures stable operation (COV_{IMEP} stays below 5%) due to trapping of residual mass that acts as an

ignition source for subsequent cycles once the initial cycle with combustion occurs.

- The NO_x emissions were very low (less than 10 ppm) for the tested conditions and do not require after-treatment. However, the UHC and CO levels are higher and would require after-treatment.
- For a particular operating condition, the presence of ethanol reduced the CO and UHC levels on this HCCI engine operating with iso-octane at a lean fuel-air equivalence ratio.

8.2.2 Experimental results: Effect of EGR

- For the same intake charge temperature and engine speed, the on-set of combustion and the HR duration increases with EGR addition irrespective of the fuel type used in this study. This influence has been reported by several other researchers elsewhere.
- The IMEP and COV_{IMEP} values also indicate that ethanol allows for the use of a higher percentage of EGR when compared to iso-octane.
- The COV_{IMEP} values for the maximum IMEP values are within the stable operating conditions (below 4%) for the tested conditions.
- The maximum thermal efficiency (30 – 40%) values obtained in this study are comparable to other HCCI experimental results reported elsewhere. The heat transfer losses decrease with engine speed and have a major effect in this IDI-type engine at lower RPM conditions.

- Trends in the thermal efficiency indicate that the residence time and combustion reaction rates play an important role at higher RPM conditions. For higher RPM conditions (1275 and 1520 RPM) fuelling with iso-octane showed slower combustion characteristics that obtained the maximum thermal efficiency when compared to 50% ethanol/iso-octane blend.
- In general, operation with ethanol present showed better emissions and more complete combustion compared to fuelling with iso-octane. The CO and UHC levels were higher when fuelled with iso-octane when compared with a 50% ethanol/iso-octane blend.
- The NO_x emissions are very low (less than 10 ppm) for the tested conditions and do not require after-treatment. However, the UHC and CO levels are higher and would require after-treatment.

8.2.3 In-cylinder fuel reformation: Numerical parametric study

- The predicted pressure and the respective rise rates after ignition were excessive compared to the experimental results. The excessive predictions in the pressure and the rise rates were due to the inherent nature of the single-zone models and similar results have been reported by other researchers.
- The trends between experimental and single-zone model were similar when analyzing a particular fuel. However, there was a reverse in the experimental and numerical trends when comparing the on-set of combustion between different fuel mechanisms (pure ethanol and pure iso-octane) for a particular operating condition.

- The in-cylinder fuel reforming using NVO extends the operational range of a HCCI engine. The no reformation fuelling condition with 45% EGR misfired, while the same condition with 30% fuel undergoing the reformation process fired.
- The NVO reforming process also showed that there is optimal reformation duration and reformation fuelling percentage depending on the HCCI engine operation condition, which varied the SOC and produced a higher IMEP during the HCCI combustion cycle.
- The in-cylinder fuel reformation using a pre-chamber also showed extension in the operating range similar to the NVO method. However, the pre-chamber method shows a higher degree of controllability in varying the HCCI combustion on-set by manipulating the time at which the reformation products are added to the main HCCI combustion event.
- Furthermore, in-cylinder reformation using a pre-chamber also showed that it can extend the HCCI operating limit to lower initial charge temperatures than the one feasible with the NVO method for a particular operating condition.
- Similar to the NVO method, the pre-chamber method also showed that there is optimal reformation duration and reformation fuelling percentage depending on the HCCI engine operation condition, which varied the SOC and produced a higher IMEP during the HCCI combustion cycle.

8.2.4 Experimental results: Effect of in-cylinder fuel reformation

- The in-cylinder reformation methodology utilizing a pre-chamber does not affect the volumetric efficiency of the engine as in the case of NVO technology and

provides control over the mixing of the reformation products with fresh charge when compared with other processes.

- Employing the proposed pre-chamber methodology results in controlling the HCCI combustion on-set (SOC) in two ways:
 - Simply manipulating the reformation chamber opening time during the compression stroke (excluding the effects of reformation products) results in temporary change in compression ratio and has a strong influence in controlling the HCCI combustion on-set (SOC).
 - Excluding the benefits of temporary change in compression ratio (that results from utilizing the proposed methodology), the fuel reformation products shows further prospects in controlling the HCCI combustion on-set. However, the influence of reformation products on the HCCI combustion on-set has a lesser influence compared to the temporary change in compression ratio that results from utilizing the proposed pre-chamber methodology.
- The experimental results from the proto-type reformation chamber demonstrate that the products from in-cylinder reformation are effective for most conditions in accelerating the HCCI combustion on-set (SOC) and reduce the regulated engine-out emissions.
- The experimental results also indicate that there is an optimal in-cylinder reformation fuelling percentage for each operating condition.

8.3 Recommendations for future work

The author suggests that future studies should cover the following areas:

- One of the major restrictions in the above reformation results is the inability to vary the CA at which the combustion products are captured and brought back into the main HCCI combustion event. This is due to the use of a compression spring to control the opening and closing of the reformation chamber valve. Hence, it is recommended to implement a Variable Valve Timing (VVT) system to control the valve, which would allow us to vary the valve opening and closing timing.
- More experimental work is needed to thoroughly investigate the many interesting details associated with the reformation strategy. It is recommended to perform a more extensive experimental matrix with varying CA at which combustion products are trapped for reformation and brought back into the main HCCI combustion event, varying reformation fuelling percentage and engine operating conditions.
- Based on the reformation fuelling results for ethanol, it is recommended to test how a hydrocarbon fuel would have behaved during this type of combustion.
- Based on the results obtained from this work it would be interesting to know what is occurring in the reformation chamber. For future experiments, it is recommended to add a piezoelectric transducer to the reformation chamber, and consider sampling from the reformation chamber for chemical analysis.

References

1. Asmus, T. and Zhou, F., "Homogeneous Charge Compression Ignition (HCCI) Engines-Key Research and Development Issues", PT-94 Society of Automotive Engineers, Chp.4, 2003.
2. Cairns, A., and Baxill, H., "The Effects of Combined Internal and External EGR on Gasoline Controlled Auto-Ignition", SAE paper 2005-01-0133, 2005.
3. Canton, P. A., Song, H. H., Kaahaaina, N. B. and Edwards, C., "Strategies for Achieving Residual-Effectuated Homogeneous Charge Compression Ignition Using Variable Valve Actuation", SAE Paper 2005-01-0165, 2005.
4. Cengel, Y., Boles, M., "Thermodynamics, An Engineering Approach, 3rd Edition," McGraw-Hill, Table A-1, pp. 898, 1998.
5. Christensen, M., Hultqvist, A. and Johansson, B., "Demonstrating the multi-fuel capability of a homogeneous charge compression ignition engine with variable compression ratio", SAE Paper 1999-01-3679, 1999.
6. Christensen, M., Einewall, P. and Johansson, B., "Homogeneous Charge Compression Ignition (HCCI) using Iso-octane, ethanol and natural gas-a comparison with spark ignition operation", SAE Paper 972874, 1997.
7. Christensen, M. and Johansson, B., "Homogeneous charge compression ignition with water injection", SAE Paper 1999-01-0182, 1999.
8. Christensen, M. and Johansson, B., "Influence of mixture quality on homogeneous charge compression ignition", SAE Paper 982454, 1998.
9. Christensen, M., Johansson, B., Amneus, P. and Mauss, F., "Supercharged Homogeneous Charge Compression Ignition", SAE Paper 980787, 1998.

10. Christensen, M. and Johansson, B., "Supercharged homogeneous charge compression ignition (HCCI) with exhaust gas recirculation and pilot fuel", SAE Paper 2000-01-1835, 2000.
11. Curran, H. J., Gaffuri, P., Pitz, W.J. and Westbrook C. K., "A comprehensive modeling study of iso-octane Oxidation" Combustion and Flame 129, pp.253-280, 2002.
12. Figure 1.2 modified based on online document available at:
"http://www.whnet.com/4x4/cgi.html"
13. Furutani, M., Ohta, Y., Kono, M. and Hasegawa, M., "An investigation into the effect of fuel composition on HCCI combustion characteristics", Proceedings of the Fourth International Symposium COMODIA; 1998. p. 173–177.
14. Goodwin, D.G., "Cantera", Proceedings of CVD XVI and EuroCVD Fourteen, Electrochemical Society, 2003.
15. Guohong, T., Wang, J., Shuai, S., Wang, Z. and An, X., "HCCI Combustion Control by Injection Strategy with Negative Valve Overlap in a GDI Engine", SAE Paper 2006-01-0415, 2006.
16. Hakan, P., Agrell, Olsson, J. and Johansson, B., "The Effect of Intake Temperature on Hcci Operation Using Negative Valve Overlap", SAE 2004-01-0944, 2004.
17. Hashimoto, K., "Effect of Ethanol on the HCCI Combustion", SAE Paper 2007-01-2038, 2007.
18. Heywood, J.B., "Internal Combustion Engine Fundamentals," McGraw-Hill, various pages, 1988.
19. Hiraya K., Hasegawa, K., Urushihara, T., Liyama, A. and Itoh, T., "A study on gasoline fuelled compression ignition engine ~ a trial of operation region expansion", SAE Paper 2002-01-0416, 2002.

20. Iida, N., Igarashi, T., “Auto-Ignition and Combustion of n-Butane and DME/Air Mixtures in a Homogeneous Charge Compression Ignition Engine”, SAE Paper 2000-01-1832, 2000.
21. Kaahaaina, N. B., Simon, A., Caton, A. P. and Edwards, C., “Use of Dynamic Valving to Achieve Residual-Affected Combustion”, SAE Paper 2001-01-0549, 2001.
22. Kamio, J., Kurotani, T., Kuzuoka, K., Kubo, Y., Taniguchi, H. and Hashimoto, K., “Study on HCCI-SI Combustion Using Fuels Containing Ethanol”, SAE Paper 2007-01-4051, 2007.
23. Kook, S., and Bae, C., “Combustion Control Using Two-Stage Diesel Fuel Injection in a Single-Cylinder PCCI Engine”, SAE Paper 2004-01-0938, 2004.
24. Koopmans, L., Ogink, R. and Denbratt, I., “Direct Gasoline Injection in the Negative Valve Overlap of a Homogeneous Charge Compression Ignition Engine”, SAE Paper 2003-01-1854, 2003.
25. Kubota Canada Ltd, retrieved November 10th, 2003, from “http://www.css-club.net/kubota_catalog/pdf/Super_Five.pdf.”
26. Kubota Corporation (n.a), “Kubota Workshop Manual 9789701642,” May 1996.
27. Lavy, J., Schulz, C., Krämer, H., Zhao, H., Damiano, L., Dabadie, J., Angelberger, C., Duret, P., Juretzka, A., Schäfle, J., Ma, T. H., Lendresse, Y. and Satre, A., “Innovative Ultra-low NO_x Controlled Auto-Ignition Combustion Process for Gasoline Engines: the 4- SPACE Project”, SAE Paper 2000-01-1837, 2000.
28. Law, D., Allen, J., Kemp, D., Kilpatrick, G. and Copland, T., “HCCI Mode of Combustion in a Single Cylinder 4-Stroke Engine Fitted With Variable Valve Train”, SAE Paper 2001-01-0251, 2001.

29. Lü, X., Chen, W. and Huang, X., "Experimental study on the auto-ignition and combustion characteristics in the HCCI combustion operation with ethanol/n-heptane blend fuels by port injection", *Fuel*, Vol. 85, Issues 17-18, p 2622-2631, 2006.
30. Mack, J.H., Flowers, D. L., Buchholz, B.A. and Dibble, R. W., "Investigation of HCCI combustion of diethyl ether and ethanol mixtures using carbon 14 tracing and numerical simulations", *Proceedings of the Combustion Institute*, Vol. 30, Issue 2, pp. 2693 – 2700, 2005.
31. Marinow, N. M., 1998, "A Detailed Chemical Kinetics Model for High temperature Ethanol Oxidation", *Inter. J. of Chem. Kin.*, Lawrence Livermore National Laboratory, Livermore, CA, UCRL-JC-131657, [Online Document], Available at:
"http://www.cms.llnl.gov/combustion/combustion2.html."
32. Mathworks, "The Matlab, the language of technical computing", The MathWorks Inc., 1994 –2005.
33. Meriam Process Technologies (n.d), retrieved December 20, 2004, from,
"http://www.meriam.com/products/default.asp?m=3&d=62&p=14."
34. Najt, P.M., and Foster, D.E., "Compression-Ignited Homogeneous Charge Combustion", SAE Paper 830264, 1983.
35. Ng, C. K. W. and J. Thomson, M. J., "A Computational Study of the Effects of Fuel Reforming, EGR and Initial Temperature on Lean Ethanol HCCI Combustion", SAE 2004-01-0556, 2004.
36. Noguchi, M., Tanaka, Y., Tanaka, T. and Takeuchi, Y., "A Study on Gasoline Engine Combustion by Observation of Intermediate Reactive Products During Combustion", JSAE 790840, 1979.
37. Oakley, A., Zhao, H., Ma, T. and Ladommatos, N., "Dilution Effects on the Controlled Auto-Ignition (Cai) Combustion of Hydrocarbon and Alcohol Fuels", SAE Paper 2001-01-3606, 2001.

38. Olsson, J., Tunestal, P., Haraldsson, G., Johansson, B., "A Turbo Charged Dual Fuel HCCI Engine", SAE Paper 2001-01-1896, 2001.
39. Olsson, J., Tunestal, P., Johansson, B., "Compression Ratio Influence on Maximum Load of a Natural Gas Fueled HCCI Engine", SAE Paper 2002-01-0111, 2002.
40. Omega International (n.d), retrieved December 2004,
"http://www.omega.com/pptst/SH_HEATER.html."
41. Omega International (n.d), retrieved December 2004,
"http://www.omega.com/ppt/pptsc.asp?ref=CNI_Series&nav."
42. Onishi, S., Jo, S. H., Shoda, K., Jo, P. D. and Kato, S., "Active Thermo Atmosphere Combustion (ATAC) – A New Combustion Process for Internal Combustion Engines", SAE 790501, 1979.
43. OTC Corporation - MicroGas Analyzer User Guide, retrieved September 10th, 2004, from,
"http://www.otctools.com/newcatalog/products/162_man.pdf."
44. Roth, K., "In-cylinder pressure measurements with optical fiber and piezoelectric pressure transducers", M.Sc. Thesis, University of Windsor, 2002.
45. Smith, G. P., Golden, D. M., Frenklach, M., Moriarty, N. W., Eiteneer, B., Goldenberg, M., Bowman, C. T., Hanson, R. K., Song, S., Gardiner, W. C., Lissianski, V. V. and Qinet, Z., "GRI Mech 3.0", Available at;
http://www.me.berkeley.edu/gri_mech/.
46. Stockinger, M. Schäpertöns, H., Kuhlmann, P., "Versuche an einem gemischansugenden Verbrennungsmotor mit Selbstzündung (Effects of air-fuel mixture on a naturally aspirated HCCI engine)" MTZ 53, vol. 2, p80-85, 1992.
47. Tabaczynski, R., "Future Powertrain Technologies", ASME ICE Meeting, Austin, Texas, USA, 2000.
48. Takeda, Y. and Keiichi, N., "Emission Characteristics of Premixed Lean Diesel Combustion with Extremely Early Staged Fuel Injection", SAE Paper 961163, 1996.

49. Tanet, A., Werner, P., Sohm, V. M., Foster, D. E., Ibara, T., Morikawa, T., Lida, M. and Waldman, J.O., "Expanding the Hcci Operation With the Charge Stratification", SAE Paper 2004-01-1756, 2004.
50. Thring, R. H., "Homogeneous Charge Compression-Ignition (HCCI) Engines" SAE paper 892068, 1989.
51. Urata, Y., Awasaka, M., Takanashi, J., Kakinuma, T., Hakozaki, T. and Umemoto, A., "A Study of Gasoline-Fuelled Hcci Engine Equipped With An Electromagnetic Valve Train" 2004-01-1898, 2004.
52. Urushihara, T., Hiraya, K., Kakuhou, A. and Itoh, T., "Expansion of HCCI Operating Region by the Combination of Direct Fuel Injection, Negative Valve Overlap and Internal Fuel Reformation", SAE Technical Paper, 2003-01-0749, 2003.
53. Hosseini, V. and Checkel, M.D., "Reformer Gas Composition Effect on HCCI Combustion of n-heptane, iso-octane, and Natural Gas", SAE paper 2008-01-0049, 2008.
54. Van Blarigan, P., Paradiso, N. and Goldsborough, S., "Homogeneous Charge Compression Ignition with a Free Piston: A New Approach to Ideal Otto Cycle Performance", SAE paper 982484, 1998.
55. Waldman, J., Nitz, D., Aroonsrisopon, T., Foster, D. E. and lida, M., "Experimental Investigation into the Effects of Direct Fuel Injection During the Negative Valve Overlap Period in an Gasoline Fueled HCCI Engine", SAE Paper 2007-01-0219, 2007.
56. Wang, Z., Wang, J., Shuai, S. and Ma, Q., "Effects of Spark Ignition and Stratified Charge on Gasoline HCCI Combustion With Direct Injection", SAE Paper 2005-01-0137, 2005.
57. Xie, H., Wei, Z., He, B. and Zhao, H., "Comparison of HCCI Combustion Respectively Fueled with Gasoline, Ethanol and Methanol through the Trapped Residual Gas Strategy", SAE paper 2006-01-0635, 2006.

58. Zhang, Y., He, B., Xie, H. and Zhao, H., "The Combustion and Emission Characteristics of Ethanol on a Port Fuel Injection HCCI Engine", SAE paper 2006-01-0631, 2006.
59. Zhao, F., Assanis, D.N., Najit, P. M., Dec, J.E., Eng, J.A. and Asmus, T.N., Editors, "Homogenous Charge Compression Ignition (HCCI) Engines; Key Research and Development Issues", SAE PT-94, 2003.
60. Zoldak, P., "Design of a Research Engine for Homogeneous Charge Compression Ignition (HCCI) Combustion", M.Sc. Thesis, University of Windsor, 2005.

Appendix A: Engine specifications

A.1: Kubota D905 engine specifications

Engine Type	Vertical 4-cycle liquid cooled diesel
Number of cylinders	3
Bore & Stroke [mm(in)]	72.0 X 73.6 (2.83 X 2.90)
Total Displacement [L(cu.in)]	0.898 (54.8)
Gross Intermittent Power [kW(HP)]	15.5 (20.8) @ 3000 RPM 18.5 (24.8) @ 3600 RPM
Net Intermittent Power [kW(HP)]	14.9 (20) @ 3000 RPM 17.5 (23.5) @ 3600 RPM
Net Continuous Power [kW(HP)]	13.0 (17.4) @ 3000 RPM 15.2 (20.4) @ 3600 RPM
No load high idling speed	3800
No load low idling speed	800
Direction of Rotation	Counter-clockwise (from flywheel side)
Dry Weight [kg(lbs)]	110.0 (242.5)
Compression Pressure	412 to 469 psi, Limit 327 psi

A.2 Factory valve timing for Kubota D905

Valve Timing	Factory Specification
Intake Valve Open	0.24 rad. (14°) before TDC
Intake Valve Close	0.52 rad. (30°) after TDC
Exhaust Valve Open	0.96 rad. (55°) before BDC
Exhaust Valve Close	0.24 rad. (17°) after TDC

A.3 Performance Curve for Kubota D905 Engine

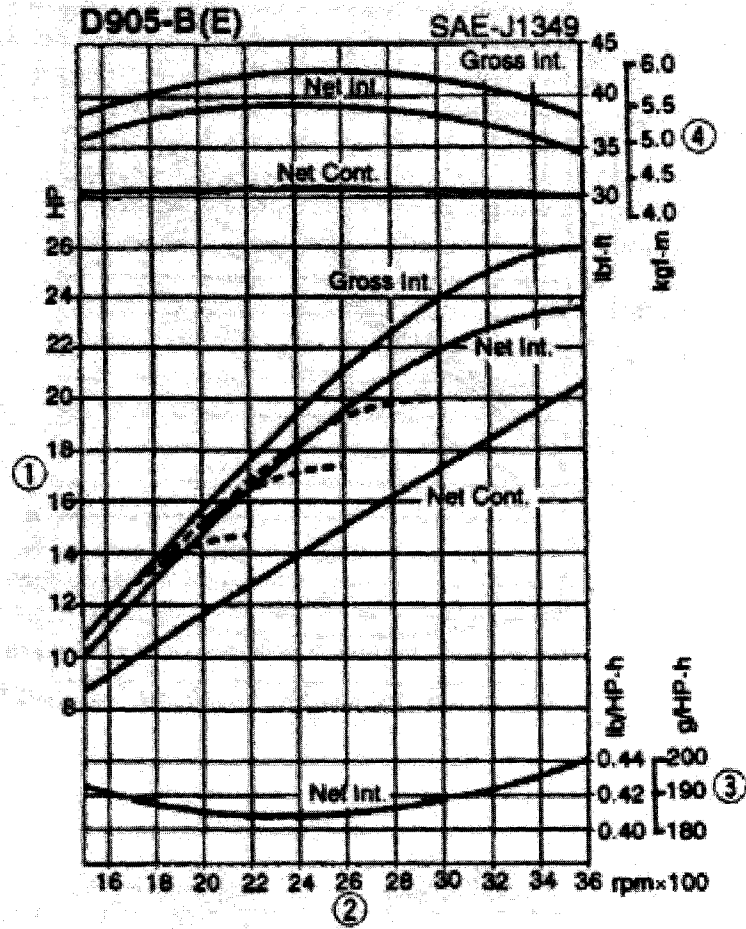


Figure A.1a: Performance Curve for Kubota D905 Engine (Units -British).

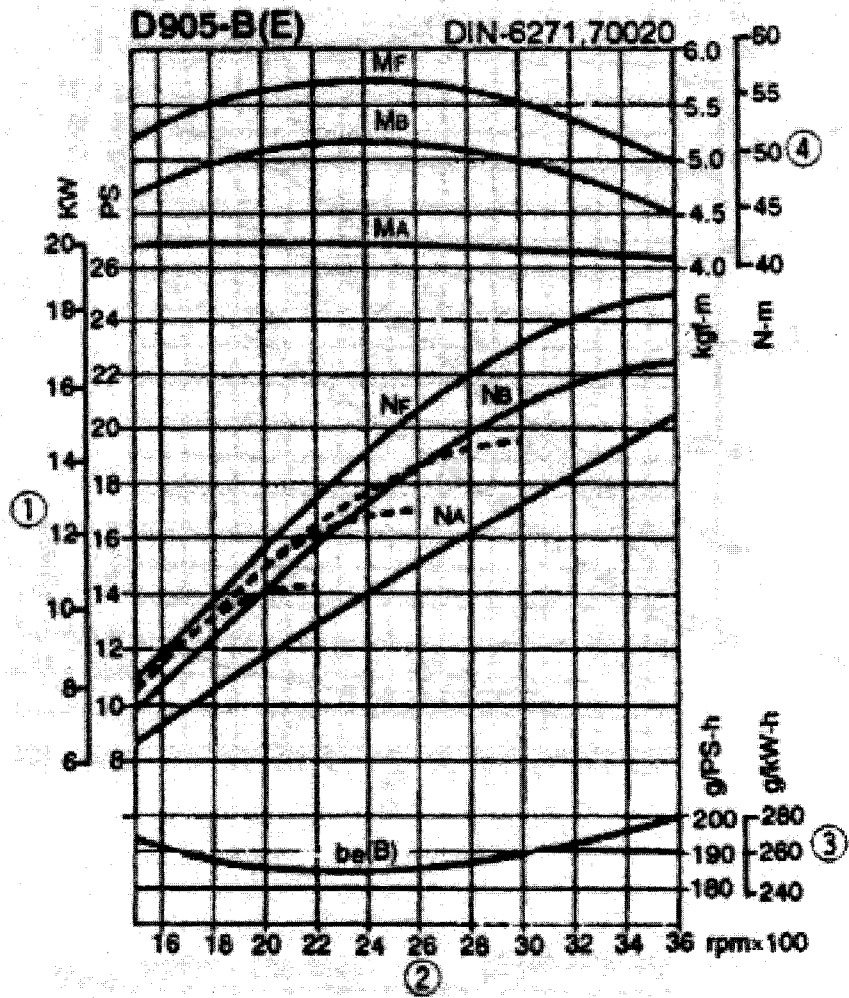


Figure A.1b: Performance Curve for Kubota D905 Engine (Units -Metric).

A.4 Cooling system specifications for Kubota D905

Thermostat's Valve Opening Temperature	69.5 to 72.5°C
Temperature Thermostat Completely Open	75°C
Radiator Water Tightness	Water tightness at 137 kPa (20 psi)
Radiator Cap Air Leakage	> 10 seconds 88 to 59 kPa, (13 to 9 psi)
Cooling System Capacity	4.73 L (1.24 gal)
Engine Block Heater Power	400 W, 120 Volt

Appendix B: Reformation chamber design

The final implemented reformation chamber design used in the experimental trials was based on modifications made to a first proto-type that was manufactured and tested. The design details of the individual components involved in manufacturing of the both the first proto-type and the final reformation chamber design are provided below.

Figure B.1 shows the complete assembly drawing of the first proto-type reformation chamber manufactured. Figures B.2 through B.7 show the individual components involved in the assembly drawing. In the first proto-type, the injector collar (Fig. B.6) and the intermediate base (Fig. B.3) were welded to the lower base (Fig. B.2). The injector sleeve (Fig. B.5) that holds the direct injector (for direct injection of fuel during reformation) is threaded to the injector collar (Fig. B.6). Figure B.4 shows the top cap that is used to pre-compress the spring and to hold the spring that acts on the valve (plunger, Fig. B.7).

The lower base (Fig. B.2) contains the reformation chamber volume for capturing the combustion products and also holds the direct fuel injector collar and sleeve. The passages at the bottom of the lower base were provided such that the volume of the manufactured chamber is maintained at 5cc and at the same time, the lift for complete opening of the reformation valve (plunger) is kept below 6mm. Figure B.7 shows the design of the plunger that slides linearly inside the reformation chamber to trap the combustion products and bring to the next cycle. The pre-compressed spring used for manipulating the CA timing at which the plunger opens (during compression stroke) and

closes (during expansion stroke) sits at the top of the plunger. The cylinder pressure acts at the bottom of the plunger. Furthermore, there is a taper provided at the end of the plunger to provide positive sealing between the lower base and the plunger (valve) when the chamber is in its closed position. The passages and the angle in the lower base were machined using Electrical Discharge Machining (EDM) for accurate machining. The machining costs for the passages and the angle in lower base were about \$800 CAD. A viton seal was used in the intermediate base (R 1.5 groove in Figure B.3) where the top of the plunger slides. The sealing is provided such that there is no leak in trapped combustion products between the reformation chamber and outside atmosphere.

During initial experimental trials, the first proto-type did mechanically perform well with both the viton seal and the bottom valve angle seal providing proper sealing when the engine is motored using the AC motor. However, once the engine is fired with a lean air-fuel mixture, the viton seal disintegrated within 5 minutes of operation due to contact with high temperature gases during combustion. This failure of viton was expected since the manufacturer rating for the viton seal is a maximum operating temperature of 350 °C. However, the shorter operating time with the viton seal was not anticipated. It should be noted that viton seal is the dynamic seal with high temperature rating available in the market for a lower price. The other option for a seal at these elevated pressure and temperature conditions is a ceramic seal. The ceramic seal is not available standard for the dimensions required here. When requested for a price quote, the manufacturers of ceramic seal provided a cost estimate of \$2000 CAD for tooling cost alone, which was outside our budget limit. These drawbacks with the viton seal lead to the modifications of

the first proto-type design to achieve the final reformation chamber design. However, it should be noted that the EDM passages with traditional angle sealing between the plunger bottom surface and the lower base worked well (when the plunger is in closed position) during both motoring and firing scenarios. Also, the seal (located in the fuel injector) between fuel injector and the collar also performed well during both motoring and firing scenarios in the first proto-type design.

In order to overcome the problem with the viton sealing, the following constraints were imposed on the next proto-type design primarily to avoid the additional cost involved in manufacturing of the component:

- To recover and use the existing lower base in order to avoid further EDM costs. Furthermore, the taper design at the lower end and the plunger provided proper sealing when the plunger is in its closed position.
- The injector collar is also to be retained and no modification is to be made to the injector the injector sleeve design (since the sealing between the injector sleeve and the collar worked fine).
- The alternative replacement seal material/design for viton should be cost effective.

The major challenge in the above mentioned constraints is to find a replacement seal that is cost effective and will withstand the high temperature and pressure conditions encountered during combustion. After reviewing several types of seals that were used in high pressure and temperature applications in various fields, flexible graphite braids used

as packing material looked promising as a replacement seal for the current application. The flexible graphite braid is cost effective, self lubricating and is applicable to an extremely wide range of temperatures and pressures applications. It has been commonly used as packing material to provide seals in pumps and valves in petrochemical/refining, hydrocarbon processing, pulp and paper, power and other industrial applications dealing with high temperatures. However, there were no examples found in literature where flexible graphite braids is used as packing material in engine valve applications. However, because to its promising properties to withstand high pressure and temperature and lower costs, it was decided to use flexible graphite material as an alternative for viton to provide sealing between the plunger and the intermediate base in the second proto-type design.

Figure B.8 shows the assembly drawing of the final proto-type design that utilizes the flexible graphite braid as the replacement seal for viton. Figures B.9 through B.14 show the individual components involved in the assembly drawing. The following methodology is adopted to achieve the final proto-type design:

- The first proto-type is cut half way in order to preserve the lower base, injector collar and the sleeve components. Then an additional piece with an internal thread is welded to it (Fig. B.9) such that the other components can be integrated using it to the existing lower base.
- An intermediate base (Fig. B.10) is threaded to the lower base that holds the flexible graphite braid as packing material around the plunger (valve). The graphite braid in the second proto-type is packed between the plunger and the

14mm bore. The plunger slides through the 8mm bore in the intermediate base. The graphite braid is compressed and kept in place by using the plug (Fig. B.11) that is threaded to the 16mm threads in the intermediate base.

- The plunger design (Fig. B.12) is also modified in the second proto-type design. The lower part of the plunger design is not changed since it is matched to bottom of the lower base that is retained from the first proto-type. However, the mid-region of the plunger is modified to incorporate a taper with an enlarged plunger diameter. This was done such a way that the plunger is stopped after 5mm rise. Furthermore, it also provides a positive seal once it comes in contact with the intermediate base and stops. A 20° angle provided in the bottom of the intermediate base (Figure B.9) and in the top of the enlarged plunger region such that a positive seal is in effect once they made contact. This way the graphite seal comes into play only during the reformation period when the plunger is in closed position and during the transient opening period of the plunger. It should be noted that the maximum pressure in the combustion chamber is attained when the reformation valve is in complete open position.
- An additional viton seal used between the plunger and the plug (Fig. B.10) above the graphite seal packing as a secondary seal for precautionary measures.

Figure B.13 shows the flange that holds the pre-compressed spring and is threaded to the top of the plunger. Figure B.14 shows the modified top cap threaded to the lower base that is used to pre-compress the spring and hold it in place.

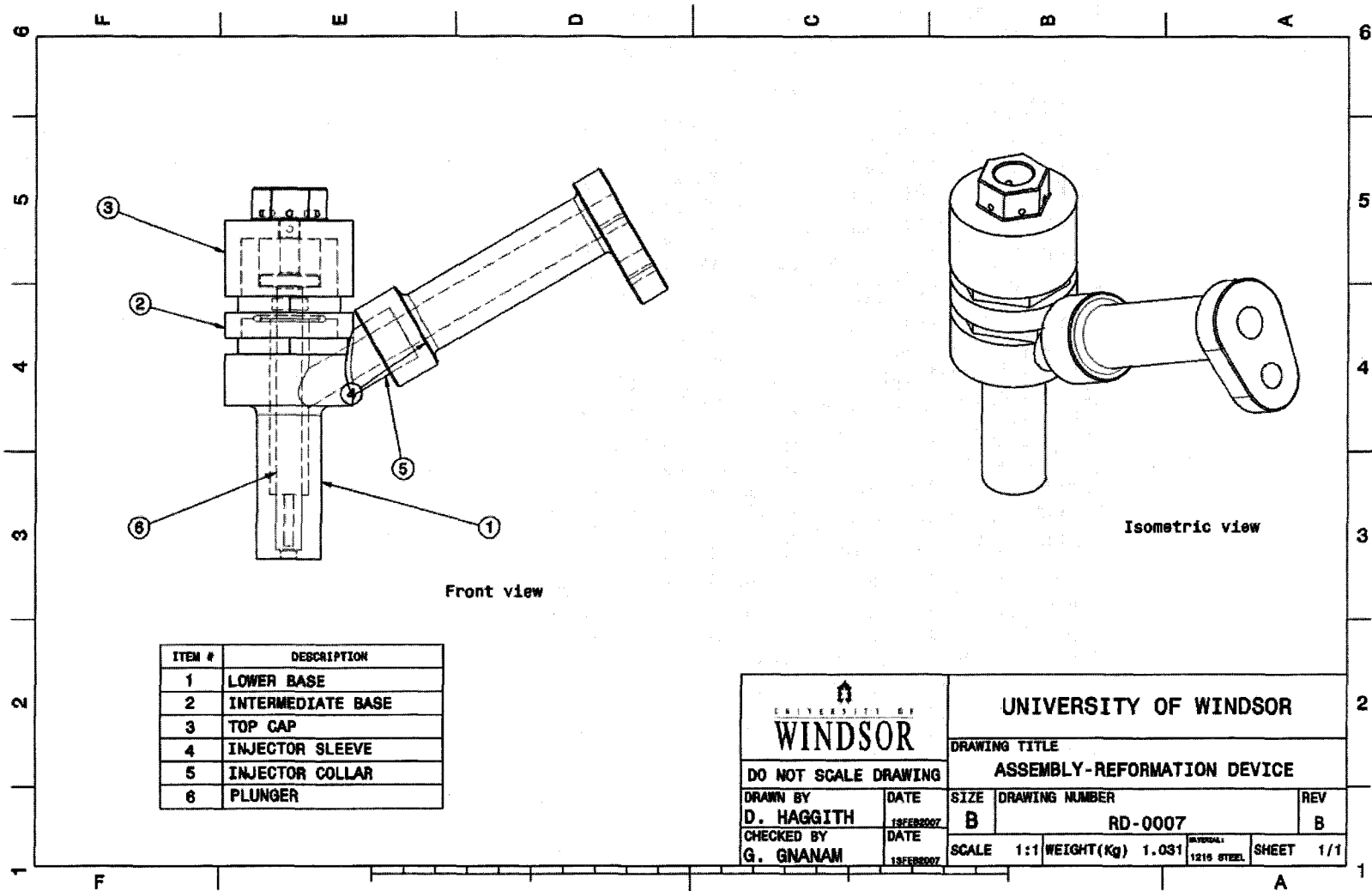


Figure B.1: Assembly drawing of the first proto-type.

Figure B.2: Lower base -- Item 1 in assembly drawing (first proto-type).

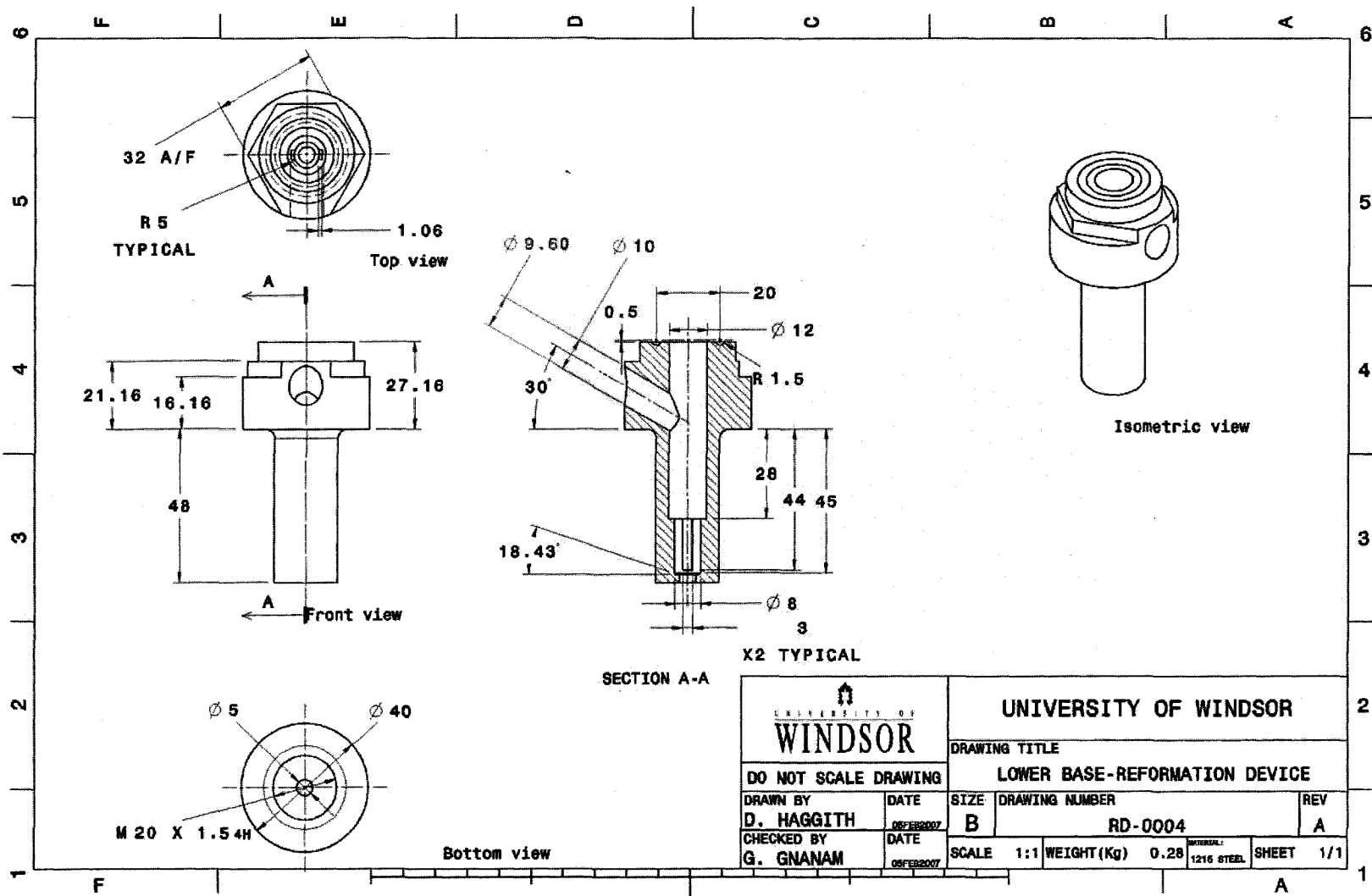
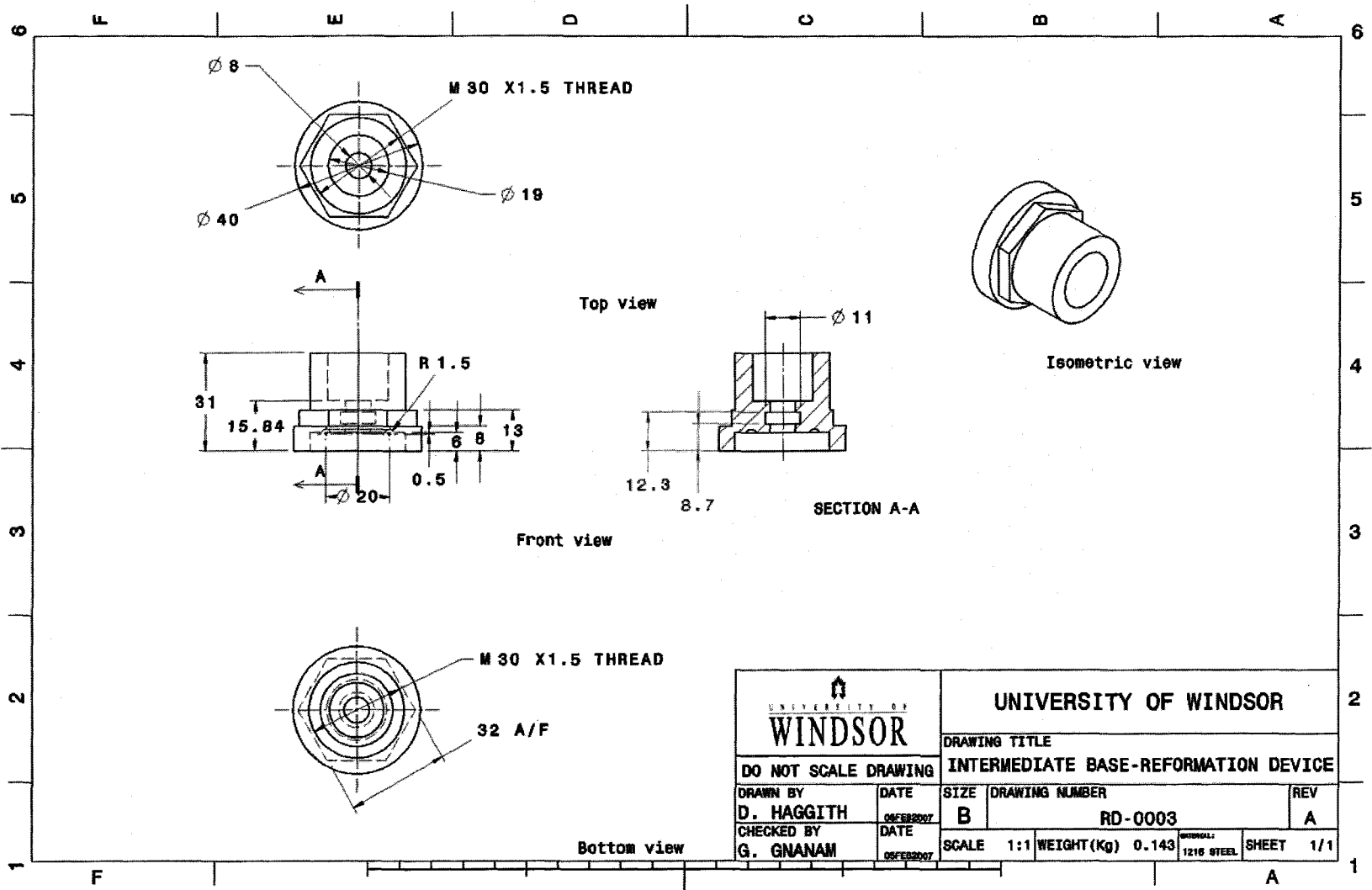


Figure B.3: Intermediate base – Item 2 in assembly drawing (first proto-type).



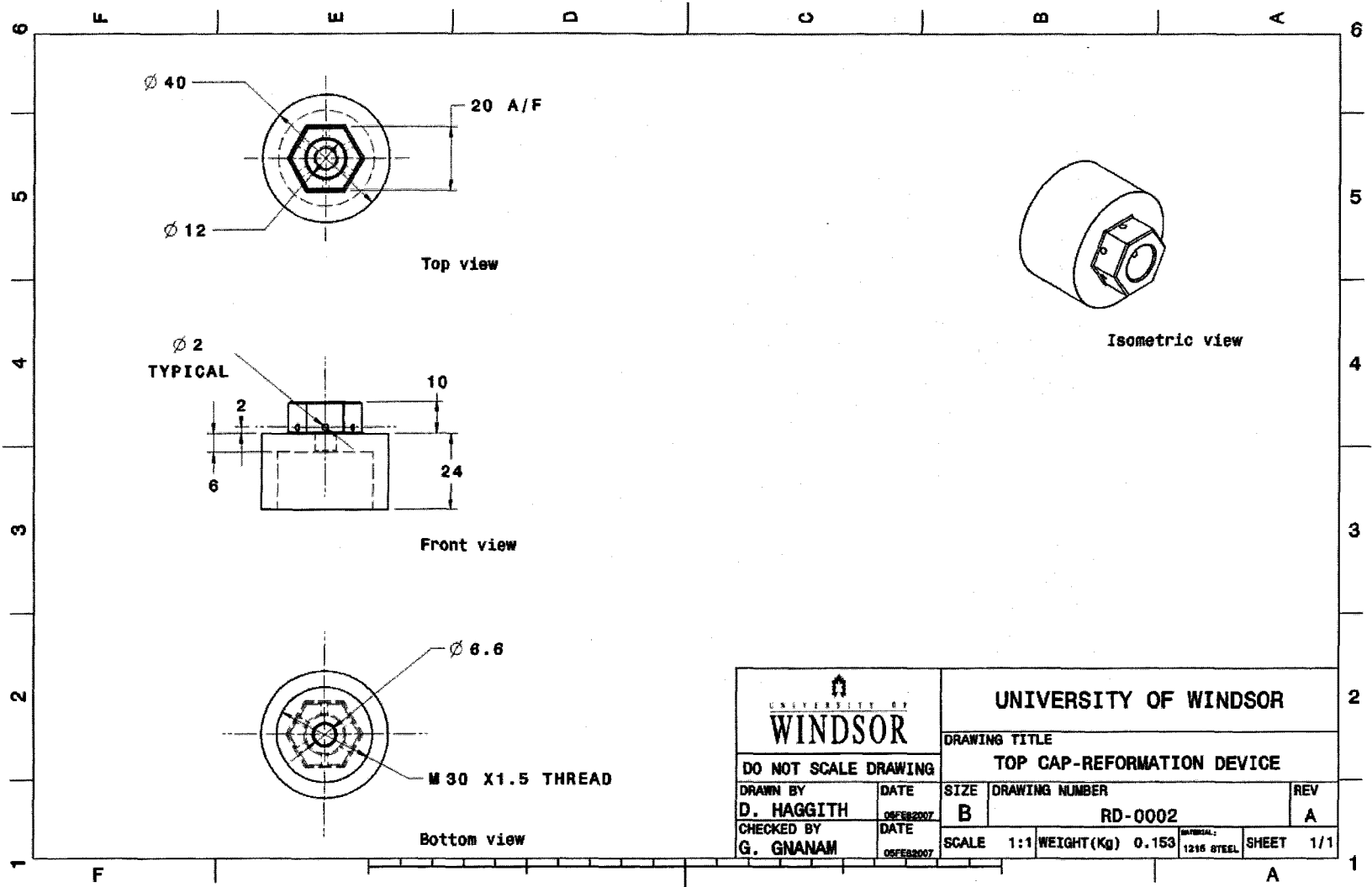


Figure B.4: Top cap – Item 3 in assembly drawing (first proto-type).

Figure B.5: Injector sleeve – Item 4 in assembly drawing (first proto-type).

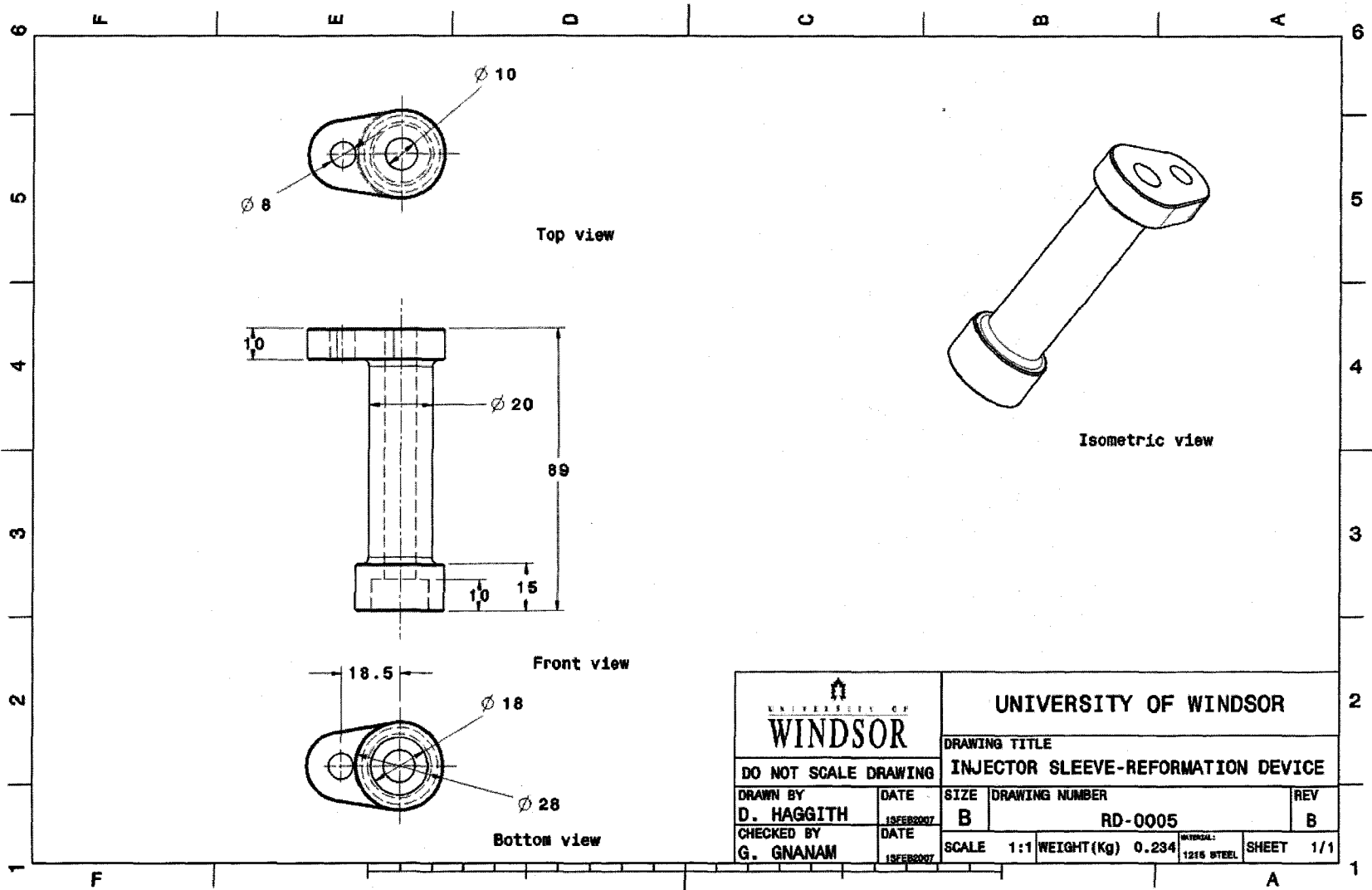
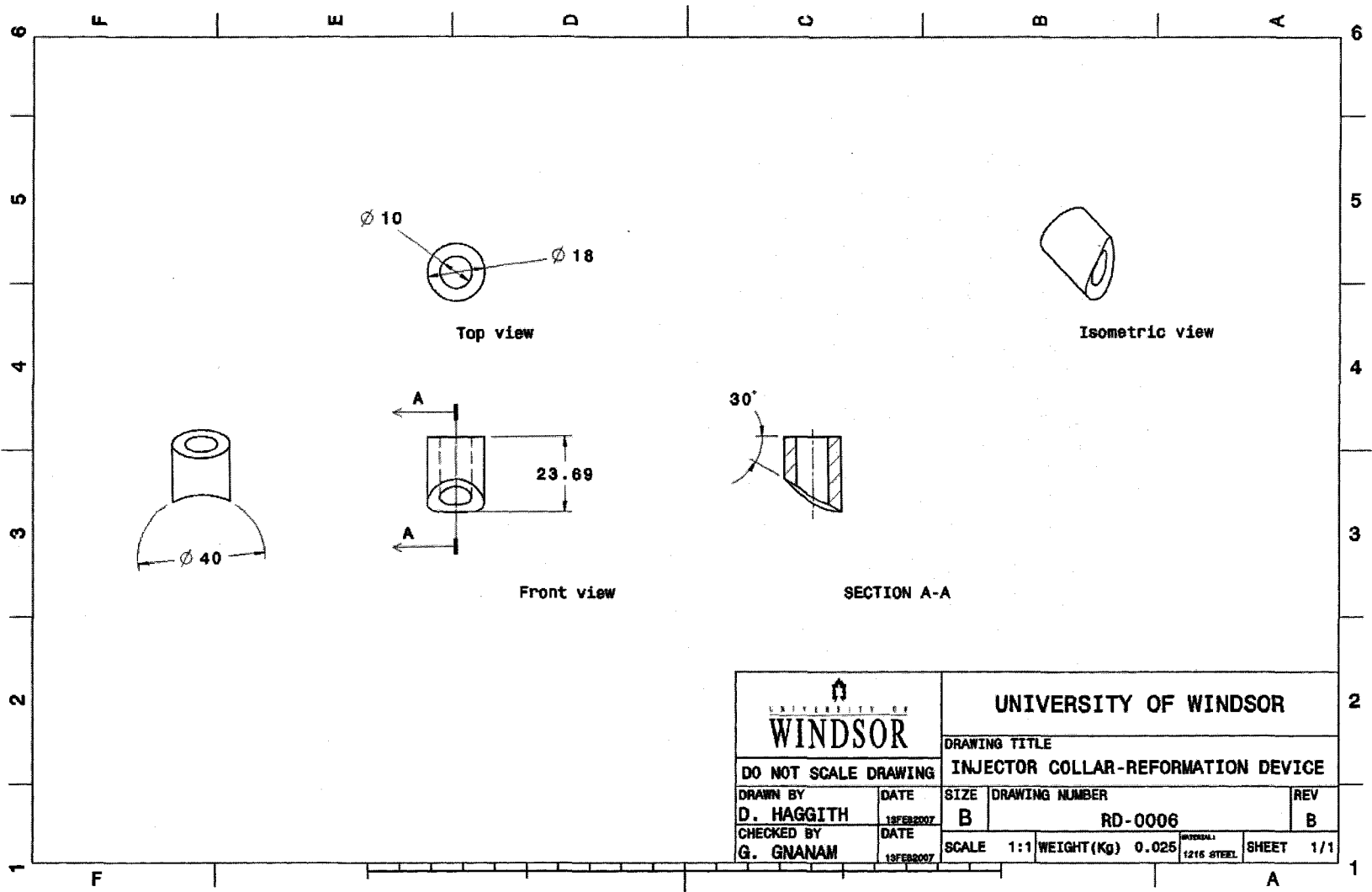
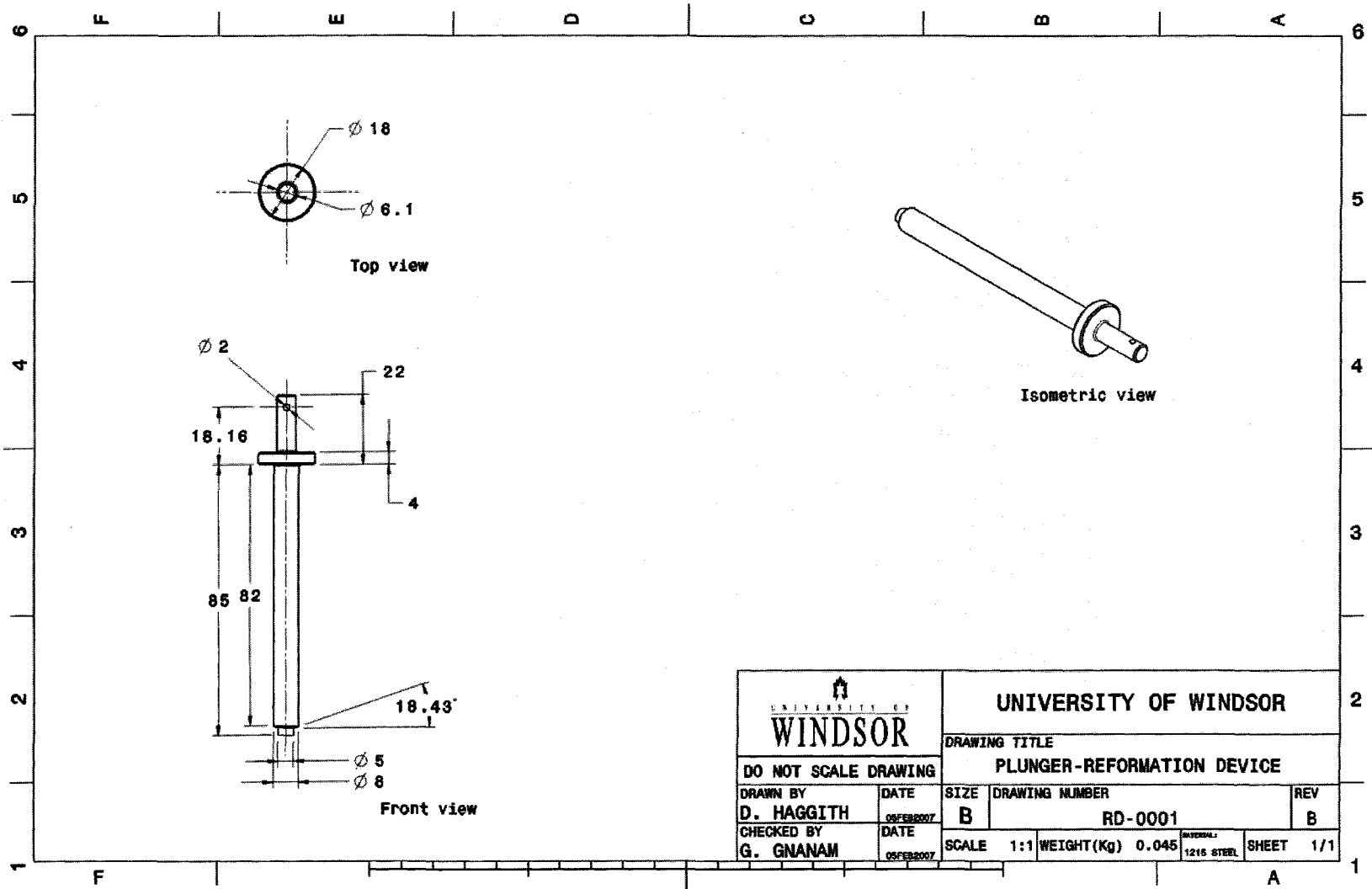


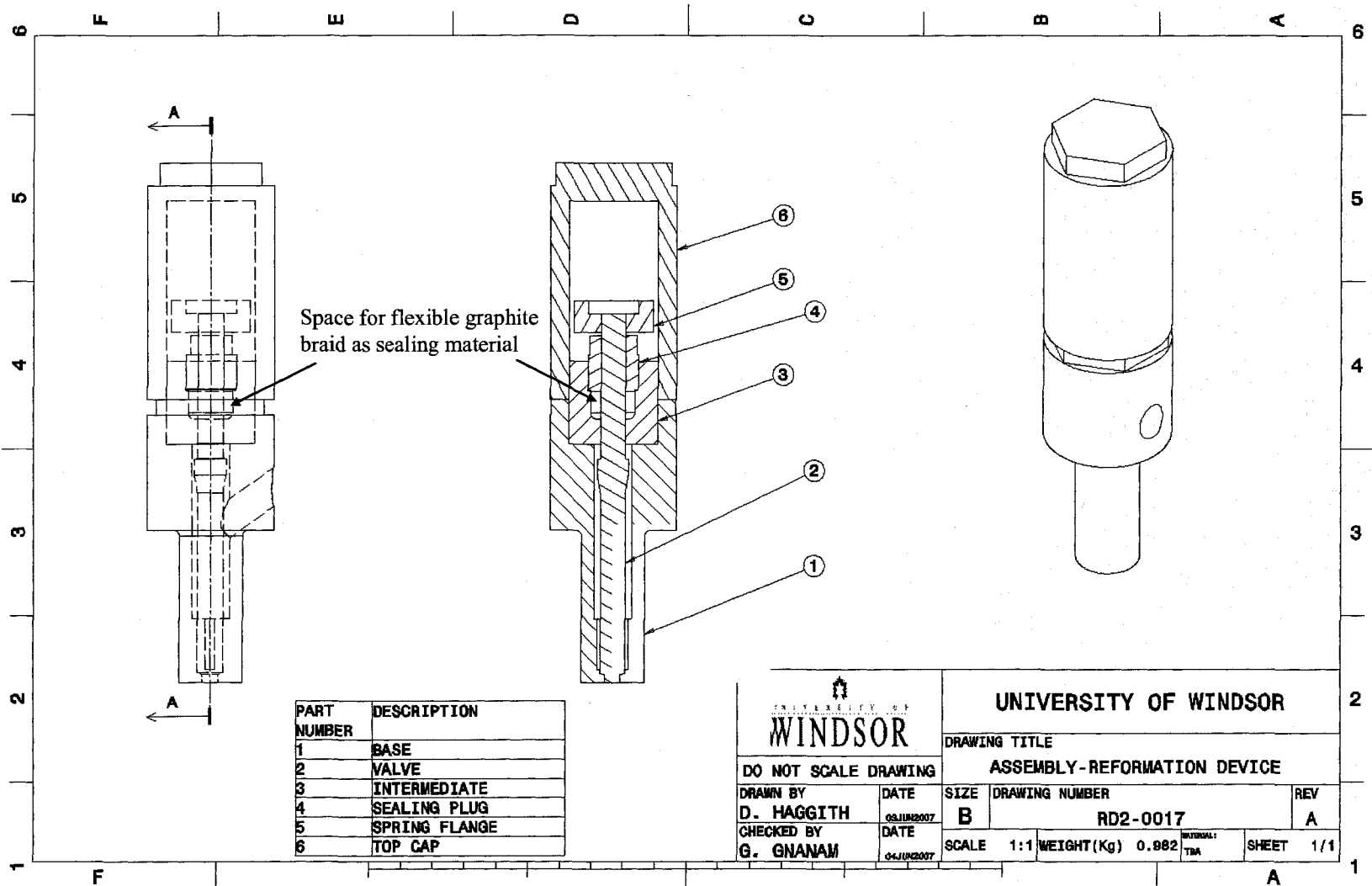
Figure B.6: Injector collar – Item 5 in assembly drawing (first proto-type).



 UNIVERSITY OF WINDSOR		UNIVERSITY OF WINDSOR			
		DRAWING TITLE			
DO NOT SCALE DRAWING		INJECTOR COLLAR-REFORMATION DEVICE			
DRAWN BY	DATE	SIZE	DRAWING NUMBER	REV	
D. HAGGITH	18FEB2007	B	RD-0006	B	
CHECKED BY	DATE	SCALE	WEIGHT (Kg)	SHEET	
G. GNANAM	18FEB2007	1:1	0.025	1/1	
			MATERIAL 1216 STEEL		

Figure B.7: Plunger – Item 6 in assembly drawing (first proto-type).





PART NUMBER	DESCRIPTION
1	BASE
2	VALVE
3	INTERMEDIATE
4	SEALING PLUG
5	SPRING FLANGE
6	TOP CAP


 UNIVERSITY OF WINDSOR WINDSOR		UNIVERSITY OF WINDSOR	
DO NOT SCALE DRAWING		DRAWING TITLE	
ASSEMBLY-REFORMATION DEVICE		ASSEMBLY-REFORMATION DEVICE	
DRAWN BY	DATE	SIZE	DRAWING NUMBER
D. HAGGITH	03 JUN 2007	B	RD2-0017
CHECKED BY	DATE	SCALE	WEIGHT (Kg)
G. GNANAM	04 JUN 2007	1:1	0.882
		MATERIAL	SHEET
		TBA	1/1

Figure B.8: Assembly drawing of the second (final) proto-type.

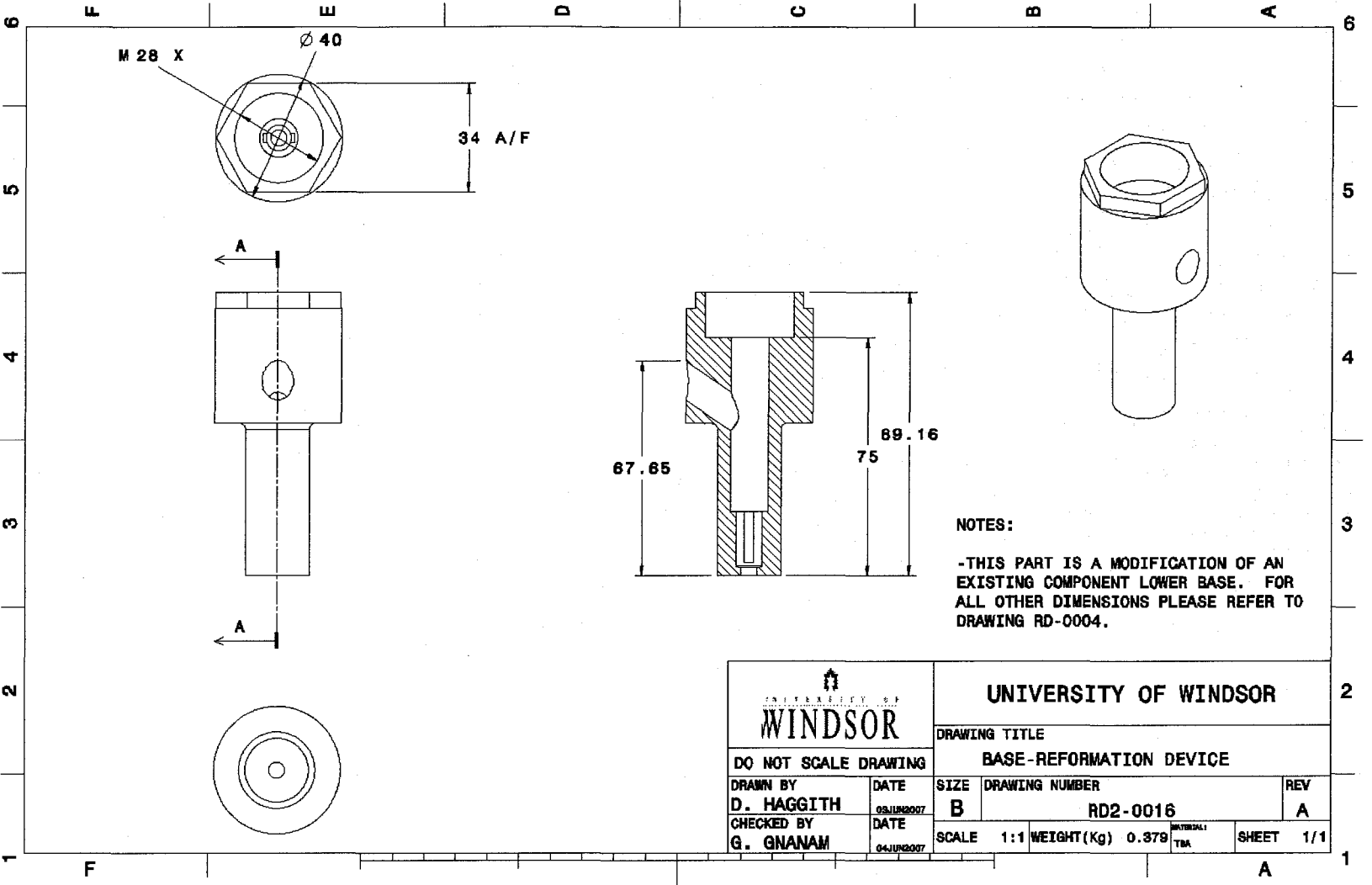


Figure B.9: Lower base restored from first proto-type- Item 1 in assembly drawing (second proto-type).

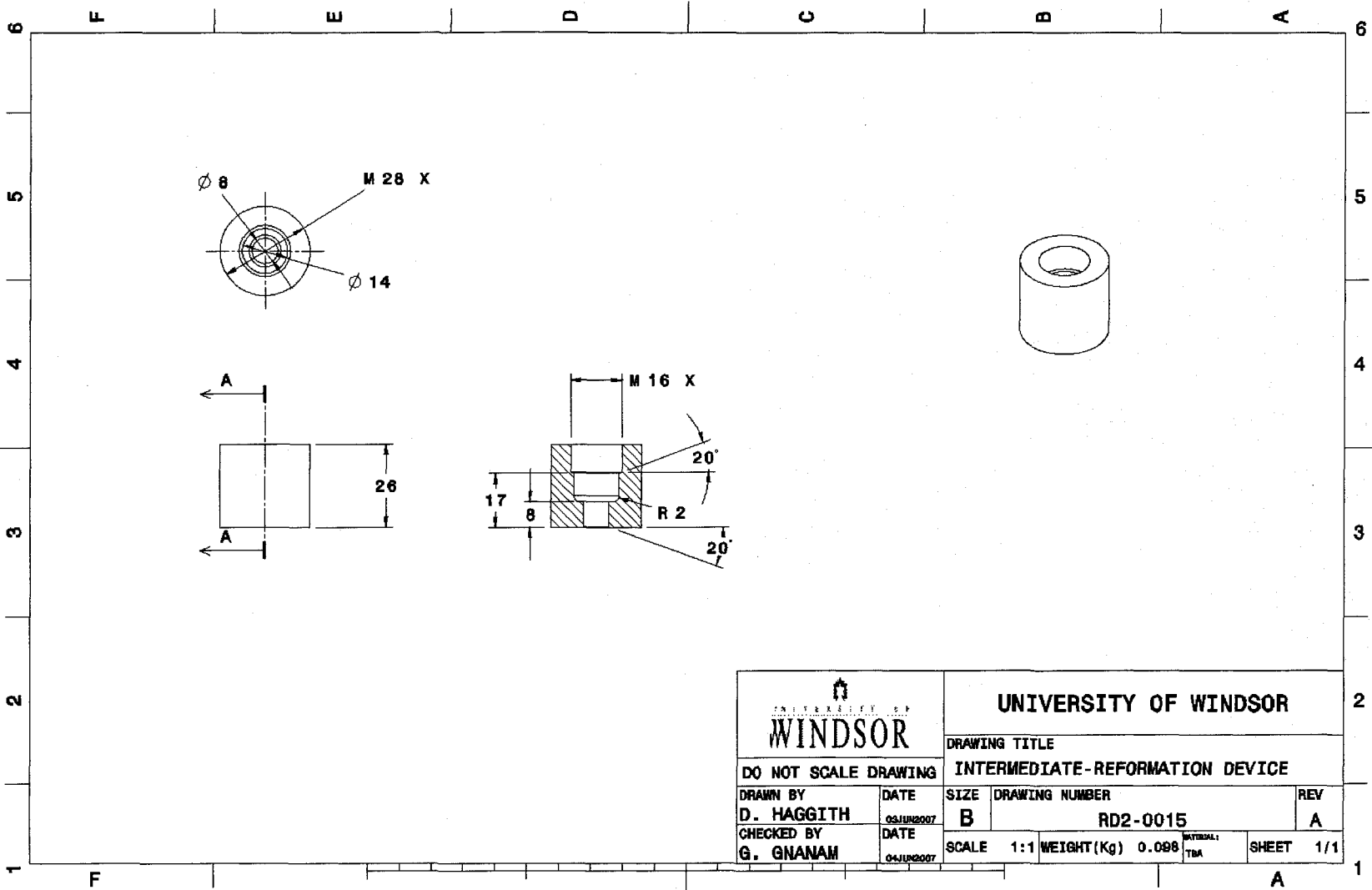


Figure B.10: Modified intermediate base – Item 3 in assembly drawing (second proto-type).


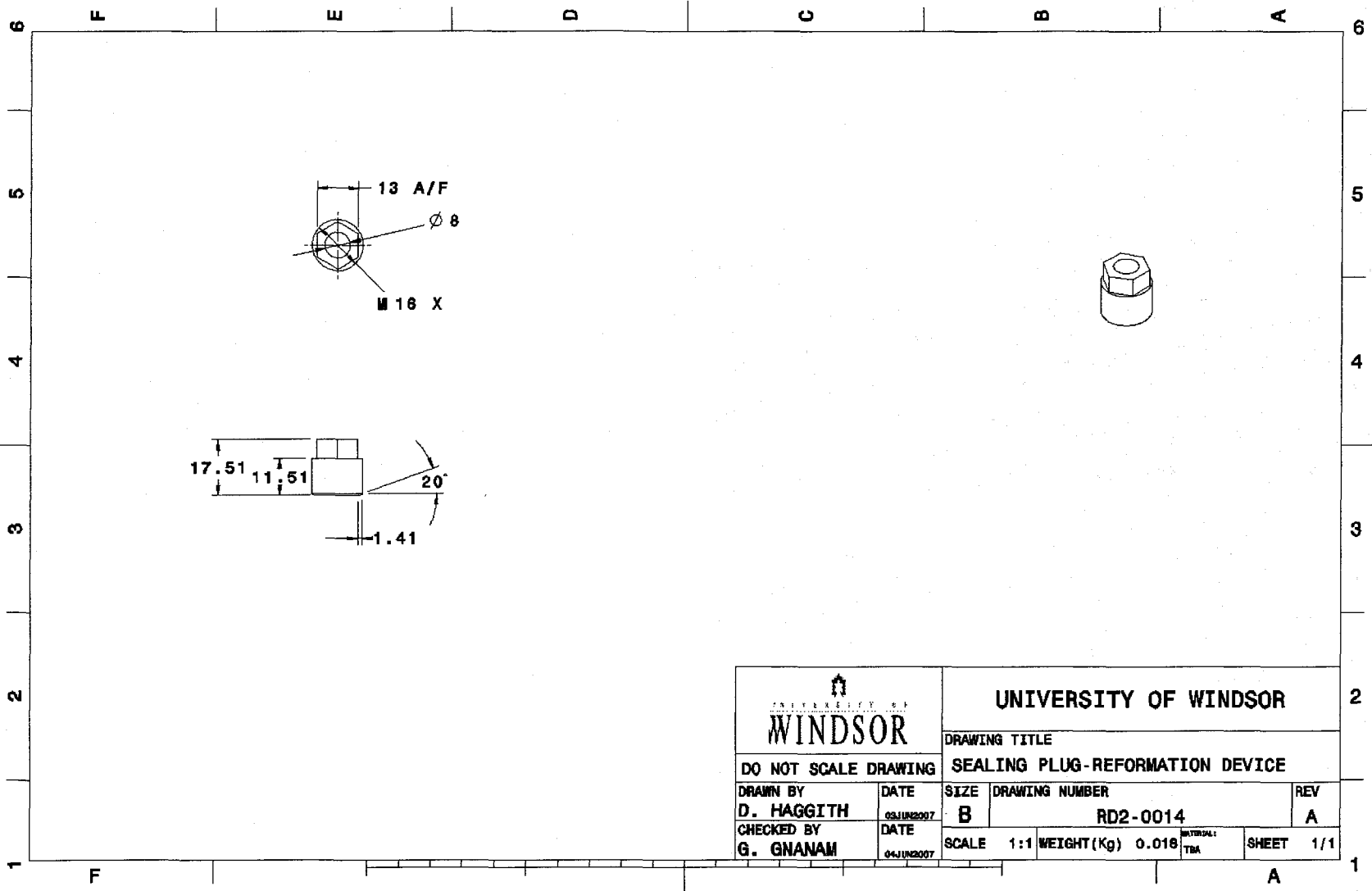
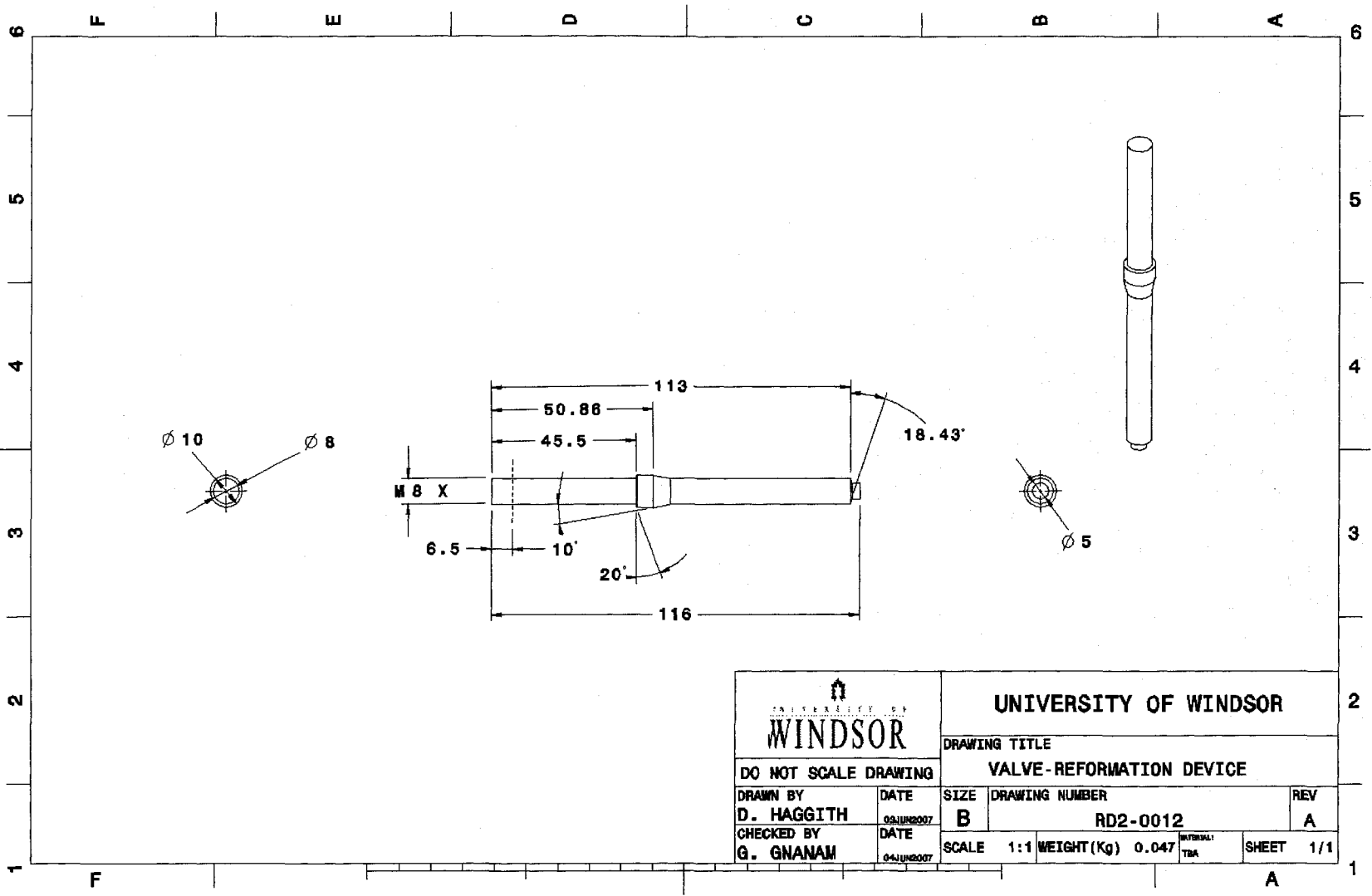
 UNIVERSITY OF WINDSOR		UNIVERSITY OF WINDSOR			
DO NOT SCALE DRAWING		SIZE B	DRAWING NUMBER RD2-0015	REV A	
DRAWN BY D. HAGGITH	DATE 03JUN2007	SCALE 1:1	WEIGHT(Kg) 0.098	MATERIAL TBA	SHEET 1/1
CHECKED BY G. GNANAM	DATE 04JUN2007				

Figure B.11: Sealing plug – Item 4 in assembly drawing (second proto-type).

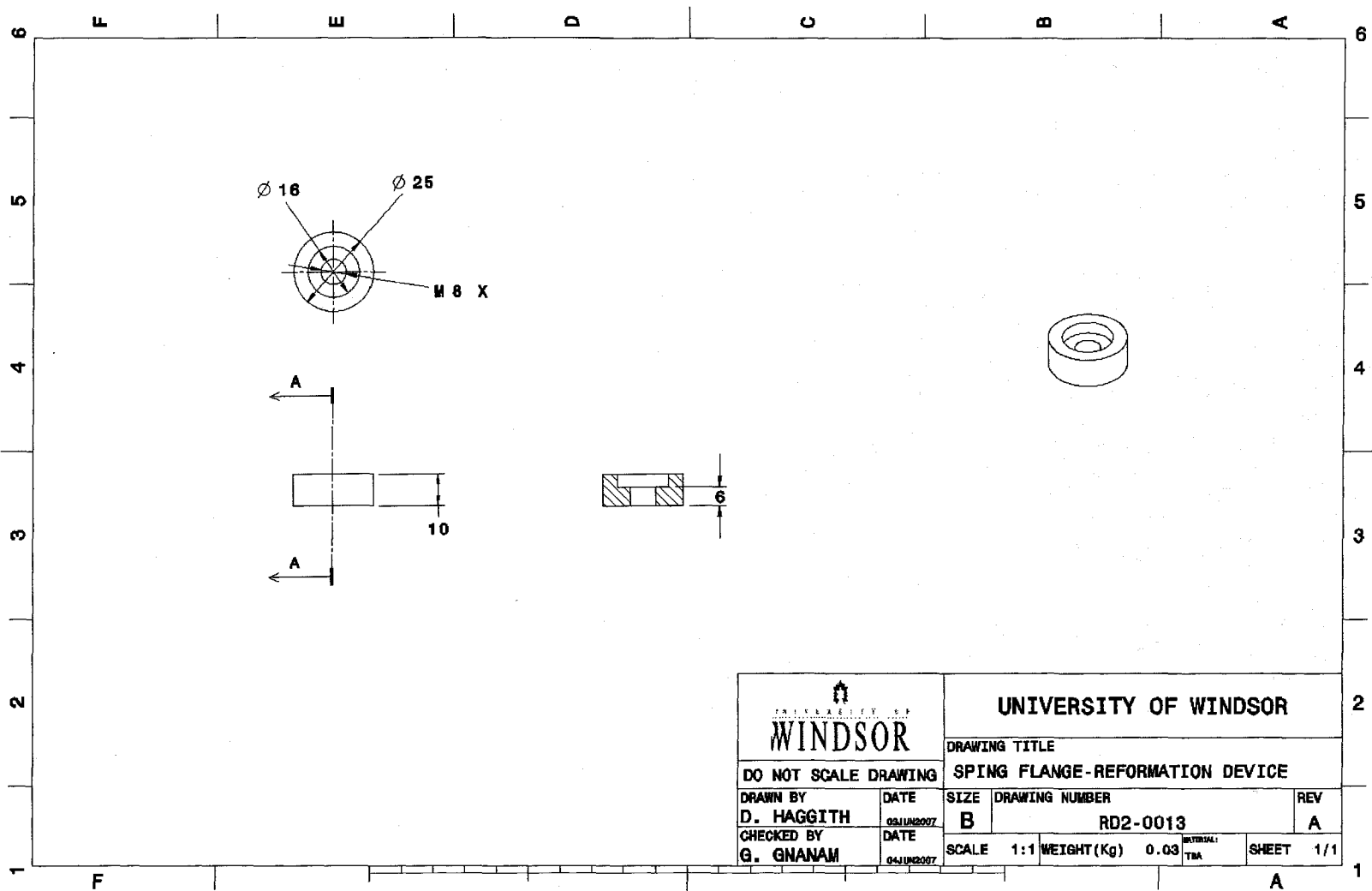


 UNIVERSITY OF WINDSOR		UNIVERSITY OF WINDSOR			
		DRAWING TITLE			
DO NOT SCALE DRAWING		SEALING PLUG-REFORMATION DEVICE			
DRAWN BY	DATE	SIZE	DRAWING NUMBER	REV	
D. HAGGITH	03JUN2007	B	RD2-0014	A	
CHECKED BY	DATE	SCALE	WEIGHT(Kg)	MATERIAL	SHEET
G. GNANAM	04JUN2007	1:1	0.018	TMA	1/1

Figure B.12: Modified plunger (valve) – Item 2 in assembly drawing (second proto-type).



 UNIVERSITY OF WINDSOR		DRAWING TITLE		REV
		VALVE-REFORMATION DEVICE		
DO NOT SCALE DRAWING	DATE	SIZE	DRAWING NUMBER	REV
DRAWN BY D. HAGGITH	03/JUN/2007	B	RD2-0012	A
CHECKED BY G. GNANAM	04/JUN/2007	SCALE 1:1	WEIGHT (Kg) 0.047	SHEET 1/1




 UNIVERSITY OF WINDSOR		UNIVERSITY OF WINDSOR			
		DRAWING TITLE			
DO NOT SCALE DRAWING		SPRING FLANGE-REFORMATION DEVICE			
DRAWN BY	DATE	SIZE	DRAWING NUMBER	REV	
D. HAGGITH	03/11/2007	B	RD2-0013	A	
CHECKED BY	DATE	SCALE	WEIGHT (Kg)	MATERIAL	
G. GNANAM	04/11/2007	1:1	0.03	TBR	
			SHEET	1/1	

Figure B.13: Flange that holds on compressed spring – Item 5 in assembly drawing (second proto-type).

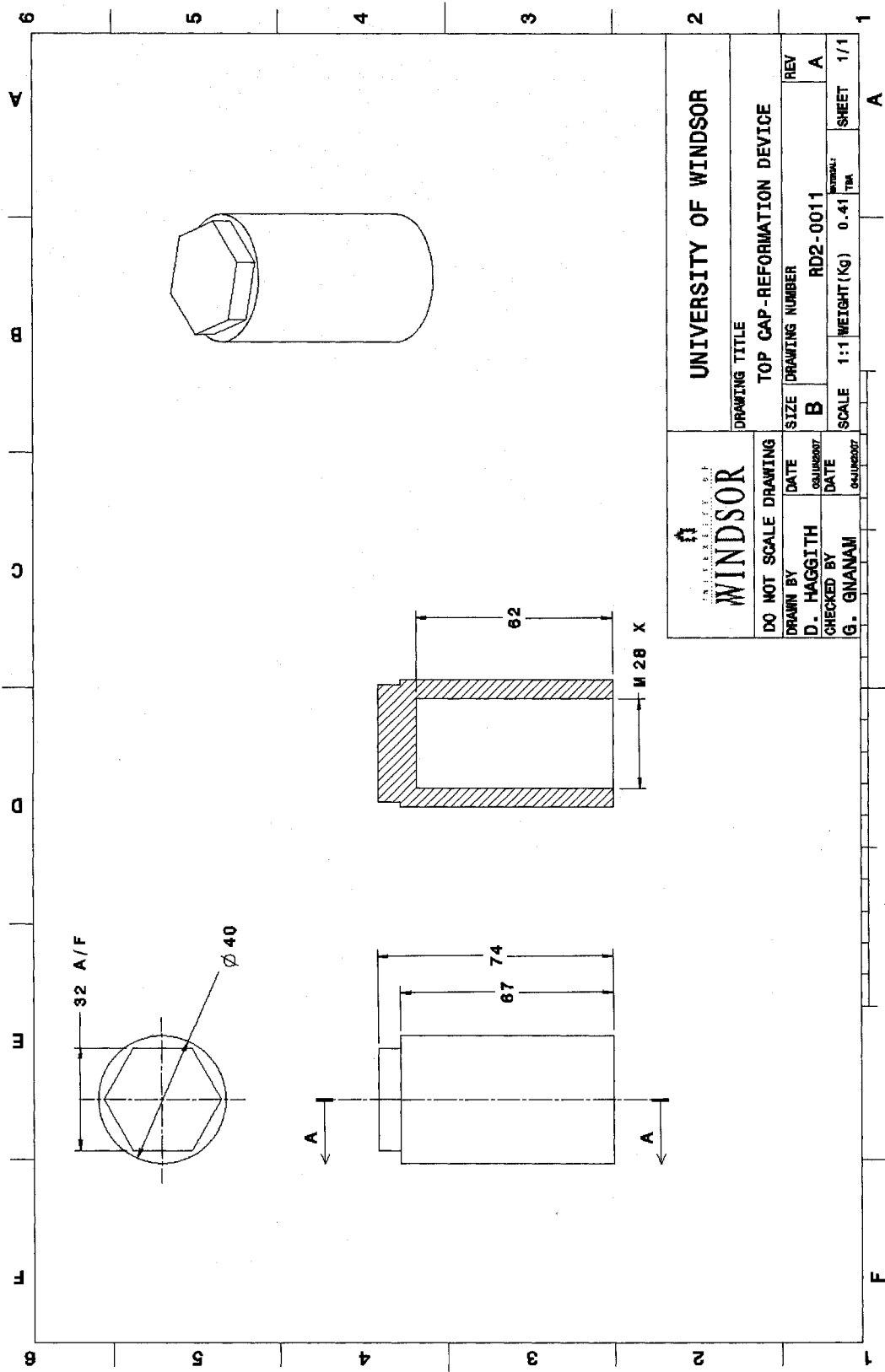


Figure B.14: Top cap – Item 6 in assembly drawing (second proto-type).

Appendix C: Precision compression springs specifications

The specification of the precision compression springs (Table C.1) used for controlling the opening and closing of the reformation chamber valve (plunger) are provided below in this section. Three different types of springs were used during the course of this work. The springs used were of same overall outside diameter (0.6 inches) and overall length (1.5 inches). The difference between the springs is the spring coil diameters which are 0.045, 0.055 and 0.063 inches. Depending on the type of the spring coil diameter used and the amount by which they are pre-compressed, the opening of valve close to TDC is manipulated.

Table C.1: Precision compression spring specifications

Type	Precision Compression Springs		
Material	Type 302 Stainless Steel		
Outer Diameter (inches)	0.6"		
Outside Diameter Tolerance	±0.015"		
Overall Length (inches)	1-1/2"		
Ends	Closed and Ground		
Wire Type	Round Wire		
Wire Size (inches)	0.045"	0.055"	0.063"
Load (lbs.)	6.01	10.62	15.39
Deflection at Load (inches)	1.11"	.85"	.77"
Rate (lbs./inch)	5.41	12.5	19.99
Rate Tolerance (lbs./in.)	± 9%		
Compressed Length (inches)	.35"	.427"	
Specifications Met	FED QQ-P-35		

Appendix D: Modifications done to the experimental set-up

The other modifications that were made to the experimental set-up during the course of this work are discussed below in this section.

D.1 Thermocouples

The thermocouple signals had significant noise interference and were unable to interpret the exact reading due to the excessive level of noise to signal ratio. A sample of the thermocouple reading is shown in Figure D.1.

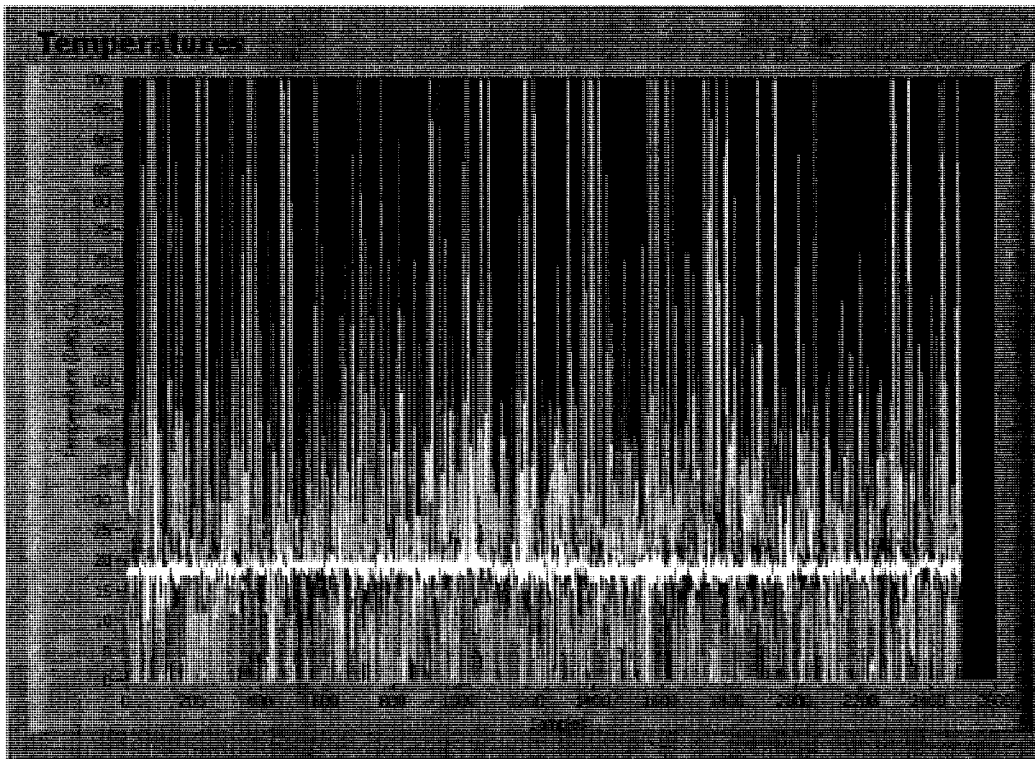


Figure D.1: Real-time unprocessed thermocouple data (Zoldak, 2005).

The excessive noise in the thermocouple reading was mainly due to the use of unshielded wires between the thermocouples and data acquisition system. The wiring between the thermocouples and the data acquisition system were replaced with shielded cables and

proper ground. This significantly reduced the noise levels in the signal and the sample of the thermocouple signal is shown in Figure D.2.

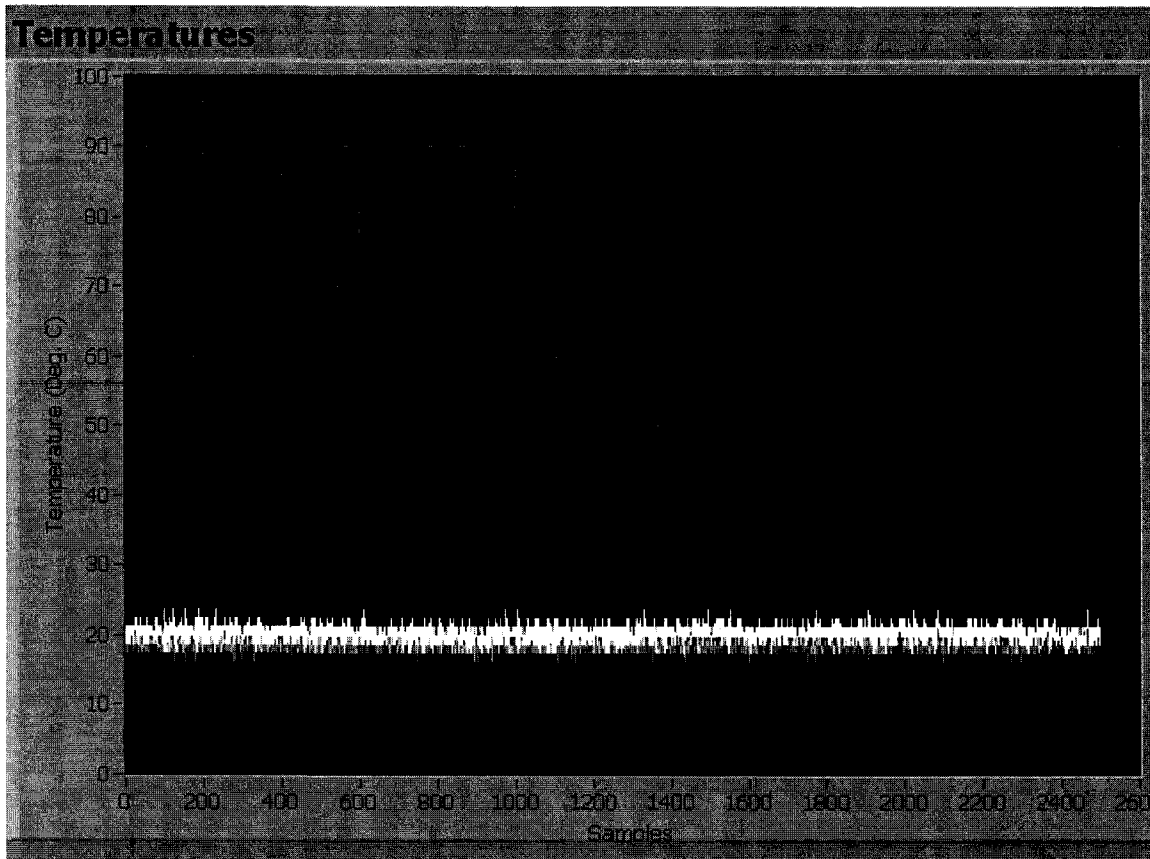


Figure D.2: Real-time unprocessed thermocouple data with shielded and grounded wires.

D.2 Intake air pre-heater

The heater element in the intake air pre-heater had failed when the experimental set-up was commissioned. The failure of the heating element was due to improper wiring between the heater and the pre-heater temperature controller (Omega CNi/32). The configuration did not use the feedback signal from the thermocouple present within the heating element. This feedback signal is vital for the controller in order to override and

cut the power to the heating element whenever the element is exposed to excessive temperatures.

The experimental set-up requirement is such that the intake air temperature has to be maintained constant (at any set value) closer to the intake valves (where the feedback thermocouple for controller is located) and not at the exit of the air-heater. Hence, there is a physical distance (about three feet) between the intake air-heater and the feedback thermocouple. This introduced significant time delay in the feedback signal for any changes made by the controller to its input signal. This delay in the feedback signal led to excessive heating and subsequent failures of the element, especially during the scenarios where there was no flow or minimum flow in the intake pipes. In the present work, a new heater element has been installed and proper wiring to include the additional feedback signal from the thermocouple present within the heating element to the controller were done. This led to operation of the air pre-heater without any failures during the experimental trials.

D.3 Oil pressure sensor

An oil pressure sensor was added to the experimental engine to monitor the engine oil pressure while the engine is in operation. The addition of oil pressure sensor is important since low oil pressure will lead to improper lubrication and mechanical failure of the engine components.

D.4 Injector cooling system

During the course of experimental runs, the fuel injector injection properties started to change when the injector is exposed to higher intake air temperatures (around 150 °C) for a period of time especially with iso-octane fuelling. The change in injection properties is due to the phase change of the fuel from liquid to gas within the injector cavity when the injector is exposed to higher intake air temperatures. It should be noted that both ethanol and iso-octane boils at around 80 °C which are well below the intake air temperatures (130 to 150 °C) used in this study. In order to overcome the fuel injector heating problem an injector cooling system was added (Fig. D.3) to the fuel injector in the experimental set-up. The injector cooling system consists of water-cooled aluminum body (part of the intake piping) that holds the fuel injector. The water is circulated through the channels in the aluminum body using a pump and a water tank. This effectively led to maintaining the fuel injector below 60°C and favorable operation of the fuel injectors during the experimental trials.

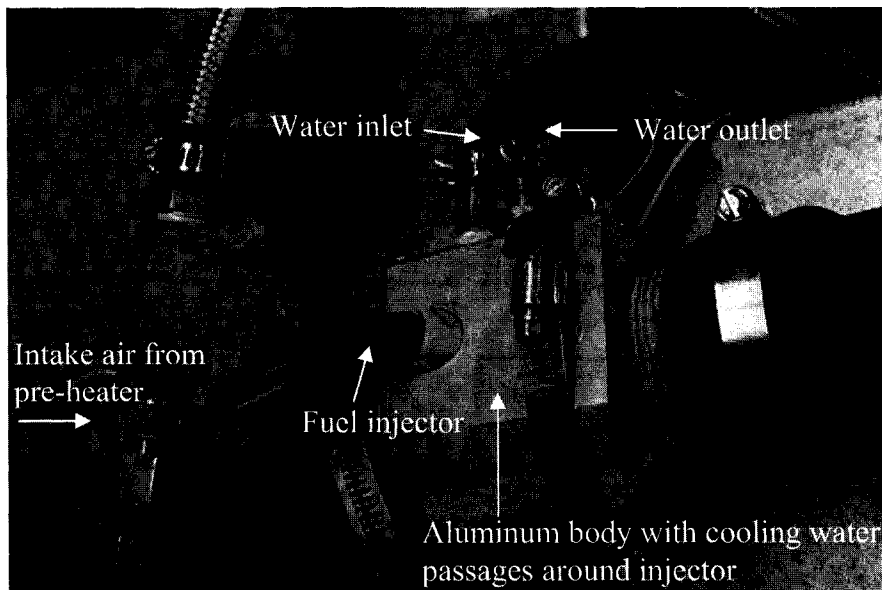


Figure D.3: Injector cooling system

D.5 Intake and exhaust pipe design

The intake and exhaust pipes were re-designed to reduce the structural vibrations in the experimental set-up especially when operating the engine at 1500 rpm. Parts of the intake pipes were replaced with flexible piping to damp vibrations. Furthermore, the overall length of the intake piping is also reduced and additional bushings/clamps were used to reduce the structural vibrations significantly.

D.6 Differential pressure transmitter for intake air-flow measurements

The Omega differential pressure used in the commissioned set-up had a wide operating range (0-100 inches of H₂O). The pressure transmitter was however re-calibrated to 0-10 inches of H₂O in order to cover the flow rate range (over the tested rpm range) of the intake air when all the three cylinders are in operation. Currently, only one cylinder is in operation and the measured differential pressure range for the single cylinder is only between 0-2 inches of H₂O for the tested rpm conditions. This led to less accuracy in the pressure readings and subsequent flow rate calculations, especially for these lower range values where the signal to noise ratio were high. In order to overcome the problem and obtain accurate air flow readings, the differential pressure transmitter was replaced with a newer one (Dwyer differential pressure transmitter) with an operating range of 0-2 inches of H₂O. The specifications of the newer transmitter are provided below in Table D.1.

Table D.1: Dwyer 616W pressure transmitter specifications

Service	Air and non-combustible, compatible gases.
Accuracy	$\pm 0.50\%$ F.S., display accuracy $\pm 0.5\%$.
Stability	$\pm 1\%$ F.S./yr.
Temperature Limits	0 to 140°F (-17.8 to 60°C).
Pressure Limits	0-2 in H ₂ O.
Thermal Effect	$\pm 0.02\%$ F.S./°F (0.036% F.S./°C).
Power Requirements	12-30 VDC (2-wire).
Output Signal	4 to 20 mA.

Figure D.4 shows the comparison of the output signal between the two pressure transmitter signals (original and replaced) when used in conjunction with the laminar flow element for intake air flow measurements. From Figure D.4 it can be seen that the Omega pressure transmitter signals are not as sensitive as the Dwyer pressure transmitter in capturing the fluctuations in the intake air flow. It should be noted that both the sensor output signal lies between 4-20 milliamps. A lower value is measure for the Omega transmitter since the measurement range of the transmitter is 0 – 10 inches H₂O for the same output signal range. In case of Dwyer pressure transmitter the measurement range is 0 – 2 inches H₂O. Furthermore, the airflow values calculated based on the measured output values from the Omega sensor are lower (4.03 CFM) compared to Dwyer sensor (4.89 CFM) when tested for the same operating condition (engine speed of 1000 RPM at STP with $r_c = 20$).

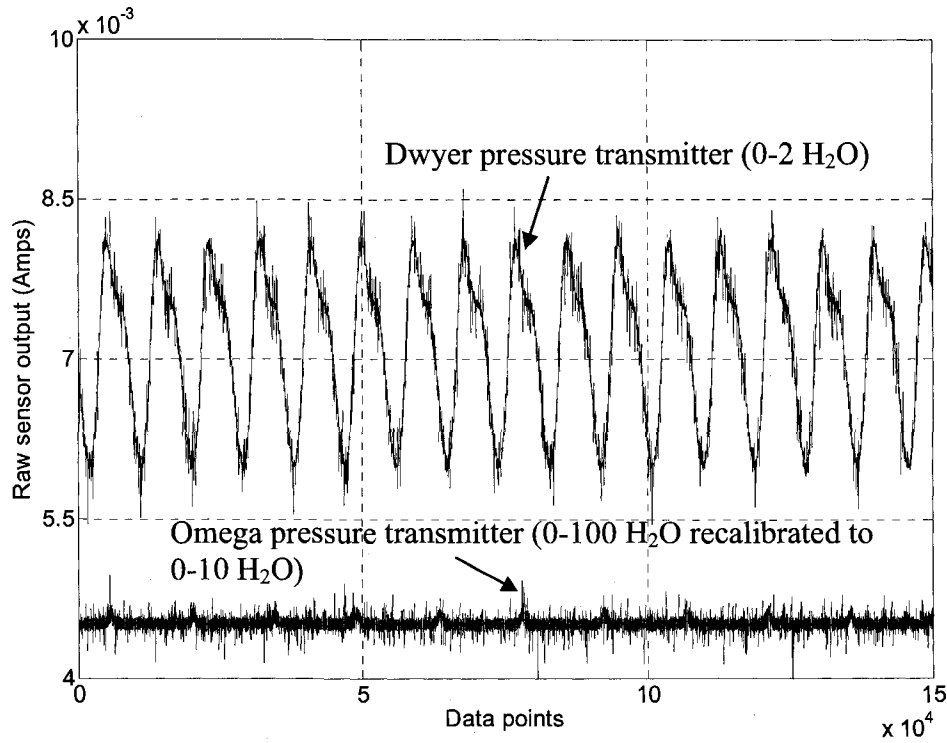


Figure D.4: Comparison between the Dwyer and Omega differential pressure transmitter (1000 RPM, $r_c = 20$, STP conditions)

D.7 ECU fuel injector calibration

Injector scalar calibrations were performed to determine the scalar values for the injector at different equivalence ratios and engine speeds. The procedures for the injector scalar calibration are provided in detail in Zoldak (2005). The ECU fuel injector calibrations done in the earlier study were incorrect primarily due to an error in the rpm sensor signal sent to the ECU at that time. The hall-effect sensor used for the ECU RPM signal had a glitch with the cam trigger mechanism and the trigger signal periodically read a higher engine speed even when the engine was running at constant RPM. In the current work,

the sensor was re-installed properly to correct the error in the signal and the injector scalar calibration was re-done using the methodology described in Zoldak (2005).

D.8 Horiba emissions bench

The Horiba emissions bench donated by the DaimlerChrysler Automotive Research and Development Centre (ARDC) was a used one and required some components to make it ready for experimentation. The control box that operates the solenoid valves in order to direct the gases (zero, span, sample) to the respective individual analyzer was absent. Also, there was no data acquisition system in place to acquire and analyze the readings from the individual analyzers. During the course of this work, a control box to operate the different solenoid valves were set-up with the help of fellow graduate students. Furthermore, a USB data acquisition card coupled with LabVIEW program running through a laptop was set-up to acquire/monitor and post-process the acquired data from different analyzers.

Appendix E: Statistical data from HCCI comparison runs

#	Fuel Type	EGR (%)	Engine speed (rpm)	Standard Deviation	% Error (RPM)	Exhaust ϕ	% Error (ϕ)	IMEP (bar)	Standard Deviation	% Error (IMEP)
1	Iso-octane	0	809.826593	14.679	0.23024	0.332321	0.33725	2.53395	0.102852	0.70589
			repeat 811.691127	18.7562		0.333441		2.51607	0.110178	
2	Iso-octane	10	810.498243	10.4861	0.15647	0.329317	0.47582	2.56457	0.093535	4.22706
			repeat 809.230035	7.49836		0.330884		2.45616	0.087285	
3	Iso-octane	20	809.028991	8.03128	0.09703	0.325202	2.14591	2.39942	0.100129	2.39562
			repeat 808.244011	7.52534		0.33218		2.34194	0.124808	
4	Iso-octane	20	1275.67576	19.8086	0.094	0.336544	1.08495	2.82823	0.268315	4.64873
			repeat 1274.47657	17.4005		0.332893		2.69676	0.305812	
5	Iso-octane	20	812.945113	19.9434	0.39046	0.447003	0.87857	3.10054	0.115868	1.15428
			repeat 809.770914	19.5856		0.443076		3.06475	0.120249	
6	Iso-octane	30	809.224924	19.2533	0.31898	0.446107	0.93692	2.89147	0.151527	1.43619
			repeat 811.806191	20.1063		0.450287		2.933	0.13712	
7	Iso-octane	20	1279.9856	20.7114	0.10794	0.438623	0.09576	3.72373	0.16295	2.4324
			repeat 1281.36725	21.0944		0.439043		3.81431	0.14834	
8	Ethanol	20	1277.03955	22.8148	0.29811	0.399865	1.4354	3.19229	0.10674	2.65768
			repeat 1280.84648	21.2876		0.394126		3.27713	0.089125	
9	Ethanol	30	1275.99142	22.9257	0.27943	0.398099	0.18505	2.95913	0.104976	3.21983
			repeat 1279.55696	20.6396		0.397362		3.05441	0.109641	
10	Ethanol	40	1274.41132	20.5607	0.1587	0.401216	0.2793	2.48691	0.201257	2.21592
			repeat 1276.43386	18.0655		0.400095		2.54202	0.21039	
11	Ethanol	0	1032.43723	22.6374	0.50362	0.319854	0.70924	2.96836	0.097242	3.03801
			repeat 1037.63678	23.1809		0.322123		3.05854	0.107525	
12	Ethanol	10	1037.51	22.7838	0.36539	0.330398	1.13008	3.03326	0.103227	0.62135
			repeat 1033.719	23.8049		0.326665		3.01441	0.091516	
Maximum % Error					0.50362		2.14591			4.64873

#	Fuel Type	COV _{IMEP}	Peak Pressure (bar)	Standard Deviation	% Error (Peak Pressure)	Intake charge Temperature (°C)	Standard Deviation	% Error (T _{in})
1	Iso-octane	0.04059	82.614548	1.192954	2.114340685	152.4	1.304405	1.6849738
		0.04379	80.867795	1.121195		149.8321	1.673635	
2	Iso-octane	0.03647	69.207949	1.639142	3.40621711	150.7147	1.313519	0.3147006
		0.03554	71.565322	1.90614		151.189	1.399724	
3	Iso-octane	0.04173	64.178299	2.399986	3.440832858	150.9113	1.223605	0.8408913
		0.05329	61.970031	2.38313		149.6423	1.878165	
4	Iso-octane	0.09487	55.59647	5.715876	4.720101834	148.2766	1.558827	0.6054226
		0.1134	52.97226	5.220021		149.1743	1.683392	
5	Iso-octane	0.03737	77.340441	1.872614	4.764637947	144.8886	1.509802	0.293881
		0.03924	73.655449	2.23455		144.4628	2.038047	
6	Iso-octane	0.0524	60.094946	4.450847	4.484370449	141.5973	1.530336	0.7188696
		0.04675	62.789826	5.799976		142.6152	1.636518	
7	Iso-octane	0.04376	69.060114	4.011105	3.028979941	145.5102	1.200521	0.488007
		0.03889	71.151931	3.873096		146.2203	1.377268	
8	Ethanol	0.03344	80.046236	1.871944	1.664992717	133.86	1.252	0.8167488
		0.0272	78.713472	2.029677		134.9533	1.901478	
9	Ethanol	0.03548	69.155159	2.386644	2.201345528	135.53	1.423856	1.4335571
		0.0359	67.632815	2.467273		133.5871	1.966408	
10	Ethanol	0.08093	57.713791	3.36552	2.116579034	135.87	1.155702	1.5486862
		0.08276	56.492233	3.463077		133.7658	1.826975	
11	Ethanol	0.03276	81.982777	1.324433	0.896245561	132.3097	2.045491	1.9654644
		0.03516	82.717544	1.823649		134.9102	1.8765	
12	Ethanol	0.03403	75.093366	1.675375	0.904834922	135.3288	1.948279	0.9063111
		0.03036	75.772837	1.948705		134.1023	1.882345	
Maximum % Error					4.764637947			1.9654644

#	Fuel Type	Coolant Temperature (°C)	Standard Deviation	% Error (T _e)
1	Iso-octane	74.57818	1.686072	0.97272
		75.30362	1.637592	
2	Iso-octane	74.41905	1.63948	0.89309
		75.08368	1.659048	
3	Iso-octane	74.14555	1.68796	1.25152
		75.0735	1.721073	
4	Iso-octane	74.03182	1.712104	0.97723
		74.75528	1.951602	
5	Iso-octane	75.35601	1.63527	0.11103
		75.43968	1.600622	
6	Iso-octane	74.53548	1.717208	0.21897
		74.37227	1.685054	
7	Iso-octane	74.90587	2.046057	0.63444
		75.3811	1.643563	
8	Ethanol	75.30502	1.26493	0.25292
		75.11456	1.674726	
9	Ethanol	74.88857	1.286583	0.90189
		74.21316	1.60522	
10	Ethanol	74.41875	1.293031	1.46729
		75.51069	1.35647	
11	Ethanol	75.59572	1.777855	0.25627
		75.78945	1.678214	
12	Ethanol	75.77111	1.711879	0.59156
		75.322875	1.873569	
Maximum % Error				1.46729

Appendix F: MATLAB program used for calculating HRR and plotting results

F.1: Calculating 125 cycle averaged HRR based on individual cycle in-cylinder pressure and CA data

```

for cond = 750:250:750% 250:1500
for cond1 = 10:10:10
    cd (strcat('D:\EGR\50iso\', num2str(cond), '\', num2str(cond1), 'egr\150comb04-3'));
    M = csvread('Data.csv',6,0);
    cd (strcat('D:\EGR\50iso\',num2str(cond),'\',num2str(cond1),'egr\150comb04-3\Post'));
    M1 = csvread('Data.csv',6,0);
    disp('Read File');
    a = 0; % updated end of cycle
    CA(:,1) = M(1:3600,21);
    V(:,1) = M(1:3600,41);
    for cycle = 1:125
        E(:,cycle) = M1(1+a:3600+a,2);
        W(:,cycle) = M1(1+a:3600+a,4);
        P(:,cycle) = M(1+a:3600+a,22);
        a = a+7200;
    end
    s = size(W);
    [b,a1] = butter(8,0.05);
    Pfavg(:,1) = sum(P,2)/125;
    Wfavg(:,1) = sum(W,2)/125;
    Ufavg(:,1) = sum(E,2)/125;
    Wf = filtfilt(b,a1,Wfavg);
    Pf = filtfilt(b,a1,Pfavg);
    Uf = filtfilt(b,a1,Ufavg);
    for ps = 2:s(1)
        if ps < 1800
            k = 1.39;
        else
            k = 1.37;
        end
        dQ(ps,1) = (((1/(k-1))*100000*((Pf(ps,1)*(V(ps,1)-V(ps-1,1)))+(V(ps,1)*(Pf(ps,1)-Pf(ps-1,1)))))+(Pf(ps,1)*100000*(V(ps,1)-V(ps-1,1)))/(CA(ps)-CA(ps-1)));
    end
    Qsum(:,1) = cumsum(dQ,1);
    dQf = filtfilt(b,a1,dQ);
    file3 = strcat('HeatRelease', num2str(cond),'phi-04tin-150',num2str(cond1),'egr-3');
    clear M

```



```

clear M1

% WRITING VARIABLE VALUES OUTPUT
mout1 = [CA dQf Qsum Pfavg];
cd (strcat('F:\EGR\50iso\'))
dlmwrite(file3,mout1);

end
end

```

F.2: Plotting the calculated HRR and in-cylinder pressure versus CA for 125 averaged cycle

```

clear all
cd (strcat('F:\EGR\50iso\'))
col = ['b:' 'k:' 'r:'];
cz = 1;
for cond1 = 10:10:30
count = 1
cycles = 125; % for 100 iso and eth
for cond = 750:250:750
file = strcat('HeatRelease', num2str(cond),'phi-04tin-150',num2str(cond1),'egr-3');
M = csvread(file,0,0);
s = size(M);
figure(count)
CA(:,1) = M(:,1);
dQ(:,1) = M(:,2);
Q(:,1) = M(:,3);
P(:,1) = M(:,4);
plot(CA(:,1),dQ(1:3600,1),col(cz:cz+1))
hold on
plot(CA(:,1),P(1:3600,1),col(cz:cz+1))%
title(strcat('50% Ethanol & 50% Iso-octane, Phi-0.4, RPM-',num2str(cond)))
xlabel('Crank Angle (CA)')
ylabel('Pressure (bar) and HRR (J/CA)')
count = count + 1;
end
cz = cz + 2;
end

```

Appendix G: MATLAB/Cantera model used for simulation

The MATLAB/Cantera modeling tools described below are based on the assumptions that the mixture in the engine system is a perfect gas, temperature and species concentrations are uniformly distributed in the cylinder, heat transfer takes place only due to convection and that radiation and crevice flows are neglected.

The model implemented using MATLAB/Cantera is a single-zone model. Cantera is used for detailed-chemistry calculations of reacting gas time evolution in a closed volume. The conservation equations governing mass, species concentration and energy were formulated in terms of a variable volume reactor. The MATLAB/Cantera code solves for the individual mass and energy conservation equations specified below:

$$\frac{dY_i}{dt} = \nu \cdot \omega_i \cdot M_i \quad i = 1, \dots, N_s$$

$$c_v \frac{dT}{dt} = -p \frac{dv}{dt} - \nu \sum_{i=1}^{N_s} e_i(T) \cdot \omega_i \cdot M_i + (dQ/dt) / (\rho V)$$

where Y_i is the mass fraction, ω_i is the species molar production term, M_i is the species molar mass, N_s is the number of species in the mixture, $\nu = \frac{V}{m}$ is the specific volume of

the cylinder, $c_v = \sum_{i=1}^{N_s} c_{v,i}(T) \cdot Y_i$ is the mixture heat capacity, T is the average gas temperature in cylinder, p is the cylinder pressure and e_i is the internal energy of the i^{th} species.

Formulas describing the piston motion specified as a function of time using MATLAB. Therefore, the cylinder volume and the volume change rate were provided as a function of crank angle degree, θ :

$$\frac{V}{V_c} = 1 + \frac{1}{2}(r_c - 1) \left[R + 1 - \cos\theta - \left(R^2 - \sin^2\theta \right)^{1/2} \right]$$

where r_c is the compression ratio, V_c is the clearance volume and $R = \frac{2l}{a}$ is the ratio of the connecting rod l and a is half of the stroke.

$$\frac{dV}{dt} = \frac{\pi B^2}{4} \left(\frac{a \sin\theta \cos\theta}{\sqrt{l^2 - a^2 \sin^2\theta}} \right) \frac{d\theta}{dt}$$

where V is the cylinder volume, B is the cylinder bore and $\frac{d\theta}{dt}$ is the rotating speed of the crankshaft and assumed to be constant. This implies that a transition has to be made from time has to be made from time to crank angle and vice versa:

$$\theta = \frac{2\pi N}{60} t$$

where N is the engine speed in revolutions per minute.

To account for heat transfer, a simplified Woschni heat transfer model was implemented. The heat transfer rate between the gas in the cylinder and the cylinder wall can be described by:

$$\frac{dQ}{dt} = hA_w(T_w - T)$$

where h is the heat transfer coefficient, A_w is the chamber surface area, T_w is the mean wall temperature and T is the cylinder gas temperature. The heat transfer coefficient is described by the original Woschni correlation (Chang, 2004).

$$h_{woschni} = B^{-0.2} \cdot p^{0.8} \cdot T^{-0.53} \left(C_1 \bar{S}_p + C_2 \frac{V_d T_r}{P_r T_r} (p - p_{mot}) \right)^{0.8}$$

$$C_1 = 2.28 + .308 \frac{\pi B \dot{\theta}}{\bar{S}_p}, C_2 = 0.00324$$

where V_d is the displaced volume, all temperature and \bar{S}_p is the mean piston speed, p_r , V_r , T_r are the working-fluid pressure, volume, and temperature at initial stage, p_m is the motored cylinder pressure at the same crank angle as p .

The system of equations for internal energy and species are solved with an ode15s solver and at each iterative step, the reacting gas is updated for the change in species concentration, specific volume and the internal energy. Below are the codes written in Matlab/Cantera using the above equations in order to simulate the results for HCCI cycle with and without reformation used in Chapter 6.

G.1: In-cylinder reformation using NVO

Step 1: Initial HCCI cycle

```
disp 'HCCI-Running'

%INPUTS

Pin= oneatm*0.8;
lam = 1/phi;
fue = 1
oxy = 3 * lam % 3 - eth, 12.5 - iso
nit = (79/21)*oxy
g=idealGasMix('chem_Mar_nox.cti');
```

```
set(g,'T',Tin,'P',Pin,'X',strcat('C2H5OH:',num2str(fue),'O2:',num2str(oxy),'N2:',num2str(
nit)));
```

```
%ENGINE PARAMETERS
```

```
bore=0.072; % m
stroke=0.0736; % m
compress=20;
conrod=.132112; %m
rpm=1000; % rpm
twall=348; % K
omega=2*pi*rpm/60.0;
engine_data=[bore, stroke, compress, conrod, rpm, twall]';
```

```
% TIMING PARAMETERS: SIMULATION CONDUCTED FOR CLOSED PART OF
THE CYCLE FROM INTAKE VALVE CLOSE (IVC) TO EXHAUST VALVE
OPENING(EVO)
```

```
ivc=-180;%degrees ATDC (negative means before TDC)
evo=180;%degrees ATDC
dtheta=.5;% crank angle resolution for output
```

```
% SIMULATION TIME PARAMTERS CONVERTED FROM DEGREES
```

```
t0=ivc*pi/180/omega;
tf=evo*pi/180/omega;
dt=dtheta*pi/180/omega;
time=[t0:dt:tf];
z = massFractions(g)';
fueltooxyperm = z(49)/z(11);
oxymassfrac = z(11);
v0=volume(t0,engine_data);
mass = 2.585e-4
z0 = [temperature(g);
      intEnergy_mass(g);
      1/density(g);
      moleFractions(g)];
gamma = cp_mass(g)/cv_mass(g)
options=odeset('RelTol', 1.e-5, 'AbsTol', 1.e-8, 'Stats', 'on', 'OutputFcn', @odeplot,
'OutputSel', [1]);
out= ode15s(@slidercrankODE,[time(1) time(end)], z0, options, g, engine_data, mass,
v0, gamma, Pin, Tin);
x=deval(out,time);
thf=time*180/pi*omega;
ns=nspecies(g);
Ru=gasconstant;
```

```

for i=1:length(time);
    r = x(4:end,i);
    for k=1:79
        if r(k) < 0;
            r(k) = 0;
        end
    end
    setmoleFractions(g,r);
    setState_UV(g,[x(2,i) x(3,i)]);
    wt1=meanmolecularweight(g);
    mfr(:,i) = massFractions(g);
    of(:,i) = moleFractions(g);
    o4(i)=cp_mass(g)/cv_mass(g);
    Tf(i) = Temperature(g);
    Pf(i) = pressure(g);
end

% ISENTROPIC EXPANSION OF GASES AT BDC

sp = [entropy_mass(g),oneatm]
setState_SP(g,sp);
Tr = temperature(g)
Pr = pressure (g)

% COMBINING BOTH DATA BEFORE CAPTURING GAS FOR REFORMATION
AND AFTER

so = size(of);
sof = so(2);
timef = zeros(1,sof);
vf = zeros(1,sof);
tof = so(2);
timef(1,1:tof) = time(1:tof);
vf(1,1:tof) = x(3,1:tof);
% WORK CALCULATIONS

for xx1 = 2:length(timef)
    work1(xx1) = ((Pf(xx1)+Pf(xx1-1))/2)*(vf(xx1)-vf(xx1-1)); % J/Kg
end
work = cumsum(work1/1000); % units J/g

% OUTPUT FOR CREATING INDEX IN EXCEL OUTPUT FILE - 1ST 10 ROWS
ARE OCCUPIED BY INDEX

spe = char(speciesNames(g));
spe1 = strvcats(char('time'), char('rad'), char('temp'), char('press'),char('work'), spe);

```

```

% CREATING FILE NAME BASED ON PHI INPUT

file = strcat('NoRef-Phi', num2str(phi),'T-',num2str(Tin));

% WRITING SPECIES INDEX ON TO FILE CREATED

dlmwrite(file,spel');

% WRITING SPECIES OUTPUT

mout = [timef thf Tf Pf work' of'];
dlmwrite(file,mout,'-append');

% ENGINE PARAMETERS AND OUTPUT CONDITIONS CREATING FILE NAME
FOR ENGINE AND INPUT PARAMETERS BASED ON PHI INPUT

file1 = strcat('Inputs', num2str(phi),'T-',num2str(Tin));
spe2 = strvcats(char('phi'), char('Pres-In'), char('Temp-In'), char('Mass'), char('bore'),
char('stroke'), char('compress'), char('conrod'), char('rpm'), char('twall'), char('Tex'),
char('Pex'), spe);

% WRITING VARIABLES INDEX ON TO FILE CREATED

dlmwrite(file1,spe2');

% WRITING VARIABLE VALUES OUTPUT

mout1 = [phi Pin Tin mass engine_data' Tr Pr of(:,end)'];
dlmwrite(file1, mout1, '-append');
%CREATING TEMP FILE FOR LOOP UNTITLED.M

file3 = strcat('Inputs-untitled');
mout2 = [phi Tin EGR reformper];
dlmwrite(file3, mout2);

%WRITING T AND PHI TO START NEXT PROGRAM

mout3 = [phi Tin EGR reformper fueltooxypemr oxymassfrac];
dlmwrite('tempref', mout3);

%WRITING T AND PHI TO START NEXT PROGRAM

mout2 = [phi Tin EGR reformper];
dlmwrite('tempegr',mout2);
if EGR > 0

```

```

    run 'ExhaustGasAdd'
end
if reformper > 0
    run 'Reformation'
else
    disp '***Done***'
end

```

Step 2: First HCCI cycle with Exhaust Gas added

```

disp 'Exhaust Gas Add - running'
g=idealGasMix('chem_Mar_nox.cti');

% READ FILE NAME INPUTS FROM TEMP.DAT

Range1 = [0 0 0 3];
filein = dlmread('tempegr',',', Range1);
phifile = filein(1);
Tfile= filein(2);
EGR = filein(3);
reformper = filein(4);

% OPEN FILE CONTAINING PARAMETERS FROM HCCI FIRST CYCLE OUTPUT

file1 = strcat('Inputs', num2str(phifile), 'T-', num2str(Tfile));

% READ PARAMETERS AND INITIAL CONDITIONS FROM HCCI FIRST CYCLE
OUTPUT

varin1 = dlmread(file1, ',', 9, 0);
phi = varin1(1);
Pin = varin1(2); %atm
Tin= varin1(3);
mass = varin1(4);
bore= varin1(5); % m
stroke= varin1(6); % m
compress= varin1(7);
conrod= varin1(8); %m
rpm= varin1(9); % rpm
twall= varin1(10); % K
Tr = varin1(11);
Pr = varin1(12);
outcond=varin1(13:end);
omega=2*pi*rpm/60.0;
engine_data=[bore,stroke,compress,conrod,rpm,twall]';

```



```

%-----
set(g,'T',Tin,'P',Pin,'X',outcond); % g based on previous HCCI cycle end conditions
Temperature(g);
Pressure(g);

% Moles of EGR added
z1 = moleFractions(g);
z1 = z1*(EGR/100);

% MOLES OF FRESH FUEL AND AIR ADDED

lam = 1/phi;
EGR
fue = 1;
oxy = 3 * lam*fue;
nit = (79/21)*oxy;
set(g,'T',Tin,'P',Pin,'X',strcat('C2H5OH:',num2str(fue),'O2:',num2str(oxy),'N2:',num2str(
nit)));
z11 = moleFractions(g);
z11(49) = (z11(49)*(1-(EGR/100)))+z1(49);
z11(11) = (z11(11)*(1-(EGR/100)))+z1(11);
z11(57) = (z11(57)*(1-(EGR/100)))+z1(57);
z11(9) = (z11(9)*(1-(EGR/100)))+z1(9);
z11(16) = (z11(16)*(1-(EGR/100)))+z1(16);
z11(10) = (z11(10)*(1-(EGR/100)))+z1(10);
z11(72) = (z11(72)*(1-(EGR/100)))+z1(72);
x111 = z11(49)
setMoleFractions(g,z11);
set(g,'T',Tin,'P',Pin);

% TIMING PARAMETERS: SIMULATION CONDUCTED FOR CLOSED PART OF
THE CYCLE FROM INTAKE VALVE CLOSE (IVC) TO EXHAUST VALVE
OPENING (EVO)

ivc=-180;%degrees ATDC (negative means before TDC)
evo=180;%degrees ATDC
dtheta=.5;% crank angle resolution for output

% SIMULATION TIME PARAMTERS CONVERTED FROM DEGREES

t0=ivc*pi/180/omega;
tf=evo*pi/180/omega;
dt=dtheta*pi/180/omega;
time=[t0:dt:tf];

```

```

z = massFractions(g);
fueltooxyperm = z(49)/z(11);
oxymassfrac = z(11);
v0=volume(t0,engine_data);
mass=density(g)*v0
z0 = [temperature(g);
      intEnergy_mass(g);
      1/density(g);
      moleFractions(g)];
gamma = cp_mass(g)/cv_mass(g)
options=odeset('RelTol', 1.e-5, 'AbsTol', 1.e-10, 'Stats', 'on', 'OutputFcn', @odeplot,
'OutputSel', [1]);
out= ode15s(@slidercrankODE, [time(1) time(end)], z0, options, g, engine_data, mass,
v0, gamma, Pin, Tin);
x=deval(out,time);
thf=time*180/pi*omega;
ns=nspecies(g);
Ru=gasconstant;
for i=1:length(time);
    r = x(4:end,i);
    for k=1:79
        if r(k) <0;
            r(k) = 0;
        end
    end
    setmoleFractions(g,r);
    setState_UV(g,[x(2,i) x(3,i)]);
    wt1=meanmolecularweight(g);
    mfr(:,i) = massFractions(g);
    of(:,i) = moleFractions(g);
    o4(i)=cp_mass(g)/cv_mass(g);
    Tf(i) = Temperature(g);
    Pf(i) = pressure(g);
end

```

% ISENTROPIC EXPANSION OF GASES AT BDC

```

sp = [entropy_mass(g),oneatm]
setState_SP(g,sp);
Tr = temperature(g)
Pr = pressure (g)

```

% COMBINING BOTH DATA BEFORE CAPTURING GAS FOR REFORMATION
AND AFTER

```

so = size(of);

```

```

sof = so(2);
timef = zeros(1,sof);
vf = zeros(1,sof);
tof = so(2);
timef(1,1:tof) = time(1:tof);
vf(1,1:tof) = x(3,1:tof);

% WORK CALCULATIONS

for xx1 = 2:length(timef)
    work1(xx1) = ((Pf(xx1)+Pf(xx1-1))/2)*(vf(xx1)-vf(xx1-1)); % J/Kg
end
work = cumsum(work1/1000); % units J/g

% OUTPUT FOR CREATING INDEX IN EXCEL OUTPUT FILE - 1ST 10 ROWS
ARE OCCUPIED BY INDEX

spe = char(speciesNames(g));
spe1 = strvcat(char('time'), char('rad'), char('temp'), char('press'), char('work'), spe);

% CREATING FILE NAME BASED ON PHI INPUT

file2 = strcat('NoRefPhi', num2str(phi), 'T-', num2str(Tin), 'EGR-', num2str(EGR));

% WRITING SPECIES INDEX ON TO FILE CREATED

dlmwrite(file2, spe1');

% WRITING SPECIES OUTPUT

mout = [timef thf Tf Pf work' of];
dlmwrite(file2, mout, '-append');

% ENGINE PARAMETERS AND OUTPUT CONDITIONS CREATING FILE NAME
FOR ENGINE AND INPUT PARAMETERS BASED ON PHI INPUT

file3 = strcat('Inputs', num2str(phi), 'T-', num2str(Tin), 'EGR-', num2str(EGR));
spe2 = strvcat(char('phi'), char('Pres-In'), char('Temp-In'), char('Mass'),
char('bore'), char('stroke'), char('compress'), char('conrod'), char('rpm'), char('twall'),
char('Tex'), char('Pex'), spe);

% WRITING VARIABLES INDEX ON TO FILE CREATED

dlmwrite(file3, spe2');

% WRITING VARIABLE VALUES OUTPUT

```

```

mout1 = [phi Pin Tin mass engine_data' Tr Pr of(:,end)'];
dlmwrite(file3,mout1,'-append');
moutegr = [phi Tin EGR reformper fueltooxyperm oxymassfrac];
dlmwrite('tempref',moutegr);

if reformper > 0
    disp '***End of HCCI cycle I with EGR***';
    run Reformation
    break
else
    disp '***Done***'
end

```

Step 3: Reforming cycle

```

g=idealGasMix('chem_Mar_nox.cti');
disp 'Reformation - running'
for refdur = 0:20:80

% READ FILE NAME INPUTS FROM TEMP.DAT

Range1 = [0 0 0 5];
filein = dlmread('tempref',',', Range1);
phifile = filein(1);
Tfile= filein(2);
EGRfile = filein(3);
reformper = filein(4);
fueltooxyperm = filein(5);
oxymassfrac = filein(6);

if EGRfile == 0

% OPEN FILE CONTAINING PARAMETERS AND OUTLET CONDITIONS
FROM HCCI FIRST CYCLE OUTPUT

file1 = strcat('Inputs', num2str(phifile),'T-',num2str(Tfile))

else

% OPEN FILE CONTAINING PARAMETERS AND OUTLET CONDITIONS FROM
HCCI WITH EGR FIRST CYCLE OUTPUT

file1 = strcat('Inputs', num2str(phifile),'T-',num2str(Tfile),'EGR-',num2str(EGRfile))
end

```

% READ PARAMETERS FROM HCCI FIRST CYCLE OUTPUT

```
varin1 = dlmread(file1,',', 9,0);
phi = varin1(1);
Pin = varin1(2); %atm
Tin= varin1(3);
massp = varin1(4);
bore= varin1(5); % m
stroke= varin1(6); % m
compress= varin1(7);
conrod= varin1(8); %m
rpm= varin1(9); % rpm
twall= varin1(10); % K
Trefst = varin1(11);
Prefst = varin1(12);
trapgas = varin1(13:end)
omega=2*pi*rpm/60.0;
engine_data=[bore,stroke,compress,conrod,rpm,twall]';
```

% RESET TO INITIAL CONDITIONS AFTER EACH REFORM DURATION

% -----

```
set(g,'T',Trefst,'P',Prefst,'X',trapgas); % g based on previous HCCI cycle end conditions
dtheta=.5;% crank angle resolution for output
ivc = -33;
evo = 39;
```

% SIMULATION TIME PARAMTERS CONVERTED FROM DEGREES

```
t0=(ivc-(refdur/2))*pi/180/omega;%convert time to crank angle (rad);
tf=(evo+(refdur/2))*pi/180/omega; %evo - time of injection - TDC
dt=dtheta*pi/180/omega;
time=[t0:dt:tf];
v0=volume(t0,engine_data);% volume of chamber - 10% of clearance volume
massr=density(g)*v0;
```

% MASS OF EACH SPECIES AT VALVE CLOSE

```
z1 = massFractions(g)*massr;
```

%-CALCULATING THE AMOUNT OF FUEL THAT CAN BE ADDED FOR THE OXYGEN PRESENT IN TRAPPED GASES AT VALVE CLOSE

```
addfuelm = z1(11)*fueltooxyperm;
massnext = massp - (massr+addfuelm);
```

```

% MASS OF FUEL THAT CAN BE BROUGHT IN NEXT CYCLE

fuelnext = fueltooxyperm*oxymassfrac*massnext

% MASS OF FUEL ADDED DURING REFORMATION

massfuelref = (fuelnext+addfuelm)*reformper/100;
percentage = massfuelref/(fuelnext+addfuelm);

% REFORMATION FUEL ADDITION
z1(49) = z1(49)+ massfuelref;

% NEW MASS FRACTIONS - INPUT FOR REFORMATION

z1 = z1/(massr+massfuelref);
setMassFractions(g,z1);
mass1 = density(g)*v0;
massnext1 = massp - mass1;
gamma = cp_mass(g)/cv_mass(g);
z0 = [temperature(g)
      intEnergy_mass(g);
      1/density(g);
      moleFractions(g)];
options=odeset('RelTol', 1.e-5, 'AbsTol', 1.e-10, 'Stats', 'on', 'OutputFcn', @odeplot,
'OutputSel', [1]);
out= ode15s(@slidercrankODE, [time(1) time(end)], z0, options, g, engine_data, mass1,
v0, gamma, Prefst, Trefst);
x=deval(out,time);
th=time*180/pi*omega;
ns=nspecies(g);
Ru=gasconstant;
for i=1:length(time);
    r = x(4:end,i);
    for k=1:79
        if r(k) < 0;
            r(k) = 0;
        end
    end
    setmoleFractions(g,r);
    setState_UV(g,[x(2,i) x(3,i)]);
    wt1=meanmolecularweight(g);
    mfr(:,i) = massFractions(g);
    ol(:,i) = moleFractions(g);
    o4(i)=cp_mass(g)/cv_mass(g);
    T1(i) = Temperature(g);
    P1(i) = pressure(g);
end

```

end

% ISENTROPIC EXPANSION OF GASES AT BDC

```
sp = [entropy_mass(g),oneatm]
setState_SP(g,sp);
Tr = temperature(g)
Pr = pressure (g)
```

% FOR CREATING INDEX IN EXCEL OUTPUT FILE - 1ST 10 ROWS ARE OCCUPIED BY INDEX

```
spe = char(speciesNames(g));
spe1 = strvcat(char('time'), char('rad'), char('temp'), char('press'), spe);
refca = 72 + refdur
```

% CREATING FILE NAME BASED ON PHI INPUT

```
file2 = strcat('Phi', num2str(phi), 'T-', num2str(Tin), 'EGR-', num2str(EGRfile), 'Ref-',
num2str(reformper), '-', num2str(refca), 'CA');
```

% WRITING SPECIES INDEX ON TO FILE CREATED

```
dlmwrite(file2,spe1);
```

% WRITING SPECIES OUTPUT

```
mout = [time' th' T1' P1' o1'];
dlmwrite(file2,mout,'-append');
```

% ENGINE PARAMETERS AND OUTPUT CONDITIONS

% CREATING FILE NAME FOR ENGINE AND INPUT PARAMETERS BASED ON PHI INPUT

```
file3 = strcat('Inputs', num2str(phi),'T-',num2str(Tin),'EGR-',num2str(EGRfile),'Ref-',
',num2str(reformper),'-',num2str(refca),'CA')
```

```
spe2 = strvcat(char('phi'), char('Pres-In'), char('Temp-In'), char('Mass'), char('bore'),
char('stroke'), char('compress'), char('conrod'), char('rpm'), char('twall'), char('mref'),
char('Tex'), char('Pex'),spe);
```

% WRITING VARIABLES INDEX ON TO FILE CREATED

```
dlmwrite(file3,spe2');
```

% WRITING VARIABLE VALUESOUTPUT

```

mout1 = [phi Pin Tin mass1 massnext1 engine_data' Tr Pr ol(:,end)'];
dlmwrite(file3,mout1,'-append');
fuelsub = fuelnext+addfuelm;
file4 = strcat('temphcci2',num2str(refca));
mout2 = [phi Tin EGRfile reformper];
dlmwrite(file4,mout2);
file5 = strcat('fuelsub',num2str(refca));
mout3 = [fuelsub addfuelm];
dlmwrite(file5,mout3);
end
disp '***End of Reformation Cycle***'
run 'HCCIcycleII'

```

Step 4: HCCI cycle with reformat products

```

g=idealGasMix('chem_Mar_nox.cti');
disp 'HCCI II running'

```

```

%% READ FILE NAME INPUTS FROM TEMP.DAT

```

```

for refca= 72:20:152
filei1 = strcat('temphcci2',num2str(refca));
filein = dlmread(filei1, ',',0,0);
phifile = filein(1)
Tfile= filein(2)
EGRfile = filein(3)
reformper = filein(4)
filei2 = strcat('fuelsub',num2str(refca));
filefuel = dlmread(filei2, ',',0,0);
fuelsub = filefuel(1)
addfuelm = filefuel(2)

```

```

% OPEN FILE CONTAINING ENGINE PARAMETERS AND END GAS
CONDITIONS FROM REFORMATION CYCLE

```

```

file1 = strcat('Inputs', num2str(phifile), 'T-',num2str(Tfile), 'EGR-', num2str(EGRfile),
'Ref-',num2str(reformper), '-', num2str(refca), 'CA');

```

```

% READ PARAMETERS AND INTIAL CONDITIONS FROM HCCI FIRST CYCLE
OUTPUT

```

```

varin1 = dlmread(file1, ',',9,0);
phi = varin1(1);
Pin = varin1(2); %atm

```



```

Tin= varin1(3);
massr = varin1(4)
massnext = varin1(5)
bore= varin1(6); % m
stroke= varin1(7); % m
compress= varin1(8)
conrod= varin1(9); %m
rpm= varin1(10); % rpm
twall= varin1(11); % K
Tpc = varin1(12);
Ppc = varin1(13);
outcond=varin1(14:end)
omega=2*pi*rpm/60.0;
engine_data=[bore,stroke,compress,conrod,rpm,twall]';

%-----

set(g,'T',Tin,'P',Pin,'X',outcond); % g based on end of reformation cycle after isentropic
expansion to Patm
u11 = intEnergy_mass(g);
svref = 1/density(g);
mr = massFractions(g)*massr; % Mass of each reformate species
if EGRfile == 0
    lam = 1/phi;
    fue = 1;
    oxy = 3 * lam
    nit = (79/21)*oxy

Set(g,'T',Tin,'P',Pin,'X',strcat('C2H5OH:',num2str(fue),'O2:',num2str(oxy),'N2:',num2str
(nit))); % without EGR
min = massFractions(g)*(massnext);
else

% OPEN FILE CONTAINING PARAMETERS FROM HCCI FIRST CYCLE OUTPUT

file2 = strcat('Inputs', num2str(phifile),'T-',num2str(Tfile))

% READ PARAMETERS AND INTIAL CONDITIONS FROM HCCI FIRST CYCLE
OUTPUT

varin2 = dlmread(file2,',',9,0);
outcond2=varin2(13:end);
set(g,'T',Tin,'P',Pin,'X',outcond2); % g based on previous HCCI cycle end conditions

% MOLES OF EGR ADDED

```

```

z1 = moleFractions(g)';
z1 = z1*(EGRfile/100);

% MOLES OF FRESH FUEL AND AIR ADDED

lam = 1/phi;
EGR = EGRfile
fue = 1;
oxy = 3 * lam*fue;
nit = (79/21)*oxy;

set(g,'T',Tin,'P',Pin,'X',strcat('C2H5OH:',num2str(fue),'O2:',num2str(oxy),'N2:',num2str(
nit)));
z11 = moleFractions(g)';
x111 = z11(49);
z11(49) = (z11(49)*(1-(EGR/100)))+z1(49);
z11(11) = (z11(11)*(1-(EGR/100)))+z1(11);
z11(57) = (z11(57)*(1-(EGR/100)))+z1(57);
z11(9) = (z11(9)*(1-(EGR/100)))+z1(9);
z11(16) = (z11(16)*(1-(EGR/100)))+z1(16);
z11(10) = (z11(10)*(1-(EGR/100)))+z1(10);
z11(72) = (z11(72)*(1-(EGR/100)))+z1(72);
setMoleFractions(g,z11);
set(g,'T',Tin,'P',Pin);
min = massFractions(g)*(massnext);
end
min(49) = fuelsub*(1-(reformper/100));
mfinal1 = (min+mr)/(massnext+massr);
setMassFractions(g,mfinal1);
set(g,'T',Tin,'P',Pin);

% TIMING PARAMETERS: SIMULATION CONDUCTED FOR CLOSED PART OF
THE CYCLE FROM INTAKE VALVE CLOSE (IVC) TO EXHAUST VALVE
OPENING (EVO)

ivc=-180;%degrees ATDC (negative means before TDC)
evo=180;%degrees ATDC
dtheta=.5;% crank angle resolution for output

%SIMULATION TIME PARAMTERS CONVERTED FROM DEGREES

t0=ivc*pi/180/omega;
tf=evo*pi/180/omega;
dt=dtheta*pi/180/omega;
time=[t0:dt:tf];
z = massFractions(g)';

```

```

fueltooxyperm = z(49)/z(11);
oxymassfrac = z(11);
v0=volume(t0,engine_data);
mass=density(g)*v0;
z0 = [temperature(g);
      intEnergy_mass(g);
      1/density(g);
      moleFractions(g)];
gamma = cp_mass(g)/cv_mass(g)
options=odeset('RelTol', 1.e-6, 'AbsTol', 1.e-9, 'Stats', 'on', 'OutputFcn', @odeplot,
'OutputSel', [1]);
out= ode15s(@slidercrankODE, [time(1) time(end)], z0, options, g, engine_data, mass,
v0, gamma, Pin, Tin);
x=deval(out,time);
thf=time*180/pi*omega;
ns=nspecies(g);
Ru=gasconstant;
for i=1:length(time);
    r = x(4:end,i);
    for k=1:79
        if r(k) <0;
            r(k) = 0;
        end
    end
end
setmoleFractions(g,r);
setState_UV(g,[x(2,i) x(3,i)]);
wt1=meanmolecularweight(g);
mfr(:,i) = massFractions(g);
of(:,i) = moleFractions(g);
o4(i)=cp_mass(g)/cv_mass(g);
Tf(i) = Temperature(g);
Pf(i) = pressure(g);
end

```

% ISENTROPIC EXPANSION OF GASES AT BDC

```

sp = [entropy_mass(g),oneatm]
setState_SP(g,sp);
Tr = temperature(g)
Pr = pressure (g)

```

% COMBINING BOTH DATA BEFORE CAPTURING GAS FOR REFORMATION AND AFTER

```

so = size(of);
sof = so(2);

```

```

timef = zeros(1,sof);
vf = zeros(1,sof);
tof = so(2);
timef(1,1:tof) = time(1:tof);
vf(1,1:tof) = x(3,1:tof);

%WORK CALCULATIONS

for xx1 = 2:length(timef)
    work1(xx1)=((Pf(xx1)+Pf(xx1-1))/2)*(vf(xx1)-vf(xx1-1));% J/Kg
end
work = cumsum(work1/1000); % units J/g

% OUTPUT FOR CREATING INDEX IN EXCEL OUTPUT FILE - 1ST 10 ROWS
ARE OCCUPIED BY INDEX

spe = char(speciesNames(g));
spe1 = strvcats(char('time'), char('rad'), char('temp'), char('press'),char('work'), spe);

% CREATING FILE NAME BASED ON PHI INPUT

file2 = strcat('HCCI-II-Phi', num2str(phi), 'T-', num2str(Tin), 'EGR-', num2str(EGRfile),
'Ref-', num2str(reformper), '-', num2str(refca), 'CA');

% WRITING SPECIES INDEX ON TO FILE CREATED

dlmwrite(file2,spe1');
% WRITING SPECIES OUTPUT

mout = [timef thf Tf Pf work' of'];
dlmwrite(file2,mout,'-append');
end
clear all
disp '****done complete cycle****';

```

G.2: In-cylinder reformation using pre-chamber

Step 1: Initial HCCI cycle

```
disp 'HCCI-Running'
```

```
% INPUTS
```

```
Pin= oneatm*0.8;
lam = 1/phi;
```

```

fue = 1
oxy = 3 * lam
nit = (79/21)*oxy
g=idealGasMix('chem_Mar_nox.cti');
set(g,'T',Tin,'P',Pin,'X',strcat('C2H5OH:',num2str(fue),'O2:',num2str(oxy),'N2:',num2str(
nit)));

```

% ENGINE PARAMETERS

```

bore=0.072; % m
stroke=0.0736; % m
compress=20;
conrod=.132112; %m
rpm=1000; % rpm
twall=348; % K
omega=2*pi*rpm/60.0;
engine_data=[bore,stroke,compress,conrod,rpm,twall]';

```

% TIMING PARAMETERS: SIMULATION CONDUCTED FOR CLOSED PART OF THE CYCLE FROM INTAKE VALVE CLOSE (IVC) TO EXHAUST VALVE OPENING (EVO)

```

ivc=-180;%degrees ATDC (negative means before TDC)
evo=180;%degress ATDC
dtheta=.5;% crank angle resolution for output

```

% SIMULATION TIME PARAMETERS CONVERTED FROM DEGREES

```

t0=ivc*pi/180/omega;
tf=evo*pi/180/omega;
tref=refca*pi/180/omega;
dt=dtheta*pi/180/omega;
time1=[t0:dt:tref];
time2=[tref:dt:tf];
z = massFractions(g)';
fueltooxyperm = z(49)/z(11);
oxymassfrac = z(11);
v0=volume(t0,engine_data);
vc=pi*bore^2/4*stroke/(compress-1);
vref = vc/3; % volume of chamber - 10% of clearance volume
mass1=density(g)*v0
z0 = [temperature(g);
intEnergy_mass(g);
1/density(g);
moleFractions(g)];

```

```

gamma = cp_mass(g)/cv_mass(g)
options=odeset('RelTol', 1.e-5, 'AbsTol', 1.e-12, 'Stats', 'on', 'OutputFcn', @odeplot,
'OutputSel', [1]);
out= ode15s(@slidercrankODE, [time1(1) time1(end)], z0, options, g, engine_data,
mass1, v0, gamma, Pin, Tin);
x=deval(out,time1);
th=time1*180/pi*omega;
ns=nspecies(g);
Ru=gasconstant;
for i=1:length(time1);
    r = x(4:end,i);
    for k=1:79
        if r(k) <0;
            r(k) = 0;
        end
    end
    setmoleFractions(g,r);
    setState_UV(g,[x(2,i) x(3,i)]);
    wt1=meanmolecularweight(g);
    mfr(:,i) = massFractions(g);
    o1(:,i) = moleFractions(g);
    o4(i)=cp_mass(g)/cv_mass(g);
    T1(i) = Temperature(g);
    P1(i) = pressure(g);
end
zr = [temperature(g)
    intEnergy_mass(g);
    1/density(g);
    moleFractions(g)];
massref = vref*density(g);
gamma = cp_mass(g)/cv_mass(g);
options=odeset('RelTol', 1.e-6, 'AbsTol', 1.e-12, 'Stats', 'on', 'OutputFcn', @odeplot,
'OutputSel', [1]);
out1= ode15s(@slidercrankODE, [time2(1) time2(end)], zr, options, g, engine_data,
mass1, v0, gamma, Pin, Tin);
x1=deval(out1,time2);
th1=time2*180/pi*omega;
ns=nspecies(g);
Ru=gasconstant;
for i=1:length(time2);
    r1 = x1(4:end,i);
    for k=1:79
        if r1(k) <0;
            r1(k) = 0;
        end
    end
end
end

```

```

setmoleFractions(g,r1);
setState_UV(g,[x1(2,i) x1(3,i)]);
wt1=meanmolecularweight(g);
mfr1(:,i) = massFractions(g);
o11(:,i) = moleFractions(g);
o41(i)=cp_mass(g)/cv_mass(g);
T11(i) = Temperature(g);
P11(i) = pressure(g);
end

```

```

% COMBINING BOTH DATA BEFORE CAPTURING GAS FOR REFORMATION
AND AFTER

```

```

so = size(o1);
sol = size(o11);
sof = so(2)-1+sol(2);
of = zeros(so(1),sof);
Tf = zeros(1,sof);
Pf = zeros(1,sof);
thf = zeros(1,sof);
timef = zeros(1,sof);
vf = zeros(1,sof);
tof = so(2)-1;
of(:,1:tof) = o1(:,1:tof);
of(:,so(2):end)=o11(:,1:sol(2));
Tf(1,1:tof) = T1(1:tof);
Tf(1,so(2):end)=T11(1:sol(2));
Pf(1,1:tof) = P1(1:tof);
Pf(1,so(2):end)=P11(1:sol(2));
thf(1,1:tof) = th(1:tof);
thf(1,so(2):end)=th1(1:sol(2));
timef(1,1:tof) = time1(1:tof);
timef(1,so(2):end)=time2(1:sol(2));
vf(1,1:tof) = x(3,1:tof);
vf(1,so(2):end)=x1(3,1:sol(2));

```

```

% WORK CALCULATIONS

```

```

for xx1 = 2:length(timef)
    work1(xx1)=((Pf(xx1)+Pf(xx1-1))/2)*(vf(xx1)-vf(xx1-1));% J/Kg
end
work = cumsum(work1/1000); % units J/g

```

```

% OUTPUT FOR CREATING INDEX IN EXCEL OUTPUT FILE - 1ST 10 ROWS
ARE OCCUPIED BY INDEX

```

```

spe = char(speciesNames(g));
spe1 = strvcats(char('time'), char('rad'), char('temp'), char('press'),char('work'), spe);

% CREATING FILE NAME BASED ON PHI INPUT

file = strcat('NoRefPhi', num2str(phi),'T-',num2str(Tin));

% WRITING SPECIES INDEX ON TO FILE CREATED

dlmwrite(file,spe1');

% WRITING SPECIES OUTPUT

mout = [timef thf Tf Pf work' of];
dlmwrite(file,mout,'-append');

% ENGINE PARAMETERS AND OUTPUT CONDITIONS

% CREATING FILE NAME FOR ENGINE AND INPUT PARAMETERS BASED ON
PHI INPUT

file1 = strcat('Inputs', num2str(phi),'T-',num2str(Tin));
spe2 = strvcats(char('phi'), char('Pres-In'), char('Temp-In'), char('Mass'), char('bore'),
char('stroke'), char('compress'), char('conrod'), char('rpm'), char('twall'), char('vref'),
char('tref'), char('Tex'), char('Pex'), spe);

% WRITING VARIABLES INDEX ON TO FILE CREATED

dlmwrite(file1,spe2');

% WRITING VARIABLE VALUES OUTPUT

mout1 = [phi Pin Tin mass1 engine_data' vref tref T1(end) P1(end) o1(:,end)'];
dlmwrite(file1,mout1,'-append');

%CREATING TEMP FILE FOR LOOP UNTITLED.M

file3 = strcat('Inputs-untitled');
mout2 = [phi Tin EGR reformper refca];
dlmwrite(file3,mout2);

%WRITING T AND PHI TO START NEXT PROGRAM

mout3 = [phi Tin EGR reformper fueltooxyperm oxymassfrac refca];
dlmwrite('tempref',mout3);

```



```
%WRITING T AND PHI TO START NEXT PROGRAM
```

```
mout2 = [phi Tin EGR reformper refca];  
dlmwrite('tempegr',mout2);  
if EGR > 0  
    run 'ExhaustGasAdd'  
end  
if reformper > 0  
    run 'Reformation'  
else  
    disp '***Done***'  
end
```

Step 2: First HCCI cycle with exhaust gas added

```
disp 'Exhaust Gas Add - running'  
g=idealGasMix('chem_Mar_nox.cti');
```

```
% READ FILE NAME INPUTS FROM TEMP.DAT
```

```
Range1 = [0 0 0 4];  
filein = dlmread('tempegr',',', Range1);  
phifile = filein(1);  
Tfile= filein(2);  
EGR = filein(3);  
reformper = filein(4);  
refca = filein(5);
```

```
% OPEN FILE CONTAINING PARAMETERS FROM HCCI FIRST CYCLE OUTPUT
```

```
file1 = strcat('Inputs', num2str(phifile),'T-',num2str(Tfile));
```

```
% READ PARAMETERS AND INITIAL CONDITIONS FROM HCCI FIRST CYCLE  
OUTPUT
```

```
varin1 = dlmread(file1,',',9,0);  
phi = varin1(1);  
Pin = varin1(2); %atm  
Tin= varin1(3);  
mass1 = varin1(4);  
bore= varin1(5); % m  
stroke= varin1(6); % m  
compress= varin1(7);
```

```

conrod= varin1(8); %m
rpm= varin1(9); % rpm
twall= varin1(10); % K
vref = varin1(11);
tref = varin1(12);
Tpc = varin1(13);
Ppc = varin1(14);
clear varin1
fileegr = strcat('NoRefPhi', num2str(phi),'T-',num2str(Tin));
varinegr = dlmread(fileegr,',',9,0);
outcond=varinegr(end,6:end);
omega=2*pi*rpm/60.0;
engine_data=[bore,stroke,compress,conrod,rpm,twall]';
set(g,'T',Tin,'P',Pin,'X',outcond); % g based on previous HCCI cycle end conditions
Temperature(g);
Pressure(g);

```

% MOLES OF EGR ADDED

```

z1 = moleFractions(g)';
z1 = z1*(EGR/100);

```

% MOLES OF FRESH FUEL AND AIR ADDED

```

lam = 1/phi;
EGR
fue = 1;
oxy = 3 * lam*fue;
nit = (79/21)*oxy;
set(g,'T',Tin,'P',Pin,'X',strcat('C2H5OH:',num2str(fue),'O2:',num2str(oxy),'N2:',num2str(
nit)));
z11 = moleFractions(g)';
z11(49) = (z11(49)*(1-(EGR/100)))+z1(49);
z11(11) = (z11(11)*(1-(EGR/100)))+z1(11);
z11(57) = (z11(57)*(1-(EGR/100)))+z1(57);
z11(9) = (z11(9)*(1-(EGR/100)))+z1(9);
z11(16) = (z11(16)*(1-(EGR/100)))+z1(16);
z11(10) = (z11(10)*(1-(EGR/100)))+z1(10);
z11(72) = (z11(72)*(1-(EGR/100)))+z1(72);
x111 = z11(49)
setMoleFractions(g,z11);
set(g,'T',Tin,'P',Pin);

```

% TIMING PARAMETERS: SIMULATION CONDUCTED FOR CLOSED PART OF THE CYCLE FROM INTAKE VALVE CLOSE (IVC) TO EXHAUST VALVE OPENING (EVO)

```
ivc=-180;%degrees ATDC (negative means before TDC)
```

```
evo=180;%degrees ATDC
```

```
dtheta=.5;% crank angle resolution for output
```

```
%SIMULATION TIME PARAMETERS CONVERTED FROM DEGREES
```

```
t0=ivc*pi/180/omega;
```

```
tf=evo*pi/180/omega;
```

```
tref=refca*pi/180/omega;
```

```
dt=dtheta*pi/180/omega;
```

```
time1=[t0:dt:tref];
```

```
time2=[tref:dt:tf];
```

```
z = massFractions(g)';
```

```
fueltooxyperm = z(49)/z(11);
```

```
oxymassfrac = z(11);
```

```
v0=volume(t0,engine_data);
```

```
vc=pi*bore^2/4*stroke/(compress-1);
```

```
vref = vc/3; % volume of chamber - 10% of clearance volume
```

```
mass1=density(g)*v0
```

```
z0 = [temperature(g);
```

```
intEnergy_mass(g);
```

```
1/density(g);
```

```
moleFractions(g)];
```

```
gamma = cp_mass(g)/cv_mass(g)
```

```
options=odeset('RelTol', 1.e-5, 'AbsTol', 1.e-12, 'Stats', 'on', 'OutputFcn', @odeplot,  
'OutputSel', [1]);
```

```
out= ode15s(@slidercrankODE, [time1(1) time1(end)], z0, options, g, engine_data,  
mass1, v0, gamma, Pin, Tin);
```

```
x=deval(out,time1);
```

```
th=time1*180/pi*omega;
```

```
ns=nspecies(g);
```

```
Ru=gasconstant;
```

```
for i=1:length(time1);
```

```
    r = x(4:end,i);
```

```
    for k=1:79
```

```
        if r(k) < 0;
```

```
            r(k) = 0;
```

```
        end
```

```
    end
```

```
    setmoleFractions(g,r);
```

```
    setState_UV(g,[x(2,i) x(3,i)]);
```

```
    wt1=meanmolecularweight(g);
```

```
    mfr(:,i) = massFractions(g);
```

```
    ol(:,i) = moleFractions(g);
```

```
    o4(i)=cp_mass(g)/cv_mass(g);
```

```

    T1(i) = Temperature(g);
    P1(i) = pressure(g);
end
zr = [temperature(g)
      intEnergy_mass(g);
      1/density(g);
      moleFractions(g)];
massref = vref*density(g);
gamma = cp_mass(g)/cv_mass(g);
options=odeset('RelTol', 1.e-6, 'AbsTol', 1.e-12, 'Stats', 'on', 'OutputFcn', @odeplot,
'OutputSel', [1]);
out1= ode15s(@slidercrankODE, [time2(1) time2(end)], zr, options, g, engine_data,
mass1, v0, gamma, Pin, Tin);
x1=deval(out1,time2);
th1=time2*180/pi*omega;
ns=nspecies(g);
Ru=gasconstant;
for i=1:length(time2);
    r1 = x1(4:end,i);
    for k=1:79
        if r1(k) <0;
            r1(k) = 0;
        end
    end
    setmoleFractions(g,r1);
    setState_UV(g,[x1(2,i) x1(3,i)]);
    wt11=meanmolecularweight(g);
    mfr1(:,i) = massFractions(g);
    o11(:,i) = moleFractions(g);
    o41(i)=cp_mass(g)/cv_mass(g);
    T11(i) = Temperature(g);
    P11(i) = pressure(g);
end

```

% COMBINING BOTH DATA BEFORE CAPTURING GAS FOR REFORMATION AND AFTER

```

so = size(o1);
so1 = size(o11);
sof = so(2)-1+so1(2);
of = zeros(so(1),sof);
Tf = zeros(1,sof);
Pf = zeros(1,sof);
thf = zeros(1,sof);
timef = zeros(1,sof);
vf = zeros(1,sof);

```

```

tof = so(2)-1;
of(:,1:tof) = o1(:,1:tof);
of(:,so(2):end)=o11(:,1:so1(2));
Tf(1,1:tof) = T1(1:tof);
Tf(1,so(2):end)=T11(1:so1(2));
Pf(1,1:tof) = P1(1:tof);
Pf(1,so(2):end)=P11(1:so1(2));
thf(1,1:tof) = th(1:tof);
thf(1,so(2):end)=th1(1:so1(2));
timef(1,1:tof) = time1(1:tof);
timef(1,so(2):end)=time2(1:so1(2));
vf(1,1:tof) = x(3,1:tof);
vf(1,so(2):end)=x1(3,1:so1(2));

% WORK CALCULATIONS

for xx1 = 2:length(timef)
    work1(xx1)=((Pf(xx1)+Pf(xx1-1))/2)*(vf(xx1)-vf(xx1-1));% J/Kg
end
work = cumsum(work1/1000); % units J/g

% OUTPUT FOR CREATING INDEX IN EXCEL OUTPUT FILE - 1ST 10 ROWS
ARE OCCUPIED BY INDEX

spe = char(speciesNames(g));
spe1 = strvcats(char('time'), char('rad'), char('temp'), char('press'),char('work'), spe);

% CREATING FILE NAME BASED ON PHI INPUT

file2 = strcat('NoRefPhi', num2str(phi),'T-',num2str(Tin),'EGR-',num2str(EGR));

% WRITING SPECIES INDEX ON TO FILE CREATED

dlmwrite(file2,spe1');

% WRITING SPECIES OUTPUT

mout = [timef thf Tf Pf work' of'];
dlmwrite(file2,mout,'-append');

% ENGINE PARAMETERS AND OUTPUT CONDITIONS CREATING FILE NAME
FOR ENGINE AND INPUT PARAMETERS BASED ON PHI INPUT

file3 = strcat('Inputs', num2str(phi), 'T-',num2str(Tin), 'EGR-',num2str(EGR));

```

```
spe2 = strvcat(char('phi'), char('Pres-In'), char('Temp-In'), char('Mass'), char('bore'),
char('stroke'), char('compress'), char('conrod'), char('rpm'), char('twall'), char('vref'),
char('tref'), char('Tex'), char('Pex'), spe);
```

```
% WRITING VARIABLES INDEX ON TO FILE CREATED
```

```
dlmwrite(file3,spe2');
```

```
% WRITING VARIABLE VALUESOUTPUT
```

```
mout1 = [phi Pin Tin mass1 engine_data' vref tref T1(end) P1(end) o1(:,end)'];
dlmwrite(file3,mout1,'-append');
```

```
% CREATING TEMP FILE FOR LOOP UNTITLED.M
```

```
file4 = strcat('Inputs-untitled');
mout4 = [phi Tin EGR reformper refca];
dlmwrite(file4,mout4);
moutegr = [phi Tin EGR reformper fueltooxperm oxymassfrac refca]
dlmwrite('tempref',moutegr);
if reformper > 0
    disp '***End of HCCI cycle I with EGR***';
    run Reformation
    break
else
    disp '***Done***'
end
```

```
Step 3: Reforming cycle
```

```
g=idealGasMix('chem_Mar_nox.cti');
disp 'Reformation - running'
```

```
% READ FILE NAME INPUTS FROM TEMP.DAT
```

```
Range1 = [0 0 0 6];
filein = dlmread('tempref',';', Range1);
phifile = filein(1);
Tfile= filein(2);
EGRfile = filein(3);
reformper = filein(4);
fueltooxperm = filein(5);
oxymassfrac = filein(6);
refca = filein(7);
if EGRfile == 0
```

```
% OPEN FILE CONTAINING PARAMETERS AND OUTLET CONDITIONS FROM  
HCCI FIRST CYCLE OUTPUT
```

```
file1 = strcat('Inputs', num2str(phifile), 'T-', num2str(Tfile))  
else
```

```
% OPEN FILE CONTAINING PARAMETERS AND OUTLET CONDITIONS FROM  
HCCI WITH EGR FIRST CYCLE OUTPUT
```

```
file1 = strcat('Inputs', num2str(phifile), 'T-', num2str(Tfile), 'EGR-', num2str(EGRfile))  
end
```

```
% READ PARAMETERS FROM HCCI FIRST CYCLE OUTPUT
```

```
varin1 = dlmread(file1, ',', 9, 0);  
phi = varin1(1);  
Pin = varin1(2); %atm  
Tin = varin1(3);  
massp = varin1(4);  
bore = varin1(5); % m  
stroke = varin1(6); % m  
compress = varin1(7);  
conrod = varin1(8); %m  
rpm = varin1(9); % rpm  
twall = varin1(10); % K  
tref = varin1(12); % time of ref  
vref = varin1(11); % ref chamber volume  
Trefst = varin1(13);  
Prefst = varin1(14);  
trapgas = varin1(15:end)  
omega = 2*pi*rpm/60.0;  
engine_data = [bore, stroke, compress, conrod, rpm, twall]';
```

```
% RESET TO INITIAL CONDITIONS AFTER EACH REFORM DURATION
```

```
set(g, 'T', Trefst, 'P', Prefst, 'X', trapgas); % g based on previous HCCI cycle end conditions  
dtheta = .5; % crank angle resolution for output
```

```
% SIMULATION TIME PARAMETERS CONVERTED FROM DEGREES
```

```
trefca = tref*omega*180/pi; % convert time to crank angle (rad);  
tf = (60/(360*rpm))*(720-trefca); %evo - time of injection - TDC  
dt = dtheta*pi/180/omega;  
time = [0:dt:tf];  
v0 = vref; % volume of chamber - 10% of clearance volume  
massr = density(g)*v0;
```

% MASS OF EACH SPECIES AT VALVE CLOSE

z1 = massFractions(g)*massr;

% CALCULATING THE AMOUNT OF FUEL ADDED MASS OF ADDITIONAL
FUEL THAT CAN BE ADDED FOR THE OXYGEN PRESENT IN TRAPPED GASES
AT VALVE CLOSE

addfuelm = z1(11)*fueltooxyperm

% MASS CAN BE BROUGHT IN NEXT CYCLE

massnext = massp - (massr+addfuelm);

% MASS OF FUEL THAT CAN BE BROUGHT IN NEXT CYCLE

fuelnext = fueltooxyperm*oxymassfrac*massnext

% MASS OF FUEL ADDED DURING REFORMATION

massfuelref = (fuelnext+addfuelm)*reformper/100;
percentage = massfuelref/(fuelnext+addfuelm)

% REFORMATION FUEL ADDITION

z1(49) = z1(49)+ massfuelref;

% NEW MASS FRACTIONS - INPUT FOR REFORMATION

z1 = z1/(massr+massfuelref);
SetMassFractions(g,z1);
mass1 = density(g)*v0;
massnext1 = massp - mass1;
gamma = cp_mass(g)/cv_mass(g);
z0 = [temperature(g)
intEnergy_mass(g);
1/density(g);
moleFractions(g)];
options=odeset('RelTol', 1.e-6, 'AbsTol', 1.e-14, 'Stats', 'on', 'OutputFcn', @odeplot,
'OutputSel', [1]);


```

out= ode15s(@slidercrankODEref1, [time(1) time(end)], z0, options, g, mass1, v0,
gamma, Pin, Tin, twall);
x=deval(out,time);
th=time*180/pi*omega;
ns=nspecies(g);
Ru=gasconstant;
for i=1:length(time);
r = x(4:end,i);
for k=1:79
if r(k) <0;
r(k) = 0;
end
end
setmoleFractions(g,r);
setState_UV(g,[x(2,i) x(3,i)]);
wt1=meanmolecularweight(g);
mfr(:,i) = massFractions(g);
o1(:,i) = moleFractions(g);
o4(i)=cp_mass(g)/cv_mass(g);
T1(i) = Temperature(g);
P1(i) = pressure(g);
end

```

% FOR CREATING INDEX IN EXCEL OUTPUT FILE - 1ST 10 ROWS ARE OCCUPIED BY INDEX

```

spe = char(speciesNames(g));
spe1 = strvcats(char('time'), char('rad'), char('temp'), char('press'), spe);

```

% CREATING FILE NAME BASED ON PHI INPUT

```

file2 = strcat('Phi', num2str(phi), 'T-',num2str(Tin), 'EGR-',num2str(EGRfile), 'Ref-',
num2str(reformper),'-',num2str(refca),'CA');

```

% WRITING SPECIES INDEX ON TO FILE CREATED

```

dlmwrite(file2,spe1');

```

% WRITING SPECIES OUTPUT

```

mout = [time' th' T1' P1' o1'];
dlmwrite(file2,mout,'-append');

```

% ENGINE PARAMETERS AND OUTPUT CONDITIONS CREATING FILE NAME FOR ENGINE AND INPUT PARAMETERS BASED ON PHI INPUT

```

file3 = strcat('Inputs', num2str(phi),'T-',num2str(Tin),'EGR-',num2str(EGRfile),'Ref-
',num2str(reformper),'-',num2str(refca),'CA')
spe2 = strvcac(char('phi'), char('Pres-In'), char('Temp-In'), char('Mass'), char('bore'),
char('stroke'), char('compress'), char('conrod'), char('rpm'), char('twall'), char('vref'),
char('tref'), char('Tex'), char('Pex'),spe);

```

```

% WRITING VARIABLES INDEX ON TO FILE CREATED

```

```

dlmwrite(file3,spe2);

```

```

% WRITING VARIABLE VALUES OUTPUT

```

```

mout1 = [phi Pin Tin massnext1 engine_data' vref tref T1(end) P1(end) o1(:,end)'];
dwmwrite(file3,mout1,'-append');
fuelsub = fuelnext+addfuelm;
mout2 = [phi Tin EGRfile reformper refca];
dwmwrite('temphcci2',mout2);
mout3 = [fuelsub addfuelm];
dwmwrite('fuelsub',mout3);
disp '***End of Reformation Cycle***'
run 'HCCIcycleII'

```

Step 4: HCCI cycle with reformat products

```

car = -15
g=idealGasMix('chem_Mar_nox.cti');
disp 'HCCI II running'
% READ FILE NAME INPUTS FROM TEMP.DAT

```

```

filein = dlmread('temphcci2','',0,0);
phifile = filein(1)
Tfile= filein(2)
EGRfile = filein(3)
reformper = filein(4)
refca = filein(5)
filefuel = dlmread('fuelsub','',0,0);
fuelsub = filefuel(1)
addfuelm = filefuel(2)

```

```

% OPEN FILE CONTAINING ENGINE PARAMETERS AND END GAS
CONDITIONS FROM REFORMATION CYCLE

```

```

file1 = strcat('Inputs', num2str(phifile),'T-',num2str(Tfile),'EGR-',num2str(EGRfile),'Ref-
',num2str(reformper),'-',num2str(refca),'CA');

```

```
% READ PARAMETERS AND INTIAL CONDITIONS FROM HCCI FIRST CYCLE
OUTPUT
```

```
varin1 = dlmread(file1,',',9,0);
phi = varin1(1);
Pin = varin1(2); %atm
Tin= varin1(3);
massnext1 = varin1(4);
bore= varin1(5); % m
stroke= varin1(6); % m
compress= varin1(7);
conrod= varin1(8); %m
rpm= varin1(9); % rpm
twall= varin1(10); % K
vref = varin1(11);
tref = varin1(12);
Tpc = varin1(13);
Ppc = varin1(14);
outcond=varin1(15:end);
omega=2*pi*rpm/60.0;
engine_data=[bore,stroke,compress,conrod,rpm,twall]';
set(g,'T',Tpc,'P',Ppc,'X',outcond); % g based on end of reformation cycle after isentropic
expansion to Patm
u11 = intEnergy_mass(g);
svref = 1/density(g);
mass11 = vref*density(g)
mr = massFractions(g)*mass11; % Mass of each reformate species
if EGRfile == 0
    lam = 1/phi;
    fue = 1;
    oxy = 3 * lam
    nit = (79/21)*oxy
set(g,'T',Tin,'P',Pin,'X',strcat('C2H5OH:',num2str(fue),'O2:',num2str(oxy),'N2:',num2str(
nit))); % without EGR
```

```
% CALCULATING THE TOTAL MASS GAS WOULD OCCUPY BASED ABOVE
CONDITIONS EGR = 0, PIN TIN
```

```
ivc=-180;%degrees ATDC (negative means before TDC)
ti=ivc*pi/180/omega;
v00=volume(ti,engine_data);
masstot=density(g)*(v00-vref)
min = massFractions(g)*masstot;
else
```

```
% OPEN FILE CONTAINING PARAMETERS FROM HCCI FIRST CYCLE OUTPUT
```

```

fileegr = strcat('NoRefPhi', num2str(phi),'T-',num2str(Tin));
varinegr = dlmread(fileegr,',',9,0);
outcond2=varinegr(end,6:end)
set(g,'T',Tin,'P',Pin,'X',outcond2); % g based on previous HCCI cycle end conditions

% MOLES OF EGR ADDED

z1 = moleFractions(g)';
z1 = z1*(EGRfile/100);

% MOLES OF FRESH FUEL AND AIR ADDED

lam = 1/phi;
EGR = EGRfile
fue = 1;
oxy = 3 * lam*fue;
nit = (79/21)*oxy;
set(g,'T',Tin,'P',Pin,'X',strcat('C2H5OH:',num2str(fue),'O2:',num2str(oxy),'N2:',num2str(
nit)));
z11 = moleFractions(g)';
z11(49) = (z11(49)*(1-(EGR/100)))+z1(49);
z11(11) = (z11(11)*(1-(EGR/100)))+z1(11);
z11(57) = (z11(57)*(1-(EGR/100)))+z1(57);
z11(9) = (z11(9)*(1-(EGR/100)))+z1(9);
z11(16) = (z11(16)*(1-(EGR/100)))+z1(16);
z11(10) = (z11(10)*(1-(EGR/100)))+z1(10);
z11(72) = (z11(72)*(1-(EGR/100)))+z1(72);
setMoleFractions(g,z11);
set(g,'T',Tin,'P',Pin);

% CALCULATING THE TOTAL MASS GAS WOULD OCCUPY BASED ABOVE
CONDITIONS EGR = 0, PIN TIN

ivc=-180;%degrees ATDC (negative means before TDC)
ti=ivc*pi/180/omega;
v00=volume(ti,engine_data);
masstot=density(g)*(v00-vref)
min = massFractions(g)*masstot;
end
min(49) = fuelsub*(1-(reformper/100));
mfinal1 = min/(masstot)
setMassFractions(g,mfinal1);
set(g,'T',Tin,'P',Pin);

```

```
% TIMING PARAMETERS: SIMULATION CONDUCTED FOR CLOSED PART OF
THE CYCLE FROM INTAKE VALVE CLOSE (IVC) TO EXHAUST VALVE
OPENING (EVO)
```

```
ivc=-180;%degrees ATDC (negative means before TDC)
evo=180;%degrees ATDC
dtheta=.5;% crank angle resolution for output
```

```
% SIMULATION TIME PARAMETERS CONVERTED FROM DEGREES
```

```
t0=ivc*pi/180/omega;
tf=evo*pi/180/omega;
tref=(car)*pi/180/omega; % **** Reformat addition at 0 CA ****
dt=dtheta*pi/180/omega;
time1=[t0:dt:tref];
time2=[tref:dt:tf];
v0 = v00-vref;
mass1=density(g)*v0
z0 = [temperature(g);
      intEnergy_mass(g);
      1/density(g);
      moleFractions(g)];
gamma = cp_mass(g)/cv_mass(g)
compress1 = v0/(2*vref);
engine_data1=[bore,stroke,compress1,conrod,rpm,twall]
options=odeset('RelTol', 1.e-5, 'AbsTol', 1.e-10, 'Stats', 'on', 'OutputFcn', @odeplot,
'OutputSel', [1]);
out= ode15s(@slidercrankODE, [time1(1) time1(end)], z0, options, g, engine_data1,
mass1, v00, gamma, Pin, Tin);
x=deval(out,time1);
th=time1*180/pi*omega;
ns=nspecies(g);
Ru=gasconstant;
for i=1:length(time1);
    r = x(4:end,i);
    for k=1:79
        if r(k) < 0;
            r(k) = 0;
        end
    end
    setmoleFractions(g,r);
    setState_UV(g,[x(2,i) x(3,i)]);
    wt1=meanmolecularweight(g);
    mfr(:,i) = massFractions(g);
    ol(:,i) = moleFractions(g);
    T1(i) = Temperature(g);
end
```

```

    P1(i) = pressure(g);
end
min1 = massFractions(g)*mass1;
for sp = 1:79
    mfinal(sp) = min1(sp)+mr(sp);
end
mfinal = mfinal/(mass11+mass1);
setMassFractions(g,mfinal);
ufinal = (u11*mass11)+(x(2,end)*mass1)/(mass11+mass1)
vfinal = ((svref*mass11)+(x(3,end)*mass1))/(mass11+mass1)
uv = [ufinal vfinal];
setstate_UV(g,uv);
xxxx = Temperature(g)
zr = [temperature(g)
    intEnergy_mass(g);
    1/density(g);
    moleFractions(g)];
gamma = cp_mass(g)/cv_mass(g);
massf = mass11 + mass1;
engine_data
options=odeset('RelTol', 1.e-5, 'AbsTol', 1.e-10, 'Stats', 'on', 'OutputFcn', @odeplot,
'OutputSel', [1]);
out1= ode15s(@slidercrankODE, [time2(1) time2(end)], zr, options, g, engine_data,
massf, v00, gamma, Pin, Tin);
x1=deval(out1,time2);
th1=time2*180/pi*omega;
ns=nspecies(g);
Ru=gasconstant;
for i=1:length(time2);
    r1 = x1(4:end,i);
    for k=1:79
        if r1(k) < 0;
            r1(k) = 0;
        end
    end
end
setmoleFractions(g,r1);
setState_UV(g,[x1(2,i) x1(3,i)]);
wt11=meanmolecularweight(g);
mfr1(:,i) = massFractions(g);
o11(:,i) = moleFractions(g);
o41(i)=cp_mass(g)/cv_mass(g);
T11(i) = Temperature(g);
P11(i) = pressure(g);
end

```

% COMBINING BOTH DATA BEFORE CAPTURING GAS FOR REFORMATION
AND AFTER

```
so = size(o1);
so1 = size(o11);
sof = so(2)-1+so1(2);
of = zeros(so(1),sof);
Tf = zeros(1,sof);
Pf = zeros(1,sof);
thf = zeros(1,sof);
timef = zeros(1,sof);
vf = zeros(1,sof);
tof = so(2)-1;
of(:,1:tof) = o1(:,1:tof);
of(:,so(2):end)=o11(:,1:so1(2));
Tf(1,1:tof) = T1(1:tof);
Tf(1,so(2):end)=T11(1:so1(2));
Pf(1,1:tof) = P1(1:tof);
Pf(1,so(2):end)=P11(1:so1(2));
thf(1,1:tof) = th(1:tof);
thf(1,so(2):end)=th1(1:so1(2));
timef(1,1:tof) = time1(1:tof);
timef(1,so(2):end)=time2(1:so1(2));
vf(1,1:tof) = x(3,1:tof);
vf(1,so(2):end)=x1(3,1:so1(2));
```

% WORK CALCULATIONS

```
for xx1 = 2:length(timef)
    work1(xx1)=((Pf(xx1)+Pf(xx1-1))/2)*(vf(xx1)-vf(xx1-1));% J/Kg
end
work = cumsum(work1/1000); % units J/g
```

% OUTPUT FOR CREATING INDEX IN EXCEL OUTPUT FILE - 1ST 10 ROWS
ARE OCCUPIED BY INDEX

```
spe = char(speciesNames(g));
spe1 = strvcats(char('time'), char('rad'), char('temp'), char('press'),char('work'), spe);
```

% CREATING FILE NAME BASED ON PHI INPUT

```
file2 = strcat('HCCI-II-Phi', num2str(phi), 'T-', num2str(Tin), 'EGR-', num2str(EGRfile),
'Ref-',num2str(reformper), '-',num2str(car), 'CA');
```

% WRITING SPECIES INDEX ON TO FILE CREATED

```
dlmwrite(file2,spel');

% WRITING SPECIES OUTPUT

mout = [timef thf Tf Pf work' of];
dlmwrite(file2,mout,'-append');

% CREATING TEMP FILE FOR LOOP UNTITLED.M

file3 = strcat('Inputs-untitled');
mout1 = [phi Tin EGRfile reformper refca];
dlmwrite(file3,mout1);
clear all
disp '****done complete cycle****';
```


Vita Auctoris

NAME: Gnanaprakash Gnanam

PLACE OF BIRTH: Salem, India

YEAR OF BIRTH: 1977

EDUCATION
Bharathiar University, Coimbatore, India
1994-1998 B.Eng.

University of Saskatchewan, Saskatoon, Saskatchewan
1999-2002 M.Sc.

University of Windsor, Windsor, Ontario
2002-2008 Ph.D.